University of Glasgow

Latorre-Barragan, Fernanda (2018) *From force generation to host cell attachment: new function of the acto-MyoA motor complex in Toxoplasma gondii tachyzoites.* PhD thesis.

https://theses.gla.ac.uk/30579/

Copyright and moral rights for this work are retained by the author

A copy can be downloaded for personal non-commercial research or study, without prior permission or charge

This work cannot be reproduced or quoted extensively from without first obtaining permission in writing from the author

The content must not be changed in any way or sold commercially in any format or medium without the formal permission of the author

When referring to this work, full bibliographic details including the author, title, awarding institution and date of the thesis must be given

Enlighten: Theses
https://theses.gla.ac.uk/
research-enlighten@glasgow.ac.uk

From force generation to host cell attachment: new function of the acto-MyoA motor complex in *Toxoplasma gondii* tachyzoites

By

Fernanda Latorre-Barragan
Licentiate in Biology

Submitted in fulfilment of the requirements for the
Degree of Doctor of Philosophy

School of Life Sciences
College of Medical, Veterinary & Life Science
Institute of Infection, Immunity & Inflammation
University of Glasgow

Abstract

The Apicomplexan parasite *Toxoplasma gondii* is considered an extremely successful pathogen for its capacity to invade virtually any nucleated cell. Host cell invasion is an active process thought to be driven by the same acto-myosin machinery that drives gliding motility. The current model suggests that at the core of the complex is MyoA, a small unconventional class XIVa myosin, which, together with its molecular partner myosin light chain 1 (MLC1), produces mechanical force on short actin (ACT1) filaments to power gliding and invasion. However, efficient conditional removal of the key components of the acto-MyoA motor complex indicated that although these proteins were important, they were not essential for motility or invasion. Some plausible explanations of this surprising finding were: probable redundancy among motor complex proteins, presence of residual protein in the conditional mutant lines, and/or compensatory mechanisms for driving these essential steps of the *T. gondii* life cycle.

Considering these hypotheses, and given that *T. gondii* encodes for 11 myosins and 7 myosin light chains, this study focused on different possibilities upon MyoA and MLC1 depletion, Therefore, overlapping subcellular localisations and functions had to be considered. Due to its structural similarity, and that it shares molecular partners with MyoA, myosin C (MyoC) was the first candidate considered to compensate for MyoA function in the *myoA* KO. In fact, a *myoA/B/C* KO was unable to grow in *in vitro* conditions due to a detrimental egress phenotype, although it could still glide and invade. Here, the *mlc1* KO, *myoB/C/mlc1* KO, and a set of MyoC complementation constructs in the *myoA* KO were analysed in deep detail to further investigate the redundancy hypothesis. The results obtained do not dismiss functional redundancies between MyoA and MyoC; on the contrary, they show that some mechanisms, such as egress, can be rescued in the *myoA* KO. However, this redundancy does not explain how *mlc1* and *myoB/C/mlc1* KO parasites remain motile and invasive in the absence of residual protein in these conditional mutants. These results make it necessary to critically revisit the current motor model and re-evaluate the functions of the proteins involved in it.

This thesis presents evidence that the acto-MyoA motor complex is involved in substrate attachment rather than in force generation. Finally, a hypothetical model for gliding motility is proposed aimed at reconciling recent observations. Together, considering different interactors and mechanisms, these results highlight the complexity of *T. gondii* tachyzoite cellular biology during progression of the lytic cycle.

Table of Contents

List of Tables

List of Figures

List of Accompanying Material

Movie 1: RHΔ*hxgprt* circular motility
RHΔ*hxgprt* expressing killer red were used to analyse gliding kinetics by time-lapse video microscopy. Ibidi glass bottom dishes pre-coated with FBS were used to assay motility. This movie shows a RHΔ*hxgprt* parasite moving in a typical helical manner. Video was recorded at 1 frame per second rate using A_{594} channel, and parasites were tracked using WrMTrck plugin (ImageJ). Movie supports Figure 3-6A. Scale bar represents 10µm. Movie saved 10X faster.

Movie 2. *mlc1* KO circular motility
mlc1 KO moving in circular motion was recorded and analysed as described for movie 1. *mlc1* KO mutants (96 hours post induction) were used to analyse gliding kinetics by time-lapse video microscopy using FITC channel. Just YFP expressing parasites (product of DiCre cassette) were considered for further examination. Movie supports Figure 3-6A. Scale bar represents 10µm. Movie saved 10X faster.

Movie 3. RHΔ*hxgprt* helical motility
RHΔ*hxgprt* moving in helical motion was recorded and analysed as described for movie 1. Movie supports Figure 3-6A. Scale bar represents 10µm. Movie saved 10X faster.

Movie 4. *mlc1* KO helical motility
mlc1 KO moving in helical motion were prepared and analysed as for described in movie 2. Movie supports Figure 3-6A. Scale bar represents 10µm. Movie saved 10X faster.

Movie 5. RHΔ*hxgprt* parasite invading host cell
RHΔ*hxgprt* invading HFF cell was recorded at 1 frame per second in DIC. Movie supports Figure 3-8A. Scale bar represents 10µm. Movie saved 10X faster.

Movie 6. *mlc1* KO mutant invading host cell rapidly
mlc1 KO parasites invading HFF cell rapidly. *mlc1* KO mutants (96 hours post induction) were used to analyse host cell penetration. Protocol for imaging was followed as described for Movie 5; however, a final image was taken in FITC channel to recognise MLC1 depleted parasites (YFP+). Movie supports Figure 3-8A. Scale bar represents 10µm. Movie saved 10X faster.

Movie 7. *mlc1* KO mutant invading host cell slowly
mlc1 KO parasites invading HFF cell slowly. Protocol for preparation and imaging was followed as described for Movie 6 and 5, respectively. Movie supports Figure 3-8A. Scale bar represents 10µm. Movie saved 10X faster.

Movie 8. RHΔ*hxgprt* vacuoles egressing by artificial induction with Ca^{++} ionophore
Live cell video microscopy was used to analyse Ca^{++} induced egress. HFF monolayer infected with RHΔ*hxgprt* expressing YFP for 36 hours was induced with Ca^{++} ionophore (A23187) at approximately 1 minute from movie start point. Images were recorded at 1 frame per second for 12 minutes. Movie supports Figure 3-9C. Numbers indicate time (minutes.seconds). Scale bars represent 5µm. Movie saved 10X faster.

Movie 9. *mlc1* KO vacuoles egressing by artificial induction with Ca^{++} ionophore
mlc1 KO mutants (96 hours post induction) were used to infect HFF monolayers. Parasites were left to replicate for 36 hours before Ca^{++} iophore (A23187) treatment. Only YFP expressing parasites were considered for examination. Movies were analysed as previously described for Movie 8. Movie supports Figure 3-9C. Numbers indicate time (minutes.seconds). Scale bars represent 5µm. Movie saved 10X faster.

Movie 10. *myoB/C/mlc1* KO smooth circular boost

myoB/C/mlc1 KO moving in circular motion was recorded and analysed as described for movie 1. *myoB/C/mlc1* KO mutants (96 hours post induction) were used to analyse gliding kinetics by time-lapse video microscopy using FITC channel. Just YFP expressing parasites (product of DiCre cassette) were considered for further examination. Movie supports Figure 4-3B. Scale bar represents 10µm. Movie saved 10X faster.

Movie 11. *myoB/C/mlc1* KO "stop and go" circular boost
myoB/C/mlc1 KO moving in circular arrested motion. Parasites were treated, recorded, and analysed as described for movie 10. Movie supports Figure 4-3B. Scale bar represents 10µm. Movie saved 10X faster.

Movie 12. *myoB/C/mlc1* KO smooth helical boost
myoB/C/mlc1 KO moving in helical motion. Parasites were treated, recorded, and analysed as described for movie 10. Movie supports Figure 4-3B. Scale bar represents 10µm. Movie saved 10X faster.

Movie 13. RHΔ*hxgprt* vacuoles egressing by artificial induction with Ca^{++} ionophore
Live cell video microscopy was used to analyse Ca^{++} induced egress. HFF monolayer infected with RHΔ*hxgprt* expressing YFP for 36 hours was induced with Ca^{++} ionophore (A23187) at approximately 1 minute from movie start point. Images were recorded at 1 frame per second for 12 minutes. Movie supports Figure 4-5B. Numbers indicate time (minutes.seconds). Scale bars represent 5µm. Movie saved 10X faster.

Movie 14. *myoB/C/mlc1* KO vacuoles egressing by artificial induction with Ca^{++} ionophore
myoB/C/mlc1 KO mutants (96 hours post induction) were used to infect HFF monolayers. Parasites were left to replicate for 36 hours before Ca^{++} iophore (A23187) treatment. Only YFP expressing parasites were considered for examination. Movies were analysed as previously described for Movie 13. Movie supports Figure 4-5B. Numbers indicate time (minutes.seconds). Scale bars represent 5µm. Movie saved 10X faster.

Movie 15-16. RHΔ*hxgprt* transiently expressing Cb-Snap
Actin signal was observed in parasites transiently expressing Cb-Snap. Prior imaging, parasites were incubated with snap-ligand for 30 min, washed twice and incubate in culture conditions for 20 min. Video was recorded at 1 frame per 100 millisec for 30 sec. Movie supports Figure 5-10E. Scale bars represent 2µm. Movie saved 1X.

Movie 17-18. loxp*mlc1* transiently expressing Cb-Snap
Cb-snap actin was visualised in lop*mlc1* parasites. Preparation of the parasites and live imaging were performed as described for movie 15. Movie supports Figure 5-10E. Scale bars represent 2µm. Movie saved 1X.

Movie 19-20. *myoA* KO transiently expressing Cb-Snap
Cb-snap actin was visualised in *myoA* KO parasites. Preparation of the parasites and live imaging were performed as described for movie 15. Movie supports Figure 5-10E. Scale bars represent 2µm. Movie saved 1X.

Movie 21-22. *mlc1* KO transiently expressing Cb-Snap
Cb-snap actin was visualised in *mlc1* KO parasites. Parasites were transfected and induced 72 hour prior imaging. Preparation of the parasites and live imaging were performed as described for movie 15. Movie supports Figure 5-10E. Scale bars represent 2µm. Movie saved 1X.

Dedication

"*The developing world is full of entrepreneurs and visionaries, who with access to education, equity, and credit would play a role in developing the economic situations in their countries"* Muhammad Yunus

This thesis is dedicated to all the people performing science in developing countries. Making the impossible possible, even in adverse circumstances.

As scientists, we should fight for the right of people to be educated to the same standard, and possess the same opportunities, no matter the country that issued their passport.

Acknowledgement

Albert Einstein once said, "*If we knew what it was we were doing, it would not be called research, would it?"*

First, and most importantly, to Prof Markus Meissner for giving me the opportunity to develop this project in his laboratory. For these four years of encouragement and guidance. Markus thank you very much for the motivation, the challenge, the generosity, and for extending your hand when the situation required.

To my advisors, Dr Richard McCulloch, Prof Margaret Harnett, and Prof Silke Müller, for their support, insightful comments, and understanding. I also want to thank Prof Gary Ward for being available for discussion and answering my questions with a big smile and great curiosity.

A special thanks to those who offered their help without being asked to proofread parts of this thesis. To Dr Jamie Whitelaw, my first friend in Glasgow, who sat next to me in the front row of this roller coaster with his actin project. To Dr Robyn Kent, who always knew if I needed a cup of tea or ten pints of beer. To Christen Klinger, who *has been correcting* my inherit ability to convert everything to passive voice, and for holding my hand in difficult times. To Matthew Gow and Kathryn Crouch, who answered rapidly and never denied help.

To all the current and former members of the Meissner lab, who made bench work enjoyable; very special thanks to the invasion group who were open for collaboration and discussion: Dr Simon Gras, Dr Gurman Pall, Dr Javier Periz, Mario del Rosario, Dr Jamie Whitelaw, Dr Nicole Andenmatten, and Dr Saskia Egarter. To Dr Mariana Serpeloni and Carmen Melatti (mama) who kept an eye on me all this time, and joined me for loud laugher in the darkest and the lightest times. To Dr Elena Jimenez-Ruiz and Aude-Anaïs Olijnik for the wisdom and the coffees shared all these years. Finally, to Dr Leandro Lemgruber, for his great job in assisting technical support with microscopy issues.

All this adventure started in the sunny days back in Quito when trying to fight Chagas disease next to my great friend Andrea Zurita. Thanks Zu for being my family in Glasgow, and an amazing friend who reminded me what great friends are made of - time, loyalty, and joy. To Helena who day by day let me get close for a chat and a hug, I deeply appreciate

your aperture. To all the people in the GBRC, especially the Sheiner, McCulloch, Hammarton, and Mottram labs for their great help and company. A special thanks to Gabriela Garcia de Anderson who always brings sun to Glasgow with her enthusiasm and commitment for studying human migration and equal rights, Gusi you are inspiring.

To those who reached me with their halo of love and support from the other side of the world. To my family, especially my mother, sister, and father, who encouraged the little me when growing tadpoles in my Barbie pool, and backing me all the way in my education since pre-kinder days. Kathy and Joy, my partners in crime and cheerleaders in life. My very best friend Luis Camacho, who keeps me updated with distribution and ecology theories, but most importantly, makes everything so much simpler. To Lu and Carli, for their unconditional friendship, and listening to every single thing I have to say about life without judgment. Finally, to all the people that in one way or another collaborated on this project. I express my gratitude to all of you, for the unconditional support and for making my life full of smiles.

My PhD education was fully funded by SENESCYT in the *Universities of Excellence* program.

Publications arising from this work and collaborations

Whitelaw*, J. A., Latorre-Barragan*, F., Gras, S., Pall, G., Leung, J. M., Heaslip, A., Egarter, S., Andenmatten, N., Nelson, S. R., Warshaw, D. M., Ward, G. and Meissner, M. 2017. Surface attachment, promoted by the Acto-myosin system of *Toxoplasma gondii* is important for efficient gliding motility and invasion. BMC Biol, 15,1. DOI: 10.1186/s12915-016-0343-5.

Periz*, J., Whitelaw*, J. A., Harding*, C., Gras, S., Del Rosario Minina, M. I., Latorre-Barragan, F., Lemgruber, L., Reimer, M., Insall, R., Heaslip, A. and Meissner, M. 2017. *Toxoplasma gondii* F-actin forms an extensive filamentous network required for material exchange and parasite maturation. eLife, 6. DOI: 10.7554/eLife.24119.

(*) Equal contribution.

Conference proceedings

This thesis has been presented at the following national and international conferences

25th Annual Molecular Parasitology Meeting in Woods Hole, MA, USA. September 2014. Poster presentation: Complementation studies of Myosin C in *Toxoplasma gondii* tachyzoites lacking key MyoA-motor complex proteins

27th Annual Molecular Parasitology Meeting in Woods Hole, MA, USA. September 2016. Poster presentation: *Toxoplasma gondii* Myosin A motor complex is necessary to regulate attachment to the surface.

British Society for parasitology BSP Spring Meeting 2017. Dundee, Scotland, UK. April 2017.Oral presentation: From force generation to substrate attachment: new functions for the Acto-Myosin A motor complex in *Toxoplasma gondii*.

Author's Declaration

I, Fernanda Latorre-Barragan, hereby declare that I am the sole author and performed all the work presented in this study. Exceptions are listed below, and mentioned in text. No part of this thesis has been previously presented for obtaining a degree at this or another university.

Fernanda Latorre-Barragan

Chapter 3:

MyoA location in the *mlc1* KO was counted by Magdalena Kujawska under my supervision during her undergraduate internship.

3D motility analysis presented in this study was performed by Dr Jacqueline Leung under Prof Gary Ward's supervision.

Chapter 5:

myoA KO 2D gliding data were taken from Dr Nicole Andenmatten to compare values to p5RT70TyMyoC data.

myoA KO qPCR and RNA seq. data were performed by Dr Nicole Andenmatten and Dr Nicholas Dickens

3D motility analysis presented in this study was performed by Dr Jacqueline Leung under Prof Gary Ward supervision.

Chapter 6:

Retention under flow conditions was performed by Dr Gurman Pall

Bead translocation of *mic2* KO, $DRPB_{DN}$ (with and without shield), RHΔ*hxgprt* under Pitstop2 and endo buffer treatment was performed and analysed by Dr Simon Gras. *act1* KO bead translocation data was collected and analysed by Dr Jamie Whitelaw.

Definitions/Abbreviations

°C	Degree Celsius	EBA	Erythrocyte binding antigen
2D	2 Dimensions	EDTA	Ethylene diamine tetraacetic acid
3D	3 Dimensions	e.g.	For example
aa	Amino acid	EGTA	Ethylene glycol tetraacetic acid
ACT1	Actin	ELC	Essential light chain
ADF	Actin depolymerising factor	EM	Electron microscopy
ADP	Adenosine diphosphate	ER	Endoplasmic reticulum
AFM	Atomic force microscopy	EtOH	Ethanol
a.k.a	Also known as	F-actin	Filamentous actin
AKTM	Apical complex lysine methyltransferase	FBS	Fetal bovine serum
ALD	Aldolase	Fw	Forward
AMA1	Apical membrane antigen 1	G-actin	Globular actin
Amp	Ampicillin	GAC	Glideosome associated connector
APR	Apical polar ring	GAP	Glideosome associated protein
Arp	Actin related protein	gDNA	Genomic deoxyribonucleic acid
ATP	Adenosine triphosphate	GFP	Green fluorescent protein
BLAST	Basic Local Alignment Search Tool	GOI	Gene of interest
bp	Base pair	GPI	Glycophosphatidylinositol
BSA	Bovine serum albumin	GRA	Dense granule proteins
C-terminal	Carboxyl terminal	GSH	Glutathione
Ca^{++}	Calcium	h	Hour
CAT	Chloramphenicol acetyltransferase	H_2O	Water
CaM	Calmodulin	HEPES	4-(2-Hydroxyethyl)-piperazineethanesulphonic acid
Cas9	CRISPR associated protein 9	HFF	Human foreskin fibroblast
Cb	Chromobody	HSP	Heat shock protein
cDNA	Complementary deoxyribonucleic acid	*hxgprt*	Hypoxanthine-xanthine-guanine phosphoribosyl transferase
CDPK	Calcium-dependent protein kinase	*i.e.*	*Id est* (that is)
CIP	Calf intestinal phosphatase	IAP	IMC associated protein
CRISPR	Clustered Regularly Interspaced Short Palindromic Repeats	IFA	Immunofluorescence analysis
CytoD	Cytochalasin D	IMC	Inner membrane complex
dd	Destabilisation domain	IPTG	Isopropyl-O-D-thiogalactopyranoside
DHFR	Dihydrofolate reductase	kbp	Kilo base pair
DiCre	Dimerisable Cre	KD	Knockdown
DMEM	Dulbecco's Modified Eagle's Medium	kDa	Kilo Dalton
DMSO	Dimethyl sulfoxide	IPP	Isopentenyl diphosphate
DNA	Deoxyribonucleic acid	M	Molar
DN	Dominant negative	mg	Milligram
dNTP	Deoxynucleotide 5'-triphosphate	MIC	Micronemal protein
Drp	Dynamin related protein	min	Minute
DS	Dextran Sulfate	ml	Millilitre
E. coli	*Escherichia coli*	MLC	Myosin light chain

mM	Milimolar	SOC	Super optimal broth with catabolite repression
MSP	Merozoite surface protein	SPN	Subpellicular network
MPA	Mycophenolic acid	spp.	Species
mRNA	Messenger ribonucleic acid	SSR	Site specific recombination
MTOC	Microtubule organising centre	SUB	Subtilisin
Myo	Myosin	t	Time
N-terminal	Amino terminal	*T. gondii*	*Toxoplasma gondii*
NCBI	National Centre for Biotechnology Information	TAE	Tris-acetate-EDTA
NEB	New England Biolabs	Taq	Thermos aquaticus
ng	Nanogram	TATi	Transactivator TRAP identified
nm	Nanometer	TEMED	N,N,N',N'-tetramethylethylenediamine
o/n	Over night	TetO	Tetracycline operator
ORF	Open reading frame	TetR	Tetracycline repressor
P. berghei	*Plasmodium berghei*	TFM	Traction force microscopy
P. falciparum	Plasmodium falciparum	TIRF	Total internal reflection fluorescence
PAM	Protospacer adjacent motif	TJ	Tight junction
PBS	Phosphate buffered saline	TM	Transmembrane
PCR	Polymerase chain reaction	TRAP	Thrombospondin related anonymous protein
PFA	Paraformaldehyde	TRE	Tetracycline responsive promoter
Pi	Inorganic phosphate	Tris	Tris [hydroxymethyl] aminomethane
PLP	Perforin like protein	Tub	Tubulin
PM	Plasma membrane	U	Unit
POI	Protein of interest	UTR	Untranslated region
PV	Parasitophorous vacuole	µg	Microgram
PVM	Parasitophorous vacuole membrane	µl	Microliter
RB	Residual body	µm	Micrometre
RBC	Red blood cell	µM	Micromolar
RBL	Reticulocyte binding like	UV	Ultraviolet
RLC	Regulatory light chain	V	Volts
ROP	Rhoptry protein	v/v	Volume/volume percentage
rpm	revolutions per min	w/v	Weight/volume percentage
RT	Room temperature	WB	Western blot
Rv	Reverse	WHO	World health organisation
RNA	Ribonucleic acid	WT	Wild-type
ROM	Rhomboid proteases	Xan	Xanthosine monophosphate
RON	Rhoptry neck protein		
s	Second		
SAG	Surface antigen		
SD	Standard deviation		
SDS-PAGE	Sodium dodecyl sulfate polyacrylamide gel electrophoresis		
SEM	Standard of the mean		
Shld-1	Shield 1		
SIM	Structured illumination microscopy		

Chapter 1 Introduction

1.1 The phylum Apicomplexa

Apicomplexan parasites are a widely diverse group of unicellular microorganisms, almost exclusively parasitic with complex life cycles (Levine, 1988). It is estimated that the group contains around 1.2-10 million species (Adl et al., 2007) that are traditionally divided into four different clades: Gregarina, Cryptosporidia, Hematozoa, and Coccidia (Figure 1-1) (Morrison, 2009, Šlapeta and Morin-Adeline, 2011, Woo et al., 2015). Apicomplexan parasites present an extensive range of morphologies, depending not only on their genus but also on life cycle stage. The members of this phylum have not only progressively lost components typical of free-living organisms, but also evolved specific parasitic factors to exploit this lifestyle (Woo et al., 2015, Klinger et al., 2016). In fact, these parasites are equally diverse in marine and terrestrial environments, certainly depending on the specific niche of their hosts. Several genera represent a potential health problem for humans and livestock, with substantial morbidity and mortality as well as financial losses every year. *Plasmodium* spp. represent some of the most prominent species within this group. According to the World Health Organisation (WHO), it is estimated that 212 million cases of malaria occurred in 2015, of these, 429 thousand deaths were reported predominantly in the African region (92%). By increasing control and prevention programmes the incidence of malaria decreased 41% between 2000 and 2015 (WHO, 2016). Equally important is *Toxoplasma gondii*, which, although largely asymptomatic in healthy people, is thought to be present in approximately 30% of the human population, residing as cysts in the brain and muscle tissue (Montoya and Liesenfeld, 2004). Importantly though, *T. gondii* can cause serious congenital malformations and miscarriage during pregnancy. Likewise, in immunocompromised patients this parasite can cause visual loss and severe illnesses (Hohlfeld et al., 1989, Ambroise-Thomas and Pelloux, 1993, Weiss and Dubey, 2009). In addition, members of the genus *Cryptosporidium* spp. are considered opportunistic pathogens able to infect hosts via food or water sources containing parasites. In humans, cryptosporidiosis is the second most common cause of diarrhoeal disease, which affects primarily children and toddlers in developing countries (Striepen, 2013). *Babesia* spp., *Theileria* spp., *Neospora* spp. and *Eimeria* spp. species are considered of high relevance for affecting agricultural industries worldwide (Trees et al., 1999, Uilenberg, 2006, Sharman et al., 2010). For instance, the agricultural industry is severely impacted by members of the genus *Theileria*, which are pathogens transmitted by ticks to ruminants and equines (Kiara et al., 2018, Ueti and Knowles, 2018). The diseases caused by these parasites (i.e. theileriosis and east coastal

fever) affect the lymphoid system, lungs and gastrointestinal tract, causing high mortality among the livestock; therefore, this is a matter of economic relevance (Morrison, 2015). Similarly, several species of *Eimeria* cause avian coccidiosis, which can develop into malabsorptive and haemorrhagic enteric diseases. These infections greatly affect egg production, feed conversion and successful offspring generation, leading to high economic loses in poultry production worldwide (Blake and Tomley, 2014).

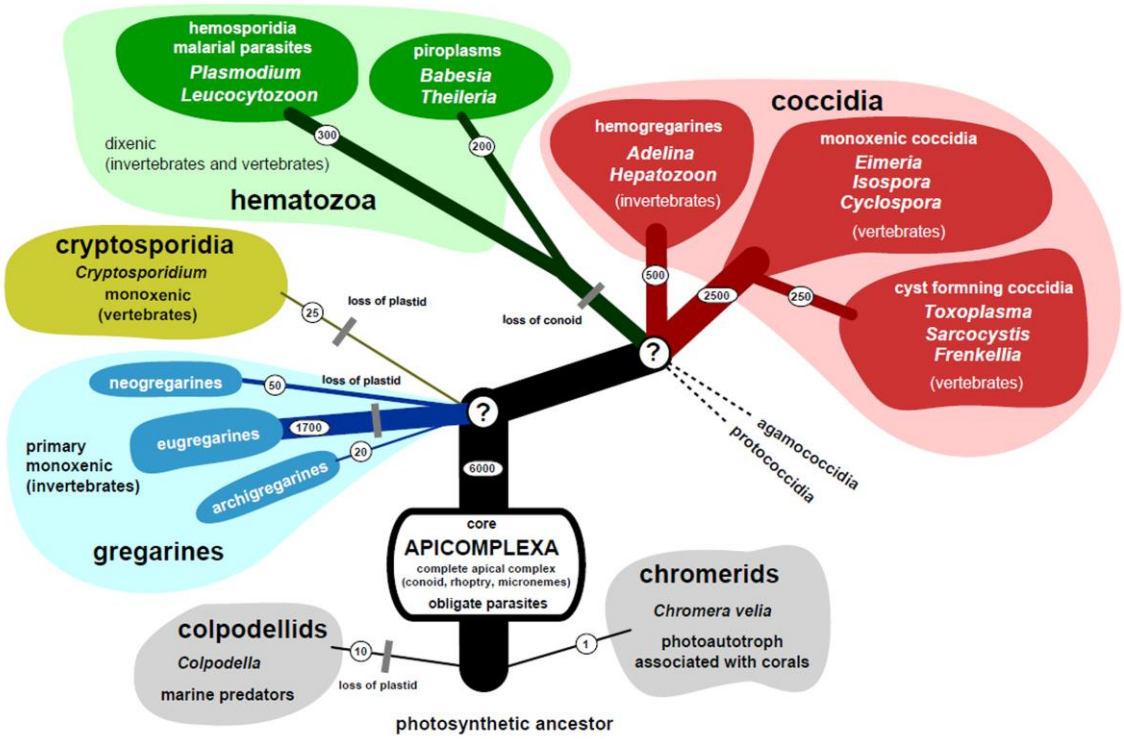

Figure 1-1. Hypothetical three of the phylum Apicomplexa.
Scheme shows a hypothetical tree of the phylum Apicomplexa. This phylum evolved from Chromerids (free-living photosynthetic ancestor) and contains four clades (coloured): gregarines, Cryptosporidia, Hematozoa, and Coccidia (Woo et al., 2015). The group is named for a particular structure situated at the anterior pole of the parasites, the “apical complex”. This complex consists of polar rings, micronemes, rhoptries, subpellicular microtubules and in some members, a tubulin-derived structure called the conoid, which is a cone-shaped organelle thought to function as a flexible scaffold, which is thought to support host cell penetration; however, this organelle is absent in hematozoans (*i.e. Plasmodium* and piroplasms *Babesia*, *Theileria*) (Morrissette and Sibley, 2002, Šlapeta and Morin-Adeline, 2011). Another shared feature among most apicomplexan parasites, except Cryptosporidia, is the presence of the apicoplast, an organelle acquired by secondary endosymbiosis (McFadden et al., 1996, Kohler et al., 1997, McFadden, 2011). Finally, apicomplexan parasites, together with ciliates and dinoflagellates, are contained in the infrakingdom Alveolata (Šlapeta and Morin-Adeline, 2011). The conserved feature that unifies this superfamily is the presence of alveoli, membrane sacks that reside underneath the plasma membrane (PM), that in this group of parasites, is organised as a set of flattened vesicles and are part of the inner membrane complex (IMC) (Gould et al., 2006). The IMC is a structural scaffold that gives rigidity to the parasite and support during cell division (Morrissette and Sibley, 2002, Harding and Meissner, 2014). Figure reprinted from (Šlapeta and Morin-Adeline, 2011, Portman and Šlapeta, 2013). Figure licensed under the Creative Commons Attribution-Non- Commercial License - Version 3.0.

1.2 *Toxoplasma gondii*, the etiological agent

Humans are among the many warm-blooded organisms this parasite can infect as an intermediate host causing toxoplasmosis. Therefore, tachyzoites and bradyzoites can be found in different human tissues. In the case of acute toxoplasmosis with tachyzoites, drugs (e.g. sulfadiazine and pyrimethamine) and the immune system can control these parasites, especially when they are extracellular (Paquet et al., 2013). However, some tachyzoites could undergo transition to bradyzoites and further develop into cysts in different tissue types such as muscular, brain, and skeletal tissue resulting in a chronic infection (Wohlfert et al., 2017). Unlike tachyzoites, tissue cysts are more elusive to both drugs and the immune system, so control of this stage is more challenging. Humans can become infected with this parasite by consumption of undercooked meat containing tachyzoites or tissue cysts. Additionally, infection can occur by drinking water containing sporulated oocysts, via transplacental transmission, or by infected organ transplantation (Kijlstra and Petersen, 2014).

1.2.1 Toxoplasmosis pathology

The seroprevalence of *T. gondii* in pregnant women around the world is around 8-75%, with this estimate giving a clear indication of wide *T. gondii* distribution (Pappas et al., 2009). Although most infections with *T. gondii* in humans are asymptomatic, they can cause severe damage when congenitally or postnatally acquired or reactivated (Hill and Dubey, 2002). The primary infection during pregnancy can occur when a woman is infected, especially during the first trimester of pregnancy (Desmonts and Couvreur, 1974). Though initially broadly distributed in the foetal tissue, *T. gondii* mainly localises in the central nervous system (Hill and Dubey, 2002). Consequently, the infection may cause severe ocular and neurological damage to the foetus or new-born child, and, in some cases, it may cause miscarriage (Dunn et al., 1999, Torgerson and Mastroiacovo, 2013). In the case of immunosuppressed individuals, for instance AIDS or chemotherapy patients, latent *T. gondii* infection can reactivate. Dormant bradyzoites burst the tissue cyst wall and transform into tachyzoites, which, after several rounds of replication can disseminate and cause tissue damage mainly in the brain, muscles, and retina. These lesions may develop into severe encephalitis or ocular disorders (Porter and Sande, 1992, Kijlstra and Petersen, 2014). Additionally, recent reports have suggested there is a link between *T. gondii* infection and neurological disorders such as behavioural changes or schizophrenia (Elsheikha et al., 2016). As this has been studied in more detail in rodent models (Kannan et al., 2010, Ingram et al.,

2013), the molecular and cellular mechanisms underlying this link in humans is matter of further research (Elsheikha et al., 2016, Sugden et al., 2016).

1.3 Overview of *Toxoplasma gondii*

T. gondii was first found in the tissues of *Ctenodactylus gundi* by Nicolle and Monceaux who were working in leishmaniasis research in 1908 (Nicolle, 1908). The name *Toxoplasma* is based on its morphology (Toxo = arc or bow and plasma = life), and *gondii* comes from the misspelled species name of the first rodent it was found in (gundi = gondii) (Nicolle, 1909) reviewed by (Dubey, 2009). The first report of *T. gondii* infection in humans was in a new born female patient in 1939. After one month, the patient developed severe encephalitis and retinitis leading to death (Wolf et al., 1939b). The examination of the tissues of the patient showed that intracellular and extracellular parasites were present. These parasites were used to perform experimental infections in mice and rabbits resulting in severe encephalitis (Wolf et al., 1939b, Wolf et al., 1939a).

T. gondii is a promiscuous parasite capable of invading a wide range of cell types of warm-blooded animals; for this reason, *T. gondii* infections are reported worldwide (Schlüter et al., 2014). This host promiscuity has, at least in part, prompted extensive scientific study of *T. gondii* biology, resulting in this parasite becoming a model organism for Apicomplexan parasites (section 1.11).

Although *T. gondii* is capable of undergoing a sexual cycle, this parasite is considered genetically clonal at a population level (Dard et al., 1992). To date, three main lineages have been recognised among species, referred to as type I, II, and III, along with “group 12”, which was acknowledged as a variation that resulted from genetic recombination in North America (Dard et al., 1992, Howe and Sibley, 1995, Khan et al., 2011). It is thought that these few lineages rose into six clades which are probably more variable than described (Su et al., 2012). Here, strains from North America and Europe have a markedly low level of genetic diversity compared to those in South America, which show an extensive genetic variation that correlates with geographical area (Khan et al., 2007), and even among habitats (Khan et al., 2011). Analysis of important phenotypic differences conferred by genetic factors showed there is a strong correlation between lineages and virulence (Taylor et al., 2006, Fentress et al., 2010, Etheridge et al., 2014).

The association between the parasite lineage, geographic area, and virulence has been broadly studied among *T. gondii* strains. In experiments performed in mice, type I isolates were shown to be highly virulent compared to type II or III strains (Sibley and Boothroyd, 1992, Gavrilescu and Denkers, 2001, Nguyen et al., 2003). Those virulent strains showed enhanced capacity to migrate across epithelia and penetrate the *lamina propia* (Barragan and Sibley, 2002). Similar patterns were reported in humans (Sibley and Boothroyd, 1992). For instance, ocular damage produced by *T. gondii* infection was found often associated with infection with type I or atypical strains in both South and North America (De-La-Torre et al., 2013). Conversely, in Europe these effects were associated with type II strain infections, which can be due to higher exposure to strains of this particular genotype (Xiao et al., 2013). Likewise, in immunosuppressed and congenitally infected patients, toxoplasmosis was associated with type II strain infections in Europe while non- type II strains were associated with more severe damage in the Americas (Xiao and Yolken, 2015). These results suggest that there is a tight association between lineages and geographic area. Despite this, further study is required to understand the link between genotype and pathology, since a plethora of factors can contribute to the effect of infection in a patient (Xiao and Yolken, 2015).

1.4 *Toxoplasma gondii* life cycle

The life cycle of *T. gondii* is complex due to its remarkable ability to infect almost all warm-blooded animals, and the different sexual and asexual stages that this parasite undergoes (Robert-Gangneux and Darde, 2012). During its asexual lifecycle *T. gondii* can infect any nucleated cell. In contrast, the sexual life cycle only occurs in felines, which are the definitive host (Dubey, 2009).

In the natural life cycle (Figure 1-2), felines become infected when ingesting food or water contaminated with oocysts, tachyzoites, or bradyzoites contained in cysts (section 1.4.1). After consumed, the cysts wall is degraded by enzymes in the feline intestinal tract, which release the bradyzoites that subsequently invade epithelial cells, and start the proliferation of new parasites. Following many cycles of asexual division, sexual development starts by the generation of male and female gametes (gametogony) in enterocytes. After fertilisation, oocysts escape the cells and disperse along the intestine of the feline; consequently, millions of unsporulated oocysts are shed in the feline's faeces. Finally, sporulation of oocysts is stimulated by environmental conditions. At this point, parasites are infective and ready to be taken up by other hosts to continue the cycle (further detail in section 1.4.1) (Dubey et al., 1970, Dubey and Frenkel, 1972, Speer et al., 1998).

Inside its intermediate host, *T. gondii* changes stage from the environmental stage to tachyzoites (section 1.4.2). Tachyzoites multiply asexually (by endodyogeny) in almost any kind of nucleated cell, then egress from the cell to infect surrounding host cells. Tachyzoites convert into bradyzoites, which are contained in tissue cysts. This stage of the parasite produces long-term infections inside cells (further detail in section 1.4.2). The natural cycle starts again when a feline consumes an intermediate host infected with tissue cysts. Humans become infected with *T. gondii* after consuming meat, fruits, vegetables or water containing oocysts. Congenital transmission represents yet another mechanism for parasitic infection to spread (Speer and Dubey, 2005, Dubey, 2009, Sibley et al., 2009).

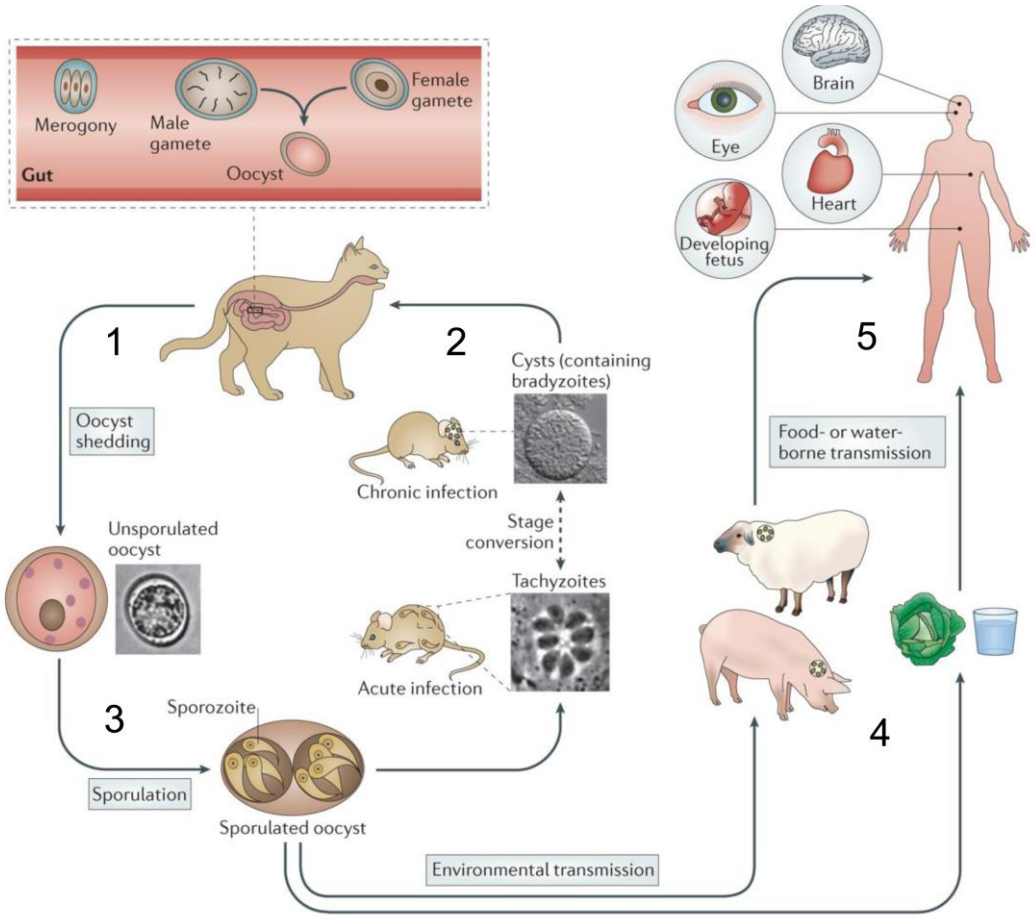

Figure 1-2. *Toxoplasma gondii* life cycle.
1. Unsporulated oocysts present in faeces of a definitive host (Felidae) sporulate in the environment and can infect an intermediate host (rodents in schematic). The infective oocyst can be found in plants material, soil and/or water **2**. After entering to the intermediate host, oocysts transform into tachyzoites and invade cells and form cyst bradyzoites **3.** After consuming the intermediate host, cats become infected by ingestion of cysts. Cats can also get infected by direct ingestion of sporulated oocysts **4.** Domestic animals and humans can get infected by ingesting sporulated oocysts present in the environment (plants material, soil and/or water) or ingesting bradyzoite cysts. Humans can acquire infection in different ways, for instance by eating undercooked meat, consuming water or food contaminated with infected-cat faeces, receiving blood transfusion or organ transplantation or from mother to child **5.** Inside the human body, parasites reside in different tissues like muscle or neural cells. Figure reprinted and adapted from (Hunter and Sibley, 2012) under license of Nature publishing group.

1.4.1 *Toxoplasma gondii* in its definitive host

Felines become infected with *T. gondii* after directly consuming sporulated oocysts, or an infected intermediate host containing tachyzoites or tissue cysts. Tissue cysts are formed by bradyzoites, named for the slow division this stage undergoes within a tissue cyst (brady = slow and zoon = animal) (Frenkel, 1973). Bradyzoite morphogenesis and further engagement to the sexual cycle has been the only stage followed in detail (Dubey and Frenkel, 1972). After ingestion, the tissue cyst wall is degraded by proteolytic enzymes in the stomach and small intestine of the host. Then, the bradyzoites are released and invade epithelial cells where they engage a last asexual division by endodyogeny (two daughters are formed from one mother cell) followed by three rounds of endopolygeny (several rounds of nuclear division precede budding) (Tenter et al., 2000, Speer and Dubey, 2005). Resulting from this, five morphologically different asexual "stages" of the parasite have been observed (Dubey and Frenkel, 1972). After this asexual development, merozoites initiate the sexual differentiation cycle that starts two days after the tissue cyst was ingested. Gamete formation results in the development of microgametocyte (male) and macrogametocyte (female) (Speer and Dubey, 2005). As a result of fertilisation, oocysts are formed and the infected cells rupture, releasing millions of unsporulated oocysts into the lumen, which are further shed with the feline's faeces. In the open environment, the excreted parasites start to sporulate, a process that leads to meiotic reduction and morphological changes; thus, when sporogony is completed, one sporulated oocyst contains two sporocyst each containing four haploid sporozoites. In this state, parasites lie in the external environment where they can survive drying and freezing conditions until an intermediate host is infected (Dubey et al., 1970, Dubey and Frenkel, 1972, Speer et al., 1998, Robert-Gangneux and Darde, 2012).

1.4.2 *Toxoplasma gondii* in the intermediate host

Having completed the sexual cycle inside the definitive host, sporulated oocysts become infective. These parasites gain access to the intermediate host via contaminated food or water. Inside the host, *T. gondii* develops exclusively into asexual stages. These stages are i) the fast replicating and propagating tachyzoites (tachy = fast and zoite = life) (section 1.4.2.1), and subsequently ii) the slow replicating and dormant bradyzoites (brady = slow and zoon = animal) (section 1.4.2.2) (Frenkel, 1973).

1.4.2.1 Tachyzoite lytic cycle

After ingestion, sporozoites transverse the intestinal epithelium to the *lamina propia* (Speer and Dubey, 1998) and transform into tachyzoites that subsequently find a suitable host cell to invade, replicate, and further disseminate, in a process called the lytic cycle (Black and Boothroyd, 2000). For completing this multistep process, the parasites employ a unique method of motility called gliding, which is an energy-dependent mechanism not associated with phagocytosis, cilia or flagella (King, 1988). For this, tachyzoites rely on the coordinated secretion of specialised organelles and substrate attachment (reviewed in section 1.5.1). At this stage, the parasite can invade virtually any nucleated cell in the organism (Carruthers, 2002). The lytic cycle (Figure 1-3) starts when the parasite actively invades a host cell, proceeded by several rounds of replication by endodyogeny (Black and Boothroyd, 2000). After division, parasites egress from the host cell and disseminate through the tissue in order to either i) engage in a new lytic cycle or ii) develop into bradyzoites (Lyons et al., 2002).

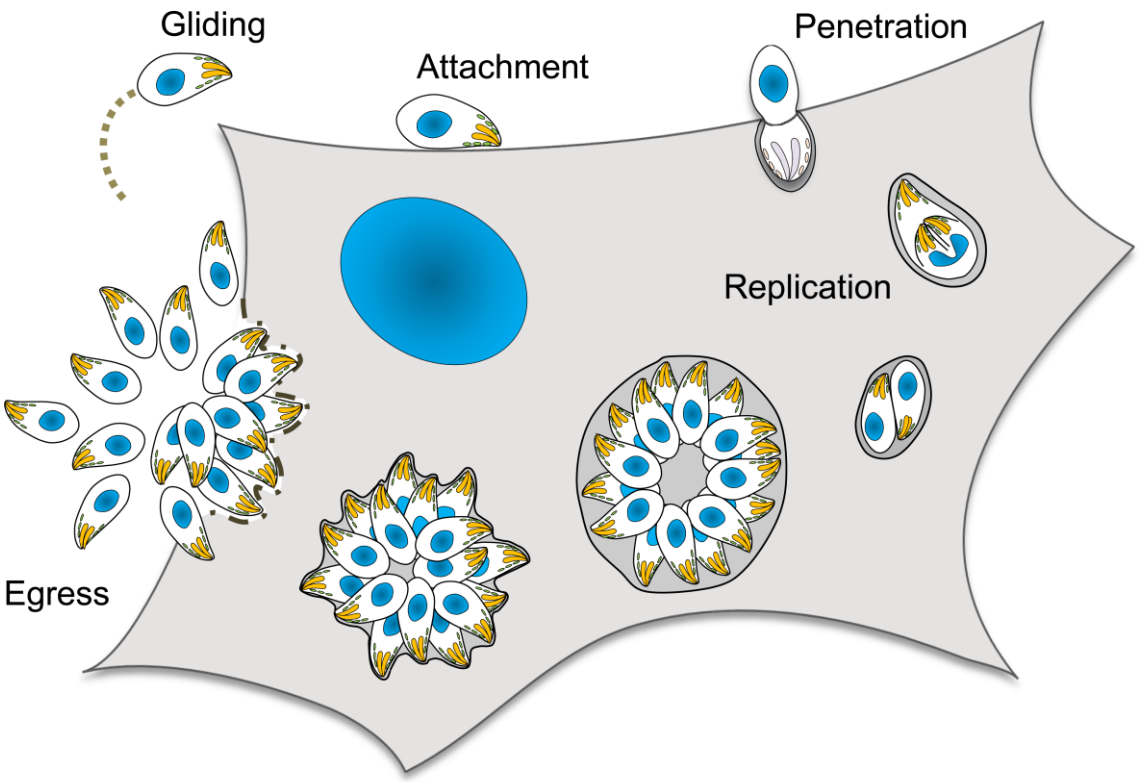

Figure 1-3. *Toxoplasma gondii* lytic cycle.
Tachyzoites use gliding motility to migrate and potentially initiate contact with a host cell. After attachment, parasites penetrate the host in an energy-dependant manner; subsequently, forming a parasitophorous vacuole (PV) that completely surrounds the parasite. Asexual replication occurs inside the PV, here, parasites engage in several rounds of replication. Proliferation continues until vacuoles reach from 32 to 64 parasites, at this point tachyzoites are ready to egress. Once free from

the host cell, parasites glide and re-invade neighbour cells. Figure adapted from Dr Nicole Andenmatten, courtesy of Dr Jamie Whitelaw.

1.4.2.1.1 Invasion

Host cell invasion by apicomplexan parasites is a fast process that relies on their ability to glide and engage a host cell. Although rapid, host cell penetration is a highly regulated multistep process. In *T. gondii* tachyzoites and *Plasmodium* merozoites this process starts with an initial attachment to the host cell PM, which is followed by reorientation of the parasite, engagement of the host cell via tight junction (TJ) formation, and finally entrance of the parasite inside the host cell. Together, these processes take up to 30 sec (Morisaki et al., 1995) (Figure 1-4).

In *T. gondii*, the first attachment of the parasite to the host cell is thought to be mediated by the GPI-anchored surface antigens (SAG1 and SAG3), which generate a low strength attachment to the host cell so the parasite has enough contact to scan for a suitable host (Carruthers and Boothroyd, 2007). Similarly, the initial attachment of merozoites to red blood cells (RBC) is mediated by merozoite surface proteins (MSP), which coat the parasite membrane and are able to interact directly with the RBC PM (Koch and Baum, 2016). Once a suitable host is found, internal calcium (Ca^{++}) levels induce microneme secretion through the apical complex, and generates a tight connection between the zoite and its host (Carruthers and Tomley, 2008, Koch and Baum, 2016). Following this tight attachment, the parasite pivots to be perpendicular with the host cell, and reduces its motion (Bichet et al., 2014). The parasite then associates with the host PM via micronemal proteins (MICs) at the entry point after discharging a second set of secretory contents resultant with TJ formation (Bichet et al., 2014). In this step, the parasite injects the rhoptry neck proteins (RONs) into the host cell to act as its own receptors while penetrating (Besteiro et al., 2011). The original model for invasion recognised the micronemal protein apical membrane antigen 1 (AMA1) and the rhoptry neck protein RON2 as the two main interactors in the junction (Lamarque et al., 2011, Bargieri et al., 2014). The penetration of the parasite through the TJ is thought be acto-myosin dependant. Therefore, AMA1 engages to the parasite cytoskeleton and drives the translocation of the TJ from the apical to the posterior pole of the parasite (Buguliskis et al., 2010). In addition to these molecules, *Plasmodium* species contain two classes of proteins that cooperate during invasion: the erythrocyte-binding antigens (EBA) and the reticulocyte binding-like proteins (RBL/Rh proteins), which are secreted from the micronemes and rhoptries, respectively (Boucher and Bosch, 2015, Koch and Baum, 2016). These form multiple interactor complexes important for initiating RBC penetration, allowing

for redundancy in the invasion process (Koch and Baum, 2016). As the parasite penetrates through the TJ, the parasite secrets a third set of proteins coming from the rhoptry bulb (ROPs), and begins the formation of the PV as it enters (Clough and Frickel, 2017). When the parasites successfully penetrated the attachment points between the host cell receptor and the parasite are cleaved by proteases such as the rhomboid-like protease 4 (ROM4), and the entry point is sealed. This step may be the initial signal for commencing intracellular replication (Besteiro et al., 2011, Santos et al., 2011).

While the model described below supported the essential functions of AMA1 and ROM4 during invasion, conditional depletion of these proteins did not affect tachyzoite survival in culture (Mital et al., 2005, Bargieri et al., 2013, Shen et al., 2014b, Rugarabamu et al., 2015). Similarly, AMA1 was deleted from the *P. berghei* genome by direct recombination, resulting in merozoites able to invade RBCs, but that presented an attachment phenotype (Bargieri et al., 2013). In contrast, a conditional *ama1* KO line established in *P. falciparum* showed that these parasites cannot form a junction, and therefore cannot invade the RBC (Yap et al., 2014). To explain these contradicting results, redundancy among microneme proteins was suggested (Lamarque et al., 2014, Yap et al., 2014). In fact, in *T. gondii* tachyzoites, AMA2 was detected in the TJ interacting with RON2, and was shown to be upregulated in long term cultured *ama1* KO mutants (Lamarque et al., 2014). However, in the case of *Plasmodium* species no obvious orthologues of AMA1 are present, making the merozoite apical erythrocyte-binding ligand (MAEBL) the strongest candidate to fulfil this function in *P. berghei* (Harvey et al., 2014, Yap et al., 2014).

In a similar scenario, the proteases in charge of surface protein cleavage in *Plasmodium* and *T. gondii* were the subject of further studies. Here, from the eight recognised ROM genes in *P. berghei*, four of them (ROM4, 6, 7 and 8) were refractory to gene deletion while ROM1, 3, 9 and 10 were shown to have redundant functions (Lin et al., 2013). Additionally, *Plasmodium* AMA1 is not only cleaved by ROMs at the transmembrane domain, but also by substilisin proteases (e.g. SUB2) at the juxtamembranous extracellular domain (Olivieri et al., 2011), indicating a high variability in surface protein processing pathways. Depletion of *T. gondii* ROM1, 4 and 5 individually and in combination, showed the importance of these proteins to process MICs in tachyzoites. However, this function is not essential for tachyzoite survival, indicating that i) there is a ROM-independent mechanism for adhesins removal and ii) AMA1 removal is not essential for host cell penetration *per se* (Shen et al., 2014b, Rugarabamu et al., 2015). Similarly, conditional depletion of acto-myosin system did not block penetration (Andenmatten et al., 2013,

Egarter et al., 2014). Furthermore, recent studies have highlighted the contribution of the host cell during the penetration process in both *T. gondii* and *Plasmodium* (Dasgupta et al., 2014, Tardieux and Baum, 2016). For instance, in tachyzoites, it was shown that RON proteins cooperate to recruit host cell components to the entry point; thus, serving as anchor to support penetration (Guérin et al., 2017).

These results together suggest that invasion mechanisms need to be revisited to reconcile current data.

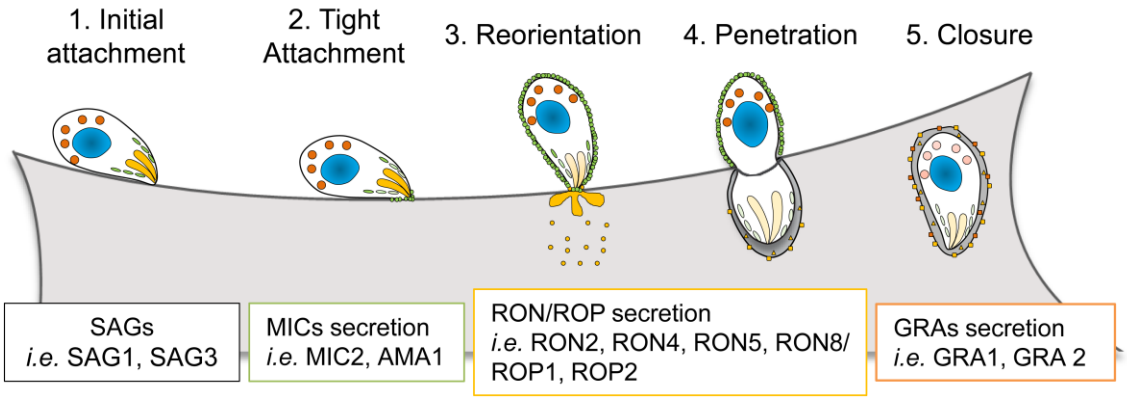

Figure 1-4. Tachyzoite invasion process
1. Tachyzoite invasion is a multistep process that initiates with weak attachment provided by SAG proteins present in the surface of the parasite. **2**. When a suitable host cell is found, secretion of MIC proteins (green) ensures a tight attachment. **3.** Alongside, the tachyzoite pivots over its apical pole and the amount of MIC proteins increase on its PM. **4.** Subsequently, RON proteins (yellow) are discharged, this step secures the association of the tachyzoite with the host. The parasite assembles a ring-shaped the TJ, which gives structural support during penetration. The tachyzoite passes through the TJ creating a visible constriction of its surface. Concomitantly, rhoptries secrete ROP proteins (yellow) to contribute with the formation of PV. Consequently, when the whole length of the parasite passed through the TJ, the connection with the host PM is released, leaving the tachyzoite surrounded by the PV in the host cytoplasm. **5.** Finally, dense granules discharge (GRA) their contents (orange) to modulate the PV that surrounds the parasite while residing in the host cell cytoplasm. Scheme inspired from Alexander *et al.*, 2005, and modified from Dr. Jamie Whitelaw.

1.4.2.1.2 Replication

During penetration, the parasite sets up its PV in the cytosol of the host cell; this structure is primarily derived from invaginated host cell PM (Suss-Toby et al., 1996). The PV is a non-fusogenic vacuole, meaning that unlike other parasites such as *T. cruzi*, *T. gondii* excludes the fusion of lysosomes and endosomes (Mordue et al., 1999). The PV assumes a location close to the mitochondria and endoplasmic reticulum of the host cell, suggesting the parasite may import nutrients during its development (Sinai et al., 1997, Pernas et al., 2014). After establishing itself inside the host, the parasite starts to replicate asexually by endodyogeny, producing two daughter cells inside a single mother cell (Hu et al., 2002a).

During this period of division, cytokinesis and daughter cell formation start before mitosis is completed (Francia and Striepen, 2014). The apical pole of the parasite is defined by the apical polar rings (APR), which act as a microtubule organisation centre (MTOC); this sets up the apical-posterior organisation of the daughter cells over a polarised microtubule scaffold (Russell and Burns, 1984, Morrissette and Sibley, 2002). The cytoskeleton keeps its development by the formation of the IMC, flattened membrane sacks linked to each other (Morrissette et al., 1997, Mann and Beckers, 2001). Following this, the Golgi apparatus, apicoplast, and nuclei are segregated to the daughter cells, and later, followed by the endoplasmic reticulum and mitochondria (Gubbels et al., 2008, Nishi et al., 2008).

The secretory organelles are not inherited form the mother cell, but thought to be produced *de novo;* for this reason, this process requires degradation and recycling of the mother cell secretory organelles. The biogenesis of these organelles remains to be studied in detail; however, some key molecules are identified, for instance, the dynamin related protein B (DrpB). Indeed, the expression of DrpB mutant ($DrpB_{DN}$) devoid secretory organelles; therefore, secretory organelle proteins were not discharged from the apical pole, but in a constitutive manner (Breinich et al., 2009). Once formed, these specialised organelles are transported to the apical pole of the daughter cells, a process that is thought to be mediated by cytoskeletal components (Francia and Striepen, 2014). The division process results in the formation of a residual body (RB) containing degraded maternal secretory organelles and parts of the mitochondrion (Nishi et al., 2008). Once the organelles have been acquired, the daughter cells inherit the maternal PM, such that when cytokinesis is completed the daughter cells are separated and able to start a new round of division (Gubbels et al., 2008). It takes between 6 and 8 hours to complete a cycle of division, depending on culture conditions and nutrient availability (Gubbels et al., 2008).

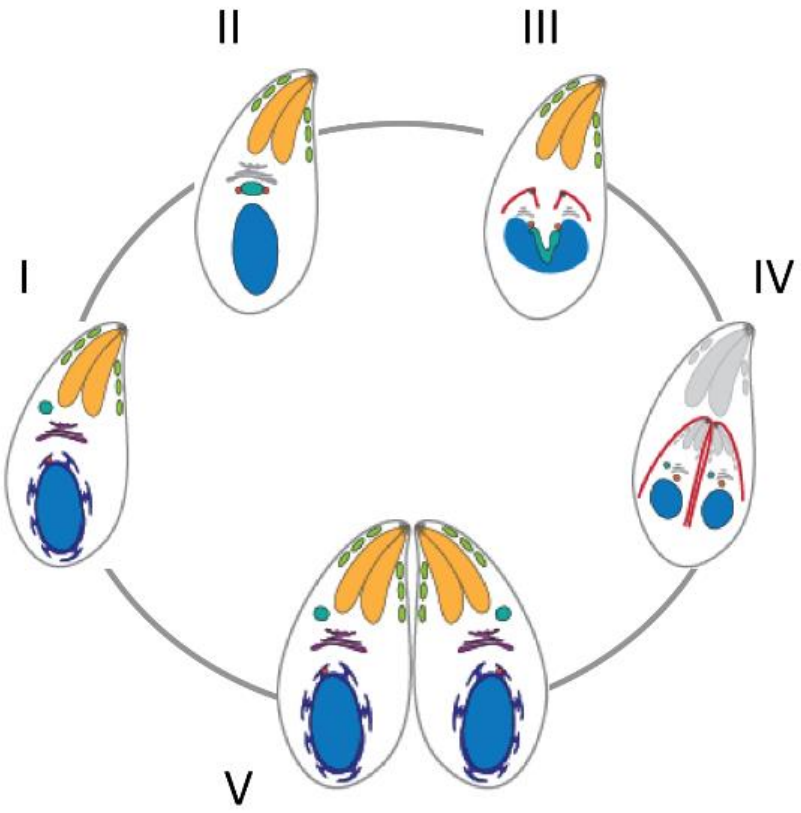

Figure 1-5. *Toxoplasma gondii* replication.
Tachyzoites employ endodyogeny to divide. This process leads to the internal budding of two daughter cells inside one mother cell. I. Fully formed tachyzoite containing all its organelles ready to start division. The diagram shows: the conoid (black), rhoptries (yellow), micronemes (green), apicoplast (turquoise), Golgi apparatus (purple), centriole (red), nucleus (blue), endoplasmic reticulum (dark blue) II. The centriole divides and associates to the apicoplast, which starts to enlarge prior to dividing in two equal parts. III. The dividing apicoplast migrates to the top of the nucleus forming a "U" shape. In addition, the formation of the apical pole sets the polarisation of the nascent buds followed by the duplication of the Golgi apparatus and the inner membrane complex (red) development IV. Centriole, apicoplast, nucleus and Golgi apparatus complete division leaving each nascent bud with one organelle of each. Elongation of the IMC is accompanied by de novo formation of secretory organelles (grey). V. After the IMC is mature and all organelles are formed and/or obtained, the now fully assembled daughter cells acquire plasma membrane leading to their separation, and finally, budding out of the mother cell (Striepen et al., 2000, Jacot et al., 2013, Ouologuem and Roos, 2014). Diagram modified from Dr. Nicole Andenmatten.

1.4.2.1.3 Egress

After five or six rounds of replication, which is between 48-72 hr after infection, the parasites exit the host cell by rupturing the PV and the host cell PM in order to disseminate (Arrizabalaga and Boothroyd, 2004). This process starts with an intracellular signal cascade that induces the discharge of MIC proteins, and stimulates the motility motor. To activate these pathways and induce egress, intracellular Ca^{++} levels increase (Black et al., 2000, Arrizabalaga and Boothroyd, 2004). The parasite contains a group of "plant-like" Ca^{++}-dependent protein kinases (CDPKs) dedicated to mediating Ca^{++} signalling. CDPKs are

kinases with Ca^{++} binding domains, and in *T. gondii*, CDPK1 and CDPK3 have been directly linked to microneme discharge during egress (Lourido et al., 2010, Garrison et al., 2012, Lourido et al., 2012). Specifically, the secretion of the micronemal perforin-like protein (PLP1) has been demonstrated to be involved in rupturing the PV and host cell PM by forming pores (Kafsack et al., 2009).

Like *T. gondii, Plasmodium* species also express the MIC proteins PLP; in fact, previous studies suggested that PLP1 contributed to membrane lysis in *P. falciparum* blood stages under Ca^{++} signalling (Garg et al., 2013). However, expression of PLP1 was not detected in *Plasmodium* asexual stages. Depletion of this protein did not affect development of these parasites during the asexual cycle (Ishino et al., 2005, Yang et al., 2017). Contrary to PLP1, subtilisin-like protease 1 (SUB1) is highly expressed at schizont maturity (Blackman et al., 1998, Blackman and Carruthers, 2013). This protein resides in specialised dense granules called exonemes until they are released to the PV lumen, and interact with different substrates (Yeoh et al., 2007). A recently published model suggests that SUB1 processes the merozoite surface protein 1 (MSP1); thus, allowing the parasite to interact to proteins in the inner membrane of erythrocyte, creating shear forces to finally disrupt the cytoskeleton of the host cell (Das et al., 2015).

In *T. gondii* tachyzoites it was suggested that the pressure generated by the increased size of the vacuole could produce enough force to disrupt the host cell indicating this process does not require movement *per se* (Lavine and Arrizabalaga, 2008). However, the association between Ca^{++} fluxes and motility, invasion, and egress supports the idea that the three mechanisms are linked (Hoff and Carruthers, 2002). Like invasion, PV disruption is rapidly achieved, and was suggested to be driven by the same machinery that controls host cell invasion and gliding (Meissner et al., 2002b). In fact, increasing the internal Ca^{++} levels, by stimulation using Ca^{++} ionophore (A23187), induces intracellular parasites to become highly motile and rapidly exit the host cell (Moudy et al., 2001). Conversely, suppression of actin dynamics in the parasite is known to be detrimental to egress. This has been demonstrated using actin depolymerising drugs, and in mutants of the motor machinery (Moudy et al., 2001, Egarter et al., 2014). Contrary to *T. gondii* tachyzoites, disruption of actin by genetic manipulation or drug inhibition did not block egress in *P. falciparum*, indicating that this process could be driven by osmotic pressure (Das et al., 2017) (further detail in section 1.7).

A recent study has exploited super resolution fluorescence microscopy together with transmission and scanning electron microscopy to study tachyzoite natural host cell egress (Caldas et al., 2017). These imaging-based results indicate that egress can occur in different ways which are: i) the host cell PM reseals after an individual parasite exit to the external milieu (non-lytic), ii) the host cell PM is burst after an individual parasite egress (lytic), iii) the host cell PM is lysed by several parasites in the PV egressing together (lytic). Moreover, lytic and non-lytic events were observed to occur within the same PV (Caldas et al., 2017). A similar scenario was observed in *P. berghei* sporozoites; indeed, motility preceded parasite egress that happened in different ways: individual exit from a specific point, and parasites budding in groups within a vesicle-like formation termed sporosome (Klug and Frischknecht, 2017). Together these results place under consideration whether egress is triggered through regulation of different pathways and/or by exploiting different routes.

1.4.2.2 Bradyzoite stage

Within the first 1-2 weeks it is estimated that tachyzoites start transforming to the slowly replicating bradyzoites (Frenkel, 1973). Some external determinants tried *in vitro* that trigger the conversion from tachyzoite to bradyzoite are: alkaline pH, heat shock and nutrient starvation (Skariah et al., 2010). During this stage, the parasites replicate by endodyogeny and generate cysts. The cysts can contain from 1000 to 2000 parasites surrounded by an elastic 0.5 μm wall (Dubey et al., 1998). Inside the cysts, the parasites are effectively dormant, and able to survive for long periods of time due to their low metabolic requirements. These parasites become infective if the cyst wall is broken, and will engage in a new cycle in either the intermediate or the definitive host (Fortier et al., 1996, Weiss and Kim, 2000).

1.5 *Toxoplasma gondii* tachyzoite ultrastructure

Tachyzoites are polarised cells with a crescent shape roughly 2 by 6 μm in dimension (Dubey et al., 1998). These are complex cells containing standard eukaryotic organelles as well as unique organelles required for the parasite's lifestyle (Dubey et al., 1998, Morrissette and Sibley, 2002) (Figure 1-6). Early studies described very accurately the ultrastructure of tachyzoites through sectioned micrographs of the parasite (Ogino and Yoneda, 1966). Among the standard organelles, tachyzoites contain a nucleus, Golgi apparatus, endoplasmic reticulum, and a single mitochondria (Ogino and Yoneda, 1966). The nucleus, containing a centrally located nucleolus, is situated towards the posterior end of the parasite and is

roughly centred (Dubey et al., 1998). The Golgi apparatus is apical to the nucleus (Ogino and Yoneda, 1966) and is in close proximity to a multi-layered endosymbiotic organelle called the apicoplast (McFadden et al., 1996, Kohler et al., 1997).

The pellicle is a three-unit membranous structure comprising the plasma membrane and an IMC of flattened vesicles. This structure is associated with 22 microtubules around 4-5 μm long that run two-thirds the length of the parasite in a spiral manner (Nichols and Chiappino, 1987, Mann and Beckers, 2001). All together, these structures are thought to act as a scaffold for mechanical support (Mann and Beckers, 2001). The microtubules originate from the apical complex, an assemblage of cytoskeletal structures including apical rings, microtubules, and conoid, and are thought to serve as tracks for transporting specialised secretory organelles (Carruthers and Sibley, 1997, Mann and Beckers, 2001). *T. gondii* harbours three sets of secretory organelles: the micronemes, rhoptries, and dense granules, all of which are essential for different steps in the parasite life cycle (section 1.5.1) (Carruthers and Sibley, 1997). Additionally, tachyzoites contain an apicoplast that is a plastid containing a genome and stroma surrounded by four membranes (section 1.5.4). This organelle is the remnant of a red algae endosymbiont that was engulfed by a common ancestor of Apicomplexans and dinoflagellates (McFadden and Yeh, 2017).

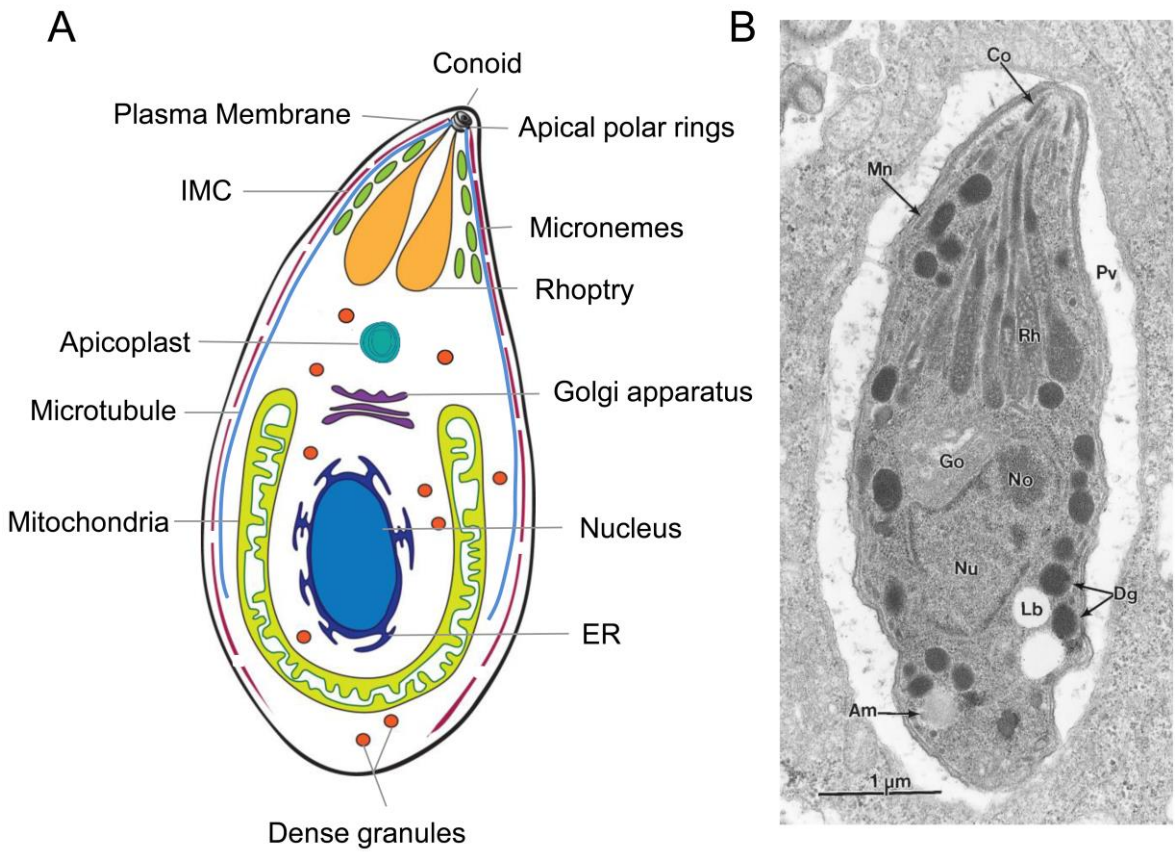

Figure 1-6. *Toxoplasma gondii* tachyzoite ultrastructure.
A. Schematic representation of a tachyzoite showing specialised and conventional organelles. In the apical pole resides the apical complex composed by apical polar rings (APR), conoid and microtubules. The rhoptries (yellow) and the micronemes (green) locate close to the apical pole while the dense granules (orange) are distributed along the cytoplasm. The apicoplast (teal), the Golgi apparatus (purple) and a single mitochondrion (lime) are located around the centre of the cell. The nucleus (blue), surrounded by the endoplasmic reticulum (ER), is located towards the posterior end. A network of 22 microtubules (sky-blue) surround the parasite creating a cage like scaffold which originates in the apical complex and run 2/3 over the parasite's length. Finally, the IMC (dark red) and PM (black) sustain the tachyzoite cellular structure. Diagram modified from Dr. Nicole Andenmatten **B.** Electron-microscopy image displaying tachyzoite organelles. Arrows indicate conoid (Co), micronemes (Mn), parasitophorous vacuole (Pv), rhoptry (Rh), Golgi apparatus (Go), nucleolus (No), nucleus (Nu), dense granules (Dg). Image reprinted from (Dubey *et. al*., 1998) under copyright permissions.

1.5.1 The secretory Organelles

1.5.1.1 Micronemes

The ellipsoidal shaped micronemes are the smallest of the secretory organelles, around 250 by 50 nm in dimension. The number of micronemes in a parasite varies from 50 to 100, and they are located towards the apical pole of the tachyzoite (Carruthers and Tomley, 2008). Early studies associated secretion of microneme contents with active penetration and gliding motility (Carruthers and Sibley, 1997). It was shown that elevation of internal Ca^{++} levels, using either Ca^{++} ionophore (A23187) or ethanol, was directly correlated to the ability of parasites to glide and invade host cells (Carruthers et al., 1999, Carruthers and Sibley, 1999). As expected, inhibition of microneme discharge had the opposite effect (Lovett and Sibley, 2003). After secretion, MICs are released onto the parasite PM and migrate from the apical pole towards the posterior pole (Carruthers and Sibley, 1997). This observation correlated with the progression of invasion and gliding, while both processes were blocked by cytochalasin D (CytoD), an actin-disrupting drug (Dobrowolski and Sibley, 1996, Dobrowolski and Sibley, 1997, Carruthers and Sibley, 1999). This was the first evidence showing a tight association between MICs and the cytoskeleton. Further studies showed there is a plethora of MICs implicated in different functions, all either from the apical membrane antigen (AMA) or thrombospondin related anonymous protein (TRAP) families (Heintzelman, 2015).

For instance, MIC2, a member of the TRAP family, was proposed to be the major virulence factor able to link the parasite cytoskeleton with the extracellular milieu (Huynh and Carruthers, 2006). The interaction between the cytoskeleton and MIC2 was suggested to be mediated via, the glycolytic enzyme, aldolase (ALD) (Jewett and Sibley, 2003). Nevertheless, neither MIC2 nor aldolase were shown essential for gliding motility (Andenmatten et al., 2013, Shen and Sibley, 2014, Gras et al., 2017), but new evidence

suggest the glideosome associated protein (GAC) serves this role in connecting the cytoskeleton to MIC2 (Jacot et al., 2016a). AMA1 binds to an assembly of RON 2/4/5/8, and these together form a complex which bridges the parasite and host cell during invasion (Besteiro et al., 2011). However, invasion and TJ formation are not blocked in a clonal *ama1* KO strain (Bargieri et al., 2013). Other proteins contained in the micronemes are pore-forming proteins, for example, PLP1 that has been shown to be essential for rapidly dismantling the PV before host cell egress (Kafsack et al., 2009). Furthermore, SUB1 also regulates adhesive activity at the PM by proteolytically cleaving other MICs (e.g. MIC2, M2AP) (Lagal et al., 2010).

1.5.1.2 Rhoptries

First called toxonemes, the rhoptries are club shaped organelles that originate from the apical end. Their shape increases towards the posterior pole and can extend from two to three μm in length. The number of rhoptries in each parasite can vary from eight to 15 and are usually located on one side on the parasite (Ogino and Yoneda, 1966, Boothroyd and Dubremetz, 2008). Proteins inside the rhoptries are not randomly mixed, but rather organised in discrete sub-compartments: the bulbous base and the neck. Remarkably, there are no internal membranes separating both "areas", and how rhoptry proteins are sorted between them remains unknown. Around 40 to 50 RONs and ROPs have been identified, of which the majority are ROPs (Boothroyd and Dubremetz, 2008, Camejo et al., 2014). Rhoptry contents are secreted during invasion, and these proteins have different functions. For instance, RON2, 4, and 5 form a complex with the micronemal protein AMA1, which intimately associates the parasite with the host cell it is invading (Alexander et al., 2005). Unlike the RONs, the ROPs migrate to three different locations: the host cell, the PV membrane, and the PV lumen; consequently, acting to preserve the integrity of the PV and to modify the host cell (Boothroyd and Dubremetz, 2008). For example, ROP16 and ROP18 are the best known of these proteins because they are involved in host cell subversion by regulating immune response genes (Boothroyd, 2013). One proposed hypothesis suggests the virulence of a *T. gondii* strain is tightly associated to allelic variations of certain ROP genes, such as correlating "virulent" ROP18 gene alleles to type I strains and "avirulent"/non-expressed ROP18 gene alleles to avirulent type III strains (Fox et al., 2016). However, these observations seem to over-simplify the infection process since many host factors could also contribute to the response, suggesting future studies are required (Jensen et al., 2011, Boothroyd, 2013).

1.5.1.3 Dense granules

These organelles were first proposed to be called round bodies for their shape (Ogino and Yoneda, 1966), but then were called dense granules because of their dense and homogeneous appearance in micrographs. These organelles are approximately 200 nm in diameter and are distributed throughout the cytoplasm of the parasite (Ogino and Yoneda, 1966). Recent studies showed that dense granules use actin tracks to move within the cytoplasm; additionally, these organelles are tremendously dynamic, with no fixed location (Heaslip et al., 2016). Despite that parasite intracellular survival depends on dense granules, they are the least studied class of secretory organelles in *T gondii*. Following secretion, GRAs locate to different areas in both the PV and host cell, and participate in maintaining the PV and regulating host cell biology. Some GRA proteins act near their secretion sites (e.g. GRA2, GRA6, MAF1), while others cross the PV and establish in the host cell organelles (e.g. GRA16, GRA24) (Hakimi et al., 2017). For instance, GRA2 and GRA6 are implicated in forming, maintaining, and stabilising the nanotubular network within the PV, thereby, participating in nutrient acquisition and providing enough physical space for the dividing parasites within the PV (Mercier et al., 2002). In addition, GRA6 manipulates the host cell response to limit parasite burden (Ma et al., 2014). Moreover, mitochondrial associated factor 1 (MAF1) locates to the PV membrane after secretion, where it is suggested to directly bind the host cell mitochondria to control the host immune response (Pernas et al., 2014). GRA17 and 23 were shown to participate in the permeabilization and stability of the PV; therefore, having a direct role in the overall intracellular development permitting the flow of small molecules between the PV and the cytoplasm (Gold et al., 2015). GRA16 is secreted to the PV lumen but crosses the PV membrane to finally migrate to the host cell nucleus, from where it controls expression of proteins involved in metabolism, progression of the manipulating/controlling the host cell cycle and promote survival of the host cell under stress conditions (Bougdour et al., 2013, Bougdour et al., 2014). Similarly, GRA24 accumulates to the host cell nucleus to regulate host gene expression; thus, controlling host inflammatory responses (Braun et al., 2013, Hakimi et al., 2017). Like ROP proteins, some GRAs are considered pathogenesis determinants for their capacity to co-opting host cell factors and interfering in host cell pathways (Hakimi et al., 2017). For example, GRA16 deficient parasites were shown to have an important role in the overall infectivity of type II but not type I strains in mice, indicating this factor relates to strain virulence (Bougdour et al., 2013).

1.5.2 The apical complex and the cytoskeleton

The first studies of the tachyzoite cytoskeleton were performed by visual examination of electron microscopy images (Nichols and Chiappino, 1987). These studies revealed the presence of a complex structure at the apical end of the cell – the apical complex, from which the phylum derives its name (Apicomplexa = apical complex). The main components of the apical complex are the conoid, APR, and microtubules. Of these, the conoid is absent in Hematozoans (*i.e. Plasmodium* and piroplasms) (Figure 1-1) (Leander and Keeling, 2003). In *T. gondii*, the conoid is a hollow funnel-shaped structure consisting of 10-14 tubulin fibres presenting a gentle left-hand torsion (Nichols and Chiappino, 1987, Hu et al., 2002b). This organelle has a diameter of around 380 nm and a length of 280 nm, and is connected to two pre-conoidal rings and surrounded by two APR, which together constitute a microtubule organisation centre (Nichols and Chiappino, 1987, Hu et al., 2002b, Hu et al., 2006). This organelle is able to extend and retract during invasion, gliding, and egress, and for this reason, early studies suggested its participation in these processes (Mondragon and Frixione, 1996). In fact, the motile conoid and the static APR are physically linked via RNG2, a protein able to flip upon conoid protrusion (Katris et al., 2014). Although conoid protrusion is not essential for these processes, this organelle and associated proteins have been implicated in the regulation of secretory organelle discharge (Heaslip et al., 2011, Katris et al., 2014) and also in invasion progression (Graindorge et al., 2016). However, the real function of the protrusion remains unknown.

The crescent shape of tachyzoites is maintained by 22 subpellicular microtubules that create a cage-like structure over two thirds the length of the parasite from the apical pole (Nichols and Chiappino, 1987). The anterior ends (minus-end) of the microtubules emerge from the inner polar rings, which serves as a MTOC (Hu et al., 2002b), and keeps the skeleton connected to the apical pole. The microtubules are left hand curved. This characteristic has been implicated in giving support and somehow direction to parasite motility in 2 dimensional (2D) and 3 dimensional (3D) environments (section 1.10) (Russell and Sinden, 1981, Leung et al., 2014).

1.5.3 The inner membrane complex and the subpellicular network

The pellicle of the parasite is a three-layered structure comprising the outer plasma membrane and IMC (Vivier and Petitprez, 1969). The IMC is composed of a set of flattened vesicles called alveoli which, together with the 22 cytoskeletal microtubules, underlay the

parasite PM (Cintra and De Souza, 1985). The IMC surrounds the cytosol, but does not reach the apical pole and is not connected to the apical or basal complex (Morrissette and Sibley, 2002). The IMC is thought to function as a lipid barrier, while the content of the alveoli is thought to be involved in storage and regulation of molecules, even though these observations have not been proven (Harding and Meissner, 2014). The cytoplasmic side of the IMC faces an organised network of 8-10 nm filaments called the subpellicular network (SPN) (Mann and Beckers, 2001). The SPN is thought to connect the IMC with the cytoskeletal microtubules and account for the shape and flexibility of the tachyzoite (Morrissette et al., 1997). The IMC also contains a group of proteins called gliding associated proteins (GAPs). Of these, GAP40, 45, and 50 have been the most studied, since they were directly implicated in gliding motility (Gaskins et al., 2004, Frenal et al., 2010). GAP45 is located in the periphery of the parasite, and contains a carboxy-terminal domain associated with the IMC, and an N-terminal acylation site, which lets it interact with the plasma membrane (Frenal et al., 2010, Ridzuan et al., 2012). This conformation makes GAP45 able to bridge and maintain a 20-30 nm separation between PM and IMC (Frenal et al., 2010, Kudryashev et al., 2010, Egarter et al., 2014). GAP40, 45, and 50 are involved in the recruitment and anchorage of the motor machinery to the cytoskeleton of the parasite (Gaskins et al., 2004, Frenal et al., 2010, Egarter et al., 2014). Moreover, depletion of GAP40 and 50 demonstrated these proteins have a role in stabilisation and biogenesis of the IMC during parasite division (Harding et al., 2016). Other examples are GAP70 and GAP80, which have been localised in the apical and posterior poles of the parasite, and are part of the apical and posterior motor complexes, respectively (section 1.9.2.1) (Frenal et al., 2014).

1.5.4 The apicoplast

The apicoplast is a non-photosynthetic vestigial plastid of red algal origin (McFadden et al., 1996, Kohler et al., 1997). This organelle is present in all apicomplexan parasites except *Cryptosporidium* species (Figure 1-1) (Zhu et al., 2000, Xu et al., 2004). The apicoplast contains its own genetic material, stroma, and four membranes. From inside to outside these membranes are: two original red algal plastid membranes, the PM of the endosymbiont, and, perhaps, a phagocytic vacuole derived from the original host (Waller and McFadden, 2005, Gould et al., 2015). The functions of this organelle are the synthesis of metabolic products for isoprenoids, fatty acids, and heme production, and have proven to be important for the parasite life cycle (Fichera and Roos, 1997, McFadden and Yeh, 2017). For instance, the generation of a precursor for isoprenoids called isopentenyl diphosphate (IPP) is a major apicoplast function (Nair et al., 2011, Yeh and DeRisi, 2011). In

Plasmodium, the removal of the apicoplast can be compensated by adding IPP to the grown media; in sharp contrast, in *T gondii* IPP addition does not compensate apicoplast loss, which may indicate the presence of other functions for this organelle in *T. gondii* (Yeh and DeRisi, 2011).

The apicoplast is segregated during endodyogeny from the mother cell to the two daughter cells, this segregation is proven to be acto-myosin F (MyoF) dependent (Jacot et al., 2013). The downregulation of MyoF had no immediate impact on the parasite, but a clear replication abrogation was observed when the mutants engaged the next lytic cycle. This phenomenon is called "delayed death", and has been described as the capacity of parasites to engage in a new round of the lytic cycle without an apicoplast but dying soon after (Fichera and Roos, 1997). The "delayed death" phenomenon can be induced by either pharmacological or genetic perturbation of apicoplast segregation (Fichera and Roos, 1997, Andenmatten et al., 2013, Jacot et al., 2013, Egarter et al., 2014, Frenal et al., 2017b).

1.6 Organelle trafficking

The correct division and functionality of cells is highly dependent on spatial and temporal organization of proteins and organelles. Early studies suggested that, during division, daughter cells inherit organelles by random events; thus, latter expand the mother material. Nevertheless, numerous evidence contradict this idea, indicating that organelle inheritance is highly regulated among different organisms (Knoblach and Rachubinski, 2016). Similarly, inside the cells, the organelles are neither uniformly nor randomly distributed, but organised in certain areas and are highly dynamic during the development of the cell.

The transport of organelles to their destination depends on motor proteins, mechanoenzymes able to convert Adenosine triphosphate (ATP) to physical movement, together with microtubule and actin cytoskeletons, which serve as tracks for the motor proteins (Rogers and Gelfand, 2000, Krendel and Mooseker, 2005). For instance, in mice melanocytes, melanosomes are transported using microtubule-dependent motors from the cytosol to the cell periphery where an acto-myosin system holds them in position to be transferred to adjacent melanocytes (Knoblach and Rachubinski, 2016). *Saccharomyces cerevisiae* uses a microtubule-independent method to deliver organelles to the nascent bud (Fagarasanu et al., 2010). In this case, organelles are transported using exclusively actin

cables which run long paths, from the mother to the bud tip, and are uniformly oriented (Hammer and Sellers, 2011).

These results indicate that actin-dependent systems can serve as tracks for organelle inheritance and trafficking. A good example of these processes is observed in *T. gondii*; here, actin has been shown to be involved in organelle segregation, trafficking, and communication among dividing parasites (Andenmatten et al., 2013, Jacot et al., 2013, Mueller et al., 2013, Egarter et al., 2014, Heaslip et al., 2016, Frenal et al., 2017b, Periz et al., 2017, Whitelaw et al., 2017). For instance, rhoptry positioning, apicoplast segregation and dense granules trafficking were severely affected upon genetic or drug mediated disruption of acto-MyoF dependent system (Jacot et al., 2013, Mueller et al., 2013, Egarter et al., 2014, Heaslip et al., 2016). In addition, recent studies showed that actin filaments serve as tracks for myosins to transport material, maintain the RB, and control synchronous division of parasites within the PV; thus, maintaining the organised appearance of the vacuole (Frenal et al., 2017b, Periz et al., 2017). Disruption of actin also caused severe phenotypes in apicoplast inheritance and efficient daughter cell separation in *Plasmodium* parasites, indicating some processes could be maintained among Apicomplexans (Das et al., 2017). Taken together these results indicate the multiple roles of acto-myosin dependent processes in *T. gondii*, which are further explained in sections 1.7.1, 1.8.1, and 1.9.1.

1.7 Actin

The assembly and disassembly of proteins is a crucial process regulating the ability of cells to move, change their shape, divide, and perform many other functions. One of the most important proteins involved in the organization of the cell is actin. Actin is a globular (G-actin) protein that organises into filaments (F-actin) to generate three different organisations: branched networks, parallel bundles, and antiparallel contractile structures. These different architectures act as mechanical scaffolds to drive changes in the cell and/or serve as tracks for other proteins to function, for instance myosins (Blanchoin et al., 2014). The actin monomer is a highly conserved protein of 42 KDa, and acts as the basic unit to generate an actin filament. Filament assembly is limited by the generation of dimers and trimers, which is the nucleation step. Nucleation is driven by different proteins (e.g. formins or actin related proteins -Arp2/3- complexes), which assist in the stabilisation of actin dimers for nucleation (Pollard et al., 2000b). The concentration of actin monomers available would permit the rapid elongation of the filament only if trimers are formed. ATP hydrolysis follows the polymerization of actin monomers in the filament. Actin filaments are polar

formations, which have a barbed end (+) on one side and a pointed (-) end on the other. Of these, the barbed end elongates faster than the pointed end, and in general is more dynamic. Under appropriate conditions, filaments can create long scaffolds up to 10 μm in length (Pollard et al., 2000a). The high dynamism of actin relies not only on the ability of filaments to form and elongate, but also in the disassembly of those filaments. There are two key F-actin depolymerisation factors: actin depolymerization factor (ADF)/cofilin and myosins (Blanchoin et al., 2014).

1.7.1 *Toxoplasma gondii* Actin

T. gondii actin (ACT1) is produced by a single-copy gene, which has been reported to exist mainly in globular form (97%) (Dobrowolski et al., 1997b). *Plasmodium* species encode two different actin isoforms called ACT1 and ACTII. ACTI is orthologous to *T. gondii* ACT1, while ACTII participates in mosquito and gametocyte stages, and seems to be essential for male gametocyte flagellation (Siden-Kiamos et al., 2012, Vahokoski et al., 2014).

Treatment of parasites with actin depolymerising -CytoD- or polymerising drugs -Jasplakinolide (JAS)- had a severe impact on the ability of parasites to glide and invade, indicating the importance of actin dynamics for these processes (Dobrowolski and Sibley, 1996, Shaw and Tilney, 1999, Wetzel et al., 2003). These results encouraged the analysis of actin binding proteins in Apicomplexan parasites. In fact, these contain a small repertory of actin binding proteins: ADF, profilin, cyclase-associated protein (CAP), coronin, formin, and capping protein (Gupta et al., 2015), but lack others as Arp2/3 complex important for actin branching in other models (Kumpula and Kursula, 2015).

ADF/cofilins contribute to F-actin dynamics by binding and sequestering actin monomers, depolymerising actin at its pointed end, and filament severing (Baum et al., 2006). While in *Plasmodium* two ADFs (ADF1 and 2) are expressed, in *T. gondii* a single ADF is recognised (Kumpula and Kursula, 2015). This protein contains a well-conserved G-actin binding domain, but lacks F-actin binding domain (Mehta and Sibley, 2010). In tachyzoites, ADF is localised diffusely in the cytosol and at the pellicle, and depletion of this protein stabilised actin filaments, and caused defective motility, invasion, and egress; mimicking JAS treatment (Mehta and Sibley, 2011). Profilins are able to sequester G-actin, and are suggested to provide polymerisable actin; therefore, these proteins participate in actin treadmilling, and accelerate actin polymerisation (Baum et al., 2006). In apicomplexan

parasites, a single profilin gene has been identified (Kursula et al., 2008), it contains a unique structural extension with an acidic tip that is directly implicated in actin monomer sequestration (Moreau et al., 2017). In *Plasmodium*, mutations generated in this particular arm confirmed the role of profilin in actin dynamics; thus, in gliding motility (Moreau et al., 2017). In *T. gondii* profilin, the length of the structural extension is shorter. It was demonstrated that the interaction between profiling and actin was weaker when compared to other profilins (Kumpula and Kursula, 2015). Depletion of this protein indicated its role in processes like gliding, invasion, and egress during tachyzoite lytic cycle (Plattner et al., 2008). Formins are actin nucleators able to elongate actin filaments by capping G-actin at the barbed end of the filament. These proteins contain two domains: i) FH1, in the C-terminal, binds the barbed end and nucleates actin filaments, and ii) FH2, in the N-terminal, binds profilin (Kumpula and Kursula, 2015). In Apicomplexan parasites, formins are currently the only candidates thought to work as actin nucleators (Gupta et al., 2015). *T. gondii* formins (formin 1, 2, and 3) are localised at the plasma membrane, pellicle, and nucleus of the parasite respectively (Daher et al., 2010, Daher et al., 2012). Formin 1 and 2 were shown to contain both domains FH1 and FH2, and to participate in actin filament polymerization (Skillman et al., 2012). Due to its localisation, formin 1 was implicated to function with the tachyzoite gliding machinery; in fact, depletion of this protein showed to have an impact on *in vitro* growth although not essential (Daher et al., 2010). Coronins are implicated in processes that require fast remodelling of actin such as leading-edge propulsion, endocytosis, cytokinesis, among others (Gandhi and Goode, 2008). These proteins are proposed to protect ADF/cofilin-mediated premature disassembly of G-actin, and to recruit Arp2/3 complex to the filaments sides, which drive actin nucleation and crosslinking (Gandhi and Goode, 2008). In *T. gondii* and *Plasmodium* a single coronin orthologue is found (Gupta et al., 2015). In *T. gondii*, coronin *in vitro* overexpression increased the rate of actin polymerisation, but no other interaction partners were found (Salamun et al., 2014). Nevertheless, it is not certain that this protein can interact/recruit polymerisation factors to rapidly elongate actin or organise already formed filaments (Salamun et al., 2014). In tachyzoites, coronin accumulates at the posterior end of invading, gliding and egressing parasites, but its conditional depletion showed a modest defect in the progression of the lytic cycle, but not gliding motility. In *Plasmodium* parasites, coronin distributes along the periphery of merozoites and sporozoites, and relocalises to the posterior end of gliding sporozoites (Olshina et al., 2015, Bane et al., 2016). Depletion of coronin in these parasites resulted in aberrant motility, indicating the role of this protein for leading directionality (Bane et al., 2016).

ACT1 filaments are not easily detectable. For instance, using standard immunofluorescence techniques with αACT1 antibodies, the ACT1 signal presents a diffuse cytoplasmic-perinuclear location (Dobrowolski et al., 1997b). However, by using immuno-electron microscopy ACT1 filaments were observed underneath the parasite PM, and scattered across the cytoplasm (Dobrowolski et al., 1997b). The fact that ACT1 filaments were not detectable raised the possibility that changes in the ACT1 amino acid sequence may cause instability in the filaments, thus limiting their length to around 100nm (Schmitz et al., 2005, Sahoo et al., 2006). Additionally, it has been suggested that, unlike conventional actin, ACT1 polymerises in an isodesmic manner lacking a lag phase and critical concentration to polymerise (Skillman et al., 2013). Therefore, actin filaments can be formed even at low concentrations of G-actin, resulting in the equally favourable formation of actin dimers, trimers or oligomers (Skillman et al., 2013). However, a recent study convincingly showed that like canonical actins, *Plasmodium* ACT1 polymerises in a cooperative manner, meaning that filament elongation occurs only if a critical concentration of free actin is available (Kumpula et al., 2017). While actin polymerisation dynamics and G-actin treadmilling rates were comparable between canonical and *Plasmodium* ACT1, overall depolymerisation rate of the latter were shown to be faster than canonical actin; therefore, suggested to be a factor that limits the length of the filament (Kumpula et al., 2017). These results are supported by *in vivo* studies suggesting *T. gondii* relies on filamentous actin structures to accomplish different functions. For instance, secretory organelle movement across the cytoplasm was shown to be acto-MyoF dependent (Heaslip et al., 2016). Here, MyoF was shown to transport dense granules along long paths; thus, ACT1 may form filaments to create extensive tracks to support continuous MyoF movement (Heaslip et al., 2016). Furthermore, actin-chromobody (Cb) probes allowed the visualisation of extensive filamentous networks. These dynamic networks are located inside the parasite and in the RB of dividing parasites. These RB filamentous structures seem to be involved in the ability of parasites to transport material, and communicate while developing inside the PV (Periz et al., 2017). A recent publication supports this observation of ACT1 filamentous structures in the RB, and that the connection of parasites inside the PV was shown to be an acto-myosin dependant process (Frenal et al., 2017b). In this study, it was demonstrated that MyoI and MyoJ actively transport material among daughter cells developing in the same PV (Frenal et al., 2017b).

1.8 Myosins

Myosins are molecular motors that mediate active actin-based locomotion. These mechano-enzymes convert energy stored as ATP into physical force that is transferred along actin filaments (Houdusse and Sweeney, 2016). The myosin holoenzyme consists of myosin heavy chains and myosin light chains; of these, the myosin heavy chains contain the actin-binding domain (Heissler and Sellers, 2014). There are around 31 myosin heavy chain families recognized at this point (Sebé-Pedrós et al., 2014), and these have been classified into two groups, the "conventional" and "unconventional" myosins, based on their structure and organisation (Krendel and Mooseker, 2005, Woolner and Bement, 2009). Myosin heavy chains consist of three regions: i) an N-terminal "head" domain responsible for binding actin and hydrolysing ATP, ii) a "neck "domain, containing IQ motifs that are basic units containing binding sites for different EF-hands proteins that can be myosin light chains or essential light chains, and iii) a C-terminal "tail" domain that serves to bind cargo or other myosins (Krendel and Mooseker, 2005). Conventional myosins (e.g. MyoII) form long polymers or bipolar filaments using their tail domains while walking on actin filaments. On the contrary, unconventional myosins act as monomers or dimers and use their tail domains to interact with other molecules as cargo (Woolner and Bement, 2009).

Myosins must adopt the correct structure in order to function properly, a process that relies on the myosin chaperones (Hellerschmied and Clausen, 2014). These proteins are in charge of folding and assembling myosins prior to or during their function. For instance, class II myosins form thick filaments that are essential for cell division. The proper formation of these filaments requires chaperone assistance, potentially by the UNC-45 group of myosin chaperones, which act in thick filament formation to direct assembly of polymers in a manner such that the myosin binding sites are kept available for other interacting proteins. Indeed, UNC-45 mutants showed a strong defect in myosin filament formation, and therefore, function (Hellerschmied and Clausen, 2014).

1.8.1 *Toxoplasma gondii* myosin heavy chain repertoire

T. gondii contains 11 recognised myosin heavy chains (Foth et al., 2006, Mueller et al., 2017) (Table 1-1). This is the largest repertoire of myosins observed in the apicomplexan phylum followed by *Eimeria* with seven myosins; *Cryptosporidium* and *Plasmodium* both have 6 recognised myosins (Foth et al., 2006).

Like in other organisms, the integrity and function of *T. gondii* myosins rely on a myosin chaperone. In this organism, a single UNC-45 homologue was identified, and showed structural similarities with these proteins (Bookwalter et al., 2014). The first identification of UNC indicated that the presence of this chaperone is essential for MyoA folding, since maintenance of myosin function and integrity is critical for its production in heterologous systems (Bookwalter et al., 2014). The *Plasmodium* UNC orthologue (PUNC) was identified, and is suggested to fulfil the same roles as *T. gondii* UNC (Bookwalter et al., 2017). Additionally, it was recently shown that UNC is involved in the assembly of the 11 myosins present in *T. gondii* (Frenal et al., 2017b). Consequently, UNC depletion resulted in severe gliding, invasion, replication, and egress phenotypes, indicating that the *unc* KO phenocopies alteration of all 11 myosins present in *T. gondii*. These results also confirmed the phenotype observed after actin depletion (Egarter et al., 2014, Frenal et al., 2017b, Periz et al., 2017, Whitelaw et al., 2017).

This section presents a compilation of the available information for the cellular location and function of myosins present in *T. gondii* (Figure 1-7). The data about the myosin molecular weights provided was taken from ToxoDB (Gajria et al., 2007).

Table 1-1. Repertoire of myosin heavy chains in *T. gondii*. Inspired by Foth *et. al*., 2006

Class	*T. gondii*	Location	Function
XIVa	MyoA	Periphery	Involved in motility, invasion and egress. Highly conserved among Apicomplexan (Hettmann et al., 2000, Herm-Gotz et al., 2002, Meissner et al., 2002b).
	MyoD	Periphery	Mainly expressed in bradyzoite stage. Not essential for lytic cycle (Hettmann et al., 2000, Polonais et al., 2011).
XIVb	MyoB/C	Posterior end	MyoB mainly expressed in bradyzoite. MyoC presents redundant roles with MyoA. Neither MyoB nor MyoC are essential for lytic cycle (Delbac et al., 2001, Foth et al., 2006, Egarter et al., 2014, Frenal et al., 2014).
	MyoE	Conoid	Unknown function. Not essential for lytic cycle (Delbac et al., 2001, Foth et al., 2006, Frenal et al., 2017b).
XIVc	MyoH	Conoid	Secretory organelles discharge in early invasion steps. Essential for invasion progression. Conserved among Apicomplexan (Foth et al., 2006, Graindorge et al., 2016).
XXII	MyoF	Cytoplasm	Apicoplast segregation during endodyogeny, and secretory organelles transport. Essential for lytic cycle. Highly conserved among Apicomplexan (Foth et al., 2006, Mueller et al., 2013, Jacot et al., 2014, Heaslip et al., 2016).
XXIII	MyoG	Periphery (weakly)	Unknown function. Not essential for lytic cycle (Foth et al., 2006, Frenal et al., 2017b).
XXIV	MyoI	RB	Formation and maintenance of communication among daughter cells within the PV. Not essential for lytic cycle (Foth et al., 2006, Frenal et al., 2017b).
VI	MyoJ	Posterior pole	Organisation of the vacuole, and involved in the communication among daughter cells. Not essential for lytic cycle (Foth et al., 2006, Frenal et al., 2017b).
	MyoK	Centrocones	Unknown function. Not essential for lytic cycle (Foth et al., 2006, Frenal et al., 2017b).
XIVe	MyoL	Conoid, cytosol	Unknown function. Not essential for lytic cycle (Foth et al., 2006, Frenal et al., 2017b, Mueller et al., 2017).

1.8.1.1 *Toxoplasma gondii* Myosin A (MyoA)

T. gondii MyoA is a 93KDa unconventional class XIVa myosin with orthologues throughout the phylum Apicomplexa (Heintzelman and Schwartzman, 1997, Foth et al., 2006). This myosin is considered unique among myosins because of its unconventional structure (Heintzelman and Schwartzman, 1997). The head domain of this protein is larger than the tail (approx. 774 aa), and contains the actin- and ATP-binding sites, which are strongly conserved. However, MyoA does not conform to the TEDS rule, which states that there is a tendency of myosins to contain phosphorylatable (T-S) or negatively (E-D) charged amino acids upstream of a highly conserved DALAK sequence. These amino acids are important for coupling acting biding with ATP hydrolysis, and have been demonstrated to be important for regulation of this interaction in other models (Heintzelman and Schwartzman, 1997). The neck domain is usually considered an important characteristic of myosins; these structures consist of between 1 and 6 IQ motifs, however, in MyoA there is a degenerated IQ motif (Heintzelman and Schwartzman, 1997). Furthermore, the MyoA tail domain is very short (just 57 amino acids), and is basically charged, a characteristic considered important in the interaction with other cellular components (Heintzelman and Schwartzman, 1997, Herm-Gotz et al., 2002). MyoA has a short "duty" cycle, which means it releases ADP fast and, consequently, the time it expends bound to actin is short (around 1.5 ms) (Bookwalter et al., 2014). Under this premise it was proposed that MyoA is a motor to produce movement rather than force (Heintzelman and Schwartzman, 1997, Herm-Gotz et al., 2002). The unitary step size of MyoA is around 5.3 nm, and it propels actin filaments towards the plus-end at a rate of 3.4 to 5μm/s (Hettmann et al., 2000, Herm-Gotz et al., 2002, Bookwalter et al., 2014). In *T gondii*, this motor lever arm comprises MyoA, myosin light chain (MLC1), and two mutually exclusive essential light chains (ELC1 and ELC2) that bind to the divergent MyoA neck domain. The lever arm both regulates, and gives rigidity to, the MyoA step in order to move on actin filaments (Herm-Gotz et al., 2002, Nebl et al., 2011, Bookwalter et al., 2014, Williams et al., 2015). A similar structure has been reported in *Plasmodium* parasites; in this case, MyoA binds a MLC (homologous to MLC1) called myosin tail interacting protein (MTIP) and ELC (Bergman et al., 2003, Bookwalter et al., 2017).

In tachyzoites, this protein is distributed beneath the PM of the parasite, a location mediated solely by the presence of MLC1 (Herm-Gotz et al., 2002, Egarter et al., 2014,

Williams et al., 2015, Whitelaw et al., 2017), similar to the interaction observed in *Plasmodium* MyoA-MTIP (Bergman et al., 2003, Sebastian et al., 2012). MyoA is the most studied of the myosins present in the phylum Apicomplexa due to its implication in the motor machinery that power motility, invasion, and egress processes in these parasites. Depletion of MyoA strongly affects the ability of parasites to complete the lytic cycle (Meissner et al., 2002b, Siden-Kiamos et al., 2011, Sebastian et al., 2012, Andenmatten et al., 2013).

1.8.1.2 Myosin B and myosin C (MyoB and MyoC)

MyoB and MyoC are two 130KDa unconventional class XIVb myosins encoded by a single gene, and produced by alternative splicing of the last intron (Delbac et al., 2001, Foth et al., 2006). Like MyoA, MyoB and MyoC have a well conserved head domain including the ATP- and actin-binding domains (Heintzelman and Schwartzman, 1997). Unlike neckless MyoA, MyoB and C have a short neck composed of a single conserved IQ motif (Heintzelman and Schwartzman, 1997). These two heavy chains differ only in the C-termini of their tail domain, with the last intron spliced in MyoC but not in MyoB (Delbac et al., 2001). Although these proteins share the same sequence for their entire head, neck, and almost all the tail domains, their localisation in the parasite is different, and also, their expression is in different stages of the parasite. MyoB is a highly soluble protein, mainly expressed in the bradyzoite stage, and its subcellular localisation remains cytoplasmic. On the other hand, MyoC is an insoluble protein, mainly produced during the tachyzoite stage, and its localisation is constrained to the posterior ring of the parasite (Delbac et al., 2001). Early studies analysed the function of MyoB and MyoC by separately overexpressing these proteins resulting in a replication abrogation in both cases (Delbac et al., 2001). The localisation of MyoC in the basal pole was associated with late daughter cell division in *T. gondii*. However, knockout of MyoB and C showed that these proteins are dispensable for the lytic cycle (Egarter et al., 2014, Frenal et al., 2014). Further analysis suggested that MyoC interacts with MLC1 in the posterior pole, and also with the structural proteins GAP80 and IMC associated protein 1 (IAP1) (Frenal et al., 2014). However, the specific function of this complex remains unknown.

1.8.1.3 Myosin D (MyoD)

MyoD belongs to class XIVa and is 91 KDa, the smallest myosin in the *T. gondii* repertoire (Hettmann et al., 2000, Foth et al., 2006, Herm-Gotz et al., 2006). Among all the *T. gondii* myosins, MyoD is the closest relative of MyoA with no orthologues in *Plasmodium* species. These proteins share high similarity in their amino acid sequence and kinetics, and

also display similar cellular distribution (Hettmann et al., 2000). Like MyoA, MyoD is located in the pellicle of tachyzoites, and in the absence of its tail domain, is mislocalised to the cytoplasm (Hettmann et al., 2000). The association between MLC2 and MyoD is similar to MyoA-MLC1. Thus, both motors require the presence of their respective light chain to stabilise and target the periphery (Polonais et al., 2011, Frenal et al., 2017b). However, contrary to phenotypes seen in the absence of MyoA in tachyzoites (Meissner et al., 2002a), the total absence of MyoD in tachyzoites show no phenotype in motility, invasion, virulence, or intracellular growth, which clearly demonstrates that MyoD is not essential during the lytic cycle (Herm-Gotz et al., 2006). Additionally, MyoD expression in bradyzoites is ten times higher than in tachyzoites, which indicates that this motor complex may have a role during cyst development (Delbac et al., 2001, Herm-Gotz et al., 2006).

1.8.1.4 Myosin E (MyoE)

Together with MyoB and MyoC, MyoE belongs to class XIVb, but is the least studied among these myosins (Foth et al., 2006). Unlike MyoB and MyoC, MyoE does not have an identifiable IQ motif and its length is 93KDa - small compared with other class XIVb myosins (Lew et al., 2002). This myosin is located at the conoid of daughter and developed tachyzoites, and its function is currently poorly understood (Frenal et al., 2017b). Since MyoE has been reported to be upregulated in bradyzoites but not in tachyzoites, it could be presumed that it has a role during bradyzoite development (Foth et al., 2006).

1.8.1.5 Myosin F (MyoF)

MyoF is a 216 KDa class XXII myosin, and is well conserved among Apicomplexa (Foth et al., 2006). Based on its sequence, this myosin shares structural similarities with myosin Va, which are well-known organelle transporters in other organisms (Foth et al., 2006, Woolner and Bement, 2009, Hartman et al., 2011). MyoF contains a conserved head domain with actin-binding and ATP-binding sites. Unlike MyoA, the MyoF neck domain is long, containing six well-conserved IQ motifs. Even though its structure suggests this myosin can interact with myosin light chains, its interactors remain unknown. Additionally, this myosin contains a coiled-coil with a specialised cargo domain that first suggested its function in the parasite (Foth et al., 2006). In dividing vacuoles, MyoF was localised in the vicinity of the apicoplast, and in non-dividing vacuoles, this myosin localised at the periphery (Jacot et al., 2013). In extracellular parasites MyoF signal was observed in the cytoplasm and in the pellicle (Jacot et al., 2013). Depletion of MyoF showed that this protein is essential for *T. gondii* tachyzoites. Further studies demonstrated that this myosin is

responsible for the correct segregation of the apicoplast during endodyogeny, for anchoring micronemes and rhoptries to the apical pole of the parasite, and for transporting dense granules to the PM of intracellular parasites (Jacot et al., 2013, Mueller et al., 2013, Heaslip et al., 2016).

1.8.1.6 Myosin H (MyoH)

MyoH is a 170KDa class XIVc myosin, and is well conserved among Coccidia, but absent in *Plasmodium* (Foth et al., 2006). Its structure contains a head domain with the conserved actin-binding and ATP-binding domains. MyoH contains a long neck domain with eight IQ motifs for interacting with light chains. The tail domain contains subdomains, previously shown to be involved in microtubule coordination in *Saccharomyces cerevisiae*, may be responsible for targeting this motor (Foth et al., 2006, Graindorge et al., 2016). This myosin localises to the apical pole of parasites in both dividing vacuoles and extracellular parasites (Graindorge et al., 2016). Specifically, MyoH is found in the tip of the conoid directly or indirectly associated to the conoid tubulin fibers (Graindorge et al., 2016). In the apical pole, MyoH interacts with three distinct light chains: MLC1, MLC5, and MLC7, the latter being dispensable for MyoH stability and function, and lytic cycle progression (Graindorge et al., 2016). Additionally, three calmodulin (CaM)-like proteins (CaM1, CaM2, and CaM3) were found in the conoid interacting with MyoH and possibly functioning as regulatory light chains (Long et al., 2017). MyoH depletion resulted in a detrimental invasion phenotype - here, parasites were unable to form a TJ and therefore blocked in host cell penetration (Graindorge et al., 2016). These results supported the hypothesis that MyoH has no role in conoid protrusion, but is actively involved in bringing transmembrane adhesins to the apical tip during secretory organelle discharge, therefore acting as a gliding motility initiator (Graindorge et al., 2016). In *Plasmodium*, it has been proposed that this function may rely on *Plasmodium* MyoB, which is a class XIVc myosin mostly located in the apical tip in motile and invasive stages (Yusuf et al., 2015). However, unlike MyoH, *Plasmodium* MyoB does not possess a tail domain this function was attributed to its unusual light chain, MLCB. Based on its location, this protein may participate in the discharge of the secretory organelles. Nonetheless, its functions and specific localisation remain unknown (Yusuf et al., 2015).

1.8.1.7 Myosin I (MyoI)

MyoI is a 200 KDa myosin is a class XXIV myosin (Foth et al., 2006). Very little is known about MyoI structure; one of the most notable sequence characteristics is its predicted

coiled-coil that would, theoretically, permit this protein to dimerize (Foth et al., 2006). However, the complete architecture and interactors of this motor remain to be studied. MyoI is located in the centre of the RB and has been recently associated to the organisation of daughter cells during replication as a synchronicity regulator (Frenal et al., 2017b). Here, MyoI is the motor responsible to maintain daughter cells connected during their development. Consequently, MyoI has been directly associated in the maintenance of the RB and is potentially associated to the organisation of F-actin network in the residual body, which have been implicated in the orientation and arrangement of the parasites in the rosette (Frenal et al., 2017b, Periz et al., 2017). It was proposed that the connection among daughter cells is actively broken in bradyzoite stage to decrease the division rate typical in the latent stage (Frenal et al., 2017b). Although the presence of the F-actin network remains to be studied in the bradyzoite stage.

1.8.1.8 Myosin J (MyoJ)

MyoJ is a 277 KDa class VI myosin (Foth et al., 2006). Class VI myosins contain a typical insert between their conserved head domain and the IQ motif. This insert is predicted to give these myosins their unusual minus-end directionality, contrary to that in the majority of myosins such as MyoA (Wells et al., 1999, Foth et al., 2006). Nevertheless, little is known about MyoJ structure and further study is required. This Myosin is associated with the basal pole in both dividing vacuoles and non-dividing parasites, forming a ring signal in the posterior end. Like MyoI, this motor participates in synchronised division during development of the vacuole. Although not essential, the idea that both myosins (MyoI and MyoJ) are involved in the synchronous replication of daughter cells, lead to the hypothesis that parasites are connected and "communicate" by transporting molecules to one to another in an acto-myosin dependent manner while developing inside the vacuole (Frenal et al., 2017b, Periz et al., 2017).

1.8.1.9 Myosin K (MyoK)

MyoK is 263KDa and belongs to class VI (Foth et al., 2006). Like MyoJ, MyoK may possess the unusual directionality observed in class VI myosins (Wells et al., 1999, Foth et al., 2006). At the moment, this characteristic is speculative, since no full characterisation of MyoK is available. In tachyzoites, MyoK localises to the centrocones in dividing parasites. *myoK* KO shows it is not essential during the lytic cycle, but its function remains unknown (Frenal et al., 2017a).

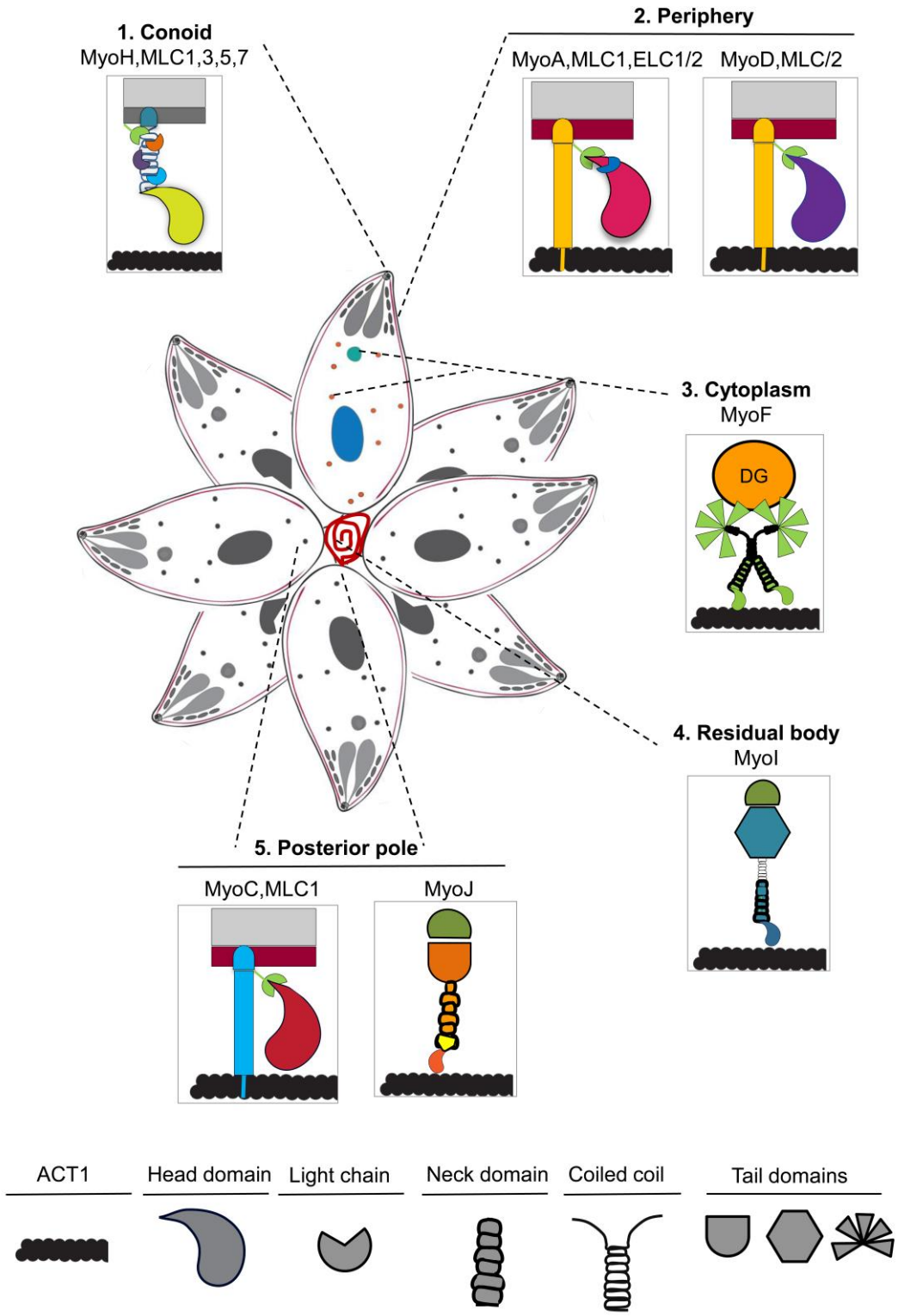

Figure 1-7. Repertoire of myosins in *T. gondii* tachyzoite.
Schematic illustration of characterised myosins expressed in tachyzoites **1.** MyoH locates at the conoid, its structure contains a long neck that permits its interactions with MLC1,3,5 and 7. MyoH functions are to give support during initial tight attachment to the host cell and penetration **2.** MyoA, locates it the periphery of the parasite via MLC1 and GAPs. Together with MLC1 and ELC1/2, MyoA powers gliding motility, invasion and egress in tachyzoites. The MyoD-MLC2 complex is located in the periphery, and is mostly expressed during bradyzoite stage **3.** In the cytoplasm, MyoF controls dense granule trafficking and apicoplast segregation during endodyogeny. This myosin contains a specialised head domain followed by a coiled coil domain and a long neck domain that permits the interaction with a yet unknown light chain(s). In the scheme of MyoF the yellow circle represents a dense granule (DG) **4.** MyoI, a long-necked myosin, is distributed in the residual body of vacuoles.

This motor was recently attributed the function of protein-transport and cell-cell communication among daughter cells in the PV. **5.** The MyoC-MLC1 complex is located at the posterior pole of the parasite, and shares functions with MyoA. MyoJ, located in the posterior pole, contains a subdomain between the head and the neck domain, which may give it an unusual directionality. Like MyoI, this motor contributes to the development and communication among daughter cells within the PV. In the scheme of MyoI and MyoJ the green semicircle symbolises cargo.

1.9 Myosin light chains

Myosin light chains (MLCs) are part of the myosin holoenzyme complex and are critical for maintaining myosin heavy chain functions. MLCs are members of the CaM and CaM-related families containing four EF motifs with a two-helix topology. This architecture is essential for binding Ca^{++}, a step crucial for associating to the heavy chains (Trybus, 1994, Gifford et al., 2007). The MLCs are able to interact with the myosin heavy chain neck domains, and to regulate the mechano-enzymatic activity of the motor complex (Heissler and Sellers, 2014). There are two kinds of light chains: the ELCs and the regulatory light chains (RLCs). Here, RLCs are the light chains involved in the regulation of the enzymatic activity of the myosin heavy chain. Consequently, the ELC associates to the light chains, which are strongly associated to the heavy chain, and enzymatic activity is fully dependent on them (Heissler and Sellers, 2014). However, this nomenclature may be misleading, as it is based on the activity and regulation of the conventional myosin II family.

1.9.1 *Toxoplasma gondii* light chains

Currently, there is a repertoire of seven recognised regulatory light chains (MLC1-7), and two characterised ELC1 and 2 in *T. gondii* (Nebl et al., 2011, Polonais et al., 2011, Williams et al., 2015). *T. gondii* MLCs display atypical EF hands where the Ca^{++} binding sites are not conserved unlike traditional MLCs (Polonais et al., 2011). Thus, this characteristic suggests Ca^{++} binding is not required for associating to the heavy chains. Additionally, all *T. gondii* MLCs possess an N-terminal extension that does not match any known domain or motif except for MLC3, which contains a coiled-coil (Polonais et al., 2011). Endogenous tagging of these proteins shows they are distributed in different locations in *T. gondii* tachyzoites, although their functions and interactors need further study. MLC1 and MLC2 locate in the periphery of the parasites where they target MyoA and MyoD, respectively (Herm-Gotz et al., 2002, Polonais et al., 2011). As opposed to the MLC1-MyoA complex that functions in tachyzoites, MLC2-MyoD are mostly expressed in the bradyzoite stage (Herm-Gotz et al., 2002, Polonais et al., 2011). MLC3, MLC5, and MLC7 were found exclusively in the apical tip (Graindorge et al., 2016). The latter, together with MLC1, has been associated with MyoH, a myosin present in the conoid and proven indispensable for

the lytic cycle (Graindorge et al., 2016). MLC4 was localised surrounding the nucleus, and MLC6, the most divergent MLC, distributed in the conoid, but was not immunoprecipitated with MyoH (Polonais et al., 2011, Graindorge et al., 2016).

T. gondii tachyzoites express two recognised ELCs: ELC1 and ELC2 (Nebl et al., 2011, Williams et al., 2015). These are calmodulin-like proteins that have well conserved EF hands, which suggest these proteins have an intact Ca^{++} binding site (Nebl et al., 2011, Williams et al., 2015). However, an *in vitro* myosin motility assay showed Ca^{++} addition had no effect on their function (Williams et al., 2015). Similar observations have been observed in *Plasmodium,* that possess one orthologue of ELC1 (ELC) (Bookwalter et al., 2017).

1.9.1.1 Myosin light chain 1 (MLC1), essential light chain 1 (ELC1) and essential light chain 2 (ELC2)

The most studied of the MLCs in *T. gondii* is MLC1 for its direct association with MyoA (Herm-Gotz et al., 2002). This protein was shown to interact at the C-terminal end of MyoA, and collocate in the periphery of the parasite with this heavy chain (Herm-Gotz et al., 2002). Similar characteristics were described for the homologous of MLC1 in *Plasmodium* MTIP, which was also described to interact with MyoA (Bergman et al., 2003). The presence of MLC1/MTIP was shown to be critical for targeting MyoA to the periphery. Thus, parasites lacking MLC1/MTIP showed relocation of MyoA, and, in the case of *Plasmodium,* the loss of MTIP resulted in degradation of MyoA (Frenal et al., 2010, Sebastian et al., 2012, Egarter et al., 2014).

Additionally, it has been shown that MLC1, together with ELC1 and 2, actively participate in stabilising the MyoA lever arm (Nebl et al., 2011, Bookwalter et al., 2014, Williams et al., 2015). ELC1 and ELC2 are the first essential light chains characterised in *T. gondii* (Nebl et al., 2011, Williams et al., 2015, Bookwalter et al., 2017). ELC1 and ELC2 colocalise with MLC1 and MyoA in the periphery of dividing and extracellular tachyzoites. These ELCs bind to the divergent MyoA neck domain, and both bind the same region in MyoA, making them mutually exclusive (Williams et al., 2015). The dependence of MyoA on MLC1 for localisation to the IMC makes the presence of MLC1 critical for MyoA peripheral location (Herm-Gotz et al., 2002, Gaskins et al., 2004, Egarter et al., 2014), however, ELC1 and ELC2 do not participate in this role (Williams et al., 2015). In fact, depletion of either ELC does not affect MyoA location, while upon MyoA removal both ELCs are mislocalised from the periphery to the cytoplasm (Williams et al., 2015). Thus, only MLC1 is essential for MyoA location. Since ELC1 and ELC2 compete for the same

region, the function of the MyoA motor relies on two light chains MLC1 and ELC1 **or** ELC2. Moreover, the MyoA motor doubled its speed when two light chains were present (from 1.5 to 3.4 μm/s), suggesting that MyoA light chains change the length of the lever arm and thus participate in regulating the speed at which actin is propelled (Bookwalter et al., 2014).

MLC1 and ELC1 can interact not only with MyoA in the periphery, but also with MyoC in the posterior pole of the parasite (Frenal et al., 2014). This association was demonstrated using immunoprecipitation assays, and suggests these proteins form a motor complex in the posterior pole (Frenal et al., 2014). However, further studies reported that ELC1 is specific to MyoA because upon its depletion, ELC1 loses its connection to the periphery of the parasite and is relocalised to the cytoplasm (Williams et al., 2015). Additionally, unlike the dependence for MyoA localisation, MyoC posterior distribution does not depend on MLC1. The only known connector of MyoC to the posterior end is the structural component IAP1 (Frenal et al., 2014). Although MyoC and its interactors in the posterior pole contain similar components to the MyoA complex in the periphery, the function of MyoC remains unknown (Egarter et al., 2014, Frenal et al., 2014). Additionally, there is no information regarding its stabilisation, or the regulation of its lever arm.

1.10 Gliding motility

Gliding motility refers to the capacity of Apicomplexan parasites to propel without the requirement of cilia or flagella, instead using their acto-myosin machinery to move along protein substrates and actively invade host cells (Vanderberg, 1974, King, 1988, Dobrowolski and Sibley, 1996, Dobrowolski and Sibley, 1997, Dobrowolski et al., 1997a). In 2D environments, *T. gondii* tachyzoites show three different kinds of motility patterns: circular, helical, and twirling (Frixione et al., 1996, Håkansson et al., 1999). During circular gliding, the parasite attaches to the substrate and moves forward producing a circular pattern. The speed of this movement is on average around 1.5μm/s. During helical motility, the parasite moves forward one body length and then rotates 180°, which leaves the parasite in a vertical angled position. Following, the parasite reorients over its apical end, and flips over rotating 180° again. Helical motion average speed varies from 1-3 μm/s, and the pattern of motility can be either straight or in a counter-clockwise circular pattern. Both circular and helical gliding result in forward movement along the substrate, which can be shown by the protein-membrane shed behind on a solid surface (Dobrowolski and Sibley, 1996, Dobrowolski et al., 1997a). Contrary to these movements, twirling is stationary (Frixione et al., 1996, Håkansson et al., 1999). In this case, the posterior pole of the parasite remains

attached to the substrate while the apical pole spins clockwise while oriented vertically. The time it takes for the parasite to complete 360° is around two seconds (Frixione et al., 1996, Håkansson et al., 1999). Parasites can rapidly change the way they move, reorienting themselves prior to starting the next movement (Håkansson et al., 1999). While these three types of movement are easily differentiated based on their particular details, their biological functions remain unknown.

Although this first description of motility remains accurate, novel tools uncovered further characteristics of apicomplexan gliding motility. For instance, *Plasmodium* sporozoite motility was studied using reflection interference contrast and traction force microscopy (TFM) to observe the dynamics of attachment sites between parasite and substrate (Münter et al., 2009). Here, they showed that the attachment points are not equally distributed during parasite motion; on the contrary, attachment points seemed to be rapidly regulated (Münter et al., 2009). Additionally, motility in 3D environments was studied in both *Plasmodium* and *T. gondii* zoites using Matrigel to create a third physical dimension (Kan et al., 2014, Leung et al., 2014). In both cases, the zoites motility critically depended on the cell shape (Kan et al., 2014, Leung et al., 2014). Also, while in 2D tachyzoites show three different motility patterns and *Plasmodium* sporozoites show circular motility, in 3D environments these parasites move in corkscrew-like trajectories only (Kan et al., 2014, Leung et al., 2014). In the case of *T. gondii*, this led to the conclusion that helical trajectories could correspond to the parasite attempting to move in a corkscrew trajectory, but lacking a third physical dimension (Leung et al., 2014).

1.10.1 The acto-Myosin A motor complex

Many human pathogens rely on cell motility to complete their life cycles. For instance, Kinetoplastids, including *Trypanosoma* and *Leishmania*, developed a specialised flagellum to propel along host tissues, and it is an essential player for their development, transmission, and pathogenesis (Langousis and Hill, 2014). Conversely, although apicomplexan zoites lack specialised motility organelles, such as cilia or flagella, they can propel themselves using their own machinery (King, 1988, Menard, 2001, Keeley and Soldati, 2004, Wetzel et al., 2005). The gliding machinery is an acto-myosin motor fixed in the pellicle of the parasite. The function of this acto-Myosin motor is thought to be in generating force to propel the parasite forward in substrates and drive rapid host cell entry (Keeley and Soldati, 2004) (Figure 1-8).

Early studies in *P. berghei* highlighted that gliding motility is substrate-dependent; the parasite's ability to glide increased in the presence of protein-coated substrates (Vanderberg, 1974). Moreover, it was shown that gliding parasites continuously deposited protein trails which demarcate the patterns of their motility (Vanderberg, 1974, Steward and Vanderberg, 1988). These insights opened the idea that secretion of proteins from the apical pole, their translocation to the posterior pole, and further shedding was an active process closely associated to gliding motility (Russell and Sinden, 1981). Drug assays were performed to study where the force for capping and gliding came from. Unlike microtubule inhibitors, both capping and motility were sensitive to the actin inhibitor CytoB (Russell and Sinden, 1981). Therefore, it was proposed that a motor, residing underneath the PM and composed of ACT1 and a Myo, was able to actively translocate secreted proteins towards the posterior end (King, 1988). In *T. gondii* the direct association between gliding and invasion was established after it was shown that CytoD not only affected motility but also the capacity of parasites to penetrate host cells (Dobrowolski and Sibley, 1996). Similar results were obtained using non-specific myosin inhibitors butanedione monoxime (BDM) and KT5926, confirming previous observations that implicated a myosin as a force producer able to drive gliding and invasion (Dobrowolski et al., 1997a). MyoA, a small unconventional myosin, was identified (Heintzelman and Schwartzman, 1997) and localised underneath the PM of the parasite, an ideal position to drive gliding motility (Hettmann et al., 2000). The confirmation of this hypothesis came after the development of the tetracycline-inducible transactivator system, which permitted the characterisation of parasites lacking MyoA (section 1.11.1.1). Here, the MyoA mutants showed a marked impairment in their ability to glide, invade, and egress (Meissner et al., 2001, Meissner et al., 2002b). The unusual structure of MyoA raised the question of its ability to reach the parasite periphery despite having a divergent neck and no tail domain, which are important features of conventional myosins. Therefore, MLC1 was recognised as the main MyoA interaction partner, able to anchor this protein to the periphery of the parasite (Herm-Gotz et al., 2002). MLC1, together with ELC1 and 2, stabilise and regulate MyoA interaction with Actin (Williams et al., 2015). In the periphery, the accessory protein GAP45 anchors MyoA to the IMC via MLC1, while GAP40 and GAP50 are thought to give stability to this complex (Gaskins et al., 2004, Frenal et al., 2010, Egarter et al., 2014, Harding et al., 2016). Altogether, the acto-MyoA motor complex functional proteins (ACT1, MyoA, MLC1, ELC1/2) and structural proteins (GAP45/40/50) have been proposed to enable gliding motility and invasion in apicomplexan parasites (Keeley and Soldati, 2004, Frenal et al., 2017a).

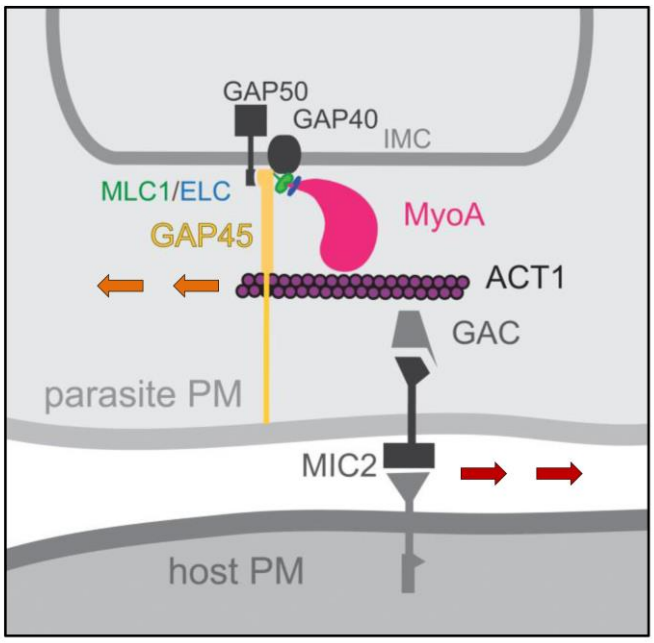

Figure 1-8. *T. gondii* tachyzoites gliding motility machinery
Schematic representation of the acto-MyoA motor complex. GAP45 (yellow), GAP40 (dark grey) and GAP50 (dark grey) are the structural support of the motor complex. MLC1 (green) targets MyoA (pink) to GAP45. MLC1 and ELC1/2 (blue) assist MyoA to walk on short ACT1 filaments (purple) that are displaced (orange arrows) contrary to parasite movement. The force that produces ACT1 translocation is indirectly transmitted to MIC proteins (pebble) in the parasite PM via GAC. MICs are associated to the cytoskeleton with one side and the substrate with the other side; thus, connecting the parasite to the milieu. Forward motility (red arrows) is product of the constant redistribution and shedding of the MICs. The force to move the MICs is generated by the acto-MyoA motor complex located in the periphery of the parasite.

1.10.1.1 Assembly of the acto-MyoA motor complex

The assembly of this motor complex divides in two steps that happen consecutively, first MyoA, MLC1 and GAP45 link together. After that, GAP50 associates resulting in the anchoring of IMC and the motor complex (Gaskins et al., 2004, Frenal et al., 2010). The tail domains in the myosins heavy chains are responsible for localizing the motor domain with the 'cargo', but as MyoA lacks a tail domain, this function is covered by an N-terminal extension of MLC1. MLC1 is a single headed myosin responsible for anchoring the motor complex to GAP45, which acts as a bridge between the IMC and plasma membrane (Herm-Gotz et al., 2002, Gaskins et al., 2004, Frenal et al., 2010). Finally, when firmly anchored to the IMC, MyoA is able to interact with ELC1/2, form here, the MyoA motor complex is assembled and ready to walk on actin filaments (Williams et al., 2015).

1.10.1.2 Architecture of the acto-MyoA motor complex

Force generation dependent on acto-myosin systems require both proteins aligned to interact. For instance, in filopodia myosin X (MyoX) tail domain transport integrins

embedded in the plasma membrane while the head domain walks along long actin scaffolds (Leijnse et al., 2015). In early studies, this architecture was proposed for the acto-MyoA motor complex (King, 1988). However, the unusual structure of MyoA suggested this protein could not sustain this architecture since it lacks a tail domain and contains a divergent neck domain. Additionally, 97% of ACT1 was found in monomeric state in *T. gondii*, while ACT1 filaments were not observable (Dobrowolski et al., 1997b). For these reasons, it was concluded that ACT1 filaments were short and unstable (Sahoo et al., 2006), and further hypothesised that MyoA may induce the formation of short ACT1 filaments (Schüler and Matuschewski, 2006b). Under these circumstances, the acto-MyoA motor complex architecture in apicomplexan parasites seemed "upside down". Here, while MyoA is fixed to the GAPs via MLC1, ACT1 would be able to interact with MIC proteins, thus linking the parasite cytoskeleton to the substrate (Keeley and Soldati, 2004, Soldati and Meissner, 2004). Even though this model is accepted, it is important to consider that both the assembly and architecture of the acto-MyoA motor complex are mainly based on immunoprecipitation studies and visualisation of fixed samples (Tardieux and Baum, 2016). While these tools lay the foundations of protein interactions, the results must be taken with great care and confirmed using other methods to consolidate *in vivo* and *in vitro* data. In addition, a limitation to define the motor complex architecture is that until today it has not been observed *in situ*, because of the difficulty in visualisation of ACT1 filaments (Tardieux and Baum, 2016), and successful endogenous tagging of MyoA without interfering with its functional domains. Considering this situation, a recent report suggested an alternative "free" acto-MyoA motor complex model. The authors propose that ACT1 is organised in filament bundles by actin binding proteins, such as coronins. These bundles are suggested to be in contact with the PM, directly linked to adhesins without the necessity of a connector. Additionally, the complex GAP-MyoA is not fixed to the antero-posterior axis; thus, directional motility would be led by orientation of ACT1 filaments or cell polarisation. Therefore, the force produced by MyoA would be transmitted to ACT1, by moving a patch of PM associated with adhesins, thereby generating forward movement (Tardieux and Baum, 2016). In order to discern the architecture and regulation of the motor in the proposed models, the authors recommend further studies of the interaction between substrate and attachment sites regulations (Tardieux and Baum, 2016).

1.10.1.3 Regulation of motility and acto-MyoA motor complex function

Gliding motility, invasion, and egress are highly controlled mechanisms, with spatial and temporal factors influencing their activation, and hence function. There are at least two

second messengers involved in this mechanism: Ca^{++} and cyclic guanosine monophosphate (GMP) (Billker et al., 2009). For instance, microneme secretion is induced by increasing intracellular Ca^{++} levels (Carruthers and Sibley, 1999, Lovett and Sibley, 2003). In *T. gondii*, the most studied Ca^{++} receptors are CDPK1 and CDPK3, due to their role during invasion and egress. CDPK1 was shown to mediate Ca^{++} dependant microneme secretion, which triggered both invasion and egress (Lourido et al., 2010), while CDPK3 was shown to be indispensable for invasion but not egress (Garrison et al., 2012, Lourido et al., 2012, McCoy et al., 2012). The CDPK3 orthologue in *Plasmodium* (CDPK1) was shown to be essential for targeting the motor complex to the periphery (Sebastian et al., 2012). These results demonstrate that i) CDPKs are conserved, but they can have different roles in different species, and ii) Ca^{++} signalling not only controls microneme secretion, but is also involved in the assembly and regulation of the acto-MyoA motor complex. For instance, a methyltransferase present in tachyzoites (AKMT) has been implicated in motility and invasion (Heaslip et al., 2011). This enzyme locates in the apical tip of immotile intracellular parasites, but upon Ca^{++} stimulation, is rapidly relocalised to the cytoplasm prior to egress. This led to the hypothesis that AKMT is sequestered in the apical pole, and Ca^{++} stimulation is the signal for releasing this protein to the cytoplasm where it is able to interact with the motor machinery (Heaslip et al., 2011). The components of the motor complex contain phosphorylation sites, suggesting they can be regulated upon Ca^{++} stimulation (Nebl et al., 2011, Treeck et al., 2011). In fact, CDPK3 was shown to specifically phosphorylate two of ten phosphorylation sites present in MyoA, which were shown to have an important role for motility and egress (Gaji et al., 2015). Unlike MyoA, phosphorylation of MLC1 and GAP45 was shown not to play a role in motility (Jacot et al., 2014). Similarly, although ELCs (ELC1 and ELC2) contain conserved Ca^{++} binding sides, *in vitro* data suggested Ca^{++} does not regulate the MyoA lever arm in either *T. gondii* or *Plasmodium*, with no change in the speed of ACT1 propulsion in the presence of Ca^{++} (Williams et al., 2015, Bookwalter et al., 2017). As such, how Ca^{++} regulates the acto-MyoA motor complex is a matter for further study.

1.10.2 The linear motor model

The linear motor model is based on the ability of parasites to translocate, or "cap", membrane proteins, a process that depends on cytoskeletal components (Russell and Sinden, 1981, King, 1988). This capping refers to the polarised migration of transmembrane proteins from the anterior pole, where they are secreted, to the posterior pole of the parasites, where they are further shed (Figure 1-8). As the transmembrane components are linked on both sides either to the substrate or the acto-MyoA motor complex, this connects the substrate to

the parasite cytoskeleton (Keeley and Soldati, 2004). Therefore, the transmembrane proteins are able to generate transient adhesion points with the substrate and allow the parasite to produce enough traction to move forward (Soldati et al., 2001). For instance, the TRAPs are transmembrane adhesins which are released from the micronemes and migrate in a polarised manner through the PM of the parasite (Heintzelman, 2015). These proteins contain extracellular adhesive subdomains that establish the interaction with the substrate (Boucher and Bosch, 2015). In *T. gondii*, MIC2 -homologous to *Plasmodium* TRAP - has been shown to interact with a variety of ligands, suggesting it can bind a great variety of substrates (Heintzelman, 2015). On the other side, the transmembrane proteins indirectly interact with actin. For over a decade, this interaction was thought to be via ALD (Jewett and Sibley, 2003). However, a conditional mutant of ALD showed this protein has no role linking the MICs to ACT1, but is essential for energy metabolism (Shen and Sibley, 2014); recently, it was shown this function is mediated by GAC (Jacot et al., 2016a). The interaction of the adhesins with ACT1 filaments allows transmission of the force generated from MyoA to the substrate (Meissner et al., 2002b). MyoA, via MLC1, is fixed to GAP45, and hence to the pellicle, and stabilised by GAP40 and 50 (Hettmann et al., 2000, Herm-Gotz et al., 2002, Gaskins et al., 2004, Frenal et al., 2010). Together, the acto-MyoA complex produces the antero-posterior migration of transmembrane proteins, which is translated into forward motion (Sibley, 2010). After their polarised translocation, the transmembrane adhesins are cleaved from the PM, which is accomplished by rhomboid proteases, such as ROM4 and ROM5 that play a major role in efficient adhesin processing (Shen et al., 2014b).

As noted, the linear motor model predicts that the peripheral arrangement and correct function of the acto-MyoA motor complex is essential for parasite motility and invasion via migration of transmembrane adhesins (Soldati and Meissner, 2004, Sibley, 2010, Heintzelman, 2015). The first indication of the acto-MyoA motor complex role in gliding and invasion came from assays performed with actin and myosin disrupting drugs (Dobrowolski and Sibley, 1996, Dobrowolski et al., 1997a). Then, the development of the inducible system based on the tetracycline repressor (TetR) permitted the generation of the first MyoA knockdown (KD) (Meissner et al., 2001, Meissner et al., 2002b). The resulting MyoA mutant exhibited significant invasion, gliding, and egress impairment, supporting previous observations (Meissner et al., 2002b). However, the use of the Tet-inducible system resulted in residual expression of the protein, which, at the time, led to the explanation that the residual invasion and gliding observed in the *myoA* KD (Meissner et al., 2002a). The development of the DiCre system (Andenmatten et al., 2013), based on site-specific recombination, permitted the creation of gene knockouts (KO) (section 1.11.1.3).

Unexpectedly, *myoA* KO, *act1* KO, *mlc1* KO, and *gap*45 KO, remained invasive and motile, although at reduced rates (Andenmatten et al., 2013, Egarter et al., 2014), contrary to results obtained upon depletion of *act1* using the DiCre system in *Plasmodium* which blocked merozoite invasion (Das et al., 2017). Additionally, depletion of the MIC proteins AMA1 and MIC2 suggested they were not critical for the parasites (Bargieri et al., 2013, Gras et al., 2017). Of these mutants, *myoA* KO, *ama1* KO, and *mic2* KO are viable in culture, and can be maintained for long periods of time, while *act1* KO, *mlc1* KO, and *gap*45 KO are blocked in egress (Andenmatten et al., 2013, Bargieri et al., 2013, Egarter et al., 2014, Gras et al., 2017). These results call into consideration the real functions of the motor complex and therefore generated a debate on i) how parasites are able to glide and invade in the absence of functional and structural proteins of the acto-MyoA motor complex (Meissner et al., 2013, Frenal and Soldati-Favre, 2015), and ii) why the ability of most mutants to egress was completely blocked (Boucher and Bosch, 2015).

The remaining invasion and gliding rates created a debate on how the parasites move, and raised different hypotheses to explain these phenomena. In the next section, I present a compilation of these proposed hypotheses.

1.10.2.1 Plasticity and redundancy among gliding components

T. gondii contains multiple myosin and MLCs genes (reviewed in section 1.8.1 and 1.9.1); therefore, in the absence of MyoA or MLC1, it is plausible to consider redundancy among complexes (Meissner et al., 2013, Egarter et al., 2014, Frenal et al., 2014, Frenal and Soldati-Favre, 2015). One of the candidates was the closely related class XIV MyoC, due to its structural similarities to MyoA. Pertinently, a triple knockout of MyoA/B/C failed to be maintained in culture due to a detrimental egress defect. These results demonstrated a certain degree of functional compensation, but did not explain why the ability of the triple KO mutant to glide and invade was not completely blocked (Egarter et al., 2014, Frenal et al., 2014). As such, the characterisation of MyoC interactors was performed (Frenal et al., 2014). In this study, three different myosin motor complexes (*a.k.a* glideosomes) were recognised: apical, peripheral, and posterior (Figure 1-9A). The three complexes depend on GAP proteins for proper targeting. Thus, in the apical motor complex GAP70, GAP40, and GAP50 recruit MyoA-ELCs via MLC1 (Figure 1-9A top panel). The peripheral motor complex (the acto-MyoA motor complex) components are the structural proteins GAP40, GAP45, and GAP50 and the functional MLC1 and MyoA-ELCs (Figure 1-9A mid panel). Finally, the posterior motor complex comprises IAP1 that recruits GAP80, GAP40, MLC1,

and MyoC (Figure 1-9A bottom panel) (Frenal et al., 2014). These results demonstrated that MyoC is part of a posterior motor complex, and shares components with the peripheral MyoA motor complex. Moreover, depletion of certain components of the machinery, e.g. GAP80 or MyoA, could be rapidly compensated by components of the neighbour motor complex, GAP45 or MyoC, respectively (Figure 1-9B/C). These data led to the hypothesis that MyoC functionally compensates for MyoA in the *myoA* KO (Frenal et al., 2014, Frenal and Soldati-Favre, 2015, Frenal et al., 2017b)

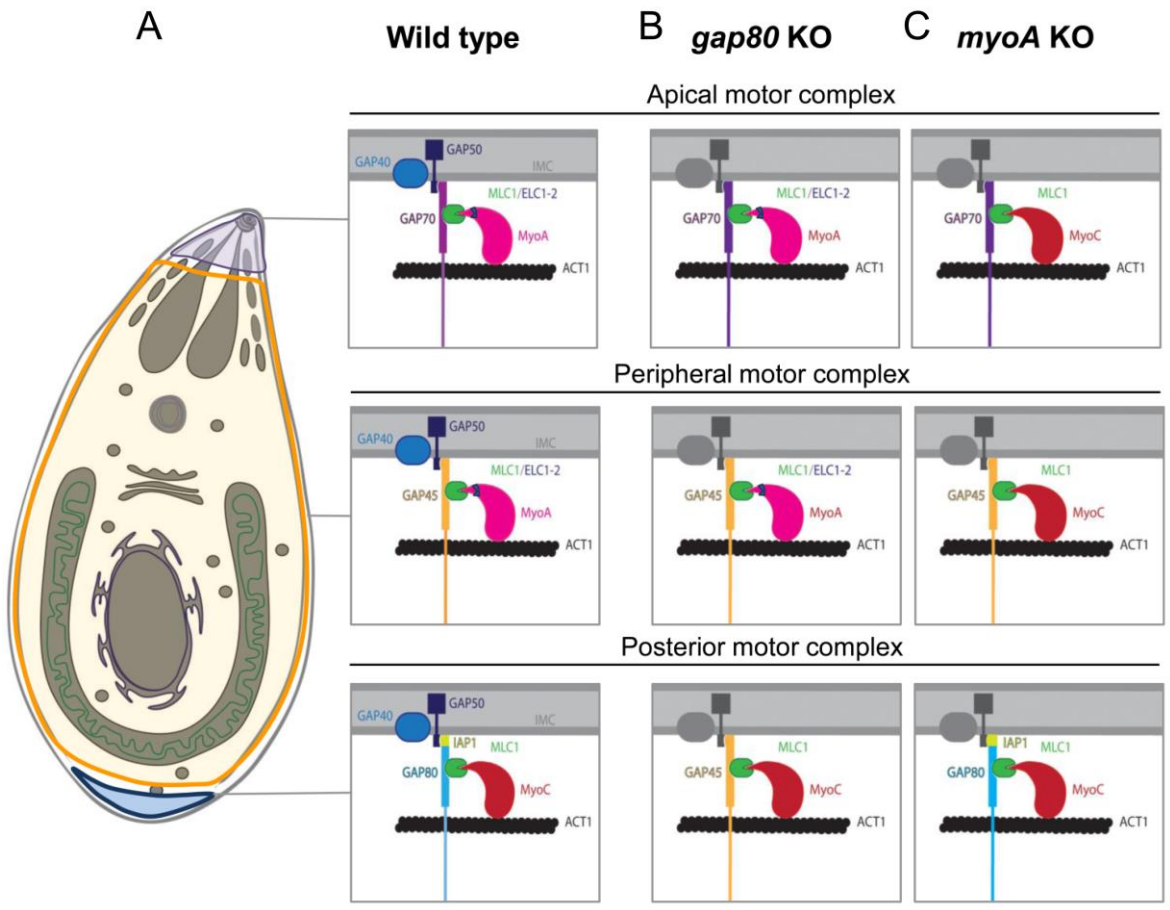

Figure 1-9. Redundancy and plasticity among myosin motor complex in tachyzoites
A. Schematic representation of the three motor complexes in wild type tachyzoites. MyoA (pink), MLC1 (green), ELC1/2 (blue), GAP70 (purple),40 and 50 (indigo) interact in the apical end. In the periphery MyoA, MLC1, ELC1/2 are anchored to the IMC via GAP45 (yellow) and supported by GAP40 and 50. In the posterior pole, MyoC (red) interacts with MLC1, GAP80 (sky blue), IAP1 (lime), Gap40 and GAP50. These components are distributed in a similar architecture than the peripheral MyoA motor complex **B.** Depletion of GAP80 is rapidly compensated by GAP45 that is relocated from the periphery to the posterior end C. Upon MyoA depletion MyoC is redistributed to the periphery to take over MyoA location and functions. Figure inspired by (Frenal *et al*., 2014).

Since a plethora of MICs are produced and secreted, similar mechanisms of redundancy among these proteins have been suggested in the case of AMA1 and MIC2 (Bargieri et al., 2013, Lamarque et al., 2014). While this sounds reasonable for these proteins, ACT1 is the product of a single gene (Dobrowolski et al., 1997b), and so its

complementation is less probable. In this case, like KO of the chaperone UNC, the *act1* KO represents a functional knockout of all acto-myosin motors in *T. gondii* (Egarter et al., 2014, Frenal et al., 2017b). However, this knockout line is still able to glide and invade (Egarter et al., 2014, Whitelaw et al., 2017).

1.10.2.2 Host cell contribution to KO mutants invasion

T. gondii host cell penetration is a smooth and fast process (taking a few seconds to complete), and was suggested to be driven by the function of the acto-MyoA motor complex (Morisaki et al., 1995, Dobrowolski and Sibley, 1997, Sibley, 2010). Hence, until now the role of the host cell during this process was considered minimal to non-existent. However, recent data suggest the host cell plasma membrane and cytoskeleton are certainly involved in the process of parasite penetration (Dasgupta et al., 2014, Bichet et al., 2016, Guérin et al., 2017). Specifically, in the case of *myoA* KO, even though these mutants enter the host cell via canonical TJ formation, they present "stop and go"-like penetration kinetics (Andenmatten et al., 2013, Egarter et al., 2014). A closer look at the penetration dynamics showed that upon contact with the host cells, *myoA* KO mutants appeared to be wrapped by the host cell PM. This "wrapping" was followed by forward displacement of the mutants into the host cells (Bichet et al., 2016). In addition, a belt of host cell actin is present around the TJ of *myoA* KO parasites. As these characteristics were absent in control parasites, it was suggested that in the absence of MyoA, the core of the motor complex, the parasites rely on host cell protrusions to penetrate (Figure 1-10A). This would explain the viability of this mutant strain in culture (Bichet et al., 2016). However, the authors suggest studying this process in control strains by adjusting the protocol of imaging to match the high speed of wild-type parasite penetration. Overall, this mechanism would explain the residual invasion capacity in MyoA motor complex component mutants, although it fails to explain residual gliding capacity.

1.10.2.3 Acto-MyoA independent motility

From early studies, the ability of Apicomplexans to move and invade has been attributed to the presence of the acto-MyoA motor complex (Dobrowolski and Sibley, 1996, Dobrowolski and Sibley, 1997, Keeley and Soldati, 2004, Soldati and Meissner, 2004, Sibley, 2010). Nevertheless, new data suggested these mechanisms can partially rely on other processes overlooked in previous studies (Münter et al., 2009, Andenmatten et al., 2013, Bargieri et al., 2013, Dasgupta et al., 2014, Egarter et al., 2014, Bichet et al., 2016, Quadt et al., 2016, Moreau et al., 2017).

Aiming to explain how *T. gondii* parasites can move in an acto-myosin independent manner, it was hypothesised that parasites rely on a gelation-isolation osmotic engine (Egarter et al., 2014). This idea suggests that at the apical pole parasites contain a gel-like structure comprising ACT1 filaments and acidic protein molecules secreted from the micronemes. This gel contains heavy and light mobile cations, with the mobile cations generating tension that is balanced by tension of the elastic gel. Degradation of macromolecules would partially disassembly the gel causing weakening of the elastic modulus, and therefore, leading to the gel swelling. This swelling will generate protrusion of the leading edge; thus, giving more area for adhesion, and pushing forward. The continuous cycling assembly of the swollen gel and disassembly of the dense gel will create a "step-like" protrusion sequence. On the other side, the posterior end of the parasite is pulled forward by the membrane tension generated by anterior pole protrusive force and the cytoplasmic flow generated by the pressure gradient (Figure 1-10B) (Egarter et al., 2014). In *Plasmodium* sporozoites, the engagement and disengagement of adhesion sides were observed in the apical and posterior pole of the parasites; thus, creating tension among poles and driving parasites to a stretching phase (Münter et al., 2009).

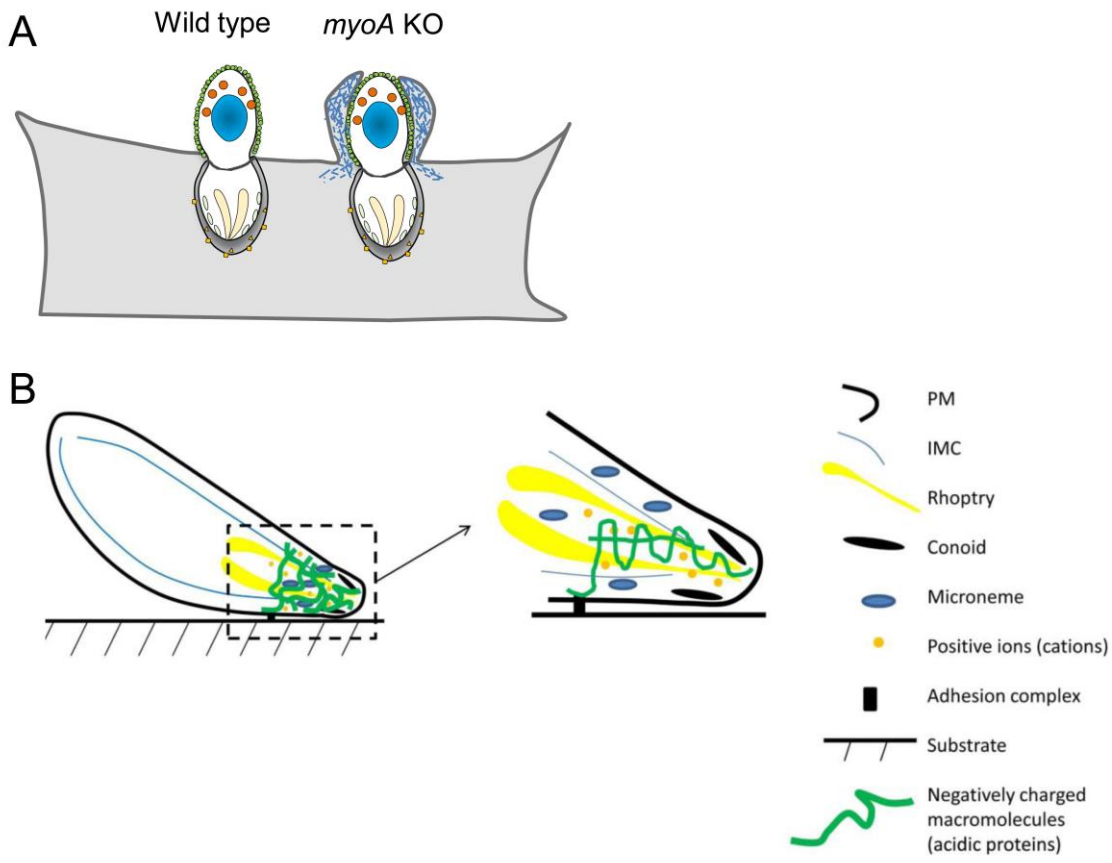

Figure 1-10. Acto-MyoA independent invasion and motility models in *T. gondii* tachyzoites

A. Host cell PM protrudes wraps and pushes *myoA* KO parasites through a canonical-assembled TJ. Scheme inspired by Bichet *et al*., 2016 **B.** Illustration of the gelation-solation hypothetical model of tachyzoite propulsion presented by Egarter *et al*., 2014. The apical pole of the parasite contains a dense gel negatively charged surrounded by mobile cations. Protrusion of the leading edge is driven by a cycle of assembly and disassembly of the gel. Here, when disassembled, the gel swells and causes the leading edge to move forward causing membrane tension, which pulls forward the posterior end. The gel reassembles again creating a dense structure in the apical end, which starts again the cycle of protrusion. Diagram reprinted from Egarter *et al*., 2014. under copyright permissions.

1.11 *Toxoplasma gondii* as a model organism

The phylum Apicomplexa comprises a number of pathogens of human and veterinary importance. From this diverse group of pathogens *T. gondii* is the most successful obligate intracellular parasite, largely due to its host cell promiscuity in the tachyzoite stage. This characteristic makes *T. gondii* parasites easy to maintain in culture, and due to their short lytic cycle, fast to propagate under laboratory conditions. Conversely, *Plasmodium* species are harder to culture because they have specialised adaptations to invade reticulocytes (Swapna and Parkinson, 2017). In addition, tachyzoites are relatively large (2x7 μm) compared to other apicomplexan parasites, like *Plasmodium* merozoites (1x1 μm). This feature facilitates the visualisation of protein subcellular distributions (Kim and Weiss, 2008). *T. gondii* tachyzoites contain a haploid genome of around 63 Mb in size, distributed among 14 chromosomes (Sibley and Boothroyd, 1992, Roos et al., 1995, Khan et al., 2005). This genetic information has been published in ToxoDB, an on-line database which provide free access to genome sequences and annotations of different parasite strains (Gajria et al., 2007). The availability of information has supported the development of different conditional systems which greatly improve the characterisation of genes and proteins (Jimenez-Ruiz et al., 2014).

Transient or stable expression of exogenous genes permit the characterisation of a great variety of proteins in *T. gondii*. The gene of interest (GOI) requires to be flanked by control elements represented by 5' and 3' regions of *T. gondii* genes in order to ensure its expression (Suarez et al., 2017). Additionally, the promoter, which must be close to the transcription start codon, regulates the level of expression. In *T. gondii*, a wide range of promoters with different expression strengths have been identified, with some showing stage specificity. For instance, the p5RT70 promoter is derived from the tubulin 1 gene (TUB1) containing five repeat elements which were shown to stimulate transcription; due to this, it is a strong constitutive promoter (Soldati and Boothroyd, 1995). Unlike TUB1-derived promoters, the dihydrofolate reductase (DHFR) promoters produce a weak constitutive expression (Matrajt et al., 2004). Transient transfection was designed to express a specific

gene product which is not integrated into the genome (Soldati and Boothroyd, 1993). This procedure is used for fast analysis, modification, and visualisation of the transfected product; however, as it is not integrated into the genome, the plasmid-DNA is not replicated and its expression will decay in a matter of days (Soldati and Boothroyd, 1993, Suarez et al., 2017). In stable expression, unlike transient transfection, the GOI is inserted into the parasite's genome. Unlike in *Plasmodium* parasites, random integration is favoured in *T. gondii*, while the frequency of homologous recombination is low. Nevertheless, a parental strain lacking KU80 (Δ*ku80*) enhances the proportion of homologous recombination. This is an element of the non-homologous end joining DNA repair pathway that can repair double strand breaks. Depletion of this element favours homologous recombination, and permit the insertion or replacement of elements in the GOI (Fox et al., 2009, Huynh and Carruthers, 2009b).

1.11.1 Reverse genetic approaches

While editing or replacement of a non-essential gene could be easily achieved, the characterisation of essential genes is challenging, and requires inducible systems for regulation or depletion of their products (Table 1-2) (Jimenez-Ruiz et al., 2014). For instance, rapid regulation of proteins can be achieved using the degradation domain system (further explained in section 1.11.1.2) (Herm-Götz et al., 2007). Similarly, the auxin-dependant degradation pathway from plants has been recently established in both *T. gondii* and *Plasmodium* species (Kreidenweiss et al., 2013, Philip and Waters, 2015, Long, 2017). This system allows the rapid and reversible degradation of a protein of interest in the presence of the plant hormone Auxin (Nishimura et al., 2009). Additionally, the tetracycline promoter system based on the transactivator protein leads to rapid repression of the GOI transcription initiation under tetracycline or tetracycline analogue induction (section 1.11.1.1) (Meissner et al., 2001, Meissner et al., 2002a, Meissner et al., 2005). Moreover, gene removal can be achieved using the DiCre system, that mediates site-specific recombination through the reconstitution of two recombinase components in the presence of rapamycin (section 1.11.1.3) (Andenmatten et al., 2013). Furthermore, U1-mediated gene silencing system regulates the expression at transcriptional level (Pieperhoff et al., 2015). Finally, a bacterial DNA recognition defence system based on clustered regularly interspaced palindromic repeats (CRISPR) has been successfully implemented in *Plasmodium*, *Cryptosporidium*, and *T. gondii* for site-specific gene editing (Lee and Fidock, 2014, Shen et al., 2014a, Sidik et al., 2014, Wagner et al., 2014, Zhang et al., 2014, Vinayak et al., 2015). This system enables a double strand break in a specific gene that is targeted by

a guide-RNA (gRNA), a 20 bps homologous region of the GOI followed by a protospacer-adjacent motif (PAM) -NGG sequence (Shen et al., 2014a, Sidik et al., 2014). Manipulation of the GOI by homologous repair requires the co-transfection of the CRISP-Cas9 with a donor vector containing the point mutation, tag or region of interest to be introduced flanked by homologous regions (Shen et al., 2014a, Sidik et al., 2014). This system permits the generation of genomic disruptions, deletions or endogenous tagging without the introduction of selectable cassettes for CRISPR/Cas9 as its expression is transient (Shen et al., 2014a, Sidik et al., 2014, Zhang et al., 2014). In *T. gondii*, constitutive expression of CRISPR/Cas9 was elegantly used to develop an extensive high throughput genetic screen in order to find proteins that contribute during host-cell infection (Sidik et al., 2016).

As described below, different conditional systems and tools are available for studying the functions of essential genes in *T. gondii*. The following sections highlight the three most used systems for functional characterisation: TetR-TATi (gene KD), ddFKBP (rapid protein degradation) and DiCre (gene KO) (Meissner et al., 2002b, Herm-Götz et al., 2007, Andenmatten et al., 2013).

Table 1-2. Systems for analysis of genes in *T. gondii*

System		Efficiency	Advantages	Disadvantages	Ref
TetR-Tati	KD	Up to 100%	Reversible	Background expression	(Meissner et al., 2002b)
ddFKBP	KD	Up to 100%	Reversible, Rapid	No under endogenous expression Background expression	(Herm-Götz et al., 2007)
DiCre	KO	variable 30-99%	No background	No reversible several cloning steps	(Andenmatten et al., 2013)
U1 snRNP	Tagging-KD	20%	Combined to DiCre	LoxP regions may affect GOI expression	(Pieperhoff et al., 2015)
CRISPR/Cas9	Various	Up to 100%	No selectable marker	Off Target	(Shen et al., 2014a)
Auxin-inducible degron (AID)	KD	No reported	Reversible, Rapid, non-toxic	Requires tagged GOI Background expression	(Long, 2017)

1.11.1.1 The tetracycline-inducible transactivator system

The tetracycline-inducible system is a powerful tool that permits the generation of gene knockdowns. This system is based on the function of TetR with a tetracycline responsive transactivator domain. Together, this allows for regulation of the expression of a GOI preceded by a tetracycline responsive promoter (TRE) containing a minimal promoter downstream of tetracycline operators (TetO). In absence of ATc, the presence of TetR and the transactivator recruit transcription factors in the TRE, which promotes the transcription of the GOI. Conversely, in the presence of ATc, competitive binding to TetR abolishes fusion of the transactivator to the TRE; thus, blocking transcription of the GOI (Meissner et al., 2001, Meissner et al., 2002b). The first transactivator used in *T. gondii* was the viron protein 16 (VP16) derived from *Herpes simplex,* but this showed inability to activate transcription (Meissner et al., 2001). Consequently, in order to find a functional activation domain, a genetic screen was performed by randomly inserting TetR in the genome, resulting in the identification of the transactivator trap identified 1 (TATi) (Figure 1-11A) (Meissner et al., 2002b), which was also shown to be functional in *P. falciparum* (Meissner et al., 2005). The functionality of the TetR-TATi regulatable system was used to generate and characterise the first MyoA conditional gene knockdown (*myoA* KD) in *T. gondii* (Meissner et al., 2002b). Since established, this system was adapted and widely used for characterising endogenous gene functions, although leaky expression of repressed genes has been reported (Jimenez-Ruiz et al., 2014).

1.11.1.2 The ligand-controlled destabilisation domain

The ligand controlled de-stabilisation domain (ddFKBP) permits rapid and reversible protein stabilisation. This system developed by mutating the rapamycin binding protein FKBP12 to respond upon induction with a rapamycin analogue shield 1 (Shld-1) (Banaszynski et al., 2006). This domain can be fused either N- or C-terminally to a protein of interest (POI). In absence of Shld-1, the fused POI is rapidly trafficked to, and degraded in, the proteasome of the cell while the presence of Shld-1 protects the POI from degradation; consequently, stabilising the protein (Figure 1-11B). Since this system requires accessibility to the proteasome, it can be challenging to use for characterising proteins residing within organelles. In *T. gondii*, the ddFKBP system induces downregulation of the protein within 6 hours after induction (Herm-Götz et al., 2007), and so it has been used for generating overexpression or dominant negative mutants (Herm-Götz et al., 2007, Agop-Nersesian et

al., 2009, Pieperhoff et al., 2013). Similarly, this system was successfully established in *P. falciparum* (Armstrong and Goldberg, 2007, de Azevedo et al., 2012).

1.11.1.3 The inducible dimerisable Cre system

The establishment of the inducible dimerisable Cre (DiCre) system allows the development of irreversible, tight, and efficient site-specific regulation of a GOI. This system is based on the function of the Cre-recombinase enzyme split into two inactive fragments; both fragments are then fused to a rapamycin binding protein, either FKBP12 or FRB. Addition of rapamycin brings together the Cre fragments and reconstitutes Cre activity to mediate excision of a gene floxed by LoxP sites (Jullien et al., 2003). In *T. gondii*, one of the most successful adaptations of this system was the development of the GeneSwap strategy. A cassette containing the floxed-cDNA of the GOI followed by a YFP-reporter and a selectable marker was integrated in the genome. This cassette was targeted to the endogenous site via homologous recombination; thus, the GOI endogenous promoter precedes the cDNA before rapamycin induction. In order to favour homologous recombination, the DiCre components were stabilised in a Δ*ku80* background (Andenmatten et al., 2013). Therefore, after rapamycin induction, the cDNA of the GOI is excised, resulting in parasites expressing the YFP reporter (Andenmatten et al., 2013) (Figure 1-11C). This strategy, with certain variations, was used to generate clean knockouts of the components of the acto-MyoA motor complex in *T. gondii* (ACT1, MyoA, MLC1, GAP40, GAP45, GAP50, MyoA/B/C, Mic2, and AMA1). These studies revealed that in these parasites, the acto-MyoA motor complex components play an important, yet not essential, role in invasion and gliding (Andenmatten et al., 2013, Bargieri et al., 2013, Egarter et al., 2014, Shen and Sibley, 2014, Harding et al., 2016). Unlike *T. gondii* ACT1, DiCre-mediated disruption of the ACT1 gene in *P. falciparum* completely blocked erythrocyte entry (Collins et al., 2013, Das et al., 2017).

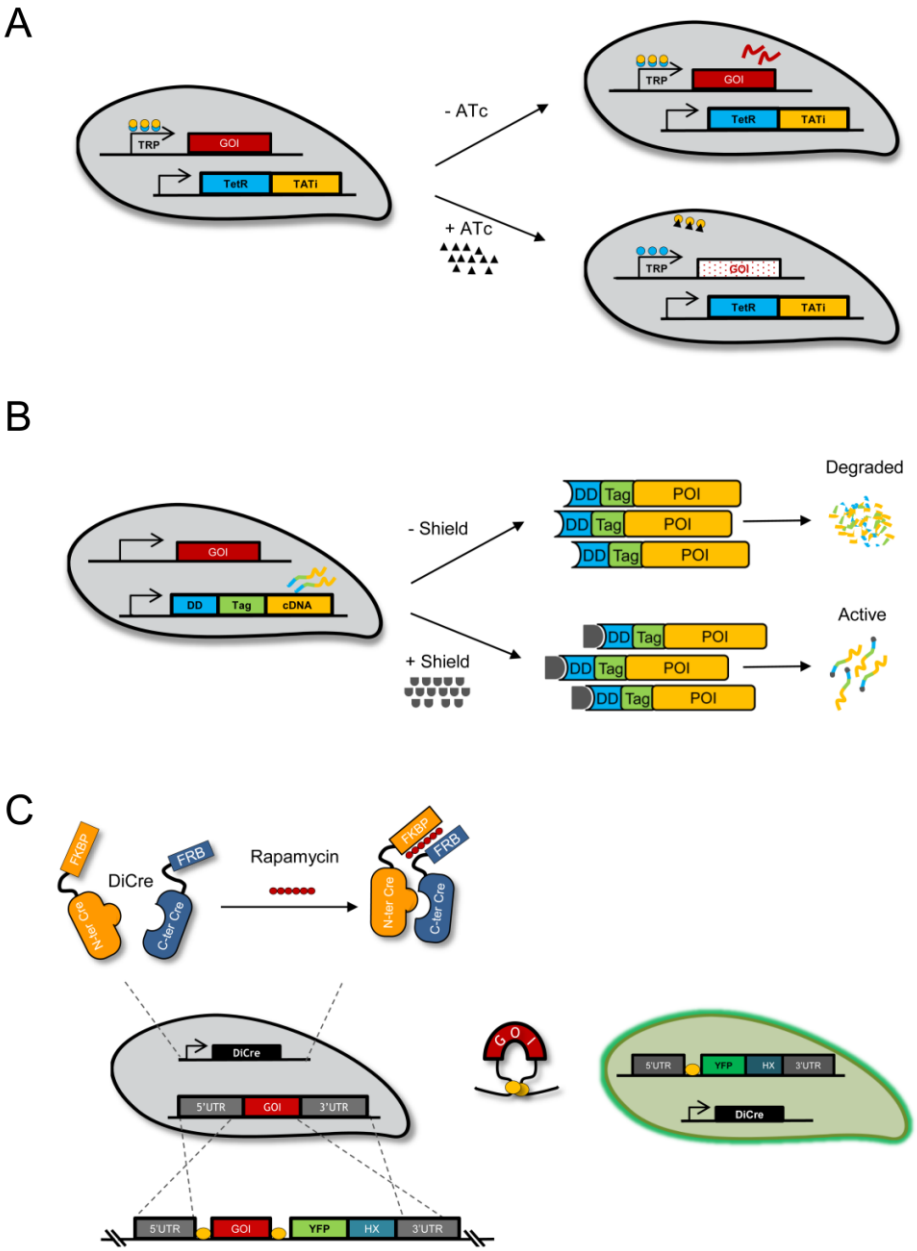

Figure 1-11. Example of three inducible systems for gene knockdown, protein degradation and gene knockout in *T. gondii*

A. Schematic representation of the tetracycline inducible transactivator system (TetR-TATi). In absence of ATc, TetR and TATi bind the TRP. the presence of TATi recruit transcription factors that ensures gene expression. Induction of the system with ATc, interfere in the interaction between TATi and the TRP; consequently, transcription is blocked by the presence of the TetR. Diagram modified from Dr. Nicole Andenmatten **B.** Scheme of the ddFKBP system. Expression of a tagged-POI fused to the dd domain triggers degradation of the protein while induction with shield-1 stabilise the POI, leading to its expression **C.** Schematic representation of the DiCre system. Endogenous GOI is replaced by a cassette containing the GOI cDNA flanked by LoxP sites, a YFP marker and a selectable marker (HX). In absence of rapamycin the GOI (cDNA) is expressed under its promoter. Upon rapamycin induction, the Cre fragments are fused, recover function, and then trigger excision of the floxed GOI cDNA. After gene removal, the YFP cassette is placed under control of the promoter; thus, knockout parasites express YFP. Figure adapted from Dr. Nicole Andenmatten.

1.12 Aim of the study

In order to migrate through tissues and infect host cells, Apicomplexan parasites rely on gliding motility (Sibley, 2010). According to the prevailing model, also called the linear motor model, the acto-MyoA motor complex is responsible for the antero-posterior translocation of transmembrane proteins; hence, this migration is translated into a forward motion (Heintzelman, 2015). Under this premise, the components of the motor machinery are indispensable for parasite motility and invasion. However, the development of the DiCre system permitted the generation of inducible knockouts (e.g. *myoA* KO, *mlc1* KO, and *act1* KO) (Andenmatten et al., 2013, Egarter et al., 2014). Against the prediction of the linear motor model, these mutant parasites remain motile and invasive, which, in case of the *myoA* KO, was explained by possible redundant functions among myosins (Egarter et al., 2014, Frenal et al., 2014). Because of its structural similarities and sharing MLC1, MyoC was suggested to take over MyoA function in the *myoA* KO line (Egarter et al., 2014, Frenal et al., 2014). Indeed, a knockout of the possible complementary myosins, *myoA/B/C* KO, failed to survive *in vitro* culture and showed reduced invasion and gliding rates compared to the *myoA* KO, although these processes were not completely blocked (Egarter et al., 2014, Frenal et al., 2014). Together, these results showed not only that additional compensatory mechanisms exist in the parasite, but also that acto-MyoA motor interactions and functions needed to be revised.

In this study, I explored the functions of the acto-MyoA motor complex by focussing on MyoA and MLC1. First, I aimed to evaluate the functions of MLC1 by characterising the capacity of the conditional *mlc1* KO to complete the lytic cycle. Additionally, I aimed to determine if the function of MyoA could be partially or fully complemented by MyoC by studying differential expression levels of MyoC in both the *myoA* KO and *mlc1* KO. Furthermore, since MyoC and MLC1 have been shown to be able to interact with MyoA and MyoC motor complexes, I directly tested the myosin redundancy hypothesis by characterising parasites simultaneously depleted of MyoB/C and MLC1. Additionally, considering the proposed functions of MyoA, I studied if the absence of MyoA and MLC1 affected formation of actin filaments and the translocation or capping of molecules at the PM. Finally, I examined alternative functions of the acto-MyoA motor complex, and studied another possible system in charge of generating and maintaining force to drive efficient gliding motility.

Aims

- Characterise the functions of MLC1 upon its removal in *T. gondii* tachyzoites
- Determine if redundant functions between MyoA and MyoC drive remaining invasion and gliding rates
- Compare if different expression levels of MyoC can fully recover for MyoA loss
- Observe if actin filament formation depends on MyoA
- Verify the functions of MyoA in terms of force generation
- Study further functions of the acto-MyoA motor complex
- Elucidate a new model for parasite gliding and invasion

2 Materials ad Methods

2.1 Equipment

Table 2-1. Equipment

Applied Biosystems	Real-time PCR light cycler (Prism 7500), MicroAmp® optical 96-well reaction plate, MicroAmp® optical adhesive film
Applied Precision	DeltaVision® Core microscope
BD Biosciences	Syringes, Needles (23-25 gauge), FACS tubes with cell strainer cap
BioRad	Agarose gel electrophoreses equipment, UV transilluminator, SDS-PAGE system, Blotting apparatus (Transblot SD and Mini transblot electrophoretic transfer cell), gel documentation system, gene Pulser Xcell, Micropulser, S3e™ Cell sorter
BTX	Electroporation cuvettes and system (ElectroSquare Pore 830)
Eppendorf	Thermocycler (Mastercycler Epgradient), Thermomixer compact
Fished Scientific	Ultrasound water bath FB15047
GE healthcare	Nitrocellulose membrane (Hybond ECL),
Grant	Water bath
Heraeus Instruments	Incubator
Ibidi	15 µ-Slide 10.8 Luer collagen IV chambers
KD scientific	Syringe pump
Kuehner	Shaking incubator (ISF-1-W)
Li-COR	Odyssey CLx
Lonza	4D-Nucleofactor™X electroporation unit, Single 100 µl Nucleovette™
Milipore	MilliQ water deionising facility, 3 µm Millipore filters
Photometrics	CoolSNAP HQ2CCD camera
Sanyo	CO2- incubator tissue culture
Satorius	Analytical balances
Sciquip	Sigma 6K 15 centrifuge (1150 rotor and 12500 rotor)
StarLab	ErgoOne Single & Multi-Channel pipettes, StarPet Pro pipette controller
Stuart	Heat block, Roller mixer, Orbital Shaker
Thermo scientific	CO2- incubator tissue culture, Nanodrop spectrophotometer, Centrifuge (sorvall legend XFR), Table top centrifuge Heraeus Pico 21, Tabletop cooling centrifuge Heraeus Fresco 21
Zeiss	Axioskop 2 (mot plus) fluorescence microscope with Axiocam MRm CCD camera, Primo Vert (light microscope), Axiovert 40 CFL fluorescence microscope with Axiocam ICc1, Axiovert A1 fluorescence microscope with Axiocam IMc1, ELYRA PS.1 Super-resolution microscope, sCMOS pco SIM camera, Plan Apochromat 63x lens

2.2 Computer Software

Table 2-2. Software

Adobe Systems Inc.	Adobe design premium CS4
AcaClone software	pDraw32
Applied Precision	SoftWoRx explorer and SoftWoRx suite
BioRad	ProSort™
Carl Zeiss Microscopy	Zen Black and Zen blue
CellProfiler	Cell Profiler 2.1.1 Analyst software
CLC Bio	CLC Genomics Workbench 6

GraphPad software Inc.	GraphPad Prism version 7.3
Li-COR	Image Studio 5.0
Microsoft Corporation	Windows 7, Microsoft Office 2010
National Institute for Biotechnology Information (*NCBI)*	Basic Local Alignment search tool (BLAST) (Altschul et al., 1990)
National Institute of Allergy and Infectious Diseases (*NIAID*)	ToxoDB (Gajria et al., 2007)
National Institutes of Health	ImageJ (Schindelin et al., 2015), Fiji (Schindelin et al., 2012)
New England Biolabs (NEB)	NEB tools™: Double Digest Finder, Enzyme Finder, NEBCutter®, NEBBioCalculator®, Tm Calculator
OligoCalc	Oligo Analysis tool (Kibbe, 2007)
PerkinElmer	Volocity 3D Image Analysis Software
Thermo Scientific	Thermo Sientific web tools: Tm Calculator
Thomson Scientific	Endnote X8
University of Utah	ApE Plasmid Editor v2.0.53c Copyright© by M. Wayne Davies

2.3 Consumables, biological and chemical reagent

Table 2-3. Biological and chemical reagents

Clontech	Shield-1
Formedium	Tryptone, yeast extract
Li-COR	Chameleon Duo Pre-stained protein ladder
Life technologies	Phosphate buffered saline 1X (PBS), Trypsin/EDTA (0.05%), PureLink® RNA mini kit, DNaseI, Platinum Taq DNA Polymerase High Fidelity, NuPage SDS loading buffer and reducing agent, Sodium bicarbonate, Ultrapure agarose
Marvel	Milk powder (skimmed)
Melford	Agar, ditriothreitol, IPTG, X-Gal
NEB	DNA ladder (1 kb), All Restriction enzymes and associated buffers, T4 DNA ligase, Taq polymerase, Phusion® and Q5® high-fidelity DNA polymerase, Calf intestinal phosphatase (CIP)
Pheonix Research Products	GelRed nucleic acid stain
Promega	pGEM®-T Easy vectors system
Roche	MgSO4 × 7H2O, potassium hydroxide, paraformaldehyde
Sigma	Ammonium persulfate, Bromophenol blue sodium salt, Casein hydrosylate, Dulbecco's Modified Eagle Medium (DMEM), Ficoll, Ethylene glycol tetraacetic acid, Ponceau S, Isopropanol, Sodium dodecyl sulfate (SDS), dimethyl sulfoxide (DMSO), N,N,N',N'-tetramethylethylenediamine, Triton X-100, Rapamycin, beta mercaptoethanol, Ca++ ionophore (A23187), Tween20, Giemsa stain, RNase-ZAP, L-glutathione reduced, Adenosine 5'-triphosphate disodium salt hydrate, Glutamine, 30% acryl-bisacrylamide mix, Sodium deoxycholate, K2HPO4, Magnesium chloride, Bleomycin (BLEO), Ampicillin sodium salt, Gentamicin, Xanthine, Chlorampehicol (CAT)
Southern Biotech	Fluoromount G (with and without DAPI)
Thermo Scientific	Bovine serum albumin (BSA), Ethylene diamine tetraacetic acid, Glycerol, Glycine, Methanol, Tris, Sodium chloride, 40 nM FluoSpheres® Carboxylate-Modified Microspheres,

	Platinum Taq DNA Polymerase High Fidelity, Restore Western blot stripping buffer
VWR	CaCl2 × 2 H2O, Glacial acetic acid, Ethanol, HEPES, Potassium chloride, Na2HPO4, KH2PO4
Zeiss	Immersion oil

2.4 Kits

Table 2-4. Nucleic acid extraction and amplification kits

Qiagen	Spin Mini-prep, Plasmid Midi-prep, MinElute PCR Purification MinElute, QIAquick gel extraction kit, DNeasy blood and tissue
Roche	PureLink® RNA isolation mini kit, high Pure PCR product purification
Thermo scientific	Maxima SYBR green/ROX qPCR Mater Mix

2.5 Buffers, solutions and media

Table 2-5. Buffers for DNA Analysis

50X TAE buffer	2M Tris, 05M Na2EDTA, 5.71% glacial acetic acid (v/v)
5X loading die	15% Ficoll (v/v), 20 mM EDTA, 0.25% Bromophenol Blue in H2O
NEB 1 kb DNA ladder	150 µl 1kb ladder (1 µg/µl), 300 µl 5X DNA loading buffer, 1050 µl H2O

Table 2-6. Buffers for protein analysis

RIPA buffer	50 mM Tris-HCl (pH 8.0), 150 mM NaCl, 1 mM EDTA, 0.5% sodium deoxycholate, 0.1% SDS (w/v), 1 % triton X-100 (v/v)
4X separating gel buffer	1.5 M Tris-HCl (pH 8.8), 0.4% SDS (w/v)
Separating gel	8-15% of 30% acryl-bisacrylamide, 25% 4X separating gel buffer, 0.1% APS 10% (w/v), 0.2% TEMED (v/v)
4X stacking gel buffer	0.5 M Tris/HCl (pH 6.8), 0.4% SDS (w/v)
Stacking gel	4% of 30% acryl-bisacrylamide, 25% 4X stacking gel buffer (v/v), 0.1% APS 10% (w/v), 0.2% TEMED (v/v)
SDS PAGE running buffer	25 mM Tris, 192 mM glycine, 0.1% SDS (w/v)
Transfer buffer for wet blot	48 mM Tris, 39 mM glycine, 20% methanol (v/v)
Blocking solution	0.2%Tween (v/v), 3% skimmed milk powder (W/v), 0.037 SDS (W/V)
Washing solution or (PBS-Tween)	0.2% tween (v/v) in 1X PBS
1 M DTT	3.085 g 1,4-dithio-DL-threitol (DTT) in 20 ml 10 mM NaAc (pH 5.2)
10 % APS	1 g ammonium persulfate in 10 ml H2O

Table 2-7. Buffers and media for bacterial culture

LB medium	10 g/l tryptone, 5 g/l yeast extract, 5 g/l NaCl
LB agar	1.5% (w/v) agar in LB medium

SOB medium	2% tryptone (w/v), 0.5% yeast extract (w/v), 0.05% NaCl (w/v), 2.5 mM KCl, 10mM MgCl2
SOC medium	20 mM glucose in SOB medium
NYZ broth	5 g/l NaCl, 2 g/l MgSO4*7H20, 5 g/l yeast extract, 10 g/l casein hydrolysate, pH adjusted to 7.5 with NaOH
Ampicillin (1000X)	100 mg/ml in H2O
IPTG (100 µl/petri dish)	100 mM IPTG in H2O
X-Gal (20 µl/petri dish)	50 mg/ml in N,N-dimethylformamide

Table 2-8. Buffers and media for *T. gondii* tachyzoites and mammalian cell culture

$DMEM_{COMPLETE}$	500 ml DMEM, 10 % FCS (v/v), 2 mM glutamine, 20 µg/ml gentamicin
2 x Freezing solution	25 % FCS (v/v), 10 % DMSO (v/v) in $DMEM_{COMPLETE}$
Electroporation buffer (Cytomix)	10 mM K2HPO4/KH2PO4, 25 mM HEPES, 2 mM EGTA pH 7.6, 120 mM KCl, 0.15 mM CaCl2, 5 mM MgCl2 with 5 mM KOH adjusted to pH 7.6, 3 mM ATP, 3 mM GSH
Giemsa staining solution	10 % Giemsa stain (v/v) in H2O
MPA (500X)	12.5 mg/ml in methanol (39 mM)
Bleomycin (4000X)	20 mg/ml in H2O
Rapamycin (1000X)	50 µM in DMSO
Calcium ionophore A23187 (1000X)	20 µM in DMSO
FACS buffer	1 % FCS, 1 mM EDTA in PBS
PFA fixing solution	4 % PFA (w/v) in PBS
Permeabilisation solution	0.2 % triton X-100 (v/v) in PBS
Blocking solution	2 % BSA (w/v) in permeabilisation solution
Hanks' balanced salt solution (HBSS)	5.33 mM potassium chloride, 0.44 mM KH2PO4, 4.17 mM sodium bicarbonate, 138 mM sodium chloride, 0.338 mM Na2HPO4, 1mM EGTA (pH=7.3), 12.5 mM HEPES
Endo buffer	44.7 mM K2SO4, 10 mM Mg2SO4, 106 mM sucrose, 5 mM glucose, 20 mM Tris, 0.3 5% (w/v) BSA, pH 8.2
Gliding buffer	1 mM EGTA, 100 mM HEPES in HBSS

2.6 Antibodies

Table 2-9. Primary antibodies

		Dilution		
Name	Species	IFA	WB	Source
Aldolase	Rabbit	1:2000	1:3000	Sibley, L. D.
AMA-1	Mouse	1:500	(-)	Ward, G.
Catalase	Rabbit	(-)	1:3000	Soldati, D.
GAP40	Rabbit	1:250	(-)	Soldati, D.
GAP45	Rabbit	1:1000	(-)	Soldati, D.
GFP	Mouse	1:500	1:2000	Roche
$Halo^{monoclonal}$	Mouse	(-)	1:1000	Promega

Halo^{polyclonal}	Rabbit	1:500	(-)	Promega
HSP60	Rabbit	1:2000	(-)	Sheiner, L.
IMC1	Mouse	1:1000	(-)	Ward, G.
IMC3	Rat	1:2000	(-)	Gubbels, M.J.
Mic2	Mouse	1:500	(-)	Carruthers, V.
MLC1	Rabbit	1:2000	1:10000	Soldati, D.
MyoA	Rabbit	(-)	1:500	Meissner, M.
RON4	Rabbit	1:5000	(-)	Lebrun, M.
SAG1 (*Toxoplasma*)	Rabbit	1:1000	(-)	ABCAM
TyTag	Mouse	1:10	1:20	Keith Gull

Table 2-10. Secondary antibodies, fluorescent ligands and stains

		Dilution			
Name	Species	IFA	WB	Live-IM	Source
Alexa Fluor350 anti-mouse	Goat	1:3000	(-)	(-)	Life Technologies
Alexa Fluor488 anti-mouse	Goat	1:3000	(-)	(-)	Life Technologies
Alexa Fluor594 anti-mouse	Goat	1:3000	(-)	(-)	Life Technologies
Alexa Fluor633 anti-mouse	Goat	1:3000	(-)	(-)	Life Technologies
Alexa Fluor350 anti-rabbit	Goat	1:3000	(-)	(-)	Life Technologies
Alexa Fluor488 anti-rabbit	Goat	1:3000	(-)	(-)	Life Technologies
Alexa Fluor594 anti-rabbit	Goat	1:3000	(-)	(-)	Life Technologies
Alexa Fluor633 anti-rabbit	Goat	1:3000	(-)	(-)	Life Technologies
Alexa Fluor350 anti-rat	Goat	1:3000	(-)	(-)	Life Technologies
Alexa Fluor488 anti-rat	Goat	1:3000	(-)	(-)	Life Technologies
Alexa Fluor594 anti-rat	Goat	1:3000	(-)	(-)	Life Technologies
IRDye680RD anti-Mouse	Goat	(-)	1:5000	(-)	Li-Cor
IRDye800CW anti-Mouse	Goat	(-)	1:5000	(-)	Li-Cor
IRDye680RDanti-Rabbit	Goat	(-)	1:5000	(-)	Li-Cor
IRDye800CW anti-Rabbit	Goat	(-)	1:5000	(-)	Li-Cor
HaloTag® TMR	N/A	(-)	(-)	1:10000	Promega
Snap-Cell®TMR-Star	N/A	(-)	(-)	1:10000	NEB
Hoechst solution	N/A	(-)	(-)	0.01%	Thermo scientific

2.7 Oligonucleotides

Name	Sequence 5’ → 3’	Enzyme	Purpose
pMyoA Fw	CCGGTACCGCCCGCGAAGCGCCTTTCTCGGATA	KpnI	pMyoATyMyoA
pMyoA Rv	CCCGAATTCTTTGCTTCAGAGAGA GATAACACGAGG	EcoRI	pMyoATyMyoA
MyoB/C locus Fw	TACTTCCAATCCAATTTAATGCCTCCCGCAGTCCGTCAGACGCAATAGATGTTCG		1-1’
MyoB/C locus Rv	TCCTCCACTTCCAATTTTAGCCGGTCTATCCGGCGCACAGGCCTCGAAGC		1-1’
5’integration Fw	GCTATCTCAACGGACAACGACTGCG		2-2’
5’integration Rv	CGTTGTCTCAGACTTTGC		2-2’
3’integration Fw	GCTGCACCACTTCATTATTTCTTCTG		3-3’

3'integration Rv	GCCAGAACCCAAAACTCTCCACTCAGACG		3-3'
MyoC ORF	GCCCTAGGATGGAGCGCAAACAAACCCAGATG	AvrII	
MyoC ORF	GCTTAATTAATCACGGTCTATCCGGCGCACAG	PacI	
pMyoC Fw	CCGGTACCTGCAACTCATGCACACGT	KpnI	pMyoCTyMyoC
pMyoC Rv	GGGCCTAGGGTCAAGTGGATCTTGGTTAGTATGGACCTCCATGGTGAAAAACAGGAAAGAAGGT	AvrII	pMyoCTyMyoC
pMyoC Fw	CCGTTAACTAGCTGGTGACGCTACCGCC	HpaI	TyMyoC-Int1
pMyoC Rv	CCGCGGCCGCaaACTAGTGTCAAGTGGATCTTGGTTAGTATGGACCTCCATGGTGAAAAACAGGAAAG	SpeI NotI	TyMyoC-Int1
5'UTR MyoC Fw	CGGGTACCGCTTCACTGGTTTATCGTGTCACGG	KpnI	TyMyoC-Int2
5'UTR MyoC Rv	GGCTCGAGGGCGGTAGCGTCACCAGCTAG	XhoI	TyMyoC-Int2
TyMyoC Fw	GCACTAGTATGGAGCGCAAACAAACCCAGATGATACTGG	SpeI	TyMyoC-Final
TyMyoC Rv	CCGCGGCCGCATCGATGAAGTGTTTTTGCAG	NotI	TyMyoC-Final
MyoC gRNA Fw	AAGTTGTCGTTCCTTTCGGCCGTGAG	(-)	Cas9-MyoC gRNA
MyoC gRNA Rv	AAAACTCACGGCCGAAAGGAACGACA	(-)	Cas9-MyoC gRNA
5'UTR-Bleo	GCTATCTCAACGGACAACGACTGCG		1-1'
5'UTR-Bleo	CGTTGTCTCAGACTTTGC		1-1'
5'Bleo-MyoC			2-2'
5'Bleo-MyoC			2-2'
3'Ty-MyoC Fw	GGA GGT CCA TAC TAA CCA AGA TCC ACT TGA C		3-3'
3'Ty-MyoC Rv	GGTCCTTGAAGGGGTTGATAGCTACC		3-3'

2.8 Plasmids

Table 2-11. Main plasmids used in this study for cloning and expression in *T. gondii*

Expression vector	Resistance	Reference
p5RT70TyMyoA	Hx	(Meissner et al., 2002b)
pMyoATyMyoA	No selection	This study
pSAG1Bleo	Bleo	(Messina et al., 1995)
P5RT70TyMyoC	No selection	(Andenmatten, unpublished)
pMyoCTyMyoC	No selection	This study
TyMyoC	Bleo	This study
5'UTRMyoCBleo3'UTRMyoC	Bleo	(Egarter et al., 2014)
P5RT70Cas9U6	No selection	(Curt-Varesano et al., 2016)
P5RT70Cas9MyoCgRNA	No selection	This study
P5RT70CbHalo	No selection	(Periz et al., 2017)
P5RT70CbSnap	No selection	(Periz, unpublished)

2.9 Cell strains

2.9.1 Bacteria strains

Bacteria strains used in this study, listed in Table 2-12, were stored at -80ºC.

Table 2-12. *Escherichia coli* competent cells for plasmid transformation

XL10-Gold	Stratagene	Chemically competent
XL1-Blue	Stratagene	Electro competent
DH5α	NEB	Chemically competent

2.9.2 *Toxoplasma gondii* strains

Table 2-13. *Toxoplasma gondii* strains used in this study

Strain	Selectable Marker	Reference
RHΔ*hxgprt*		(Donald and Roos, 1993)
RHΔ*hxgprt* p5RT70TyMyoC	Bleo	This study
RHΔ*hxgprt* ddDrpB$_{DN}$	HX, CAT	(Pieperhoff et al., 2013)
RHΔ*hxgprt* pMyoCTyMyoC	Bleo	This study
RHΔ*ku80*		(Huynh and Carruthers, 2009b)
RHΔ*ku80*TyMyoC	Bleo	This study
loxp*myoA*	HX, DHFR, CAT	(Andenmatten et al., 2013)
myoA KO	HX, DHFR, CAT	(Andenmatten et al., 2013)
myoA KO p5RT70TyMyoC	HX, DHFR, CAT, Bleo	This study
myoA KO pMyoCTyMyoC	HX, DHFR, CAT, Bleo	This study
myoA KOTyMyoC	HX, DHFR, CAT, Bleo	This study
Triple KO	HX, DHFR, CAT, Bleo	(Egarter et al., 2014)
loxp*mlc1*	HX	(Egarter et al., 2014)
loxp*mlc1* pMyoATyMyoA	HX, DHFR, CAT, Bleo	This study
loxp*mlc1*TyMyoC	HX, DHFR, CAT, Bleo	This study
MyoB/CKO loxp*mlc1*	HX, DHFR, CAT, Bleo	This study
loxp*act1*	HX	(Egarter et al., 2014)
mic2 KO	HX	(Andenmatten et al., 2013)

2.9.3 Mammalian cell lines

Tachyzoites were grown in human foreskin fibroblasts (HFFs, purchased from ATCC). HFFs are primary cells with contact inhibition and limited growth (cultured up to passage 23). HFFs were used for maintenance, transfection, subcloning of parasites and phenotypic characterisation of *T gondii*.

2.10 Molecular biology

2.10.1 Isolation of genomic DNA from *T. gondii*

The extraction of genomic DNA (gDNA) was performed using the DNeasy® blood & tissue Kit. Parasites were collected either from the media when freshly egressed or from heavily infected cells by scratching and syringing through a 25-gauge needle. In both cases,

extracellular parasites were pelleted by centrifugation (600 g for 5 min), and resuspended in 200 µl of PBS1X. gDNA extraction was accomplished by following the protocol described by the manufacturer with a final elution in 100 µl H2O.

2.10.2 RNA extraction, cDNA precipitation and qPCR techniques

Approximately $2x10^7$ parasites were used for RNA extraction, this number of parasites were collected from a heavily infected culture of around 36 hours post inoculation. These parasites were pelleted by 600 g centrifugation for 5 min at 4ºC and kept on ice all the time. Total RNA was isolated using the PureLink® RNA mini kit following the manufacturer's specifications. Prior manipulation of the samples and RNA extraction all the equipment was cleaned using RNase-ZAP. The integrity of the RNA material was evaluated by measuring the concentration using a nanodrop spectrophotometer and running an agarose gel (app. 6ng per lane). In the gel, separation of the 28S and 18S bands can be observed after 10-15 min at 100V (Aranda et al., 2012).

1 µg of total RNA was used as template to synthetize cDNA using the reverse transcriptase SuperScript™ III kit (Invitrogen©). Samples were prepared with the manufacturer's specifications; then, amplification of the reaction was performed with an initial incubation at 25ºC for 10 min, followed by 50ºC for 15 min, and 85ºC for 5 min to terminate the reaction.

The Maxima® SYBR Green/ROX qPCR master mix (Thermo scientific) was prepared in duplicate per each sample, containing a negative control to discard contamination of the mix components or DNA material. All the reactions were set up in MicroAmp® optical 96-well reaction plates and sealed with MicroAmp® optical adhesive films. The samples were run and analysed in the Prism 7500 thermocycler (Applied Biosystems) using the default thermic profile settings for standard samples (Table 2-15). Primer efficiency and analysis were performed by Dr Nicole Andenmatten.

Table 2-14. qPCR master mix

Component	Volume (µl)
Maxima SYBR® green (2X)	6.25
Fw primer	0.5
Rv primer	0.5
Nuclease free H2O	4.25
Template [50ng]	1

Table 2-15. qPCR thermic profile

Temperature	Time	Cycles
50ºC	2 min	
95ºC	10 min	
95ºC	15 sec	x40
60ºC	1 min	

2.10.3 Polymerase chain reaction

During this study, PCR was used mainly to amplify DNA fragments for molecular cloning, colony screening in transformed bacteria and controlling correct insertion of the different plasmids stabilised in tachyzoites.

For molecular cloning, high fidelity polymerases were used because they contain proof-reading activity, which reduces the error rate during amplification. Platinum® Taq DNA polymerase high fidelity (Invitrogen) by preference in this study. The mix preparation and thermic profiles were followed under the manufacturer's specification. These details are listed in Table 2-16 and Table 2-17.

Table 2-16. Platinum® Taq reaction

Component	Volume (µl)
10X high fidelity PCR buffer	2.5
50mM $MgSO_4$	1
10mM dNTP Mix	0.5
10 µM Fw primer	0.5
10 µM Rv primer	0.5
Platinum® Taq DNA pol	0.1
Template (10-50 ng)	1
H_2O	To 25

Table 2-17. Platinum® Taq amplification thermic profile

Temperature	Time	Cycles
94ºC	30 sec	
94ºC	15 sec	X30
55ºC-68ºC*	30 sec	
68ºC	1 min/kb^	
68ºC	5 min	
4ºC	indefinitely	

(*) Calculated based on primers Tm
(^) Calculated based on amplicon size

Taq DNA polymerase (NEB) was used to amplify products for colony screening and analytical purposes. PCR reaction and thermal cycler conditions are detailed in Table 2-18 and Table 2-19.

Table 2-18. Taq DNA polymerase PCR reaction

Component	Volume (µl)
10X ThermoPol buffer	2.5
10mM dNTP Mix	0.5
10 µM Fw primer	0.5
10 µM Rv primer	0.5
Platinum® Taq DNA pol	0.125
Template (>1000 ng)	1
H_2O	To 25

Table 2-19. Taq DNA polymerase thermic profile

Temperature	Time	Cycles
95ºC	30 sec	
95ºC	30 sec	X30
45ºC-68ºC*	60 sec	
68ºC	1 min/kb^	
68ºC	5 min	
4ºC	indefinitely	

(*) Calculated based on primers Tm

(^) Calculated based on amplicon size

2.10.4 Agarose gel electrophoresis

Agarose gel electrophoresis was used to separate DNA fragments and amplicons (Lee et al., 2012). Gels were prepared diluting agarose (0.8 - 2%) in 1XTAE (W/V) by boiling in a microwave; after completely dissolved, 0.01% GelRed was added to visualise the bands. 6X DNA loading buffer was added to the samples before loading in the pre-casted gel; also, 5 µl 1kb DNA ladder (NEB) was used to reference the size and concentration of the sample in the gel. Loaded agarose gels were run in an electrophoresis chamber filled with 1X TAE for around 1 hour at 80-120 V. The DNA was visualised using a UV transilluminator.

2.10.5 Restriction endonuclease digest

Restriction endonuclease mediated digestion was used in this study for molecular cloning, verification of plasmids and linearization of constructs prior transfection. For

molecular cloning, 2 µg of PCR products or 0.5 µg of plasmids were digested with the appropriated restriction enzymes following specifications of the manufacturer. Diagnostic digestions were performed in DNA plasmids; for this, 100 ng of DNA was digested using the necessary enzymes following the manufacturer's protocol.

Before transfection, the plasmids of interest were linearized with a single cutting enzyme; also, certain plasmids were double cut to dispose of the backbone. For transfections in BioRad© electroporator, 60 µg of the plasmid of interest was digested; in the case of co-transfections, 30 µg of the linearized selectable marker construct was included. For Amaxa© transfections, 20 µg the plasmid of interest was digested following manufacturer's directions.

For all reactions, the digestions were incubated at 37ºC for 3 hours in a water bath. To note, all enzymes used in this study were ordered at NEB.

2.10.6 Dephosphorylation of digested DNA plasmids

Alkaline calf intestinal phosphatase (CIP) was added to the DNA plasmids after restriction enzyme digestion. This enzyme mediates the dephosphorylation of the 5' end DNA, preventing the re-ligation of the backbone. Incubation of 10 U/µl (0.5 µl) of CIP with the sample at 37ºC for 1 hour is enough to treat the plasmids before purification.

2.10.7 Purification of DNA

Purification of DNA backbones and inserts was performed using the QiAquick gel Extraction kit and the MinElute DNA extraction kit (Qiagen©), respectively.

For the backbone purification, QiAquick gel Extraction kit was used to isolate DNA bands form agarose gels. The desired band was cut from the agarose gel using a sterile scalpel blade over a UV transilluminator. The piece of agarose containing the band was weighed, and extracted following the specifications of the manufacturer. DNA inserts that did not need to be separated were directly purified and eluted from silica spin columns supplied in the MinElute DNA extraction kit following manufacturer's protocol. The presence and correct purification of the bands were analysed by running an agarose gel.

2.10.8 Determination of nucleic acid concentrations

The concentration of plasmid DNA, DNA fragments, amplicons and RNA was determined using a nanodrop spectrophotometer adjusted at 260 nm absorbance.

2.10.9 Ligation of DNA fragments

DNA ligase are widely used to catalyse the formation of covalent bonds between two DNA fragments; thus, joining insert and plasmid.

Before ligation into a backbone of interest, some inserts were cloned into pGEM® T-easy, a standard bacterial vector, that harbours T-overhangs, and join inserts containing 3' poly-A tails. This reaction was performed mixing 1 µl of the insert and 1 µl pGEM® in presence of 2X rapid ligation buffer and ligase. Samples were incubated at room temperature for 1 hour.

Ligations of backbones and inserts of interest were performed using T4 DNA ligase (NEB®). The reaction was performed by mixing the backbone and the insert at a molar ratio of 1:1, 1:3 and 1:5. T4 DNA ligase Buffer, T4 DNA Ligase and H_2O were added, and adjusted to a final volume of 10 µl. Ligations were incubated overnight at room temperature. After this time, the reaction was verified by running 2 µl of the mix in an agarose gel.

2.10.10 Plasmid transformation into bacteria

Ligated plasmids were amplified using chemically competent *E. coli*. Bacterial recipients were thawed on ice, 50 µl of bacteria were mixed with 5 µl of the ligation reaction and incubated together for 30 min. Following, bacteria were heat shocked at 42ºC for 30 sec, and returned to ice for 2 min. 450 µl of NZY rich broth was added to the cells, and incubated at 37ºC for one hour shaking. After this time, bacteria were plated on LB-ampicillin agar plates, and incubated at 37ºC overnight. Colony PCR was performed next day as described in section 2.10.3. using primers specifically designed for binding outside and inside the insertion. Colonies containing the plasmid of interest were cultured in LB broth at 37ºC overnight shaking.

2.10.11 Isolation of plasmid DNA from bacteria

To extract plasmid DNA from bacteria, overnight grown cultures were pelleted by centrifugation. Following, the pellet was resuspended and lysed in alkaline detergents containing NaOH and SDS aimed to destabilise the bacterial cell wall, nucleases, and denature DNA material. The latter convert gDNA and plasmid DNA from double stranded DNA (dsDNA) to single stranded DNA (ssDNA). Alkaline mediated lysis was later controlled by adding potassium acetate containing solution; thus, permitting reestablishment of dsDNA. The small size of plasmid DNA facilitates its re-naturation from ssDNA to DsDNA unlike gDNA. Separation of gDNA and proteins from plasmid DNA can be achieved by ultracentrifugation since dsDNA dissolve easily in solution. From this point, plasmid DNA was purified by either ethanol precipitation or silica columns provided in QiAprep spin Miniprep and Midiprep kits (Qiagen®).

2.10.11.1 Small scale DNA plasmid extraction

Subcloning of intermediate constructs require relatively small amounts of DNA plasmid yields. For this, colonies containing the plasmid of interest were grown overnight in 4 ml of LB broth shaking. After this time, cells were pelleted and DNA was extracted using QIAprep spin Miniprep kit (Qiagen®) following the manufacturer's protocol. The DNA material was eluted in a final volume of 50 µl in ddH_2O, yielding around 5-20 µg of plasmid.

2.10.11.2 Medium and large scale DNA plasmid extraction

Final vectors require large amount of DNA concentration for further transfection, for this reason, cells containing the plasmid of interest were grown overnight in 50 ml LB broth shaking. Bacteria were pelleted by centrifugation; next, plasmid DNA was extracted by following QIAprep spin Miniprep kit (Qiagen®) specifications. This protocol yields between 50 and 300 µg of plasmid DNA diluted in a final volume of 50 µl in ddH_2O.

Ethanol was also used for obtaining large amounts of plasmid DNA. Here, the construct of interest was precipitated after separation step (section 2.10.11) by adding ethanol 100%. The precipitation was facilitated by keeping the mix at -80ºC for 30 min or -20ºC overnight. DNA and ethanol 100% were separated by ultracentrifugation, followed by one washing step with ethanol 70%. Finally, plasmid DNA was eluted in 100 µl ddH_2O yielding around 500 µg to 1 mg of DNA material.

2.10.12 DNA sequencing

DNA sequencing was used to verify the integrity of inserts and final vectors prior transfection. DNA samples were prepared under specifications of GATC© Biotech (sanger sequencing) in a final volume of 10 µl containing 5 µl of purified DNA [80-100 ng/µl], and 5 µl of primer [5 pmol/µl].

2.10.13 RNA sequencing

RNA sequencing was performed at the Glasgow polyomics facility. Samples were run on the Ion torrent PGM TM (Life technologies). The reads were analysed single ended with a fragment size of 200 to 400 bps. The differential expression between conditions was calculated by qualification of the reads and normalised based on the gene size within the genome. Transcriptome and heat maps were analysed and generated by Dr. Nicholas Dickens.

2.10.13.1 Quality control (Fast QC)

The reads were inspected in various quality metrics, which reported the information of visualisation. This process considered the total reads, obtained for all sequences, generated from the initial sample. Phred score indicated the accuracy of the read. Here, 20 phred score demonstrated 99% of accuracy of the read. This was taken as the base line for base-accuracy. Considering each read base-accuracy, the quality of the fragment was then summarised as the per-sequence quality score.

2.10.13.2 Trimming

Reads containing low base-accuracy were trimmed or removed from the sample. Removing deletes the whole read, whereas, trimming removes only the low-quality ends of the reads. For instance, adapter sequences or any base pair in the ends of the sequence with low score (Phred >20%) were trimmed, leaving 100 bps long sequences. This process was performed using FastX quality trimmer (HannonLab). By this point, a second FastQC was run in order to analyse the quality of the sequences again.

2.10.13.3 Reads alignment to reference genome

Hisat uses a multitep process which start by aligning all the sequences to the genome of interest (Kim et al., 2015). This program was used to align the trimmed sequences to the

genome of interest, in this study all annotation references were taken from ToxoDB (Gajria et al., 2007). Then, transcriptome alignment, genomic alignment and spliced alignment were annotated and mapped. The aligned reads were indexed using SAM tools suite (Li et al., 2009).

2.10.13.4 Abundance calculation

After alignment and annotation, the reads abundance was quantified using Cuffquant (Cufflinks). This program starts by creating a graphic, which parsimoniously explain the obtained data. The quantification abundance was output as fragment per kilobase per million mapped reads (FPKM), which is used to correct the number of reads in terms of library size and transcript length (Korpelainen et al., 2014). From here the data produced become a table containing the annotation and the reads counts (FPKM).

2.10.13.5 Differential expression analysis

The standard normalisation method was used to diminish the possible differences in read abundance and transcriptome composition caused by sampling variability. Next, Cuffdiff (Cufflinks) (Trapnell et al., 2012) was used to calculate the abundance of transcripts and to compare the expression of the genes. The samples (in replicas) were analysed in base of the normalised dataset.

2.10.13.6 Analysis of gene expression

The output of the combination performed in Cuffdiff was directly load in R (CummeRbound) (Galaxy Biostarts). This program was used to analyse the fold change of the reads over the different conditions. The outcome of selected genes was visualised in a heatmap displaying the expression value of the genes of interest. The graphic contained the conditions (strains) in columns and the genes of interest in rows. Each condition was represented with one square that is coloured according its fold change (Korpelainen et al., 2014).

2.10.14 Cloning performed in this study

The vector maps and cloning strategies are illustrated in Figure 2-1 and Figure 2-2.

The parental strain p5RT70TyMyoA was used to generate the plasmid pMyoATyMyoA. Briefly, p5RT70 was excised and replace for pMyoA via KpnI and EcoRI. This plasmid was cotransfected with pSAG1BleoSag1 vector (Figure 2-1).

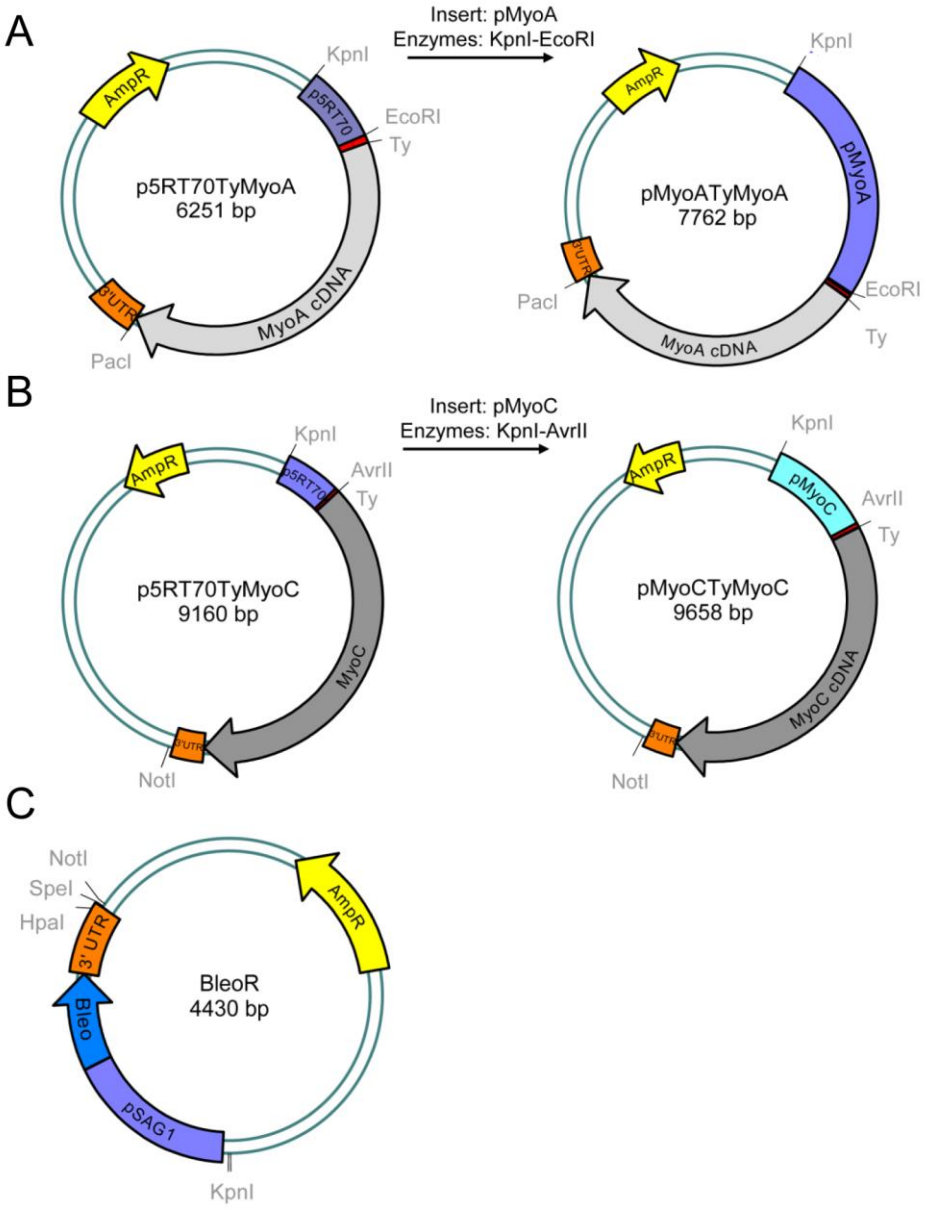

Figure 2-1. Plasmid maps, cloning and transfection strategy of pMyoATyMyoA and pMyoCTyMyoC
A. pMyoA was cloned into pP5RT70TyMyoA expression vector using KpnI and EcoRI restriction sites **B.** pMyoC was cloned into pP5RT70TyMyoC expression vector using KpnI and AvrII restriction sites. The selectable marker pSAG1Bleo was co-transfected using REMI (NotI) (C) Selectable marker pSAG1Bleo was cotransfected using REMI (KpnI). All plasmids were checked by sequencing

MyoC overexpression vectors were generated from the parental plasmid p5RT70TyKillerRed. MyoC cDNA was placed under p5RT70Ty via AvrII and PacI. This plasmid was expressed and used as template for the pMyoCTyMyoC vector, where pMyoC was cloned upstream TyMyoC ORF via KpnI and AvrII (Figure 2-1).

The endogenous tagging MyoC vector, 5'UTRMyoCpSagBleo3'Sag1pMyoCTy*myoC*$_{gene}$, (abbreviated from here as TyMyoC) was generated from the parental strain pSAG1BleoSag1 (Messina et al., 1995). First (TyMyoC-Int1), pMyoC was obtained by amplification of a 1 kb fragment upstream of *myoC* start codon using HpaI and NotI. Second (TyMyoC-Int2), 5'UTR MyoC, was obtained by amplifying a 1.5 kb region located 1 kb upstream of the *myoC* start codon and cloned via Kpn1 and XhoI. Third (TyMyoC-Int3), MyoC$_{gene}$ corresponds to a 2.2 kb fragment of 5' *myoC* genomic sequence. This insert was cloned using enzymes SpeI/NotI. The resulting plasmid (TyMyoC-Int1) was cut via EcoRI to excise a one-point mutation generated during cloning. The final plasmid (TyMyoC-Final) contains the first 500 bp of 5'*myoC* genomic sequence to mediate crossover. To facilitate insertion of the plasmid, this was cotransfected with p5RT70Cas9CRISPR::sgMyoC (Cas9MyoCgRNA) that was generated from the parental p5RT70Cas9CRISPR::sg (Curt-Varesano et al., 2016). MyoC gRNA was cloned using the golden gate strategy via BsaI (Figure 2-2).

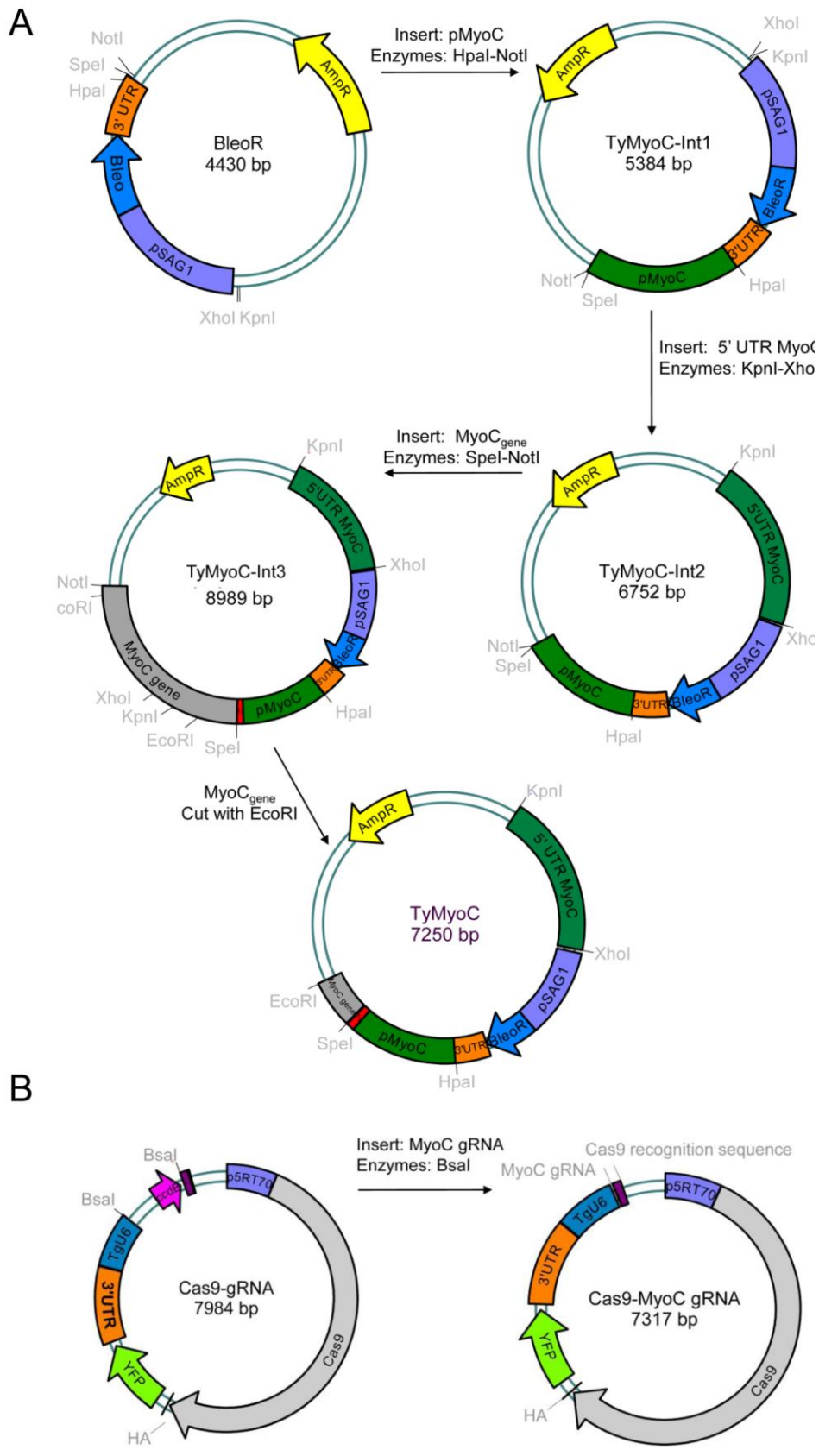

Figure 2-2. Plasmid maps, cloning and transfection strategy of endogenous tagging MyoC vector (TyMyoC)

A. TyMyoC vector was generated from three intermediate vectors. pMyoC was first inserted via HpaI-NotI into the parental vector pSAG1Bleo. Following, 5'UTRMyoC was inserted upstream pSAG1Bleo cassette via XpnI-KpnI. Next, a 2.2Kb *myoC* 5' genomic sequence was inserted via SpeI-NotI. EcoRI was used to cut the latter fragment to avoid a point mutation generated during cloning. TyMyoC final vector contains a 500 bp *myoC* genomic sequence **B.** p5RT70Cas9CRISPR containing a MyoC

specific gRNA to facilitate integration of the plasmid. MyoC gRNA was cloned via BsaI using gold gateway strategy (Weber et al., 2011). All plasmids were checked by sequencing

2.10.15 Ethanol precipitation

Verified and purified final vectors were precipitated using ethanol prior transfection. For this, plasmid DNA was mixed with 1/10 of its volume of 3M sodium acetate (pH 5.2), and 3 volumes of ice-cold 100% ethanol. Plasmids were precipitated by centrifugation at 13,000 rom at 4ºC for 30 min, followed by two washes with 70% ethanol aimed to remove salts. Ethanol was discarded and the pellet was air-dried before resuspending in either cytomix or P3 buffer, depending on the electroporator used (BioRad©) or (Amaxa©), respectively.

2.11 Cell biology

2.11.1 *Toxoplasma gondii* tachyzoites and mammalian cells *in vitro* culturing

Toxoplasma gondii tachyzoites were grown and maintained in human foreskin fibroblast monolayer (HFF). HFF cells were maintained in Dulbecco's modified Eagle's medium (DMEM), supplemented with 10 % fetal bovine serum (FBS), 4 mM L-Glutamine and 10 µg/ml gentamycin. Incubation conditions were considered 37°C, 5% CO_2. For culture maintenance, extracellular tachyzoites were inoculated to fresh confluent HFF monolayers. In cases where the line presented an egress defect, intracellular parasites were mechanically released by scratching and syringing through 25-gauge needle three times prior inoculation. The volume of parasites passaged varied according the maintenance or experiment to perform. Host cells were passaged in a dilution of 1:4 once a week to new flasks.

2.11.2 Trypsin/EDTA treatment of mammalian cell lines

Before passing, mammalian host cells were washed three times with 1XPBS to remove all residual media. Following, host cells were detached from the bottom of the culturing flask by covering all the monolayer with trypsin/EDTA. Enzymatic reaction was proceeded at 37ºC for 5 min; then, flasks were gently tapped to mechanically facilitate detachment. The reaction was stopped by adding $DMEM_{COMPLETE}$ to a volume 1:4 to pass the cells to new containers.

2.11.3 Cryopreservation of *T. gondii* and thawing of stabilates

For preservation of parasites, the media of a heavily infected culture was exchanged for 900 µl of fresh media. Cells were gently scratched using a cell scraper, and the suspension was transferred to a 2 ml cryotube. 900 µl of freezing media (Table 2-8) were added to the parasite suspension. Tubes were left overnight at -20ºC; then, they were transferred to -80ºC freezer where they were stored for several weeks. For long term preservation, cryotubes were stored in liquid nitrogen. Similarly, confluent monolayers were detached, resuspended in 900 µl of fresh media and pelleted by centrifugation (200 g for 5 min). Supernatant was exchanged by 900ul of fresh media and 900 µl of freezing media. The process of freezing was followed as described for parasites.

Frozen stabilates or host cells were reanimated by thawing the content of the cryotubes at 37ºC. Following, cells were resuspended in 4 ml of pre-warmed media. Tachyzoites were added to confluent host cells overnight in culture conditions. After this time, media containing residues of freezing media was changed for fresh $DMEM_{COMPLETE}$.

2.11.4 Transfection of *T. gondii*

Exogenous DNA was expressed in tachyzoites in transient or stable manner. Transfection of plasmids was performed by electroporation (Soldati and Boothroyd, 1993) using either BioRad or Amaxa electroporators. Both systems have similar principle, but require different buffers and DNA concentrations for transfections. BioRad uses homemade buffer cytomix (Table 2-8) that resembles intracellular ionic composition, this buffer was used to dilute both DNA and parasites before transfection. Transfection in BioRad equipment using cytomix buffer yields up to 30% transfection efficiency. In contrast, Amaxa® nucleofactor works with commercially available buffer P3 that is used to dilute parasite and plasmids, but yields up to 90% transfection efficiency. Since both electroporators were used along this study, the transfection mixes of BioRad and Amaxa are listed in Table 2-20.

Table 2-20. Transfection mix for transfection

BioRad©(Cytomix)			Amaxa® (buffer P3)		
	[Concentration]	Volume		[Concentration]	Volume
Precipitated plasmid	[60 µg]	100 µl	Precipitated plasmid	[30 µl]	50 µl
ATP	[100 mM]	30 µl	Parasites	(app. $1x10^5$)	50 µl
GSH	[100 mM]	30 µl	Final volume	(-)	100 µl

Parasites	(app. $1x10^7$)	640 µl		
Final volume	(-)	800 µl		
Cuvette BioRad©	4mm		Cuvette Nucleovette™	100 µl
Program	Square wave		Program	Lonza® F158
Voltage	1700 V			
Pulse	200 µs			
Pulse number	2			
Interval	5 ms			

2.11.4.1 Transient transfections

Transient transfection is a useful and fast technique designed to introduce and express circular exogenous DNA. However, since it is not integrated into the genome, the extrachromosomal DNA is not replicated; consequently, lost over cell divisions (Suarez et al., 2017). Transient transfections were performed by electroporation (section 2.11.4) (Soldati and Boothroyd, 1993) preferably using Amaxa® equipment to achieve high transfection efficiency; following, parasites were inoculated onto HFFs grown on coverslips and incubated between 24 and 72 hours prior to fixation and analysis.

2.11.4.2 Stable transfection

In many protozoans, such Kinetoplastids, integration of foreign DNA occurs by homologous recombination, requiring a short homology sequence to be targeted into a specific locus. In contrast, only 5-10% of integration in *T. gondii* happens by homologous recombination; hence, exogenous DNA is majorly randomly integrated in the genome (Donald and Roos, 1993). The presence of Ku80 has a pivotal role in non-homologous end joining DNA repair (Huynh and Carruthers, 2009b).

In tachyzoites, random integration (i.e. overexpression vectors) was performed by using linearized plasmid DNA [20-60 µg] (Table 2-20). In case plasmid DNA did not contained a selectable marker, 60 µg of linearized plasmid DNA was co-transfected with a 30 µg of the selectable marker linearized plasmid (section 2.10.5). In both cases, DNA was transfected as described in section 2.11.4. Restriction enzyme mediated insertion (REMI) was used to increase the transfection efficiency; to perform this procedure, 10 units of restriction enzyme used for linearization were added to the transfection mix before electroporation (Black et al., 1995). REMI activates DNA repair machinery, resulting in

elevated recombination events; indeed, NotI was reported to increase 400 fold the transfection efficiency (Black et al., 1995).

Homologous recombination is necessary to target plasmids (i.e endogenous tagging or knockout) to specific locus. In order to target specific locus, Ku80 was depleted (ΔKu80), which dramatically increased gene targeting for both endogenous tagging and gene replacement (Fox et al., 2009, Huynh and Carruthers, 2009a). Similarly, CRISPR-cas9 containing specific gRNAs plasmids can be transiently expressed with the plasmid of interest to target the edition machinery to a specific locus (Shen et al., 2014a, Sidik et al., 2014). After edition, the plasmid of interest act as a donor vector containing homology arms to facilitate correct integration (Shen et al., 2014a, Sidik et al., 2014).

In this study, homologous recombination was performed using 60 µg of plasmid DNA linearized at both ends of the DNA cassette to dispose of the backbone. Endogenous tagging was achieved by co-transfecting 60 µg of the plasmid of interest with 20 µg of gRNA-specific CRISPR/Cas9 vector. Following, transfection was performed as described in section 2.11.4 without the addition of restriction enzyme to the transfection mixture.

2.11.4.3 Drug mediated positive selection

Drug selection is a widely used strategy to separate parasites expressing a plasmid of interest over non-expressers. There are numerous markers available such as: chloramphenicol acetyl transferase (CAT) that is selected with Chloramphenicol (Kim et al., 1993), dihydrofolate reductase-thymidylate synthase allele (DHFR-TD) that is selected with pyrimethamine (Donald and Roos, 1993), HXGPRT that is selected with mycophenolic acid and xanthine (Donald et al., 1996), and *Tn5 ble* that is selected with phleomycin (*a.k.a.* Bleomycin) (Messina *et al.*, 1995).

Along this study bleomycin (Bleo) was the only selection drug used to positively select parasites. This marker is able to intercalate into the DNA and cause irreparable DNA lesions that inhibit the cells growth (Gatignol et al., 1987). Toxicity of bleomycin is neutralised by the action of BLE protein which from a 1:1 complex with the drug; thus, inhibiting its activity (Gatignol et al., 1987). Three distinct BLE proteins have been isolated *Sh ble*, *Sa ble*, *Tn5 ble*. The latter was cloned and successfully expressed in *T. gondii* making it a functional and efficient selectable marker (Messina et al., 1995).

Bleo selection in *T. gondii* tachyzoites is achieved in four different sets of administration with two distinct concentrations 50 µg/ml and 5µg/ml in $DMEM_{COMPLETE}$ (pH 7.6). DMEM-Bleo 5 and 50 µg/ml were prepared at least one day in advance, and left in the incubator with loose cap to maintain pH. The first set of administration was performed just 48 hours after electroporation. Here, parasites were mechanically egressed, pelleted and resuspended in 1 ml of DMEM-Bleo [50 µg/ml], and left in the incubator for four hours. After this time, parasites were pelleted at 1500 g for 5 min, and washed twice in PBS. Following, the parasites were resuspended in DMEM-Bleo [5 µg/ml] and added to fresh confluent host cells. The second set of Bleo selection was maintained for around 10-15 days after transfection, constantly changing host cells since monolayer is partially affected by Bleo. The third set of administration was done in extracellular parasites that survived selection in similar conditions as the first administration. Finally, the fourth set of administration was maintained during subcloning by limiting dilution in 96-well plates (section 2.11.5) in DMEM-Bleo [5 µg/ml].

2.11.5 Isolation of clonal parasite lines by limited dilution

After selection, integration of the plasmids in the genome varied in number; thus, the resulting in parasite mixed populations. To obtain homogenous populations, clonal parasite lines containing the plasmid of interest were isolated by limited dilution in 96-well plates containing HFFs monolayers.

Here, 50 µl of extracellular parasites were added to the first well (A1) of the plate followed by seven successive 1:4 dilutions in the first column of the plate (B1 to H1). Then, 11 successive 1:4 dilutions from left to right in each row (2 to 12) using a multichannel pipette in a final volume of 150 µl. The plates were incubated from 7-14 days at normal growth conditions (37 °C, 5 % CO_2), without disturbance. Finally, the plate was inspected for wells containing only one plaque in the monolayer, meaning plaque was originated from a single parasite that engaged several rounds of the lytic cycle. These parasites were then selected and analysed.

2.11.6 Induction and maintenance of DiCre conditional mutants

Conditional DiCre mutant lines were induced for four hours using rapamycin 50 nM to the parental loxp strain. Rapamycin was used to reconstitute the Cre recombinase domains; therefore, mediating the excision of the GOI. For obtaining fresh *myoA* KO lines,

loxp*myoA* line was induced for four hours with rapamycin, then the population was subcloned by limited dilution, in a similar process as described in section 2.11.5. Since this strain is able to survive *in vitro* (Andenmatten et al., 2013), the parasites were kept in constant culture with extra care since they grow slower than control strains (RHΔ*hxgprt* or loxp). In contrast, *act1* KO, *mlc1* KO and triple KO cannot survive in culture for long periods for its detrimental egress defect (Egarter et al., 2014). To reduce the outgrowth of unexcised parasites in these cultures, dextran sulfate 2.5 % in $DMEM_{COMPLETE}$ (DS-media) was added in order to inhibit reinvasion of egressing parasites (unexcised) (Coleman and Gubbels, 2012). Before releasing mutants with egress defect, DS-media was removed from the dish and washed three times with $DMEM_{COMPLETE}$. This process was repeated every 36 hours.

2.12 Tachyzoite phenotypic analysis

2.12.1 Immunofluorescence assay

Infected HFF monolayers or extracellular parasites were fixed in 4% paraformaldehyde for 20 min at room temperature, and washed once with PBS. Next, coverslips containing parasites were blocked for 30 min in either non-permeabilising (2% BSA in 1X PBS) or permeabilising (0.2% triton X-100, 2% BSA in 1X PBS) conditions. Primary antibodies (20µl) were incubated for 1 hour on blocking buffer on a wet chamber (petri dish containing humid absorbent towel papers) followed by 4 washes with the respective blocking solution for five min. Secondary antibodies were incubated for 40 min in blocking buffer, followed by four washes as previously described. Finally, coverslips were fixed using Fluoromount™ (with or without DAPI). All procedures were performed at room temperature.

2.12.2 Plaque assay

$1x10^3$ parasites were seeded on confluent HFF monolayers previously grown in 6-well plates. The plates were incubated at 37°C, 5% CO2 for 5-7 days. After this time, monolayers were gently washed once in PBS and fixed with cold methanol or PFA 4% for 20 min. Fixative was washed, and cultures were stained with Giemsa (1:10 in H2O) for 45 min, and washed three times on PBS. Images were acquired using Axiovert 40 fluorescence microscope with Axiocam. The size of each plaque was measured using ImageJ software and normalized to the appropriate control.

2.12.3 Trail deposition assay

Trail deposition assay was used to examine 2D motility gliding by detecting surface proteins that are deposited by the parasites while gliding (Dobrowolski and Sibley, 1996). Glass coverslips were incubated with 100 % fetal bovine serum (FBS/ H_2O) for 2 hours. Before used, FBS was removed and coverslips were washed three times in PBS. 2 X 10^6 freshly lysed parasites or mechanically egressed parasites were washed in pre-warmed PBS once, and resuspended in 500 µl in pre-warmed gliding buffer. Parasites were incubated at room temperature for 15 min, then at 37°C, 5% CO_2 for 30 min. Coverslips were fixed in 4% paraformaldehyde for 20 min. Visualization of the trails was achieved by using αSAG1-Alexa Fluor 594 antibodies. Assays were analyzed in triplicate, three times. 400 parasites were counted and gliding rate was assessed.

2.12.4 Synchronised invasion assay

T. gondii invasion was assayed using the synchronised "red/green" or invasion assay (Huynh and Carruthers, 2006). For this experiment, $5x10^6$ parasites were inoculated on HFFs, and brought to the monolayer by centrifugation at 200 g for 2 min. Infection was allowed at standard culture conditions for 15 min prior fixation. IFA was performed by labelling extracellular and intracellular parasites using green and red fluorochromes before and after host cell permeabilization, respectively. Here, extracellular parasites were labelled with αSAG1-red and intracellular parasites were labelled using αIMC1-green, resulting in dual labelled sample. Parasites contained in 10 fields of view (100X objective) were counted and analysed as a percentage of RHΔ*hxgprt*.

2.12.5 Replication assay

1×10^5 tachyzoites were inoculated onto HFF monolayers previously grown on 24-well plates containing glass coverslips. Infection was allowed under normal growth conditions for 1 hour; after this time, coverslips were washed in PBS to remove extracellular parasites and therefore synchronise replication. Parasites were allowed to replicate under standard culturing conditions for 24 hours prior fixation (Kremer et al., 2013). Samples were labelled using αIMC1-red; following, 100 vacuoles were counted, and categorise by number of parasites contained in each vacuole (2, 4, 8, 16, >32). Numbers were expressed as percentage. Assays were done in triplicate in three independent experiments.

2.12.6 Apicoplast maintenance

To investigate if apicoplast maintenance is affected by the absence of MLC1, parasites were allowed to replicate for 24 hours as described in section 2.12.5 at 0, 24, 48, 72 and 96 hours post induction. Fixation and IFA were conducted as described in section 2.12.1. Visualisation of apicoplast was achieved by immunostaining using αHSP60 kindly provided by Dr Sheiner. Ratio 1 apicoplast per parasite was considered correct. 100 vacuoles per experiment were counted.

2.12.7 Ionophore- induced egress

The ability of parasites to egress the host cell was assayed with Ca^{++} ionophore (A23187) (Black et al., 2000). To note, *mlc1* KO parasites were assayed from 96 hours after rapamycin induction. For this experiment, $2.5X10^4$ freshly lysed or mechanically egressed parasites were seeded on HFF monolayers on coverslips, and incubated for 36 hrs at standard culturing conditions. To induce artificial egress, media was exchanged for serum free DMEM containing 2 µM Ca^{++} ionophore (A23187). After 10 min, infected cells were fixed and stained with αSAG1 antibodies. 200 vacuoles were counted in each assay, experiments were analysed in triplicate, three times.

2.12.8 Ionophore- induced PV permeabilization

To analyse if parasites were able to permeabilize the PV, 36 hours infected HFF monolayers were treated and fixed as described in section 2.12.7 (Kafsack et al., 2009). Following, an IFA in non-permeabilising conditions was performed using αSAG1 antibodies. Permeabilisation was analysed by presence or absence of signal in vacuoles (intracellular).

2.12.9 Time-lapse video microscopy

This microscopy technique was used to analyse 2D gliding, penetration and egress kinetics of mutant parasites. (Håkansson et al., 1999). All experiments were performed in glass bottom live cell dishes (Ibidi µ-dish$^{35mm\text{-}high}$). These assays were carried out in a DeltaVision® Core microscope, equipped with a temperature and gas control chamber which was used to maintain culture conditions (37ºC and supplying 5% CO_2). Obtained videos were analysed using SoftWoRx® or Fiji software.

2.12.9.1 Invasion kinetics analysis

Heavily infected HFF monolayers were gently scratched and syringed though a 25-gauge needle to mechanically induce egress. Extracellular parasites were added to fresh HFF monolayers previously grown on glass bottom live cell dishes (Ibidi µ-dish$^{35mm\text{-}high}$). Cultures were transported using a safety plastic chamber. Videos were taken using the 40X oil objective lens, and recorded at 1 frame per second for 35 min. All samples (RHΔ*hxgprt*, loxp*mlc1* and *mlc1* KO) were imaged using DIC light for the full length of the video; however, to recognize *mlc1* KO parasites, a final image using FITC filter was taken.

2.12.9.2 Gliding kinetics

For gliding movies, Ibidi µ-dish$^{35mm\text{-}high}$ were coated with FBS 100% for 2 hours in advance. FBS was removed from the dishes, and washed twice with PBS. Parasites were prepared as described in section 2.12.3. Briefly, extracellular parasites were washed in pre-warmed PBS, resuspended in gliding buffer, and added to the dish. Movies were taken using 20X objective lens, and recorded at 1 frame per second for 30 min after parasites settled. For this experiment, RHΔ*hxgprt* expressing killer red was used since automatic tracker recognizes only fluorescent parasites. Videos of *mlc1* KO and RHΔ*hxgprt* were taken in FITC and red (A_{594}) channels, respectively. 20 videos of each motility, circular and helical, were analyzed using wrMTrck plugin designed for Fiji (imageJ).

2.12.9.3 Egress movies

To analyse *mlc1* KO egress upon Ca^{++} ionophore induction, 36 hour infected monolayers in glass bottom live cell dishes (Ibidi µ-dish$^{35mm\text{-}high}$) were imaged. For this experiment, RHΔ*hxgprt* expressing YFP was used to visualize host cell disruption. Vacuoles of interest were focused using 63X immersion oil objective lens. Parasites were imaged using DIC and FITC channels at 1 frame per second for 15 min. 2 µM Ca^{++} ionophore (A23187) were directly added above the region of interest after 1 minute from video start point (Frame 1).

2.12.9.4 Analysis of intracellular parasites expressing Cb

To analyse Cb-actin dynamics in intracellular parasites, 24 hour infected monolayers in glass bottom live cell dishes (Ibidi µ-dish$^{35mm\text{-}high}$) were incubated in presence of snap ligand (1:10000) diluted in $DMEM_{COMPLETE}$ for thirty min. After this time, cultures were

washed three times using pre-warmed PBS, then fresh media was added to the dishes and incubated in standard culture conditions for 15 min. Vacuoles of interest were focused with 100X immersion oil objective lens, and imaged in the red (A_{594}) channels at 1 frame per 100 millisec for 30 sec.

2.12.10 Fluorescence-based analysis

2.12.10.1 Quantitative immunofluorescence analysis

Wild-type and parental loxp*mlc1* strains were used as controls. For *mlc1* KO, parasites were induced with rapamycin as described in section 2.11.6, and cultured for 24 hours on HFFs prior to fixation. An IFA was conducted using αMLC1 kindly provided by Prof Soldati in a 1:2000 dilution, and AlexaFluor 594 in a 1:3000 dilution (Molecular Probes). Analysed images were obtained using a DeltaVision® Core microscope equipped with a CoolSNAP HQ2 CCD camera. The obtained images were saved as single red and green channel files.

For analysis and quantification of fluorescence intensities CellProfiler 2.1.1 software (www.cellprofiler.org) was used. Images were transformed from RGB to greyscale in Fiji (ImageJ) before import to the program. The pipeline was adjusted to detect vacuoles within the range of 5 to 40 pixels. Objects were identified using a global threshold strategy with a three class-Otsu threshold and weighted variances. Here, the fluorescence of the red-coloured region of interest (MLC1 signal) was measured on the basis of the total pixel occupied by the vacuoles (YFP+). Information about MLC1 intensities was exported to an Excel spreadsheet. The data obtained was filtered manually using area and integrated intensity parameters to include all parasites in a vacuole and exclude clustered vacuoles or random objects. 60 vacuoles were measured in each time point (0, 24, 48, 72 and 96 hours after induction) and processed to remove the calculated internal background.

2.12.10.2 Cell fluorescence measurement

For measuring the differential signal, IFA was performed using respective primary and secondary antibodies (section 2.6). Following, images were obtained using ELYRA PS.1 microscope (Zeiss). SIM images were collected at the same exposure and resolution parameters. Images were obtained using Zen Black (Zeiss) program and analysed using ImageJ. Vacuoles to be analysed were manually selected and traced using the ImageJ drawing tool. Measurements considered were: area, integrated density and mean grey value.

Data were plotted by using the corrected total cell fluorescence (CTCF) (Potapova et al., 2011).

2.12.11 Fluorescence activated cell sorting

Fluorescence activated cell sorting (FACS) was used to enrich and separate *mlc1* KO (YFP+) parasites for culturing and western blot analysis, respectively. Prior to sorting, *mlc1* KO parasites were scratched, syringed through a 25 G needle and filtered through a 3 micron Millipore filter (Millipore Merck) for purification of the sample. S3e™ Cell Sorter (Bio-Rad Laboratories, Inc.), equipped with a 488 nm laser, was used to sort *mlc1* KO (YFP+) expressing parasites. Parasites were sorted into 5 ml tubes. Before sorting parasites, the equipment was calibrated using ProLine™ universal calibration beads (Bio-Rad Laboratories, Inc.). Gates were adjusted to separate and collect YFP expressing population (*mlc1* KO).

For long term culturing experiment, sorting was performed in single cell mode to obtain the purest population possible. Sample loading stage and collection area was set at 37°C. After sorting, parasites were cultured under standard conditions. Egress was mechanically induced each 48 hours; in addition, non-induced extracellular parasites were controlled using DS-DMEM.

For western blot analysis, sorting was performed in enrichment mode to obtain the highest number of parasites possible. The temperature for sample loading stage and collection area was set at 4°C. After collection parasites were prepared for SDS-PAGE and western blot as described in section 2.13.

2.12.12 Retention under shear flow

The ability of parasites to retain on substrates was analysed under physiologic shear stress using microfluidics “open flow” system (KD Scientific Legato 200 syringe pump) (Harker et al., 2014). 4 x 10^5 extracellular parasites, contained in a final volume of 250 µl, were added to a collagen IV coated fluidic chambers (Ibidi IB-80192), and allowed to attach for 20 min under static condition at 37ºC with 5% CO2. After this time, the chamber was placed onto a Zeiss AxioVert.A1 microscope (40X lens), and connected to an “open circuit” loop containing at one extreme a syringe pump filled with $DMEM_{COMPLETE}$. An initial flow of 0.1 ml/min (equivalent to 0.3 dyn/cm2) was streamed to remove non-attached parasites, this was considered the started point (100% parasites). 1 minute before the flow rate

increased, an image was taken in FITC and DIC in each region of interest. In each flow rate, control and mutant parasites were counted from 5 fields of view. Counts were normalised to the 100%. Data collected and analysed by Dr. Gurman Pall.

2.12.13 Bead translocation fixed assay

For fixed translocation assays, Ibidi µ-dish$^{29mm\text{-}high}$ were coated with 0.1 % poly-L-Lysine for 30 min, and washed once with MilliQ water. 40nm fluorescent latex beads FluoSpheres® (Invitrogen) were diluted (1:80) in Hanks Balanced Salt Solution (HBSS) supplemented with 25mM HEPES (H-H buffer). To avoid clumps, beads were sonicated twice for 2 min and centrifuged for 10 sec; following, supernatant was separated and kept on ice until used.

Parasites were scratched, syringed through a 25-gauge needle, and filtrated through a 3 micron Millipore filter (Millipore Merck) for purification of the sample. Next, parasites were diluted to 2.5x10^7/ml and pelleted by centrifugation at 1500g for 5 min at 4ºC, at this point parasites were maintained on ice during preparation. Pellet was resuspended and incubated with 5 µl beads diluted in 250 µl cold H-H Buffer. The final dilution of parasites in H-H buffer was 1X10^7/ml. The mixture was added to poly-L-Lysine coated dishes and left on ice for 20 min. After this time, dishes were incubated at standard culturing conditions for 15 min prior fixation 4 % PFA for 20 min. PFA was removed gently; following, parasite nuclei were stained using Hoechst 0.01 %. Non-fluorescent parasites were stained with αSAG1 to define their shape. Images of beads were taken in DeltaVision® Core microscope. Three situations were considered for analysing the experiment: unbound (no beads signal was observed), bound (signal of the beads can be seen in the periphery), and capped (signal of the beads is polarised to the polar ends).

2.12.14 3D motility assays

3D motility assays were used for further examination of gliding motility, this protocol was followed as described in (Leung et al., 2014). Briefly, parasites were released from host cells by scratching and syringing through a 27-gauge needle followed by purification by filtration using a 3 µm Nuclepore filter. The parasites were pelleted by centrifugation at 1000 g for 4 min, the pellet was washed twice, and resuspended in a final concentration of 1-2 x 10^8 parasites/mL in 3D Motility media (1X Minimum Essential

Medium lacking sodium bicarbonate, 1 % FBS, 10 mM HEPES pH 7.0 and 10 mM GlutaMAX L-alanyl-L-glutamine dipeptide) containing 0.3 mg/mL Hoechst 33342.

The suspension was mixed with 3 volumes of 3D Motility Media and 3 volumes of Matrigel (BD Biosciences, San Jose, CA), prechilled on ice. 3D Matrigel motility was imaged, tracked and processed using Imaris x64 v. 7.6.1 software (Bitplane AG, Zurich, Switzerland) (Leung et al., 2014). Three independent biological replicates, each with three technical replicates, were performed. This experiment was standardised, performed and analysed by Dr. Jacqueline Leung under supervision of Prof Gary Ward in the University of Vermont, USA.

2.13 Biochemistry

2.13.1 Preparation of parasite cell lysates

Mechanically induced or freshly egressed parasites were pelleted by centrifugation at 1500 g for 5 min at 4ºC, and washed twice in cold PBS. Parasites were resuspended in fresh $DMEM_{COMPLETE}$ and counted; then, the volume containing around $1x10^7$ parasites was pelleted, supernatant was removed, and the pellet was kept on ice. The parasites were resuspended in a final concentration of $1x10^{5-6}$ parasites/µl in 10X NuPage® reducing agent and 4X NuPAGE™ LDS sample buffer (Thermo scientific©). The mixture was boiled at 95ºC for 5 min, and samples were kept at -20ºC until used.

2.13.2 Sodium dodecyl sulphate polyacrylamide gel electrophoresis

Material of $5x10^5$ – $1x10^6$ parasites were loaded in each well for further protein separation by sodium dodecyl sulphate polyacrylamide gel electrophoresis (SDS-PAGE) (Laemmli, 1970). Here, the presence of SDS in the gel permits to run proteins of different sizes by using voltage. Polyacrylamide gels are prepared in two phases: stacking and running, which preparation is detailed in Table 2-6. To note, 10% APS and TEMED were used to catalyse polymerisation; therefore, they were added right before gel was poured in glass cassettes (1.50 mm thick). In addition, 500 µl of isopropanol was used to ensure a straight termination of the running gel; after its polymerisation, stacking gel mix was added on top, and a 10-well comb was placed. After polymerisation parasite lysates, and 2µl Chameleon ™ Duo protein ladder (Li-COR) was included to visualise gel migration and protein size.

Proteins migrated through the stacking gel at 120V (10 min), and separated in the running buffer at 150V (50 min).

2.13.3 Western blotting

After separation, proteins were transferred from the polyacrylamide gel to Hybond® ECL™ nitrocellulose membranes (Sigma-Aldrich®). For transferring, membrane and gel were "sandwiched", in each side, by 2xWhatman filter paper and a foam pad all pre-soaked in transfer buffer. The gel holder cassette was closed and introduced in the electrode assembly, maintaining the membrane to the anode (+) and the gel to the cathode (-) side. The assembly was placed in Bio-Rad©

Mini-PROTEAN® tank filled with transfer buffer (Table 2-6) and containing a cooling unit. Subsequently, the tank was introduced into a Styrofoam box with ice to keep cold temperature during the process. Transference was run at 110V for 60-75 min.

2.13.4 Ponceau-staining

Ponceau staining is a fast way to verify correct protein transference. Here, the membrane was stained with Ponceau S solution for 2 min at RT shaking until bands revealed. After visualization, the dye was removed by washing twice with PBS for 5 min.

2.13.5 Immunostaining

Blotted membranes were blocked overnight in 5% skimmed milk in PBST at 4ºC shaking (Table 2-6). After blocking, membranes were incubated in 1 ml primary antibody (diluted over blocking solution) for one hour in a wet chamber as described for IFA (section 2.12.1). Afterwards, primary antibodies were washed away three times with PBST, following, membranes were incubated in 5 ml secondary antibody IRDye® (LiCor®) diluted over blocking buffer. Finally, the membranes were washed three times in PBST and stored in PBS until visualisation.

2.13.6 Visualisation and quantification of the protein bands

Proteins were detected using the Li-Cor® Odyssey® equipment. This system allows highly accurate quantitative infrared detection of the protein of interest. Quantification of protein abundance in bands was performed in Image Studio 5.0 software (LiCor®).

2.13.7 Stripping

Membranes could be re-probed by removing previous antibodies. This was achieved by incubating membranes in Li-COR® stripping buffer for 20 min shaking. Afterwards, membranes were washed three times in PBS to remove all the stripping buffer and detached antibodies. By this end, membranes could be blocked and start the immunostaining procedure again (section 2.13.5).

2.14 Bioinformatics

2.14.1 Sequence alignments

DNA and protein sequences were aligned using CLC genomics workbench 6.5 (Qiagen). In addition, this program was used to observe the chromatogram of sequenced samples.

DNA or amino acid sequences were searched and/or aligned using BLAST® local alignment tool (Altschul et al., 1990) available in either (http://toxodb.org/toxo/) (EuPathDB) or (https://blast.ncbi.nlm.nih.gov/Blast.cgi) (NCBI) web pages.

2.14.2 Data and statistical analysis

Primary data entry was done using Microsoft Excel and GraphPad Prim® 7.03. Statistical analysis was performed using GraphPad Prim® 7.03. When comparing two groups, the P value was calculated using an unpaired Student's t-test. When comparing multiple groups, the P value was determined using One-way ANOVA accompanied by Tukey's-post hoc test, or a two-way ANOVA accompanied by Dunnet's multiple comparison test. P values were symbolised as follows: not significant *ns* ($P>0.05$), significant * ($P\leq0.05$), very significant ** ($P\leq0.01$), highly significant *** ($P\leq0.001$), extremely significant **** ($P\leq0.0001$).

Chapter 3 Characterisation of MLC1 depleted mutant line

3.1 Characterisation of *mlc1* KO

The mechanisms underlying *T. gondii* invasion into host cells has been strongly associated with gliding motility, a substrate-dependent process supposedly driven by the acto-MyoA motor complex, also known as the glideosome (Dobrowolski et al., 1997a, Meissner et al., 2002b, Soldati and Meissner, 2004). This motor complex is thought to be located between the plasma membrane (PM) and the inner membrane complex (IMC), in a limited space called the pellicle (Opitz and Soldati, 2002, Keeley and Soldati, 2004). The suggested architecture of this motor includes three glideosome associated proteins: GAP40, 45 and 50, which are considered structural components of the motor (Gaskins et al., 2004, Frenal et al., 2010). MyoA, a fast myosin heavy chain, is believed to be the functional core of the motor complex (Meissner et al., 2002b). This unconventional myosin presents limitations for interacting with other proteins due to its short neck domain and lack of a tail domain (Hettmann et al., 2000). To interact with the structural backbone of the proposed motor, and maintain its rapid and constant speed, MyoA relies on three light chains; myosin light chain 1 (MLC1), essential light chain 1 (ELC1) and essential light chain 2 (ELC2) (Herm-Gotz et al., 2002, Nebl et al., 2011, Bookwalter et al., 2014, Williams et al., 2015).

The peripheral arrangement and function of these proteins supported the development of the linear motor model that predicts that MyoA moves on short actin (ACT1) filaments to generate force (Dobrowolski et al., 1997a, Dobrowolski et al., 1997b, Meissner et al., 2002b, Opitz and Soldati, 2002). The force is transmitted to the substrate via force transducers like adhesive transmembrane proteins derived from micronemes, for example microneme protein 2 (MIC2). Consequently, the smooth redistribution to the posterior pole and subsequent disengagement of the force transducers is translated into forward motion (Soldati and Meissner, 2004, Carruthers and Blackman, 2005, Heintzelman, 2015).

The development of the DiCre system, based on site-specific recombination, enabled the generation of genetic knockouts of core acto-MyoA motor complex proteins in *T. gondii* (Andenmatten et al., 2013). Mutants of structural (*gap40* KO, *gap45* KO, *gap50* KO) and functional proteins of the motor complex (*myoA* KO, *mlc1* KO, *act1* KO) presented significantly reduced invasion and gliding rates. However, these processes were not completely blocked as would be expected by the linear motor model (Andenmatten et al.,

2013, Egarter et al., 2014, Williams et al., 2015, Whitelaw et al., 2017). A reduction, but not complete elimination, of the parasites ability to glide and invade presented the possibility that compensatory mechanisms exist to preserve motility. As Myosin C (MyoC) shares MLC1, its main interaction partner with MyoA, and is structurally homologous, it was proposed as the compensatory protein upon loss of MyoA (Herm-Gotz et al., 2002, Polonais et al., 2011, Frenal et al., 2014). MyoC is the core motor protein of the MyoC-motor complex, also called MyoC glideosome, located at the posterior pole of the parasite (Frenal et al., 2014). At the posterior pole, MyoC and MLC1 interact with the structural proteins GAP80, GAP40 and IAP1, the latter being responsible for targeting the MyoC motor complex to the posterior pole (Frenal et al., 2014). Depletion of GAP80 or IAP1 can be rescued by GAP45, a typical protein from the peripheral MyoA-motor complex (Frenal et al., 2014).

The observation that partial rescue upon loss of components was capable between motor complexes, combined with the redundancy of the myosin interacting partners (MLC1 and ELC1) lead to the plasticity and redundancy hypothesis between myosin motors in *T. gondii* tachyzoites (Meissner et al., 2013, Frenal and Soldati-Favre, 2015). With these reasons in mind, an inducible *myoA/B/C* KO (triple KO) was generated (Egarter et al., 2014, Frenal et al., 2014). Since MyoB and MyoC are alternatively spliced proteins transcribed from the myoB/C gene, the deletion of this gene resulted in depletion of both proteins (Delbac et al., 2001). The triple KO strain presented a more severe phenotype compared to the *myoA* KO, however, these parasites remained motile and invasive, although at lower rates (Egarter et al., 2014, Frenal et al., 2014). Despite this, it cannot be excluded that other myosins, apart from MyoA and MyoC, can functionally complement for their loss.

These studies demonstrated that there is a certain degree of plasticity between components of the MyoA and MyoC motor complexes. However, the fact that invasion and gliding were not completely blocked opened a new question regarding redundancy within these motor complexes. Thus, to test the hypothesis regarding overlapping functions between MyoA and MyoC, we further analysed MLC1 because it is central for stabilisation of the MyoA lever arm, and, therefore, critical for the function of the acto-MyoA motor complex (Hettmann et al., 2000, Herm-Gotz et al., 2002, Williams et al., 2015). Previously it has been shown that MLC1 is required for the correct location of MyoA to the periphery of the parasite, serving as an anchor to the proteins in the IMC (Egarter et al., 2014). Additionally, MLC1 is a central component of both MyoA and MyoC motor complexes, and has the capacity to interact with both MyoA and MyoC. For these reasons, to test this

versatile, complex and redundant system, this chapter focuses on the deep characterisation of MLC1 functions. To study redundancy in the motor complexes, the inducible *mlc1* KO line (Egarter et al., 2014) was used to test the ability of the mutant parasites to complete the lytic cycle, and understand which steps were affected by the depletion of this protein.

3.1.1 Depletion of MLC1

Previous studies stabilised the DiCre cassette in the Δ*ku80* line in order to increase the homologous recombination rate of the loxp cassette, containing the CDNA of the GOI flanked by loxp sites, a YFP reporter and the 5' and 3' endogenous regions of the GOI (Egarter et al., 2014). Upon rapamycin induction, the lines containing this optimised loxp cassette delete the floxed GOI, leaving the YFP reporter under the control of the endogenous promotor. This strategy permitted the visualisation of YFP+ KO parasites; thus, the efficiency of the induction could be directly assessed based on the percentage of YFP expressing parasites in the induced population (Egarter et al., 2014). For instance, depletion of MLC1 was observed in a conditional *mlc1* KO around 48 hours after induction with 50 nM rapamycin (Egarter et al., 2014). Extracellular parasites were induced for four hours and after 24 hours the proportion of YFP positive vacuoles was 35%, indicating inefficient activity of the Cre-Lox system when compared to other conditional mutants that yield an induction rate >90% (Andenmatten et al., 2013). Therefore, it was necessary to optimise the induction strategy to obtain a higher proportion of *mlc1* KO (YFP+) parasites within the population (section 2.11.6). To enhance excision of MLC1, extracellular loxp*mlc1* parasites were incubated with different concentrations of rapamycin for 4 hours at 37^{o}C. Parasites were then inoculated on confluent HFF cells and grown for 48 hours before fixing with 4% paraformaldehyde (PFA) and assaying by immunofluorescence (IFA). The efficiency of induction was evaluated considering the percentage of YFP expressing parasites (*mlc1* KO) in the induced population. As depicted in Figure 3-1A, when inducing with 50 nM rapamycin, the percentage of parasites expressing YFP, which are therefore *mlc1* KO, was 25 ± 5.7 %. Increasing the concentration of rapamycin from 50nM to 100nM increased the percentage of *mlc1* KOs in the population to 36.3 ± 5.1% %. The rate of YFP turnover after rapamycin induction in the loxp*mlc1* is low compared to more efficient lines such as loxp*act1* or loxp*gap45* (Egarter et al., 2014). This can be explained since excision rates can vary according to the GOI even if the same DiCre containing strain was used to generate the loxp stable lines. Under this premise, the location, orientation, number and space between the loxp sites can influence the efficiency of the DiCre system (Nagy, 2000, Zheng et al., 2000). In addition, some genes are located in areas not easily accessible in the genome, which

could potentially affect the recombination rate. Under this premise, it is conceivable that any of these factors could explain the low induction efficiency observed in the loxp*mlc1* line. However, no further analysis of the loxp*mlc1* genome was conducted.

Following with the characterisation, using the optimised induction strategy, depletion of MLC1 was demonstrated using an αMLC1 antibody. MLC1 is peripherally detectable in the parental line (RHΔ*hxgprt*) and the loxp*mlc1* line, but after induction the majority of YFP positive vacuoles showed no MLC1 staining while a small proportion showed residual MLC1 staining (Figure 3-1B) (Egarter et al., 2014).

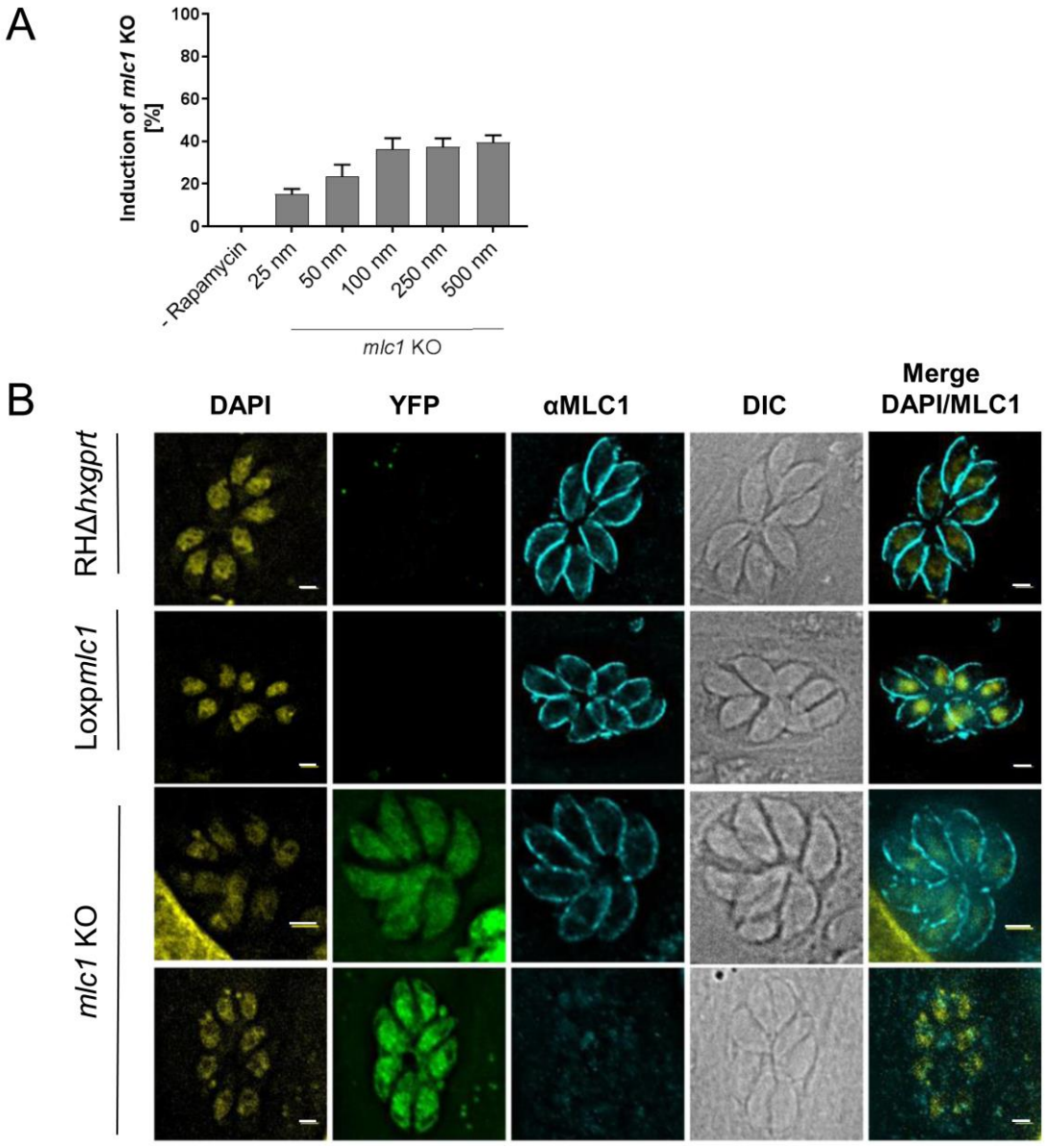

Figure 3-1. Optimisation of *mlc1* KO and verification of protein depletion
A. loxp*mlc1* line was treated with different concentrations of rapamycin for four hours. YFP production was determined 48 hours after treatment. Fifty vacuoles were counted in three repetitions. Graph shows mean values from three independent experiments ± SD **B.** IFA of MLC1 localisation in

RHΔ*hxgprt,* loxp*mlc1* and *mlc1* KO after 48 hours induction. αMLC1 antibody was used to verify protein expression. Scale bar represents 2 µm.

3.1.2 MLC1 down-regulation in *mlc1* KO

To study the dynamics of downregulation and depletion of MLC1 in the *mlc1* KO, we performed a quantitative immunofluorescence assay. For this experiment, parasites were induced using 100 nM rapamycin in the conditions described below, and allowed to invade for one hour. After infection, three washes with PBS were used to remove extracellular parasites, and intracellular parasites were cultured for at least 24 hours prior to fixation. The experiment was performed from 24 to 96 hours after induction, at 24-hour intervals. An IFA was performed using αMLC1 antibody previously described, and AlexaFluor-594 as secondary antibody (Figure 3-2A). Background intensity of the red channel was calculated by using YFP only expressing parasites with no antibodies added for the red channel. Images were taken as single red and green channels using consistent exposure parameters for control (RH*Δhxgprt* and loxp*mlc1*) and *mlc1* KO samples in both channels. No processing or colour enhancement was performed to maintain intact red channel signal (Figure 3-2A). CellProfiler_2.1.1 free software (www.cellprofiler.org) was used to analyse and quantify fluorescence intensities (Carpenter et al., 2006). In each image taken, the red-stained (MLC1) area was analysed based on the total pixel occupied by each vacuole. In the *mlc1* KO line, only YFP expressing vacuoles were analysed and quantified (Figure 3-2B).

The measured intensities presented no significant differences between the control strains, RH*Δhxgprt* and loxp*mlc1*, with all vacuoles exhibiting staining above background level (Figure 3-2B). In control parasites, MLC1 is uniformly and sharply distributed to the pellicle with no observable difference in the signal distribution or thickness (Figure 3-2A, top panels). In the *mlc1* KO (YFP+), MLC1 signal reduces visibly 24 hours after induction (Figure 3-2B), though the intensity does not fall below background intensity at this time point (Figure 3-2B). This may be due many parasites start expressing YFP, but remnants of the protein are still present in the pellicle as shown in Figure 3-2A, third panel and Figure 3-2B. At 48 hours post induction, MLC1 cannot be detected in the pellicle in most of the vacuoles (Figure 3-2A), and the average intensity levels falls below background level (Figure 3-2B). At 48 hours, a small number of vacuoles still display MLC1 signal that overlaps with the intensity of low-expressing control parasites, although this trend is less common at later time points. This intensity variation can be due to antibody signal, which is a typical limitation of immunofluorescence quantification assays (Zinchuk et al., 2007). 96

hours after induction, MLC1 signal falls below background level in virtually all YFP+ vacuoles (Figure 3-2A/B), for this reason, all phenotypic analyses performed in this study used this time point.

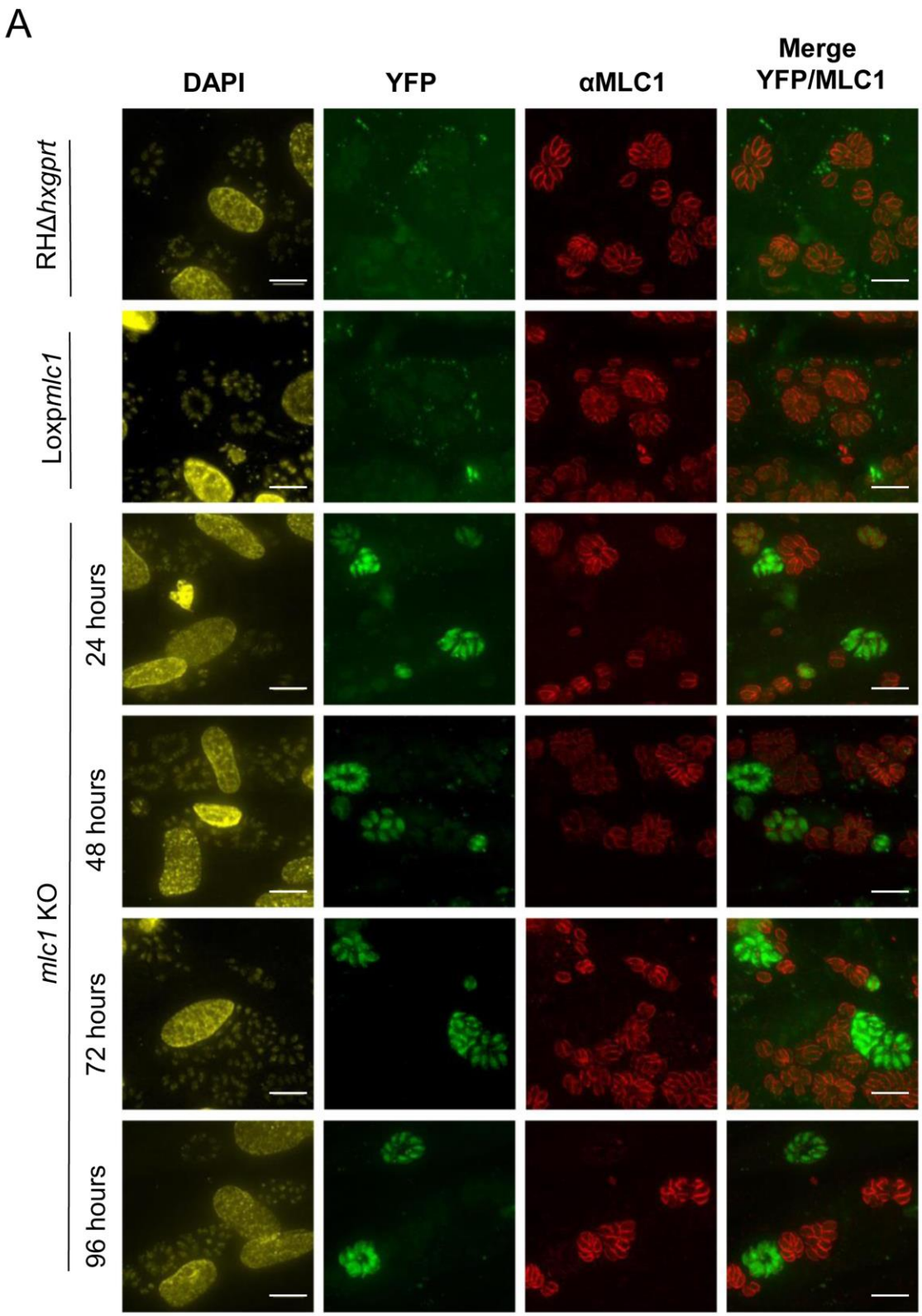

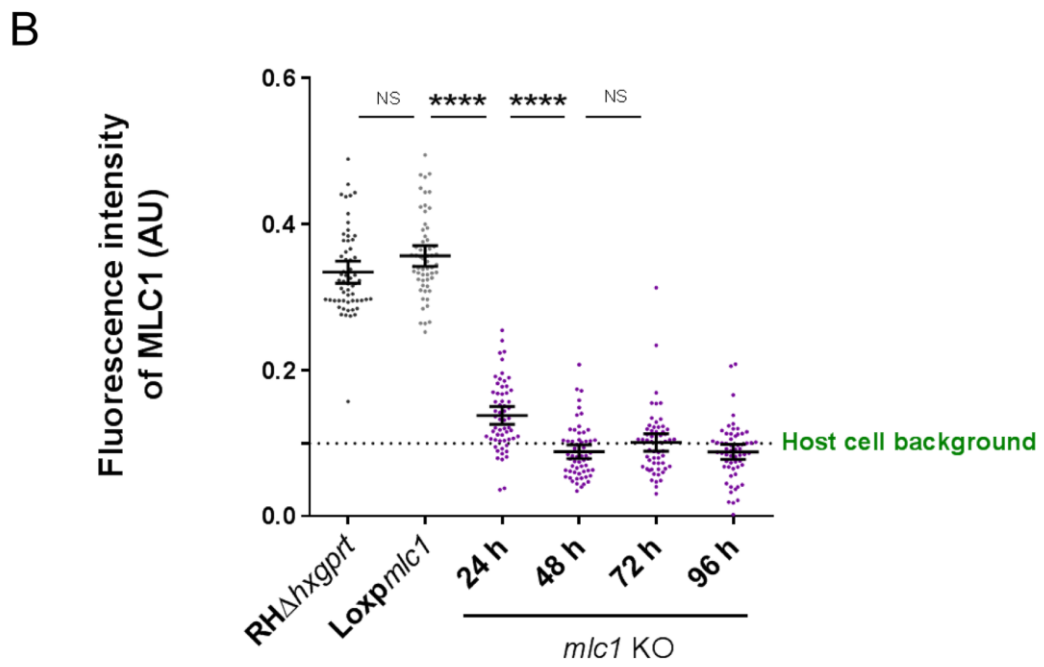

Figure 3-2. Quantitative Immunofluorescence analysis of MLC1 depletion
A. IFA analysis using αMLC1 in RHΔ*hxgprt*, loxp*mlc1* and *mlc1* KO. Non-processed images showing typical background noise in control lines in the green channel. Analysis of MLC1 depletion in the inducible strain was carried out 96 hours after induction at 24-hour time points. Scale bar represents 2 µm. **B.** Fluorescence intensity analysis was used to measure MLC1 depletion. IFA using α-MLC1 at 24, 48, 72, and 96 h post induction was carried out. Sixty vacuoles per strain were analysed using CellProfiler software. Dashed line represents fluorescence background of the red channel obtained by an RH RHΔ*hxgprt* YFP expressing strain. *mlc1* KO red signal falls below background line meaning MLC1 has been correctly depleted after rapamycin induction. Bars indicate mean ± SD. Means among groups were compared using one-way ANOVA followed by Tukey's post-hoc test. **** P<0.0001, not significant (ns) P>0.05. Figure modified from (Whitelaw et al., 2017) under Creative Commons Attribution 4.0 International License.

3.1.3 MyoA localisation fully depends on the presence of MLC1 in the periphery

Previous studies showed that MTIP (an orthologue of MLC1) deletion produced MyoA degradation, which indicated that association of MyoA with its light chain was necessary for maintaining localisation and function (Sebastian et al., 2012). A similar scenario was observed by IFA in the *mlc1* KO: here, MyoA relocalised to the cytosol (Egarter et al., 2014). In this section, we attempted to ascertain if degradation of MyoA occurred following MLC1 depletion.

First, we aimed to detect protein levels of MyoA in the *mlc1* KO by using Western Blot. Since the *mlc1* KO mutant line is not viable in culture, we were forced to work with the mixed population after induction. To separate both populations, we employed FACs sorting to select YFP-expressing parasites only, and then perform the protocol. By using tight parameters for fluorescence separation, isolation of YFP expressing parasites was

possible. However, although several attempts were made to separate later time points (Appendix 2), it was only possible to isolate a sufficient number of events ($1x10^6$) to perform the immunoblot 48 hours after induction. After isolation, western blot was performed using antibodies αMLC1, to confirm excision, and αMyoA, to study regulation of this protein. As shown in Figure 3-3A, correct excision of MLC1 is apparent from a sharp reduction in staining. In the same experiment, MyoA levels are visibly reduced, although the protein is still present. This signal may come from YFP expressing mutants, which still present remnants of MyoA 48 hours post induction (explained in section 3.1.2).

This result made me interested in further investigating the state of MyoA after excision. Of note, one of the major limitations in studying MyoA is that the antibodies against this protein are not specific and cross-react with other epitopes for IFAs. For this reason, I generated and stabilised a construct to tag a second copy of MyoA in the inducible *mlc1* KO line (Figure 3-3B). The plasmid contained a 2000 bp fragment of the 5' UTR region (-2000 to 0 from the start codon), a Ty Tag, and MyoA cDNA. This construct (pMyoATyMyoA) was co-transfected with a bleomycin selectable cassette in the loxp*mlc1* line. The localisation of MyoA was assayed by IFA using αTy antibodies. As expected, TyMyoA signal localises in the pellicle of the parasite (Figure 3-3C, top panel), whereas, upon MLC1 depletion, this protein either changes its location from the periphery to the centre of the cytoplasm (Figure 3-3C, mid panel) or is completely absent (Figure 3-3C, bottom panel). Following this observation, a quantification of this phenomenon was performed (Figure 3-3D). As speculated before, these data show that depletion of MLC1 drives relocalisation and, possibly, degradation of MyoA as described for *Plasmodium* (Sebastian et al., 2012, Egarter et al., 2014).

Together with data shown in section 3.1.2, the downregulation of MLC1 directly affects MyoA localisation in the pellicle of the parasite. Under this premise, we have shown that after 24 hours of induction MLC1 and MyoA drastically reduce their signal in the periphery in the inducible *mlc1* KO. To confirm possible degradation, further investigation into protein and transcript levels is needed. However, this approach is challenging considering that the *mlc1* KO line available is not clonal and the presence of uninduced parasites is difficult to avoid.

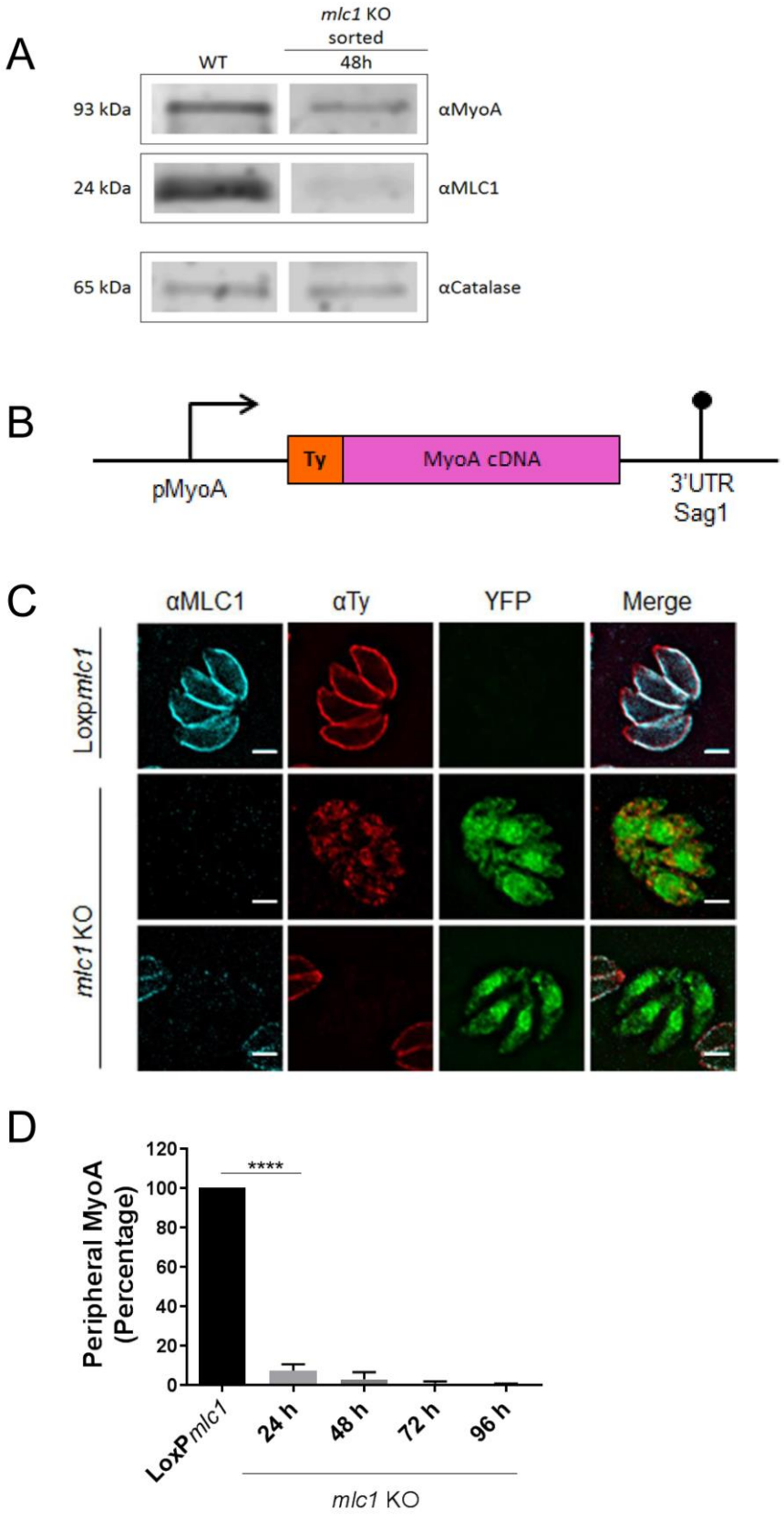

Figure 3-3. MyoA relocalises to the cytoplasm in the absence of MLC 1
A. Immunoblot of sorted *mlc1* KO (48-hour post induction). Levels of MyoA and MLC1 were determined using respective antibodies. Catalase was used as loading control. Bands show dramatic drop of MLC1 and MyoA signal upon excision of the *mlc1* gene **B.** Scheme of pMyoATyMyoA construct that was randomly integrated into the loxp*mlc1* genome. MyoA cDNA was fused to a Ty tag under the pMyoA promoter **C.** Immunofluorescence analysis of TyMyoA in loxpa*mlc1* and *mlc1*

KO parasites using αTy and αMLC1 antibodies **D.** Percentage of correctly localised MyoA in the *mlc1* KO line. MyoA localisation was assessed using αTy at 0, 24, 48, 72, and 96 h after induction of loxp*mlc1*. Graphic shows mean ± standard deviation of three independent experiments. Comparison between groups used one-way ANOVA followed by Tukey's post-hoc test. **** P< 0.0001. Figure modified from (Whitelaw et al., 2017) under Creative Commons Attribution 4.0 International License.

3.1.4 Long term culture of *mlc1* KO

Previous data suggest that the reduction in gliding and invasion is comparable when MyoA or MLC1 are knocked out (Egarter et al., 2014). However, in contrast to *myoA* KO parasites, egress is strongly delayed in *mlc1* KO parasites, meaning isolation of a *mlc1* KO line was impossible (Egarter et al., 2014). Nevertheless, it was possible to maintain these parasites in *in vitro* culture for up to 14 days if the vacuoles were artificially released. After this time, a dramatic reduction of *mlc1* KO parasites was reported in the population, likely as a result of non-induced parasites outcompeting the induced KO parasites (Egarter et al., 2014). Under this premise, it is central to mention that the conditional *mlc1* KO strain presents low induction efficiency. We have determined that the induction efficiency is not greatly enhanced by increasing rapamycin concentration or exposure time (Figure 3-1A). After reaching an average YFP+ population of 40% at 24-48 hours post induction, the mutant population decline rapidly until disappearance. This phenomenon is clearly observed in plaque assays, where loxp*mlc1* populations overgrow in induced cultures and *mlc1* KO (YFP+) parasites don't form plaques (Egarter et al., 2014). Considering these results, a long-term *mlc1* KO culture was sought to rule out the possibility that the *mlc1* KO not only exhibits a significant egress defect but also presents an uncharacterised detrimental phenotype.

There are several factors affecting the ability of uninduced parasites to outgrow *mlc1* KO parasites in culture. Firstly, the *mlc1* KO is unable to naturally egress, and secondly, its motility and invasive capability is reduced compared to uninduced parasites. Additionally, considering that apicoplast segregation is acto-MyoF dependant (Jacot et al., 2013, Whitelaw et al., 2017), it would be plausible that MLC1 participates in this process. Thus, *mlc1* KO parasites could present deficient apicoplast inheritance, manifesting in a delayed death phenotype upon completing one round of the lytic cycle (Fichera et al., 1995). To determine if extended culture, exceeding the previously reported 14 days, was achievable, these two parameters were altered to enhance the proportion of *mlc1* KO parasites in the population. Induced parasites were mechanically egressed after 36 – 48 hours, and subjected to culture conditions to enhance survival of the *mlc1* KO in the mixed population. For this, parasites were allowed to invade in normal conditions for 24 hours, then dishes were washed and 2.5%

dextran sulphate was added to complete DMEM. Dextran sulphate (DS) is a glycan competitor, which avoids re-invasion of egressed parasites (Carruthers et al., 2000, Coleman and Gubbels, 2012). As *mlc1* KO parasites do not egress they were not affected by addition of DS. By following this protocol, I controlled re-invasion events and extracellular parasites were washed away, which enhanced the number of induced parasites in culture. Between 24 to 96 hours post induction, the percentage of YFP expressing parasites in the population dropped significantly. At this point, the YFP+ population was enriched using fluorescence-activated cell sorting (FACS) to isolate the mutant population from non-induced parasites (YFP negative). A constant protocol of mechanical release every 36 hours, usage of DS-DMEM media 24 hours after infection, and sorting YFP+ parasites was used to enable maintenance of *mlc1* KO parasites in culture for 7 weeks (Figure 3-4).

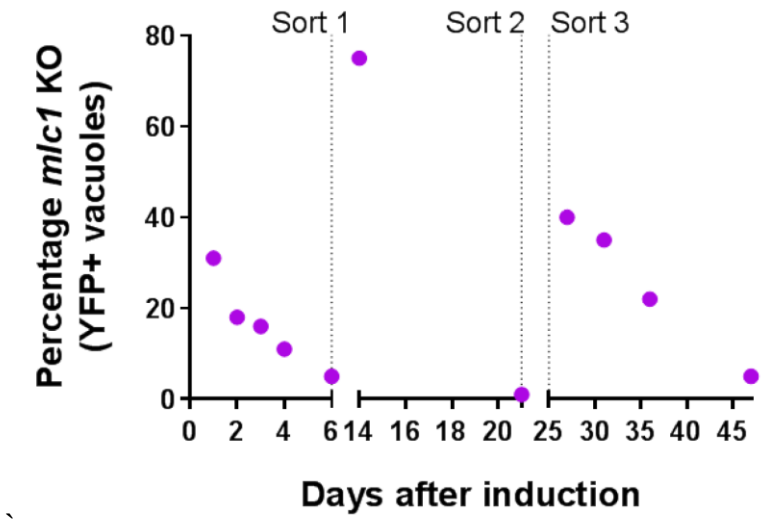

Figure 3-4. Long term culture of *mlc1* KO
Long term culture of *mlc1* KO parasites was achieved by combining FACs sorting (vertical dashed lines) and mechanical parasite egress. Parasites were sorted for YFP signal produced by the DiCre cassette marker. Percentage of parasites was measured by counting YFP+ vacuoles over the total number of vacuoles contained in 20 fields of view using a 40X objective. MLC1 depleted parasites can be kept in culture for long periods if non-induced parasites are removed and YFP+/MLC1- parasites are enriched. Figure modified from (Whitelaw et al., 2017) under Creative Commons Attribution 4.0 International License.

I obtained a peak of 80% YFP+ parasites using FACs. However, despite strict parameters for gating and single-cell sorting, non-induced parasites were always present in the population. Thus, it was not possible to isolate a pure *mlc1* KO population. As previously reported, separation of populations by FACs is influenced by many factors including: number of parasites sorted, proportion of parasites of interest in the population,

fluorochrome brightness and equipment power (Eidell et al., 2010, Coleman and Gubbels, 2012).

Although a clonal *mlc1* KO population couldn't be isolated through bypassing egress and enriching the YFP+ population, *mlc1* KO parasites could be continuously maintained in culture, which demonstrates that MLC1 is dispensable for all steps of the lytic cycle except egress. It would be interesting to explore if an adaptation occurs after several rounds of *mlc1* KO enrichment, given the remarkable capacity of *myoA* KO parasites to adapt to the loss of MyoA in terms of gliding and invasion rates (Andenmatten, unpublished data) (Appendix 3). Unlike the *mlc1* KO, MyoA null parasite egress was not completely blocked, but only reduced, which makes *mlc1* KO adaptation less plausible. Nevertheless, an adaptation of the *mlc1* KO is a possibility that would require further investigation.

3.1.5 MLC1 is dispensable for replication and apicoplast division

Endodyogeny, the process of replication in tachyzoites, is a highly coordinated process in which two daughter cells are formed within a single mother cell (Sheffield and Melton, 1968, Francia and Striepen, 2014). During progression of replication, the apicoplast, a multimembrane secondary plastid (Fichera and Roos, 1997, Kohler, 2005), is actively segregated by myosin F (MyoF) into the daughter cells (Jacot et al., 2013). The presence of this organelle is essential for parasite survival because it is important for biosynthesis of fatty acids, isoprenoids, and heme (Fichera and Roos, 1997, Sheiner et al., 2013). Parasites lacking the apicoplast are able to complete one round of the lytic cycle normally, but die following subsequent invasion, a phenomenon called "delayed death" (Fichera et al., 1995, Fichera and Roos, 1997). Apicoplast inheritance can be affected or blocked with either pharmacological compounds (such as Ciprofloxacin), or by depleting components of the acto-MyoF complex (Fichera and Roos, 1997, Andenmatten et al., 2013, Jacot et al., 2013, Egarter et al., 2014, Frenal et al., 2017b).

MyoF, a class XXII myosin, contains a conserved motor domain, a long neck domain composed of six light chain binding motifs and a coiled-coil domain that supports a double head and a cargo binding domain at the C-terminal end of the protein (Foth et al., 2006). MyoF subcellular localisation varies during the different stages of the lytic cycle, but it is predominantly found in the cytoplasm and, to a lesser extent, in the periphery (Jacot et al., 2013, Heaslip et al., 2016). Even though the acto-MyoF motor complex is important for

apicoplast positioning and dense granule trafficking (Jacot et al., 2013, Heaslip et al., 2016), the proteins associated with this myosin and/or its interactors are unknown.

Previous reports suggested there was no replication effect on parasites lacking MLC1 (Figure 3-5A), however this replication analysis did not closely examine the formation and delivery of the daughter apicoplast (Egarter et al., 2014). To study if apicoplast replication or segregation was affected in parasites lacking MLC1, we used apicoplast markers on replicating vacuoles. *mlc1* KO parasites (96 hours post induction) were allowed to replicate for 24 hours before being fixed and assayed for apicoplast replication and segregation.

Using the apicoplast marker HSP60, as shown in Figure 3-5B, no loss of the apicoplast was seen in *mlc1* KO parasites. Furthermore, correct separation and delivery of the apicoplast was confirmed by quantifying the number of apicoplast per daughter parasite (expected ratio 1:1) after depletion of MLC1 (Figure 3-5C). No appreciable difference was observed between the *mlc1* KO and control RHΔ*hxgprt* parasites. Taken together, these results confirm that apicoplast segregation does not depend on the presence of MLC1, which implies that MyoF function is not based on an interaction with MLC1 in the tachyzoite stage.

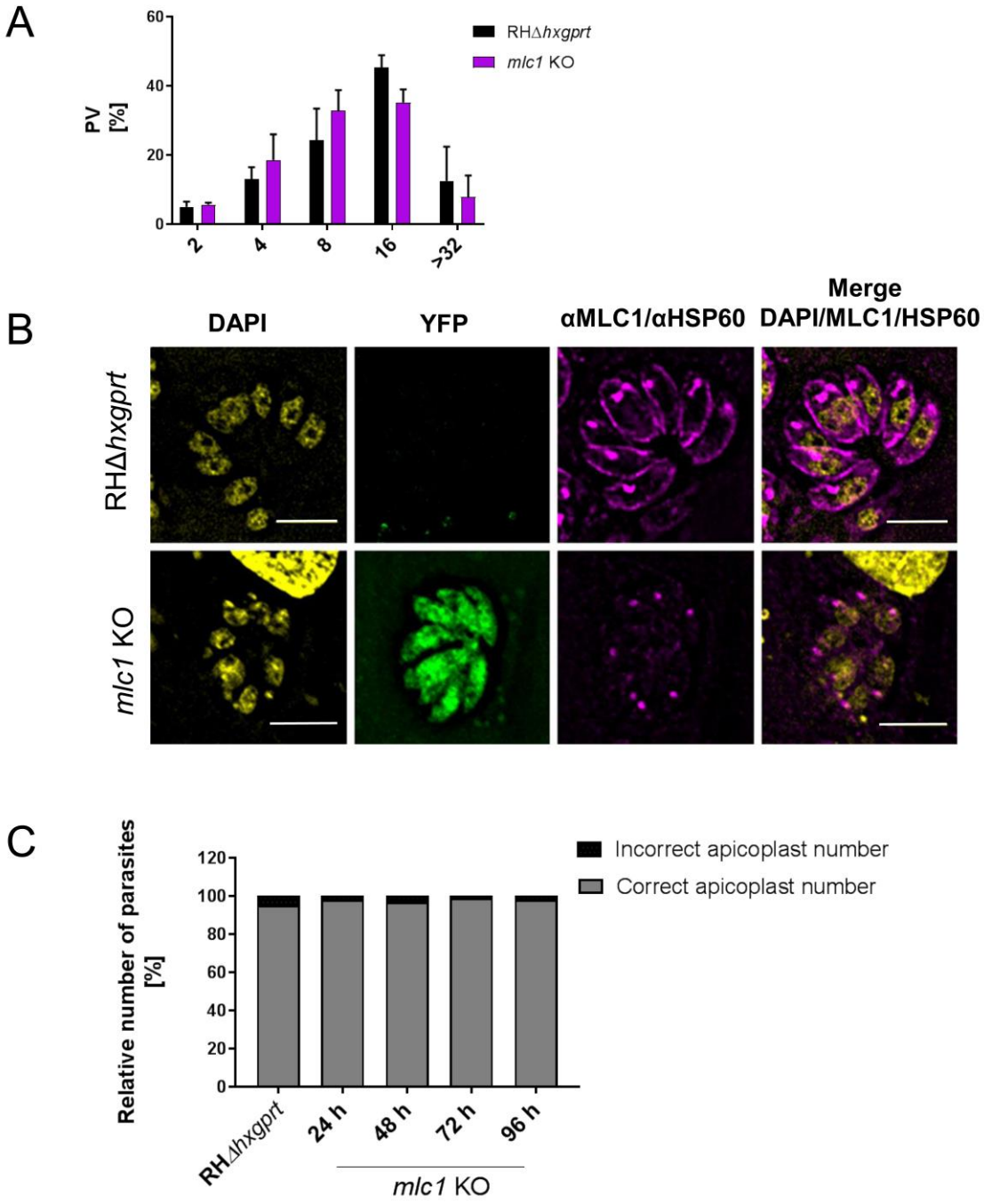

Figure 3-5. Replication and apicoplast segregation analysis in *mlc1* KO
A. Replication assay of RHΔ*hxgprt and mlc1* KO parasites 96 hours after induction to yield maximum MLC1 depletion within the population. Parasites were allowed to infect HFFs for 1 hour and replicate for 24 hours. Data were quantified in terms of number of parasites per vacuole. No important replication delay is seen in these parasites. Values are expressed as average ± SD. Experiment performed by Dr. Saskia Egarter **B.** αHSP60 antibody was used to test apicoplast maintenance in the *mlc1* KO strain. Scale bar represents 5µm **C.** Quantification of apicoplast loss was carried out. A 1:1 ratio (apicoplast: parasite) was considered correct apicoplast number. No apicoplast loss was found in the MLC1 depleted line compared to the control line

3.1.6 *mlc1* KO gliding kinetics

T. gondii tachyzoites rely on gliding motility to disseminate to find a suitable host cell. Early studies assayed motility by detecting surface proteins that the parasite deposits as it glides over protein coated surfaces on coverslips. These trails could be visualised using immunofluorescence against deposited proteins; this protocol is known as a trail deposition assay (Dobrowolski and Sibley, 1996, Dobrowolski et al., 1997a). Although informative, this assay examines motility solely in static 2-dimensional (2D) samples, and no quantitative information of kinetics could be measured. Frixione and colleagues further analysed gliding capability of tachyzoites in 2D using time-lapse video microscopy (Frixione et al., 1996). This analysis reported that the parasites were able to move in three different ways: circular, helical, and twirling, and that all of these were affected if actin or myosin inhibitors were added to the media (Håkansson et al., 1999). Moreover, circular and helical motility were thought to result in forward clockwise movements, which led to the generation of a 360° path (circular) or a corkscrew 180° flip trail (helical). Twirling is characterised by fast circular motility of the anterior pole, while the posterior pole remains attached to the substrate (Håkansson et al., 1999). Studies carried out in *Plasmodium berghei* and *T. gondii* using 3-dimensional (3D) matrices have reported parasites moving in an irregular corkscrew motion, with the trajectory of this corkscrew being influenced by cell shape (Kan et al., 2014, Leung et al., 2014). These results provide insight into how 2D motility patterns are translated to a unique complex helical movement in a non-limiting environment (Frevert et al., 2005, Kan et al., 2014, Leung et al., 2014).

Gliding ability of the *mlc1* KO was first assessed using the well-established trail deposition assay. The results suggest that, compared to control parasites normalized at 100% gliding (circular and helical trails), 42% of *mlc1* KO mutants exhibit exclusively circular residual motility (Egarter et al., 2014). This phenotype was similar to that of the *myoA* KO (Egarter et al., 2014). Although trail deposition is an excellent tool for qualitatively analysing motility, quantitative information associated with these trails is limited, imprecise, or absent.

Next, we assessed the kinetics of *mlc1* KO motility by time-lapse video microscopy analysis. For this, parasites were allowed to glide for 30 minutes on glass-bottom live-cell dishes previously coated with 100% FBS. 20 helical and 20 circular trails were imaged and tracked using WrMTrck plugin designed for ImageJ/Fiji (Nussbaum-Krammer et al., 2015). In good agreement with previous results, parasites lacking MLC1 remain motile, albeit in a lower proportion compared to wild type parasites (Egarter et al., 2014). Overall, these

mutants displayed continuous movement, similar to WT parasites, meaning they can smoothly move in complete circles. This contrasts with *myoA* KO parasites, which seem to have a "stop and go" like motion (Figure 3-6A, Movie 1-2) (Egarter et al., 2014). While trail deposition assays showed that *mlc1* KO parasites mostly deposited circular trails, live-cell imaging revealed the presence of short helical trails, not detectable using the trail deposition assay and also not previously described in the *myoA* KO (Figure 3-6A, Movie 3-4). The average distance of these helical trails was significantly shorter (16 ± 2 µm) than those made by RHΔ*hxgprt* parasites (55 ± 5 µm). In contrast, the average distance of circular trails (33 ± 4 µm) was not significantly different compared to RHΔ*hxgprt* (41 ± 4 µm) (Figure 3-6B). Furthermore, when considering circular motion, *mlc1* KO parasites show a slight difference in average (0.4 ± 0.2 µm/s) and maximum speeds (1.2 ± 0.1 µm/s) compared to RHΔ*hxgprt* parasites (0.7 ± 0.08 µm/s and 1.7 ± 0.1 µm/s, respectively). Whereas parasites performing helical gliding show significantly slower average (0.2 ± 0.02 µm/s) and maximum (1 ± 0.1 µm/s) speeds (Figure 3-6C/D) when compared to RHΔ*hxgprt* (1 ± 0.1 µm/s and 2 ± 0.2 µm/s, respectively). Taken together, these results show that *mlc1* KO parasites can glide in a constant circular and helical manner, unlike *myoA* KO parasites. As shown in section 3.1.3, MyoA loses its peripheral location in *mlc1* KO parasites 96 hours post induction (time point these data were collected). Under this premise, we can conclude that neither MyoA nor MLC1 is driving this process; however, we still cannot disregard the possibility that MyoC is compensating in this case.

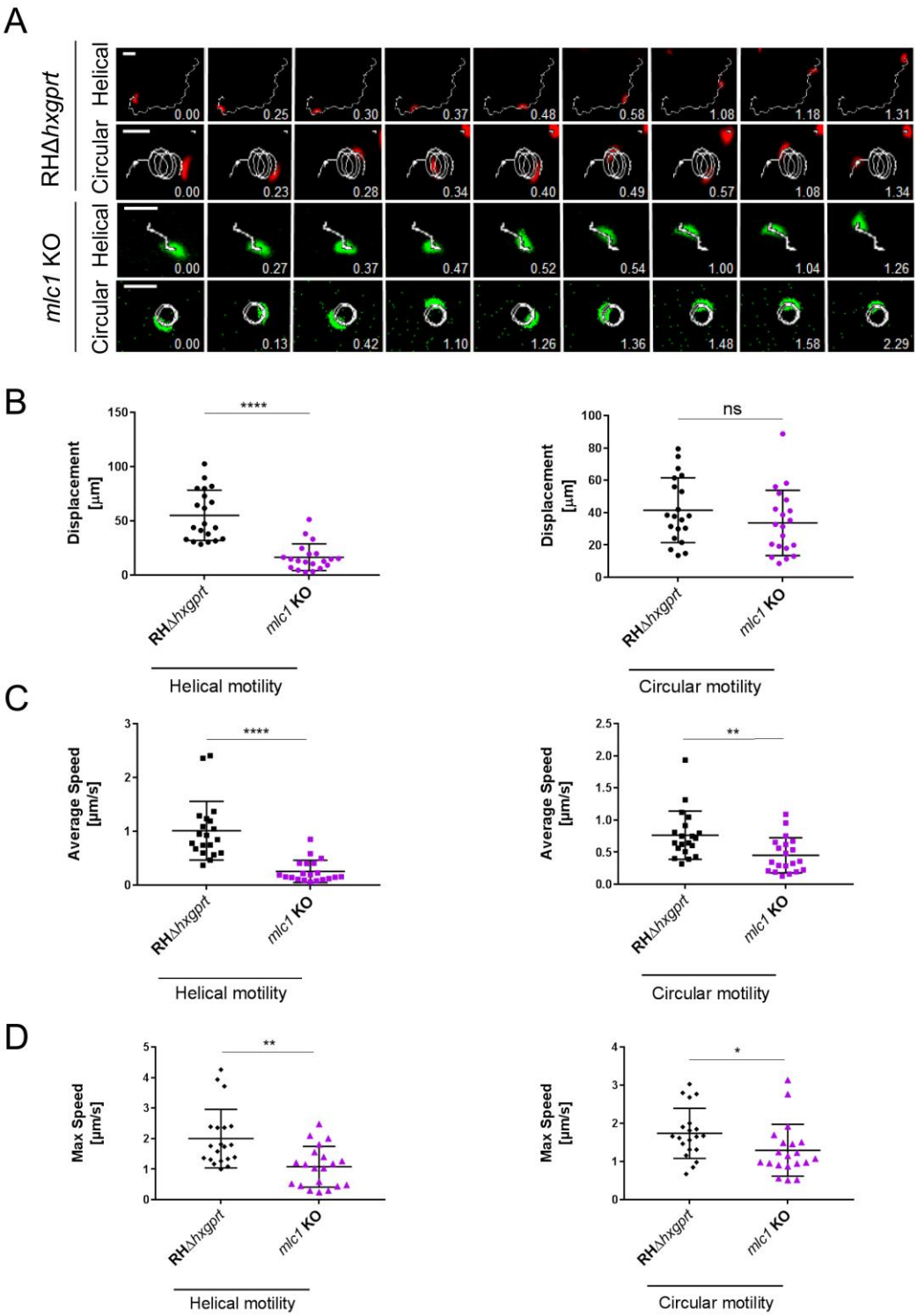

Figure 3-6. 2-D gliding kinetics analysis of *mlc1* KO mutant parasites
A. RH*Δhxgprt* and *mlc1* KO tachyzoites gliding in a 2D environment were recorded at 1 frame per second. Twenty circular and helical trails were tracked using the Fiji wrMtrck plugin. Trails generated were superimposed on the time-lapse images. Time stamp indicates minute.seconds. Scale bar represents 10µm **B.** Displacement, **C.** average speed **D.** and Maximum speed of tracked parasites moving in circular and helical manner were quantified. In the *mlc1* KO, helical motility shows slower speeds with shorter tracks when compared to control parasites, compared to circular gliding, which is faster and presents longer tracks. Unpaired t-test was used to measure statistical differences between groups. **** P≤0.0001 ** P≤0.01 * P≤0.1 ns P>0.05. Figure modified from (Whitelaw et al., 2017) under Creative Commons Attribution 4.0 International License.

Our collaborator Dr. Jacqueline Leung, under the supervision of Professor Gary Ward at the University of Vermont, studied the motility kinetics of *mlc1* KO parasites using a 3D assay (Leung et al., 2014). In these experiments, mutant parasites were allowed to glide in a 3D extracellular matrix (Matrigel). Similar to results obtained in 2D gliding analysis, the number of parasites moving was greatly reduced (Figure 3-7A) from approximately 40% in non-induced parasites to 3% in MLC1-depleted parasites. Additionally, the distances moved are significantly shorter in the *mlc1* KO (7 ± 0.6 µm) compared to control parasites (14 ± 1 µm) (Figure 3-7B). Although the number of parasites moving and the distance parasites moved are significantly reduced, the average (0.7 ± 0.1 µm/s) and maximum (1.99 ± 0.35 µm/s) speed is comparable to control parasites (0.7 ± 0.07 µm/s and 2 ± 0.09 µm/s, respectively) (Figure 3-7C/D). This suggests *mlc1* KO parasites can generate the necessary force to glide in 3D environments.

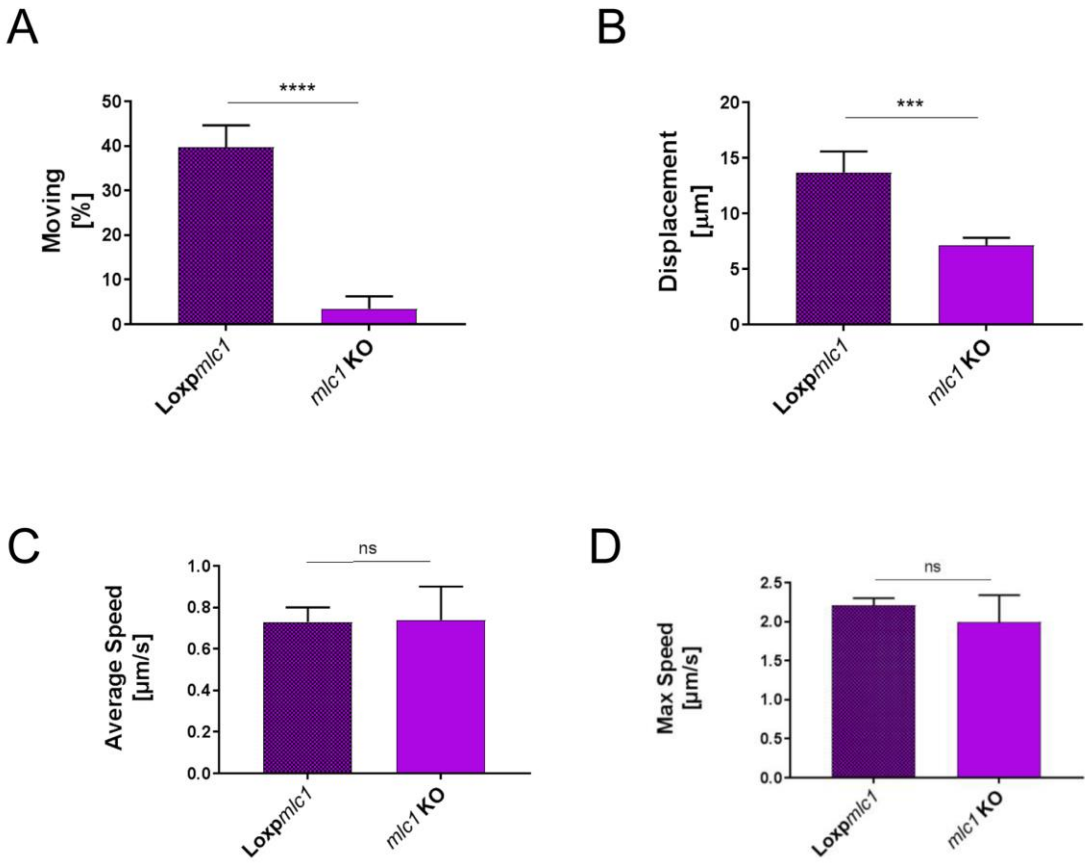

Figure 3-7. 3D gliding kinetics analysis of *mlc1* KO mutant parasites
Results obtained by Dr. Jacquelin Leung and Prof Gary Ward
A. loxp*mlc1* and *mlc1* KO tachyzoites gliding in a 3-D matrix were recorded and the percentage of total parasites moving was quantified (only tracks greater than 2µm were considered as moving parasites). The number of *mlc1* KO parasites moving drops significantly when compared to the loxp*mlc1* control line. **B.** Gliding trail distances are significantly shorter in the *mlc1* KO line **C.** Average speed **D.** and maximum speed of tracked parasites present no statistical differences compared to control parasites. Graphs show mean ± SD of six replicates per induced knockout sample. Two-way ANOVA followed by Sidak's test was used to compare between groups. **** P≤0.0001 *** P≤0.001

ns P>0.05. Figure modified from (Whitelaw et al., 2017) under Creative Commons Attribution 4.0 International License.

Taken together, the 2D and 3D gliding kinetics confirm that MLC1 is important for gliding motility. Both 2D and 3D analyses show a reduction in the percentage of motile *mlc1* KO parasites. In terms of trail length, the displacement in the 3D environment is reduced compared to the 2D. This could be explained by the resistance that parasites need to overcome when moving in Matrigel, which exceeds that experienced in a 2D assay. When gliding in a 2D assay, MLC1 depleted parasites showed significant differences in terms of average and maximum speeds when compared to control parasites. Such difference was not evident in 3D experiments, which highlights the importance of combining assays to obtain accurate quantitively and qualitatively analysis of gliding motility.

3.1.7 *mlc1* KO penetration kinetics and analysis

T. gondii tachyzoite invasion is a smooth multi-step process that can be completed in a short time, usually ranging between 25 to 40 seconds (Morisaki et al., 1995). During this process parasites engage with the host cell plasma membrane via the tight junction (TJ) that consists of a multi-subunit protein complex secreted by the parasite to establish a bridge with which to enter the host. This junction moves continuously over the parasite from the apical to posterior pole as invasion proceeds, and has been shown to be indispensable for apicomplexan zoite penetration processes (Besteiro et al., 2011, Bargieri et al., 2014). In the case of *myoA* KO parasites, host cell penetration shows a normal TJ formation but presents a significant defect in attachment and an arrested "stop and go" motion during penetration. These characteristics slow the invasion process to times ranging from 25 seconds to 10 minutes (Egarter et al., 2014). The remaining invasion rate in the *myoA* KO has been suggested to be host cell-dependent. According to a recent study, host cell plasma membrane protrusions can be pulled over the parasite, resulting in host cell force to facilitate *myoA* KO mutant penetration (Bichet et al., 2016). In the case of the *mlc1* KO, previous reports suggest it is not essential for either TJ formation or host cell invasion (Egarter et al., 2014). This observation was confirmed by long term culture of *mlc1* KO parasites facilitated by mechanical egress and population enrichment (Figure 3-2B).

I was curious to know if *mlc1* KO parasites present an arrested phenotype while invading, similar to that of *myoA* KO parasites. Time-lapse microscopy was used to evaluate the invasion process in *mlc1* KO parasites. Extracellular parasites were inoculated into confluent cell cultures and imaged for 30 minutes. Seventeen invasion events were recorded

in bright field with a final FITC image taken to identify mutant parasites (YFP+) from un-induced parasites (YFP-). Unlike the *myoA* KO, *mlc1* KO parasites can invade host cells in a smooth manner (Figure 3-8A/B). The average penetration time is significantly slower than in RHΔ*hxgprt* parasites (Figure 3-8A, top panel. Movie 5), with times ranging from 22 sec, comparable to the control strain (Figure 3-8A, bottom panel. Movie 6), to 6 min (Figure 3-8A, mid panel. Movie 7).

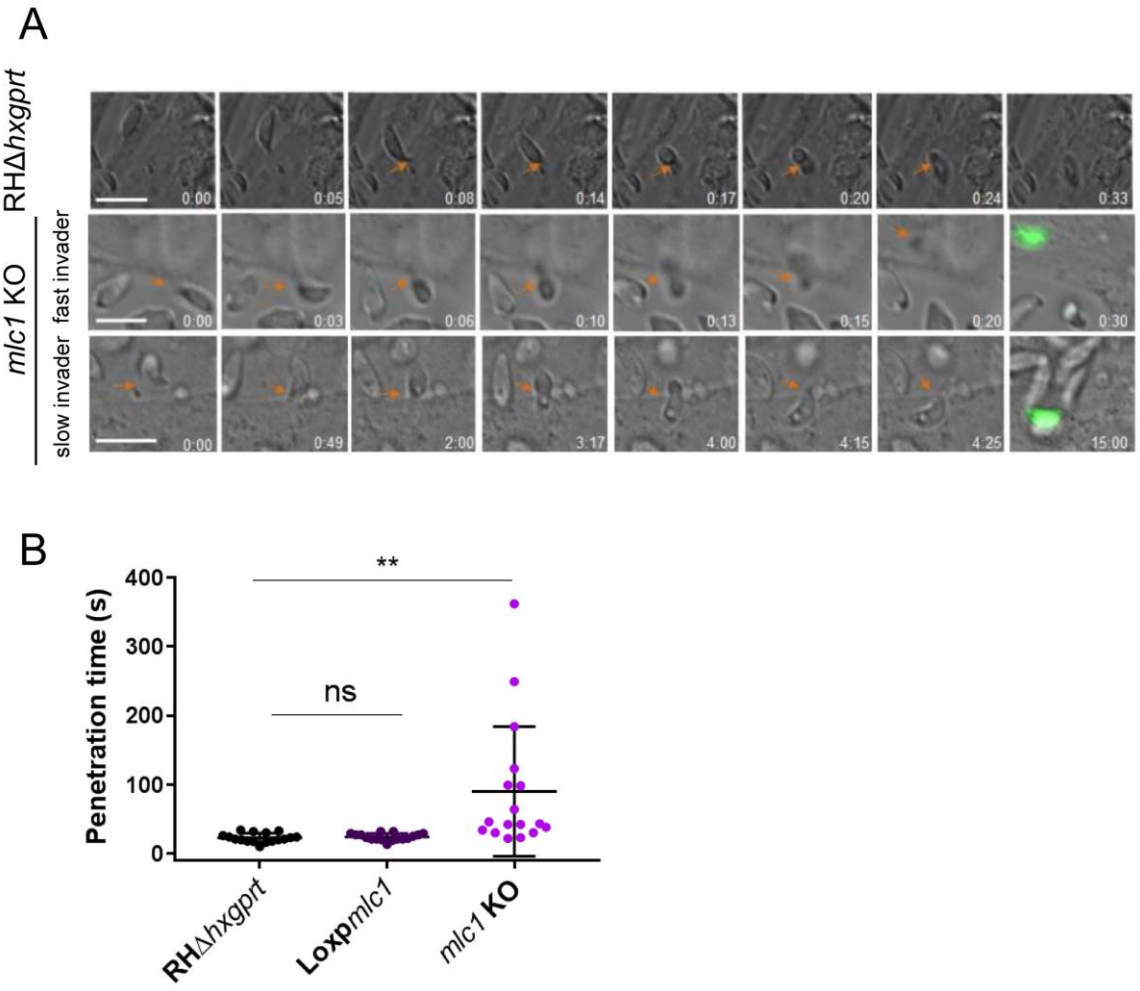

Figure 3-8. Host cell invasion kinetics of *mlc1* KO mutant strain.
A. Time-lapse analysis of RH*Δhxgprt* and *mlc1* KO tachyzoites penetrating HFFs. Videos were recorded at one frame per second in DIC. A final image in FITC was taken to identify YFP+ parasites, which was used to determine that the *mlc1* gene had been excised. Arrows follow tight junction formation until closure. Representative images of fast and slow MLC1 depleted invaders are shown in the panel. Time stamp indicates minute.seconds. Scale bar represents 10µm **B.** Graphic displays penetration time of RHΔ*hxgprt*, loxp*mlc1* and *mlc1* KO. Seventeen events for each strain were tracked manually from tight junction formation to closure. *mlc1* KO parasites show a delay in penetration time, but an open distribution of penetration speeds (min: 22 sec) (max: 362 sec). Graphic shows average ± SD. One-way ANOVA followed by a Tukey's test was used to calculate differences among means. **, $p<0.01$. ns $P>0.05$. Figure modified from (Whitelaw et al., 2017) under Creative Commons Attribution 4.0 International License.

These data suggest that *mlc1* KO parasites do not show an attachment phenotype or display a "stop and go" penetration motion, in contrast to *myoA* KO parasites (Egarter et al., 2014). On the contrary, a continuous invasion process was observed. Yet, the average penetration time shows slower kinetics compared to control parasites. Taken together, we have shown that *mlc1* KO parasites are able to generate enough force to invade host cells, but that this process shows a wide range of penetration times. However, we cannot discard the possibility that partial force for entry is generated by the host cell, as observed for the *myoA* KO (Bichet et al., 2016). Deeper characterisation of this process using more advanced microscopy tools is needed to understand the role of the host in *mlc1* KO penetration.

3.1.8 MLC1 is essential for host cell egress

Host cell egress is a highly coordinated process required for *T. gondii* to move from one host cell to another following completion of replication. Early studies showed that a calcium signalling cascade triggers stimulation of several processes producing physiological changes in intracellular parasites that result in egress (Endo et al., 1982). Host cell egress can be artificially induced by increasing intracellular calcium levels using Calcimycin (Ca^{++} Ionophore A23187) or dithiothreitol (DTT) (Endo et al., 1982, Stommel et al., 1997). Prior to host cell rupture and dissemination, parasites change their morphology, become highly motile, and secrete perforins to permeabilise the parasitophorous vacuole (PV) and host cell plasma membrane (PM) to exit the host cell (Black et al., 2000, Kafsack et al., 2009). Regulation of these processes is associated to calcium-dependant plant-like kinases (CDPKs) and protein kinases (PKs) (Lourido and Moreno, 2015). In *T. gondii*, protein kinase G (PKG), calcium-dependant plant-like kinase 1 (CDPK1), and calcium-dependant plant-like kinase 3 (CDPK3) have been implicated in egress through their phosphorylating proteins of the motor complex and triggering microneme secretion (Dvorin et al., 2010, Lourido et al., 2010, Garrison et al., 2012, Lourido et al., 2012, McCoy et al., 2012, Gaji et al., 2015). In the case of TgCDPK3, studies show that MyoA is a main substrate of this kinase, which is further supported by their colocalisation at the periphery of the parasite (Gaji et al., 2015).

Although not essential for gliding, invasion, or replication, MLC1 has been shown to be essential for host cell egress, either naturally or upon induction with Ca^{++} ionophore (Figure 3-9A) (Egarter et al., 2014). Considering that motility via phosphorylation of the motor complex is strongly associated with egress, I took a closer look at *mlc1* KO parasites to determine how egress is blocked in these mutants. First of all, the integrity of the PV was examined upon induction of internal Ca^{++} influx using antibodies against parasite plasma

membrane proteins (αSAG1) under non-permeabilising conditions (section 2.12.7 and 2.12.8). Therefore, SAG1 signal is only visible if the PV and host cell PM are disrupted and the parasites are directly exposed to the antibody (Black et al., 2000). For this, $1x10^4$ parasites were induced 96 hours prior to infecting host cells and left to invade for one hour. Note that a low number of parasites were used to observe well separated/isolated vacuoles, such that egress of induced and non-induced vacuoles could be observed independently. After invasion, extracellular parasites were washed away and intracellular parasites were left to replicate for 48 hours. Ca^{++} influx was induced with Ca^{++} Ionophore (A23187) for 10 minutes before fixation, and an IFA using antibodies against SAG1 in non-permeabilising conditions was performed.

Within the population, virtually all RHΔ*hxgprt* vacuoles egressed after 10 minutes of induction (Figure 3-9B top-panel). SAG1 signal was observed in 100% of extracellular parasites (freshly egressed) as well as all the parasites within disrupted vacuoles. In the case of *mlc1* KO, 96±1 % vacuoles (YFP+) remained internalised within the host cell. From this, 61±14 % of the parasites presented SAG1 signal (Figure 3-9 bottom-panel); and the remaining proportion did not show detectable SAG1 staining inside the host cell (Figure 3-9 mid-panel). These results suggest that *mlc1* KO parasites are not able to egress a permeabilised vacuole, and also present a delay in membrane permeabilisation.

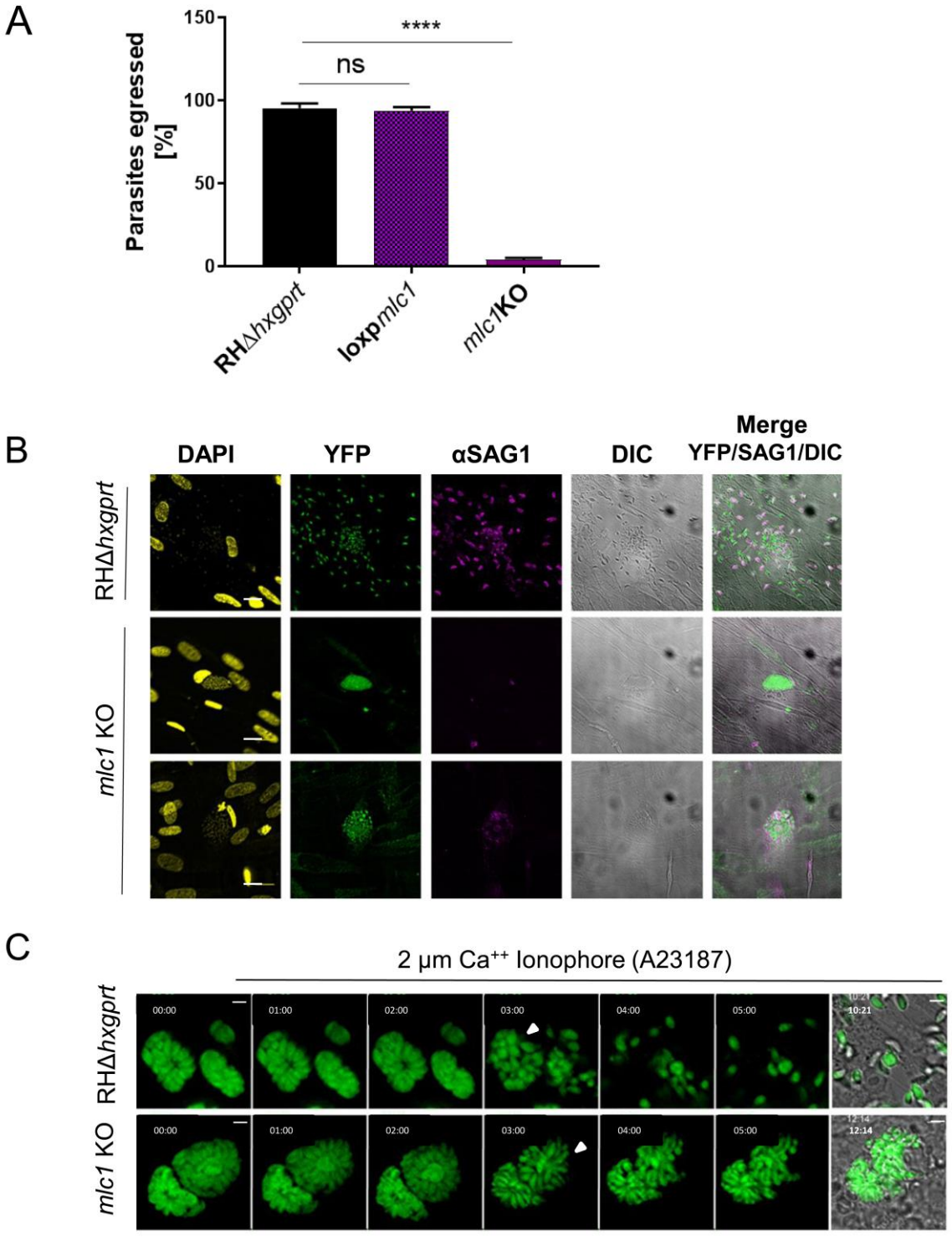

Figure 3-9. Host cell egress is blocked in the *mlc1* KO

A. Quantification of RHΔ*hxgprt*, loxp*mlc1,* and *mlc1* KO egress after Ca^{++} Ionophore induction (10 minutes). *mlc1* KO is severely impaired in its ability to egress. Graphic displays mean values ± SD of three replicates. One-way ANOVA followed by a Tukey's test was used to calculate differences among means. ****, p<0.0001 **B.** IFA using αSAG1 staining under non-permeabilising conditions was used to visualise PV disassembly and parasite dissemination upon Ca^{++} ionophore stimulation (10 minutes). Even though most vacuoles remained completely intracellular (mid panel) upon Ca^{++} stimulation, perforation of the PV can be observed in a small population. This was observed in vacuoles with intravacuolar SAG1 signal. Scale bar represents 20µm **C.** Time-lapse microscopy was used to follow egress progression after Ca^{++} Ionophore induction. Videos were recorded at 1 frame per second. Stimulation with Ca^{++} ionophore was completed within the first minute at timepoint, 0:00. *mlc1* KO strain is responsive to internal calcium flux stimulation (white arrows), but no rupture of the

PV or dissemination is evident in the mutant line when compared to control parasites. Numbers indicate time (minutes.seconds). Scale bars represent 5um.

As permeabilisation of the PV and host cell PM are motility independent, we investigated further if the *mlc1* KO parasites were delayed in their response to Ca^{++} ionophore (A23187) treatment. For this, live imaging of egressing parasites was carried out. Briefly, cultures were infected with *mlc1* KO parasites (96 hours post induction) in glass bottom dishes as described below (section 2.12.9.3). After 36 hours of replication, vacuoles of interest were identified and imaged at 1 frame per second. Egress was induced with 2 µM Ca^{++} ionophore A23187, one minute after imaging commenced. As expected, in control parasites calcium triggered morphological changes and stimulated motility in virtually all vacuoles of the culture approximately 1 minute after Ca^{++} influx. Following this, the RB of the vacuoles collapsed, the PV ruptured, and finally, the host cell PM was disrupted (Figure 3-9C, Movie 8). The *mlc1* KO vacuoles, identified by their YFP+ signal, changed their morphology and became slightly motile after one minute of Ca^{++} ionophore induction. However, by this point, it cannot be ruled out that the movement observed in the parasites reflects the host cell movement, which also seems to move. Following, the RB of the vacuole collapses, but no apparent PV rupture was observed. The host cell PM did not collapse and parasites did not disseminate (Figure 3-9, Movie 9).

As shown in control parasites, Ca^{++} ionophore increases intracellular Ca^{++} levels and triggers cytoskeletal changes, motility induction, and microneme secretion, resulting in permeabilization of the PV rapid parasite release. Results presented here show that *mlc1* KO parasites are responsive to increased Ca^{++} levels at the same time as control parasites (approximately one minute after treatment), demonstrated by morphological changes and slight movement; however, these mutants were unable to egress permeabilised PVs. In addition, around 70% of *mlc1* KO vacuoles showed αSAG1 signal in the absence of detergent permeabilisation, indicating that the egress block is not due to PV permeabilisation *per se.* In fact, these data partially resemble the egress block observed in the absence of apical complex lysine methyltransferase (AKMT). *akmt* KO mutants did not affect either PV nor host PM permeabilisation, yet, the egress phenotype corresponded to deficient motility activation (Heaslip et al., 2011). Unlike *mlc1* KO and *akmt* KO, depletion of the permeabilisation protein, perforin-like protein 1 (PLP1), caused egress delay, but host cell disruption was eventually achieved due to vigorous movement of the parasites (Kafsack et al., 2009). These results point to motility as a major factor for egress; thus, in the case of the *mlc1* KO, suggesting peripheral motor location is necessary for host cell disruption. Consistent with this premise, CDPK3 was shown to be able to phosphorylate MyoA and

actively participate in an egress signalling cascade (Garrison et al., 2012, Lourido et al., 2012, McCoy et al., 2012, Gaji et al., 2015). Therefore, absence of MLC1-MyoA in the periphery impedes regular cascade events, resulting in a motility activation block. Finally, the motor complex function can be related to regulation, initiation, or mediation of efficient motility prior to rupture and microneme secretion, or relevant signalling pathways, but this remains an open question for future experiments.

3.2 Summary and conclusions

Previous studies suggested that force generation for motility and invasion relied on the acto-MyoA motor complex (Dobrowolski et al., 1997a, Soldati and Meissner, 2004). The studies discerned the essentiality of ACT1 and MyoA based on inhibition with drugs and the generation of inducible knockdowns using the tetracycline trans-activator system (Dobrowolski et al., 1997a, Dobrowolski et al., 1997b, Meissner et al., 2002b). The residual invasion and gliding seen in these studies was attributed to a lack of specificity and the "leakiness" of the systems used. However, the essentiality of these proteins was not questioned due to the strong phenotypes of the mutants (Dobrowolski et al., 1997b, Meissner et al., 2002b). The establishment of the DiCre system in *T. gondii* allowed for generation of knockouts of MyoA, MLC1 and ACT1, all key functional components of the acto-MyoA motor complex (Andenmatten et al., 2013, Egarter et al., 2014). While clearly reduced, gliding and invasion were not blocked in any of the named mutants, contrary to egress, which was significantly affected in the *mlc1* KO, *act1*KO and *gap45* KO (Egarter et al., 2014).

One explanation for the residual gliding motility and invasive capability seen in the *myoA* KO line was a recovery of some MyoA functions by the closely related MyoC, whose specific functions remain unknown (Egarter et al., 2014, Frenal et al., 2014). For this reason, a *myoA/B/C* KO (triple KO) was generated by (Egarter et al., 2014), and replicated in (Frenal et al., 2014). These conditional mutants were not viable in culture because they have a significant egress defect, but remained invasive (Egarter et al., 2014, Frenal et al., 2014). In both cases, removal of MyoB/C in the *myoA* KO had a great impact on parasite fitness; for this reason, redundancies among the heavy chains was considered a key point to explain the residual invasive capability of the *myoA* KO strain.

Toxoplasma gondii contains a repertoire of seven MLCs, but only MLC1 is responsible for MyoA location in the pellicle; a similar interaction has been shown for *P. falciparum* MTIP-MyoA (Bergman et al., 2003, Polonais et al., 2011, Sebastian et al., 2012,

Egarter et al., 2014). Recent studies have co-precipitated MyoC and MLC1 and concluded they interact at the posterior pole of tachyzoites with other elements in the so called MyoC glideosome (Frenal et al., 2014). Under this premise, we considered that any interaction between MyoC and the rest of the motor complex must be mediated via MLC1.

For this reason, this chapter focused on characterising a *mlc1* KO in greater detail, as information gleaned from characterising this mutant represents a key point in explaining the loss of peripheral MyoA localisation and other recognised essential light chains that interact with it (Egarter et al., 2014, Williams et al., 2015). Depletion of MyoA results in relocation of ELC1 from the periphery (Williams et al., 2015) and, predictably, ELC2, which is explained as both light chains competing for the same binding site in the MyoA neck domain.

Analysis of MLC1 levels and MyoA peripheral localisation confirmed these proteins are significantly lost 36-48 hours after rapamycin induction in the conditional *mlc1* KO line (Egarter et al., 2014). This implies that MLC1 is essential for MyoA localisation at the pellicle, as MLC1 depletion causes loss of the MyoA-MLC1 complex. Additionally, through bypassing egress and enriching the induced population, I maintained the *mlc1* KO for a prolonged period, suggesting that, although this protein is essential for egress, it is dispensable in all other steps of the lytic cycle. This is consistent with the lack of a delayed death phenotype from impaired apicoplast segregation, unlike that observed for ACT1 and MyoF disruption (Jacot et al., 2013, Whitelaw et al., 2017). Similarly, the *mlc1* KO parasite replication rate is comparable to control parasites. Moreover, by using time-lapse microscopy and automated tracking, I measured gliding displacement and speed, and confirmed that *mlc1* KO mutants can glide in circular and helical manners. These findings were supported using Matrigel to perform 3D gliding characterisation (Leung et al., 2014, Whitelaw et al., 2017). Here, mutants moved at an average and maximum speed comparable to control parasites even though the length of the trails was significantly reduced. Similarly, invasion kinetics of the *mlc1* KO showed a wide distribution of invasion speeds. Thus, some mutants presented fast penetration kinetics (minimum 23 sec), while others exhibited slow invasion kinetics (maximum 362 sec). However, egress assays showed that *mlc1* KO mutants are capable of reshaping and slightly move inside the PV, but that disruption of the PV and dispersion of the parasites was not observed, consistent with an egress defect.

Considering that both MyoA-MLC1 and MyoC-MLC1 interactions are lost in the *mlc1* KO, these results show that MyoC can partially rescue the *myoA* KO line phenotype

(Frenal et al., 2014, Frenal and Soldati-Favre, 2015). Under this premise, the ability of parasites to disrupt the PV and exit the host cell is a key fact that supports overlapping roles of these proteins. On the other hand, other functions, like gliding speed, are enhanced in absence of MLC1, which calls into question the ability of MyoC to compensate for MyoA motor functions.

These findings raise questions about the probability of direct compensation between MyoA and MyoC. Considering there are seven MLCs recognised in *T. gondii*, we cannot discard the possibility of MyoC working together with another light chain, or simply that another motor complex (such as MLC2-MyoD) has taken over these important roles in the parasite.

Chapter 4 Generation and characterisation of *myoB/C/mlc1* KO

MyoB and MyoC are products of alternative splicing of the same gene, and are expressed predominantly in the bradyzoite and tachyzoite stage, respectively. Like MyoA, MyoC is classified as an unconventional myosin containing a conserved head domain, a divergent neck domain, and an atypical short tail domain responsible for its localisation to the posterior pole of the parasite (Delbac et al., 2001, Foth et al., 2006). Overexpressed MyoC co-immunoprecipitates with structural proteins -GAP80, GAP40, GAP50, IAP1- and functional light chains -MLC1 and ELC1- (Frenal et al., 2014). However, the ELC1 has been highlighted as specific for MyoA, for it is mislocalised upon MyoA depletion, losing its association with the periphery while no posterior pole relocation was observed (Williams et al., 2015). The association of MyoC with these proteins indicates a similar composition to the MyoA motor complex, for this reason, the complex was named the MyoC-glideosome or MyoC motor complex. Early studies associated MyoC with parasite division, however actin-disrupting drugs did not affect this process, demonstrating that cytokinesis is myosin-independent (Delbac et al., 2001, Gubbels et al., 2006). Further studies focused on identifying MyoC motor complex functions. Several attempts to knockout the main components of the MyoC motor complex failed to show a clear phenotype in the tachyzoite stage (Egarter et al., 2014, Frenal et al., 2014). Another unconventional myosin present in *T. gondii* is MyoH (Foth et al., 2006), which is located in the apical pole and associated with the microtubules present in the conoid. This heavy chain can interact with three light chains, namely MLC1, 3, 5, and 7, and contains a tail domain, which gives it the capacity to anchor to the conoid (Graindorge et al., 2016). Disruption of the MyoH gene impaired the capacity of parasites to glide, invade, and egress, but no effect on replication was observed (Graindorge et al., 2016). MyoH mutant parasites showed that this protein has a role during host cell entry, demonstrated by a defect on the formation and progress of the moving junction (TJ) (Graindorge et al., 2016).

As MyoA and MyoC share the same interacting partner, MLC1, and have structural similarities, both myosins are good candidates to complement each other either is lost. The potential redundancies between MyoA and MyoC raised two questions regarding phenotypes seen in previous studies. First, are *myoA* KO parasites able to invade and glide because of direct compensation by MyoC**?** Second, is the lack of phenotype upon removal of MyoC in tachyzoites because of rapid complementation by MyoA**?** (Egarter et al., 2014, Frenal et al., 2014). In order to find an answer to these questions, inducible systems were

used to disrupt MyoA/B/C together, the mutant lines generated were: DiCre inducible *myoA* KO in the *myoB/C* KO (*myoB/C* KO loxp*myoA*), also known as triple KO (Egarter et al., 2014), and TetR inducible MyoB/C KD in the *myoA* KO (*myoA* KO imyoC KD) (Frenal et al., 2014). As MyoB and MyoC are protein products from the same gene (Delbac et al., 2001), disruption of the gene abolishes expression of both myosins (Egarter et al., 2014, Frenal et al., 2014). In both previous studies, it was not possible to isolate a viable triple KO line. Removal of all three myosins blocked parasite progression through the lytic cycle, observed by the absence of plaques in growth assay (Egarter et al., 2014). However, a closer examination revealed, 2-5% of the parasites remained invasive after respective gene excision and no significant intracellular growth phenotype was observed (Egarter et al., 2014, Frenal et al., 2014). However, natural and Ca^{++} induced host cell egress was completely blocked when the myosins were no longer expressed. Based on these results, the ability of MyoA-MyoC to functionally compensate for the loss of the other myosin was a plausible explanation (Egarter et al., 2014, Frenal et al., 2014, Frenal et al., 2017a).

Considering the presence of seven light chains and the plasticity suggested for *T. gondii* myosins, a plausible idea to explain the remaining invasiveness and motility in the *myoA/B/C* KO (triple KO) is due to the availability of MLC1 in the pellicle that could target another unconventional myosin to complement for the loss of *myoA/B/C*. Similarly, remaining invasion and gliding rates in the *mlc1* KO could be driven by MyoC accompanied by another light chain. This idea is reasonable as MyoC location in the posterior pole depends on the structural protein IAP1, but not MLC1 (Frenal et al., 2014, Whitelaw et al., 2017).

To test this hypothesis and study if invasion and gliding can happen in absence of MLC1 and/or MyoA/B/C, this chapter focuses on the generation and characterisation of a conditional *myoB/C/mlc1* KO mutant. This knockout line allowed us to study the phenotype of parasites directly lacking MLC1 and MyoC, key proteins associated to the MyoA- and MyoC-motor complexes. Additionally, this conditional line permitted us to observe the effect of parasites indirectly lacking MyoA as this protein relocates to the cytoplasm and is probably degraded upon MLC1 depletion (section 3.1.3) (Egarter et al., 2014). Furthermore, previous studies showed that MyoA possess two specific light chains, ELC1 and ELC2, which depend on MyoA to keep their peripheral location (Williams et al., 2015). By directly and indirectly removing these six components of the motor-complex machinery, I speculated this conditional knockout would allow us to assess and distinguish between different potential redundancies from both MLC and myosin side. Under this premise, If MyoC fully

rescues for MyoA phenotype via interaction with MLC1 in the periphery (Frenal et al., 2014, Frenal et al., 2017a), the *myoB/C/mlc1* KO mutant here characterised would present a detrimental phenotype for motility and invasion. While in case MyoA is directed to the periphery by other light chain there is a potential possibility to recover for the detrimental egress phenotype.

4.1.1 Generation of *myoB/C/mlc1* KO

To generate this line, I obtained a *myoB/C* KO in the loxp*mlc1* line using a similar *myoB/C* KO plasmid and protocol as previously described (Egarter et al., 2014). Briefly, a bleomycin resistance cassette was flanked with 2000 bps of MyoC 5' and 3' UTR regions (Figure 4-1A). Validation of correct integration of the *myoB/C* KO cassette was achieved by analytical PCR. Here, we used three sets of primers. The first amplifies the *myoB/C* gene product (1-1') which will be lost upon successful gene replacement. Two sets of oligonucleotides specifically designed to bind outside the homology region and inside bleomycin cassette at the 5' (2-2') and 3' (3-3') ends show successful replacement with the resistance marker. As shown in Figure 4-1B, a clonal line myoB/C loxp*mlc1* was successfully isolated after bleomycin selection. Loss of *myoB/C* gene confirmed in the *myoB/C* loxp*mlc1* line and integration was validated by the 5' and 3'correct integration of bleomycin resistance cassette.

Since this inducible line, *myoB/C/mlc1* KO, was generated in the previously described loxp*mlc1* (section 3.1.1) (Egarter et al., 2014), the same conditions for induction were applied for depletion of MLC1 (section 3.1.1). Induction with rapamycin [100 ng] was used and all experiments were performed 96 post induction.

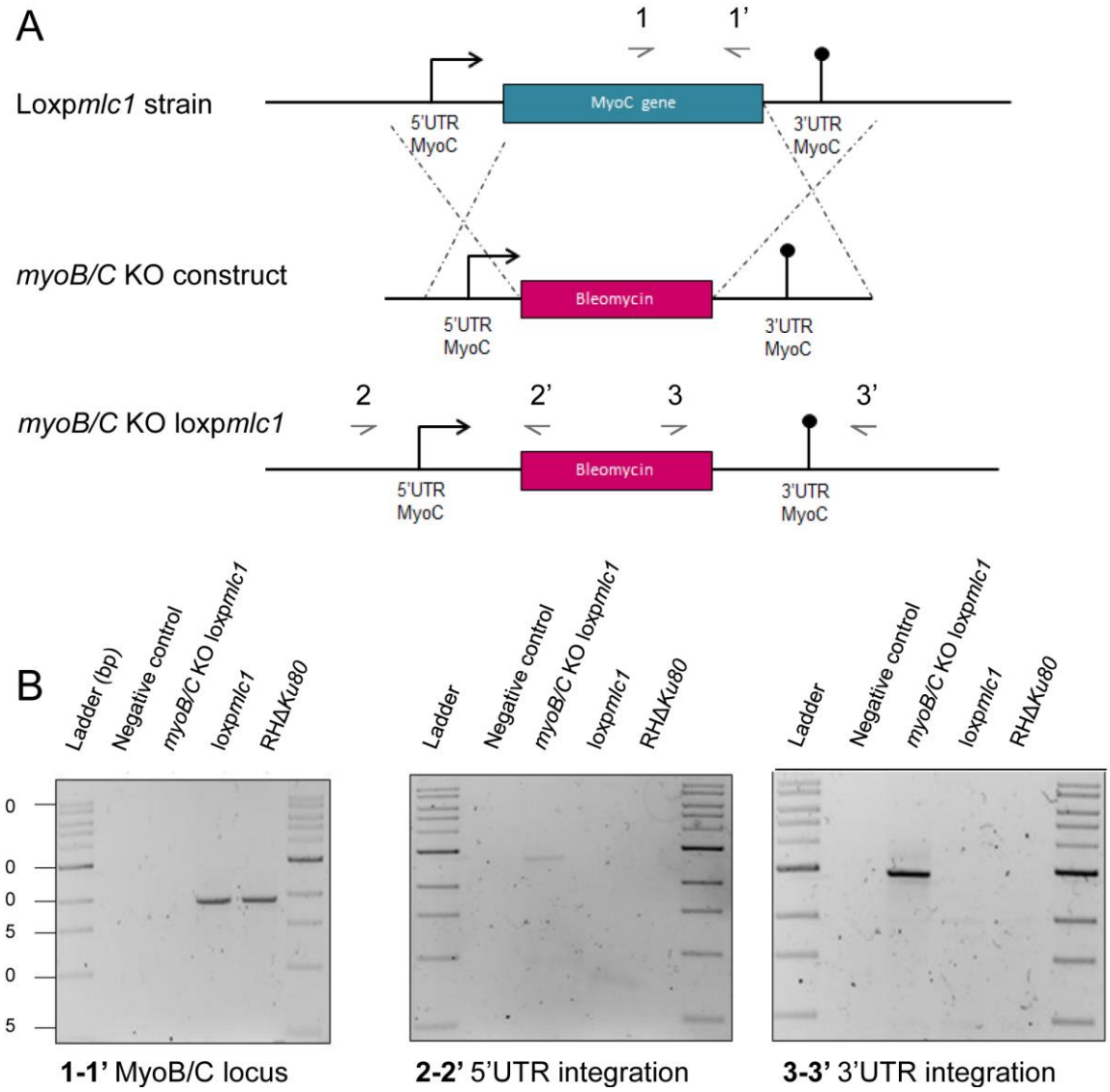

Figure 4-1. Generation of an inducible *myoB/C/mlc1* KO strain
A. Scheme of the *myoB/C* KO plasmid integrated in the loxp*mlc1* line. Double homologous recombination was used to introduce a Bleomycin cassette in the *myoB/C* locus. **B.** Confirmation of integration of the *myoB/C* KO cassette by PCR. Correct excision of myoB/C gene was confirmed by using primer pair 1-1' (expected size: 1.9 Kbp), whereby loss of the amplification product demonstrates loss of the gene in the genome. To verify correct integration of the *myoB/C* KO vector at 5' and 3' ends, the set of primers 2-2' (expected size: 2.8 Kbp) and 3-3' (expected size: 2.7 Kbp) were used, and can only amplify if the bleomycin cassette has been integrated at the MyoB/C locus; as seen in the schematic (A). DNA ladder shows molecular standard weights. Numbers expressed in Kbp.

4.1.2 *myoB/C/mlc1* KO cannot progress through the lytic cycle

To determine the ability of these parasites to complete the lytic cycle, a five-day plaque assay was carried out. Briefly, extracellular *myoB/C* KO loxp*mlc1* parasites were induced with 100nM rapamycin for four hours prior to infection as shown in section 3.1.2. Confluent monolayers of HFF cells were then infected with $1x10^3$ parasites. Cultures were incubated under normal conditions for 5 days without disturbance to give parasites enough

time to engage in several rounds of the lytic cycle. After this time host cells were fixed with 4% PFA.

As shown in Figure 4-2A, no difference was observed between RHΔ*hxgprt* and *myoB/C* KO loxp*mlc1* strains (top panels) confirming the observation that removal of MyoB/C does not impair the *T. gondii* lytic cycle (Egarter et al., 2014, Frenal et al., 2014). On the other side, monolayers containing *myoB/C/mlc1* KO parasites presented fewer plaques when compared to control lines. The induction rate of the *myoB/C* KO loxp*mlc1* line was around 25-35%, for this reason, it was possible to visualise two different populations in the plaque assay corresponding to non-excised YFP- (*myoB/C* KO loxp*mlc1*) parasites and excised YFP+ (*myoB/C/mlc1* KO) parasites (bottom panels). All plaques formed were YFP-negative corresponding to parasites still expressing MLC1, while no plaques of YFP-positive parasites were observed (bottom panel/expansion). In this case, individual rosettes were seen but no dissemination was evident. Thus, this phenotype resembles to results previously reported for *mlc1* KO growth (Egarter et al., 2014).

Furthermore, I was curious to investigate if *myoB/C/mlc1* KO parasites were able to survive for longer periods if egress was bypassed and the population was enhanced. For this reason, mutant parasites were mechanically released from the host cells each 36-48 hours, and the population of uninduced parasites was controlled using DMEM media supplemented with 2.5% dextran sulphate (DS). Since DS prevents re-invasion of egressed parasites, it prevented overgrowth of the uninduced population, while *myoB/C/mlc1* KO mutants remained intracellular, most probably reflecting the detrimental egress phenotype observed in the *mlc1* KO (section 3.1.8). By using these constant procedures, *myoB/C/mlc1* KO parasites were kept in culture for up to 12 days (Figure 4-2B).

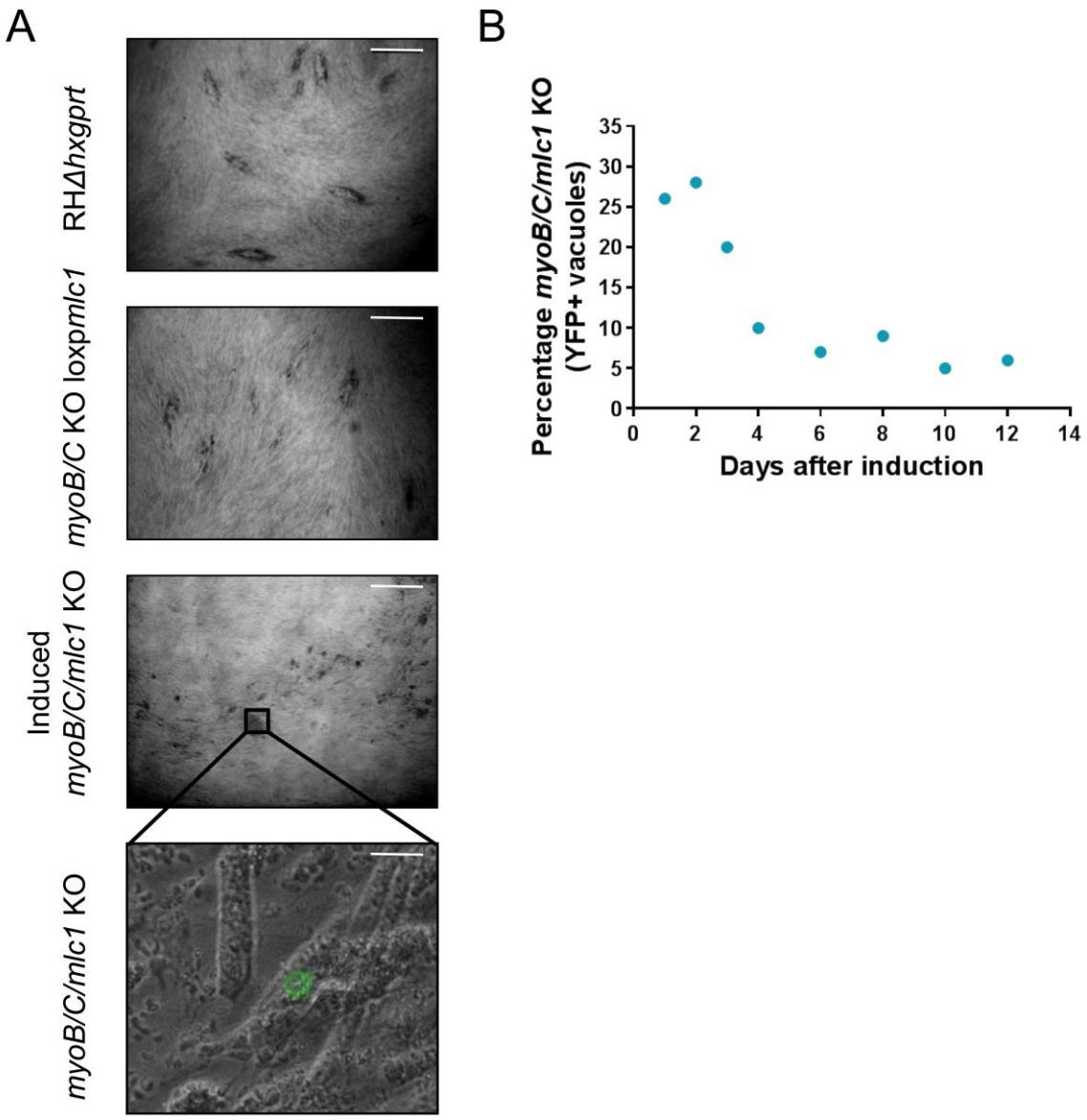

Figure 4-2 *myoB/C/mlc1* KO **can be maintained in culture if egress is mechanically induced**
A. Five-day plaque assay to analyse growth ability of RHΔ*hxgprt* and *myoB/C/mlc1* KO. Inducible line presents two independent populations: YFP- populations dispersed and forming plaques and YFP+ parasites not forming plaques (*myoB/C/mlc1* KO). Scale bar represents 0.2 mm (top panels) and 20 µm (bottom panel) **B.** *myoB/C/mlc1* KO was maintained in culture by controlling uninduced population and mechanically assisting egress of YFP+ vacuoles. Percentage of parasites was measured by counting YFP+ vacuoles over the total number of vacuoles contained in 20 fields of view using a 40X objective lens.

These results suggested that the *myoB/C/mlc1* KO strain was blocked in egress, as large vacuoles could be observed, but no propagation of the YFP+ population was seen. Like data shown for *mlc1* KO (section 3.1.4), these parasites could be maintained in culture for longer than 96 hours if egress was bypassed.

It is plausible to think that if egress is mechanically induced and the population enriched, these parasites could be maintained for longer periods, like demonstrated for the *mlc1* KO (section 3.1.4). This data resembled the *mlc1* KO and triple KO phenotype, re-

affirming the observation that the loss of a motor localised at the periphery causes a block in egress. Furthermore, the fact that *myoA* KO parasites are delayed, but not blocked, in egress confirms the observation that MyoC can indeed complement for egress in this absence when MLC1 is present.

4.1.3 *myoB/C/mlc1* KO can glide in circular and helical manner

The accepted linear motor model suggests that gliding motility and invasion rely on MyoA, and its light chain MLC1, to generate force by moving along short actin filaments, which redistributes transmembrane proteins from the apical tip to the posterior pole resulting in forward motion (Meissner et al., 2002b, Soldati and Meissner, 2004). Contrary to what was predicted by the linear motor model, *myoA* KO, *mlc1* KO and *act1* KO strains presented residual gliding and invasion capacities (Meissner et al., 2002b, Andenmatten et al., 2013, Egarter et al., 2014). In terms of gliding, 40% (normalised to RH) of the *myoA* KO mutants could move, albeit with significantly slower speed, and formed mainly circular trails in a stop and go fashion (Egarter et al., 2014). In the corresponding experiments, the *mlc1* KO and *act1* KO conditional lines showed reduced gliding rates, but enhanced average speeds (Whitelaw et al., 2017). Additionally, both mutant lines move smoothly in a circular and helical manner (Whitelaw et al., 2017). Analysis of the *myoB/C* KO in tachyzoite stage demonstrated no observable or significant gliding phenotypes when compared to RHΔ*hxgprt* (Frenal et al., 2010, Egarter et al., 2014). Taken together these results show that, while gliding rates are similar among *myoA* KO, *mlc1* KO and *act1* KO, gliding kinetics present important differences and are key to understand the function of the motor complex. For this reason, we investigated the gliding capacity of the *myoB/C/mlc1* KO strain. First, a trail deposition assay was performed to assess the percentage of parasites moving. For this, motility was assayed by immunofluorescence detection of SAG1, a surface protein, which is deposited behind the parasite while moving (Dobrowolski and Sibley, 1996, Dobrowolski et al., 1997a). Here, only YFP expressing parasites were considered to ensure only *myoB/C/mlc1* KO trails were analysed. As shown in Figure 4-3A approximately 15% [25% normalised] of the parasites remained motile after excision of *mlc1* gene. These parasites formed predominantly circular trails [13%] but short helical trails were also found [2%] (Figure 4-3B). *myoB/C* KO loxp*mlc1* gliding rates were comparable to RH mutants with 59% and 58% [normalised] of the parasites moving in circular and helical manner, which confirms earlier results suggesting that MyoB/C does not contribute significantly to gliding in presence of MyoA.

Second, we were interested in analysing the gliding kinetics of these mutant parasites using time-lapse microscopy. For this, I followed the protocol described in section 3.1.6 used for analysing the *mlc1* KO parasites. Here, parasites were recorded at 1 frame per second. Distance, average and maximum speeds were analysed using WrMTrck plugin as described above (section 3.1.6). As shown in Figure 4-3C, *myoB/C/mlc1* KO parasites can move in both circular and helical manner. Interestingly, although circular gliding (47 ± 10 µm) presented comparable distances to RHΔ*hxgprt* (41 ± 4 µm), the average (0.4 ± 0.07 µm/s) and max (1 ± 0.1 µm/s) speeds were significantly slower (0.7 ± 0.08 µm/s and 1.7 ± 0.14 µm/s, respectively) (Figure 4-3 D/E). Moreover, even though the majority of parasites completed a circular boost in a clear smooth movement (Figure 4-3B mid panel, Movie 10), few glided in semicircles with a stop and go fashion as described for *myoA* KO (Figure 4-3B, bottom panel, Movie 11) (Egarter et al., 2014). In addition, twelve helical trails were recorded that presented shorter gliding displacement (24 ± 4 µm), but average (0.8 ± 0.3 µm/s) and max (1.9 ± 0.4 µm/s) speeds no different than RHΔ*hxgprt* parasites (1 ± 0.1 µm/s and 2 ± 0.2 µm/s, respectively) (Figure 4-3 D/E, Movie 12)

These results show the remarkable capacity of parasites lacking MyoA-MyoC and MLC1 in the pellicle to move in circular and helical manner with speeds comparable to RHΔ*hxgprt*. Here, we showed that circular movement results in similar displacement distances as RHΔ*hxgprt* parasites, but present a slight difference in terms of speed. 65% of trails were completed in smooth gliding boosts while 35% of the analysed parasites presented ‘stop and go’ like movement. Conversely, helical trails showed shorter distance displacement, while the average and max speeds are comparable to RHΔ*hxgprt* parasites

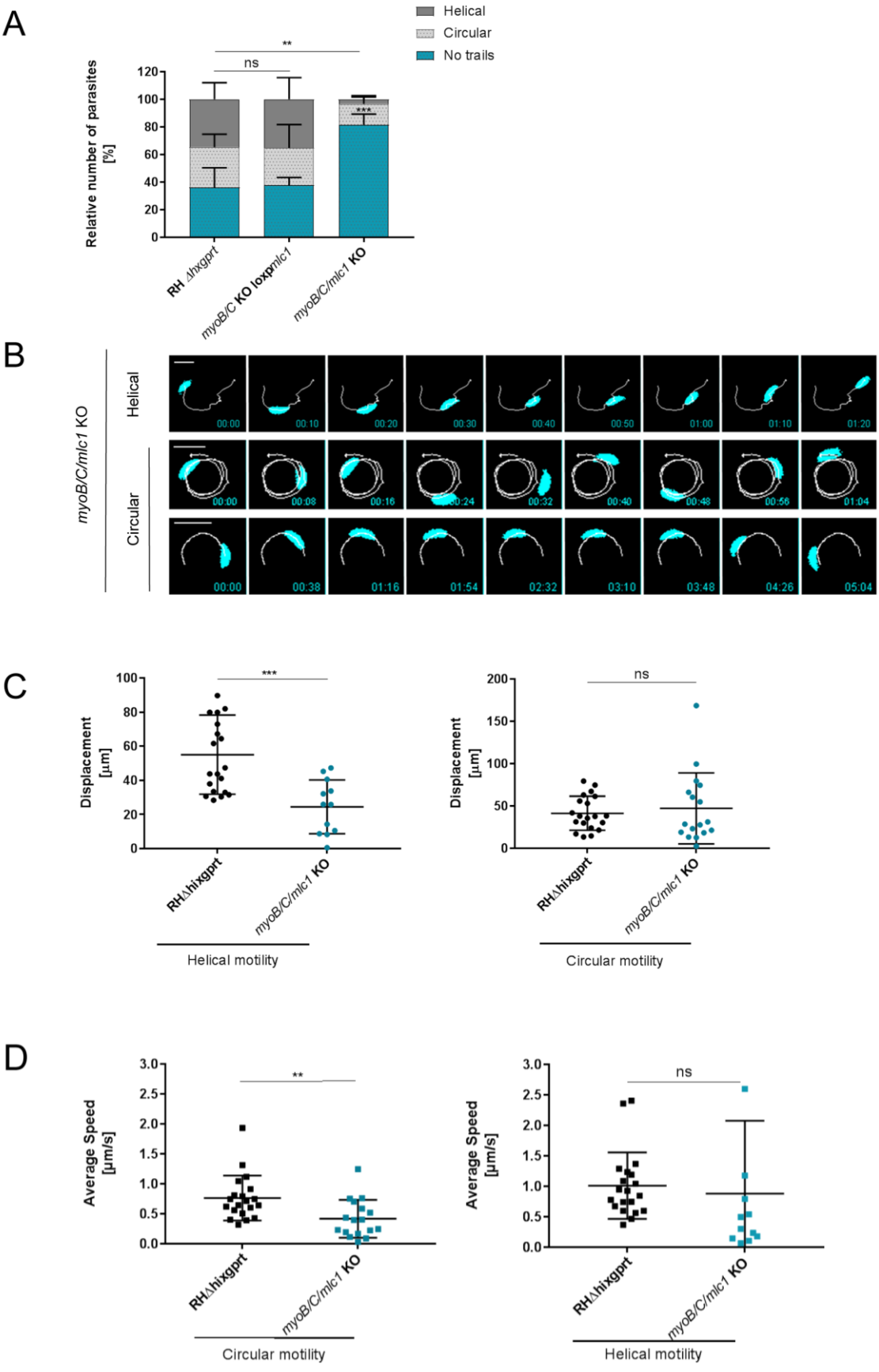
A
Helical
Circular
No trails
Relative number of parasites [%]
ns
**
***
RH Δhxgprt
myoB/C KO loxpmlc1
myoB/C/mlc1 KO
B
myoB/C/mlc1 KO
Helical
Circular
C
Displacement [µm]
***
ns
RHΔhixgprt
myoB/C/mlc1 KO
Helical motility
Circular motility
D
Average Speed [µm/s]
**
ns
RHΔhixgprt
myoB/C/mlc1 KO
Circular motility
Helical motility

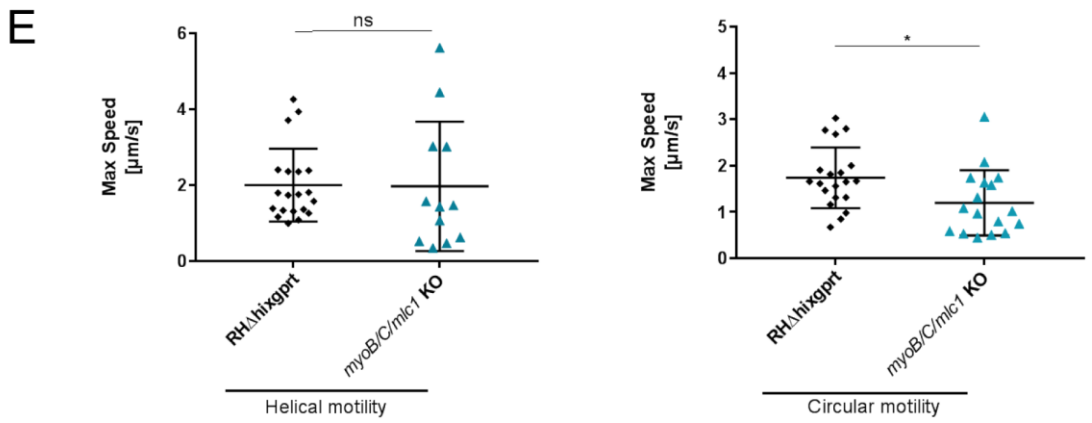

Figure 4-3. 2D gliding Kinetic analysis of *myoB/C/mlc1* KO mutant parasites
A. Quantification of trail deposition assay on RH*Δhxgprt, myoB/C* KO lox*pmlc1 and myoB/C/mlc1* KO. IFA using antibody αSAG1 was used to detect trails. Graphs displays mean values of three independent assays in triplicate ± SD. Two-way ANOVA followed by Tukey's post-hoc test was used to measure statistical differences among strains. *** P≤ 0.001, ** P≤ 0.01, not significant (ns) P>0.05 **B.** Tachyzoites gliding in a 2D environment were recorded at 1 frame per second. Seventeen circular and twelve helical trails were tracked using the Fiji wrMtrck plugin. Generated trails were superimposed on the time-lapse images to highlight movement. Time stamp indicates minute.seconds. Scale bar represents 10µm **C** Displacement, **D** average speed, and **E** Max speed of tracked parasites moving in circular and helical manner were quantified. In the *myoB/C/mlc1* KO, short helical tracks were recorded with no significant difference in terms of speed compared to control parasites. Circular tracks present longer distances but with slower speeds when compared to RH*Δhxgprt*. Unpaired t-test was used to measure statistical differences between groups. *** P≤ 0.001, ** P≤ 0.01, * P≤ 0.1, not significant (ns) P>0.05.

4.1.4 . Replication analysis of *myoB/C/mlc1* KO

Although first observations of MyoB and C overexpression showed a cell division abrogation (Delbac et al., 2001), neither *myoA* KO, *myoB/C* KO, *mlc1* KO nor the triple KO presented a severe replication defect (Meissner et al., 2002b, Andenmatten et al., 2013, Egarter et al., 2014, Frenal et al., 2014). Here, we analysed if the *myoB/C/mlc1* KO showed a delay in parasite division and replication inside the host cell. Replication assays were performed by using mechanically released parasites 96 hours post induction, these were incubated with HFFs for one hour, followed by several washes to remove extracellular parasites, and replication was allowed to progress for 24 hours prior to PFA fixation. The number of parasites per vacuole was analysed by IFA using α-IMC antibody. Counting determined vacuoles containing 2, 4, 8, 16, or >32 parasites.

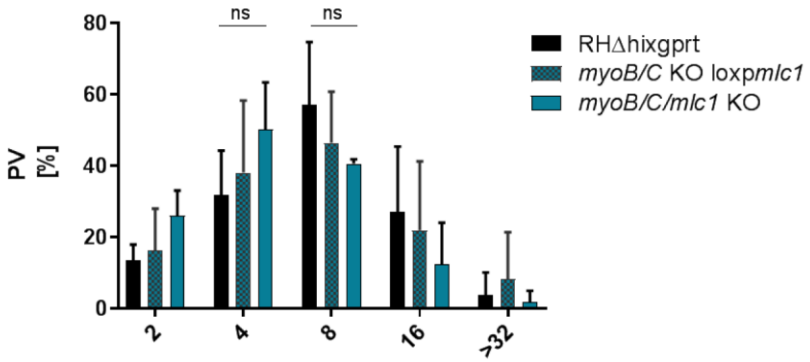

Figure 4-4. Characterisation of *myoB/C/mlc1* KO replication
Replication assays using RHΔ*hxgprt*, *myoB/C* KO loxp*mlc1* and *myoB/C/mlc1* KO were performed 96 h post induction. Parasites were allowed to invade for one hour and replication progressed for 24 hours prior to fixation, after which the number of parasites per parasitophorous vacuole was quantified. Graphs display mean values for three experiments in triplicate. Two-way ANOVA and Tukey's test were used to compare means among groups. No significant difference was found between strains. Not significant (ns) P>0.05

As shown in Figure 4-4 no replication defect was detected in the *myoB/C/mlc1* KO strain when compared to the uninduced line and RH*Δhxgprt*. In good agreement with previous data, depletion of myoB/C and MLC1 neither affects parasite division nor presents a cumulative division phenotype.

4.1.5 *myoB/C/mlc1* KO cannot egress

Artificial induction of *T. gondii* tachyzoites vacuoles with Ca^{++} Ionophore A23187 triggers internal Ca^{++} signalling, which is followed by cytoskeletal changes, rapid motility, microneme secretion, disruption of the parasitophorous vacuole, and dispersion of the parasites (Black et al., 2000, Kafsack et al., 2009). Gliding motility has been shown to be important for mechanical disruption of the PV, which facilitates egress, and so this process was analysed in the motor complex knockouts. Here, it was observed that the MyoA null parasites presented a delay in egress that was not associated with microneme secretion, but rather poor gliding capacity (Meissner et al., 2002b, Egarter et al., 2014). However, egress was completely blocked in *mlc1*, triple, *gap45*, and *act1* KOs, preventing these parasites from completing the lytic cycle, and resulting in an impediment for isolating clonal lines (Andenmatten et al., 2013, Egarter et al., 2014).

In this section, the ability of *myoB/C/mlc1* KO to egress the host cell was analysed by fixed and live cell imaging protocols as described in section 3.1.8. First, confluent HFF monolayers, growing on glass bottom live cell dishes, were infected for 1 hour with *myoB/C/mlc1* KO (96 hours post induction). Following this, the monolayer was washed several times to remove extracellular parasites, and intracellular parasites were allowed to

replicate for 36 hours. After this time, cultures were incubated with 2 µm of Ca^{++} ionophore (A23187) for ten minutes under standard culture conditions. Coverslips were fixed and immunoassayed using αSAG1 antibodies in non-permeable conditions. As shown in Figure 4-5A, while RHΔ*hxgprt* parasites egress was evident in virtually all the infected cells, *myoB/C/mlc1* KO parasites were unable to egress from the host cell, resembling the *mlc1* KO phenotype which were unable to rupture the PV (section 3.1.8). Once again, 70.6±9.4 the *myoB/C/mlc1* KO vacuoles remained inside the host cell showing SAG1 signal (bottom panel), lack of SAG1 staining could be seen in a remaining percentage of vacuoles (mid panel).

Next, we took a closer look at the egress process to determine if *myoB/C/mlc1* KO, as with the *mlc1* KO, could move and dissemble rosettes but unable to rupture the host cell and spread upon Ca^{++} stimulation. This protocol was carried out using the same steps as described in section 3.1.8. As observed previously, RHΔ*hxgprt* parasites changed morphology, rapidly moved, and perforated the PV and the host cell in around 1 minute after Ca^{++} ionophore induction. Additionally, these parasites disseminated among neighbouring cells in a rapid manner, and several reinvasion events could be observed (Figure 4-5B, top panel, Movie 13). In contrast, although *myoB/C/mlc1* KO parasites responded to the Ca^{++} ionophore (A23187) by changing shape, rapid movement was not observed. In addition, disintegration of the PV and dissemination of the mutants was seen only in 4% of the population (Figure 4-5B, bottom panel, Movie 14). These results resemble the *mlc1* KO phenotype previously described in section 3.1.8. Here, it is clear that the loss of MLC1 from the periphery causes egress impediment in 96% of the vacuoles, reaffirming the hypothesis that activation of motility inside the PV is essential for parasites to disrupt permeabilised vacuoles.

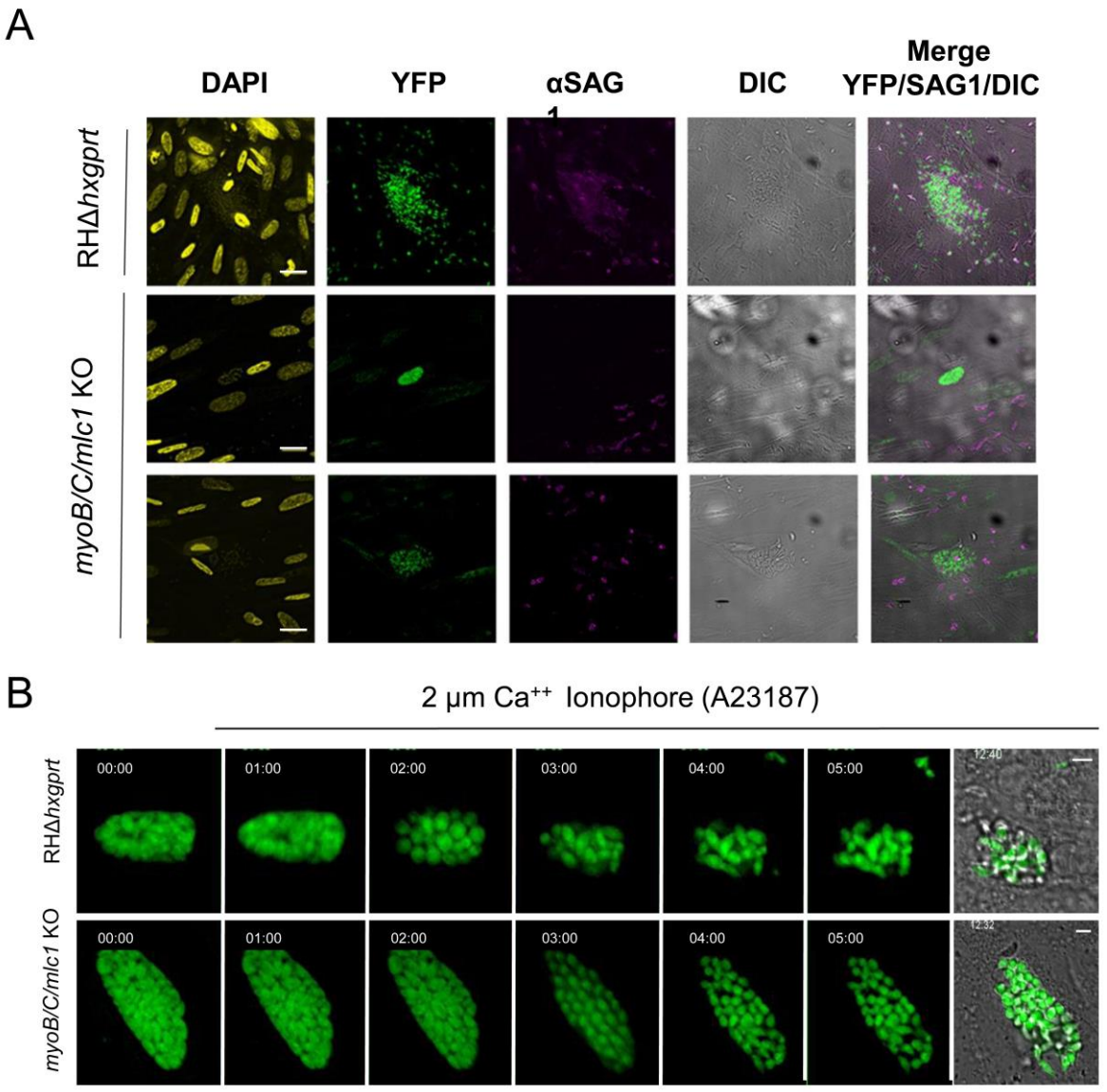

Figure 4-5. Host cell egress presents a severe phenotype in *myoB/C/mlc1* KO
A. SAG1 staining was used to visualise PV disassembly and parasite dissemination upon Ca^{++} ionophore stimulation (10 minutes). In the case of the *myoB/C/mlc1* KO mutants most of the vacuoles remained intracellular with no visible permeabilization of the vacuole (second panel), but a few events of intracellular SAG1 signal could be observed (bottom panel). Scale bar represents 20µm **B.** Time-lapse microscopy was used to follow egress progression after Ca^{++} Ionophore induction. Videos were recorded at 1 frame per second. Calcium stimulation was performed within the first minute from 0:00. *myoB/Cmlc1* KO strain reacted upon Ca^{++} ionophore stimulation resulting in intracellular parasite movement, but apparent rupture of the PV or dissemination were not observed in the mutant line. Time stamp displays (minutes.seconds). Scale bars represent 5um.

4.2 Summary and conclusions

Toxoplasma gondii encodes five myosins class XIV A and B, which include MyoA, MyoB, MyoC, MyoD and MyoE (Foth et al., 2006) and seven light chains (MLC1-7) (Polonais et al., 2011). MyoA is a small unconventional neck-less myosin that has been broadly studied for its participation in parasite gliding motility (Dobrowolski et al., 1997a, Heintzelman and Schwartzman, 1997, Keeley and Soldati, 2004). In fact, parasites showed

a significant decrease in motility upon depletion of MyoA but, surprisingly, this function was not completely blocked (Meissner et al., 2002b, Andenmatten et al., 2013, Egarter et al., 2014). These results highlighted the possibility of compensatory mechanisms to retain motility and invasion. Considering evidence in other models (Venit et al., 2013, Okumura et al., 2015), and the large repertoire of myosins present in the parasite, other myosins were proposed to provide compensatory function following loss of MyoA.

MyoC was suggested to be functionally redundant to MyoA because of its structural similarities and capacity to interact with the same interaction partners such as MLC1 (Egarter et al., 2014, Frenal et al., 2014). For this reason, a triple KO for MyoA/B/C was generated and could not be maintained in culture, although invasion and gliding occurred at reduced rates (Egarter et al., 2014, Frenal et al., 2014). As previously shown (section 3.1.3), depletion of MLC1 results in the relocation of MyoA from the periphery to the cytoplasm of the parasite and is hypothesised to result in its degradation, as shown for *P. falciparum* MyoA in the absence of its light chain MTIP (homologous to MLC1) (Sebastian et al., 2012). However, depletion of MyoA does not affect MLC1 localisation at the periphery, which gives credence to the possibility that another myosin relocates to compensate for MyoA loss (Andenmatten et al., 2013, Egarter et al., 2014). To study this option, MLC1 was depleted (Egarter et al., 2014), and the mutants presented an aberrant egress phenotype, but gliding motility and invasion were not abrogated (section 3.1.8). This indicated that if another myosin could compensate for MyoA loss it was not doing so by interacting with MLC1 as its light chain.

Considering the large repertories of myosins and myosin light chains in *T. gondii* (Foth et al., 2006, Polonais et al., 2011), the possibility of MyoC interacting with another light chain to target to the pellicle in the absence of MLC1 was plausible. For this reason, in this chapter I generated a *myoB/C/mlc1* KO and studied in detail its phenotype. This mutant let me observe the phenotype of *T. gondii* tachyzoites lacking several components of the motor complex. The proteins directly depleted were: MLC1, the only myosin light chain directly involved in gliding motility to date, and MyoC, the most suitable candidate to assume MyoA functions. In addition, other proteins were indirectly affected; for instance, MyoA, which loses its location in the absence of MLC1 (section 3.1.3), together with ELC1 and ELC2, whose location in the periphery fully depends on MyoA (Egarter et al., 2014, Williams et al., 2015). Additionally, the previously published triple KO (*myoA/B/C* KO) did not contain a marker for visualising the parasites directly, which limited its analysis to fixed assays (Egarter et al., 2014). The inducible *myoB/C/mlc1* KO is a *myoB/C* KO that was generated

from the loxp*mlc1* strain (Egarter et al., 2014). This line allowed the direct visualisation of the mutants as they express YFP from the DiCre cassette upon MLC1 removal.

Like the *mlc1* KO and the triple KO, the *myoB/C/mlc1* KO couldn't be isolated as a clonal line, most likely due to the essentiality of MLC1 for the parasite survival. For this reason, *myoB/C/mlc1* KO parasites were kept as a mixed population, which, by bypassing egress, could be maintained in culture for prolonged time. These results resemble the *mlc1* KO previously discussed in section 3.1.4 (Whitelaw et al., 2017), which was identified as essential for egress but not for other steps of the lytic cycle. Additionally, even though greatly reduced in gliding rates, *myoB/C/mlc1* KO parasites could move in both helical and circular motilities in 2D environments, generating longer distances compared to the *mlc1* KO, but at comparable gliding speeds. When compared to the "stop and go" circular movement of the *myoA* KO (Egarter et al., 2014), the *myoB/C/mlc1* KO seemed to present enhanced motility because it moves in both circular and helical manners, and in an apparent smooth trend (results summarised in Table 4-1). These results may suggest two different scenarios: i) there are a small number of functional MLC1-MyoA motors able to power motility or ii) the absence of MLC1-MyoC complex in the pellicle enhances motility. The first is a plausible possibility since small traces of MLC1 can remain functional in the *myoB/C/mlc1* KO. However, a careful characterisation of the *mlc1*, *act1*, *gap45* KO showed that some essential steps of the lytic cycle, like egress, were affected in >95% of the mutant population; whereas other steps, like invasion and gliding, were affected in a lower percentage of parasites and some happen in similar kinetics as control parasites (Andenmatten et al., 2013, Egarter et al., 2014, Harding et al., 2016, Whitelaw et al., 2017). Under the second scenario that is supported in this thesis, the fact that MyoA and MyoC present similar structures (Foth et al., 2006) and share interaction partners (Frenal et al., 2014) does not necessarily guarantee a full recovery of functions. It has been previously shown that gliding quality, displacement, and speed is highly dependent on MyoA and its interaction partners (MLC1, ELC1-ELC2), who stabilise the lever arm and its step size (Bookwalter et al., 2014, Williams et al., 2015). According to immunoprecipitation studies, MyoC is able to precipitate with both MLC1 and ELC1 (Frenal et al., 2014); however, further studies showed ELC1 is specific for MyoA because it is mislocalised upon MyoA excision (Williams et al., 2015). Considering that in *T. gondii* and *Plasmodium* MyoA step is regulated by specific interactors (Bookwalter et al., 2014, Williams et al., 2015, Bookwalter et al., 2017, Green et al., 2017), it is possible that MyoC cannot by stabilised and regulated in a similar way causing a defect in the step on actin filaments and further deficient motility seen in the *myoA* KO. For instance, differences between both myosins at

submolecular level and/or phosphorylation dynamics could affect the function of MyoC, so full functional recovery cannot be achieved following MyoA loss. In addition, no replication defect was evident in this mutant line, which, again, discards the role of MyoB/C in replication as previously described (Delbac et al., 2001). Unlike replication, egress was severely affected in the *myoB/C/mlc1* KO line. Egress was monitored by using artificial induction with Ca^{++} ionophore (A23187). Here, *myoB/C/mlc1* KO parasites seemed responsive to Ca^{++} induction because vacuole collapse, slight movement, and perforation of the PV were observed, but spreading from the host cell was not seen. This phenotype is the same as that observed in the *mlc1* KO (section 3.1.8), indicating that the MLC1-Myosin complex(es) have an essential role in a step upstream of PV disruption during egress. Lastly, SAG1 staining in impermeabilized conditions is a basic tool to estimate PV and host cell perforation; nonetheless, it is not clear if the PV was disrupted in vacuoles without SAG1 signal. For this reason, in order to further study if the permeabilisation of the host cell plasma membrane shows a delay, deep analysis of egress with different markers would be useful. For instance, the progression of PV and host cell PM disruption can be followed by microneme secretion with MIC markers and permeabilisation of the PV with GRA markers as done by Kafsack (2009).

Altogether these results show that in the absence of MLC1, MyoC, MyoA and most probably its specific light chains (ELC1-ELC2), tachyzoites can move and invade host cells (Meissner et al., 2002b, Andenmatten et al., 2013, Egarter et al., 2014, Frenal et al., 2014, Williams et al., 2015, Whitelaw et al., 2017). However, these components are required for maintaining efficient motility and invasion rates. These data support results displayed in Chapter 3, as the *myoB/C/mlc1* KO resembles the *mlc1* KO phenotype in terms of gliding, replication and egress rates. Moreover, invasion rates, most likely, resemble those of *mlc1* KO since this line was used as the recipient strain for the *myoB/C* KO plasmid. This indicates that the observed phenotype of the *myoB/C/mlc1* KO is predominantly an effect of MLC1 removal. When compared to the *myoA* KO, the improvement of gliding distances and speeds observed in the *myoB/C/mlc1* KO suggests that MyoC cannot compensate for MyoA in terms of motor function. Albeit, by this point, there is not enough evidence to support this observation, so characterisation of MyoC structure, lever arm stabilisation, and step size is needed. Another possibility to explain the remaining gliding rate in this conditional line could be that other complexes, such as MyoH-MLC3/5/7, are compensating for MyoA/B/C and MLC1 loss. However, this possibility is less plausible since, unlike MLC1, MLC5 and 7 were shown to be disposable for MyoH function (Graindorge et al., 2016).

To this end, the possibility that the MLC1-MyoC complex could fully complement upon MyoA depletion has been discarded, but a characterisation of the roles which MyoC can takeover is necessary to understand the function(s) of MyoA in different steps of the lytic cycle. Additionally, this information would clarify which roles are specific and which are redundant in between both heavy chains.

Table 4-1. Summary of mutants characterisation

		Control	***myoA* KO**	***mlc1* KO**	***myoB/C/mlc1* KO**	***act1* KO**
2D	Gliding (%)	39%	10%	12%	19%	22%
	Displacement Circular (µm)	41±4	11±5	33±4	47±10	36±14
	Displacement Helical (µm)	55±5	(*)	16.± 2	24 ± 4	36±8
	Speed Circular (µm/s)	0.7±0.08	0.2±0.08	0.4±0.2	0.4±0.07	1±0.3
	Speed Helical (µm/s)	1±0.1	(*)	0.2±0.02	0.8±0.3	0.8±0.2
3D	Gliding rate (%)	39%	5%	3%	N/A	5%
	Displacement (µm)	14 ±1	3±0.2	7±0.6	N/A	7±1
	Speed (µm/s)	0.7±0.07	0.3±0.07	0.7±0.1	N/A	0.7±01
Penetration (s)		25±4	245±49	89±22	N/A	119±42
Egress		Normal	Delayed	Blocked	Blocked	Blocked
Reference		[1][2]	[1][2]	[1][2]		[1][2]

(*) not observed (N/A) not applicable [1](Egarter et al., 2014) [2] (Whitelaw et al., 2017). In 3D motility assays, control parasites are considered loxp*mlc1* while for the rest of assays refers to RHΔhxgprt.

Chapter 5 Visualisation and Analysis of proteins associated with MyoA

The importance of acto-myosin systems is based on the ability of both proteins to interact to produce and transmit force. The typical arrangement of these complexes consists of myosin polymers or soluble monomeric myosins walking on long actin filaments, which serve as the scaffold for force production (Krendel and Mooseker, 2005, Hartman et al., 2011). Myosins belong to a superfamily of proteins having diverse molecular and structural motifs that give rise to different properties. The molecular structure of many myosin heavy chains consist of a conserved N-terminal motor domain containing ATP- and actin-binding sites, a neck domain to interact with myosin light chains, and a tail domain responsible for cargo binding (Krendel and Mooseker, 2005). The variations within this architecture make these proteins extremely diverse in their mechanochemical properties and functions. For this reason, myosins have been shown to be involved in a plethora of functions; for example, cell motility, actin organisation, cell adhesion, membrane trafficking, and organelle and protein localisation, among others (Krendel and Mooseker, 2005, Hartman et al., 2011). Considering these diverse roles, and the fact they contain conserved domains, overlapping functions among myosins is a plausible mechanism to ensure that important cellular functions are accomplished. For instance, a knockout line of mouse nuclear myosin 1 (NM1) showed it was not essential as Myo1c presented redundant functions within the cell (Venit et al., 2013). A similar scenario has also been described in *Drosophila* left/right embryonic development where Myo31Df and Myo61F showed overlapping functions (Okumura et al., 2015).

T. gondii contains seven myosin light chains (MLC1-7) and eleven myosin heavy chains (MyoA, B/C, D, E, F, G, H, I, J, K and L), of which just two of them are conserved across the phylum Apicomplexa (MyoA and F) (Foth et al., 2006, Polonais et al., 2011, Frenal et al., 2017b). In tachyzoites, these myosins participate in motility, organelle segregation, protein trafficking, and communication among daughter cells during division (Delbac et al., 2001, Meissner et al., 2002b, Heaslip et al., 2010, Jacot et al., 2013, Mueller et al., 2013, Frenal et al., 2017b, Periz et al., 2017). The most studied myosin, in both *Toxoplasma* and *Plasmodium*, is MyoA, for its important roles during gliding motility and invasion (Pinder et al., 1998, Meissner et al., 2002b, Soldati and Meissner, 2004). The arrangement of the acto-MyoA motor complex derives from immunoprecipitation assays that suggested the interaction among the proteins (Tardieux and Baum, 2016). The accepted architecture proposes an atypical “upside-down” organisation of the components based on the unconventional neckless structure of MyoA (Opitz and Soldati, 2002, Sibley, 2010).

Consequently, the inner membrane complex (IMC) proteins GAP40, 45, and 50 constitute a structural scaffold for MyoA, which is targeted there via myosin light chain 1 (MLC1). Once fixed, MyoA moves along short actin (ACT1) filaments that interact indirectly with adhesive proteins (e.g. MIC2) in the PM via the glideosome-associated connector (GAC) (Herm-Gotz et al., 2002, Sibley, 2010, Heintzelman, 2015, Jacot et al., 2016b). Thus, the force generated by the acto-MyoA motor complex produces the antero-posterior migration of the adhesins in the parasite's PM, which translates to forward motion (Sibley, 2010). This model predicts that the peripheral arrangement and correct function of this complex are essential for parasite motility (Heintzelman, 2015).

To study the functions of each protein in the gliding machinery, conditional mutants of GAP40, GAP45, GAP50, MyoA, MLC1, and ACT1 were produced (Andenmatten et al., 2013, Egarter et al., 2014). Motility and invasion could not be analysed in the GAP40 and 50 mutants since their depletion results in a severe defect in daughter cell formation (Harding et al., 2016). In contrast, *gap45* KO, *myoA* KO, *mlc1* KO, and *act1* KO mutants remained motile and invasive, albeit at reduced rates (Meissner et al., 2002b, Andenmatten et al., 2013, Egarter et al., 2014). Of these, *myoA* KO parasites were the only knockout strain viable in culture. However, these mutant parasites presented an arrested 'stop and go' circular motility phenotype in terms of gliding and invasion (Egarter et al., 2014). Additionally, when left in culture for prolonged periods, *myoA* KO parasites adapted and showed increased gliding, invasion, and egress rates. However, while the gliding rate was enhanced, gliding kinetics did not improve, indicating that *myoA* KO adaptation cannot be directly attributed to a myosin motor function (Andenmatten, unpublished data) (Appendix 3). Consequently, the remaining gliding capacity and invasiveness of the *myoA* KO was attributed to molecular redundancies among myosins present in *T. gondii* (Meissner et al., 2013, Frenal and Soldati-Favre, 2015). Four of the ten myosins present in *T. gondii* are structurally related to MyoA (MyoB/C/D and E), all belonging to either class XIVa or b (Delbac et al., 2001, Foth et al., 2006, Polonais et al., 2011). In tachyzoites, MyoC forms a motor complex at the basal pole of the parasite, where it shares components with the acto-MyoA motor complex (Frenal et al., 2014). For these reasons, it was considered plausible that MyoC could be redundant with MyoA (Egarter et al., 2014, Frenal et al., 2014). Indeed, in the absence of MyoA, overexpressed MyoC relocates to the periphery of the parasite, and leads to an immediate adaptation of the *myoA* KO in terms of growth, gliding, and invasion rates (Frenal et al., 2014). Together these results supported the hypothesis that MyoC can compensate for the loss of MyoA in *myoA* KO parasites (Frenal et al., 2014, Frenal and Soldati-Favre, 2015).

This chapter is focused on analysing the capacity of MyoC to recover for MyoA functions in the *myoA* KO strain. Under this premise, I characterised the phenotype of three different expression levels of MyoC in the *myoA* KO line throughout the lytic cycle. Additionally, since both myosins share the same interaction partner (MLC1), I analysed if MyoC can relocalise in the pellicle of *T. gondii* tachyzoites after MLC1 depletion in the conditional *mlc1* KO. Finally, to increase our understanding of the arrangement and functions of the acto-MyoA motor complex, I employed the recently established tool for visualising actin filaments (Periz et al., 2017) in the acto-MyoA motor complex mutant parasites.

5.1 Expression of MyoC in the *myoA* KO

The viability of MyoA null mutants *in vitro* demonstrated that this motor is not essential for completing the lytic cycle; thus, compensatory mechanisms could be taking place. MyoC was speculated to be responsible for compensating MyoA loss in the DiCre KO because of its similar structure and shared interaction partners, (Egarter et al., 2014, Frenal et al., 2014). To study this possibility, *myoA/B/C* KO (triple KO) and *myoB/C/mlc1* KO were generated and characterised (Chapter 4) (Egarter et al., 2014, Frenal et al., 2014). Indeed, these mutant lines could not be maintained in culture indefinitely and showed a detrimental egress phenotype, but again, gliding and invasion were not blocked (Chapter 4) (Egarter et al., 2014). Additionally, MyoC expressed under either a T7S4 or p5RT70 constitutive promoter (Frenal et al., 2014) (Andenmatten, unpublished data), showed a relocation of this protein to the pellicle of *myoA* KO parasites. These results suggested that MyoC can partially complement for MyoA functions and location, and possibly drive fast adaptation in the MyoA null mutants, leading to the idea of plasticity between motor complexes (Frenal et al., 2014, Frenal and Soldati-Favre, 2015). This hypothesis suggests that endogenous MyoC complements to some degree for MyoA loss, but data of endogenous MyoC were not available. In this chapter, I tested the MyoA-MyoC redundancy hypothesis by comparing how different levels of MyoC complement for MyoA functions. Hence, three different complementation constructs allowed establishment of different expression levels of MyoC in the *myoA* KO parasites. Furthermore, these lines were characterised to examine the ability of MyoC to recover for MyoA in different steps of the lytic cycle.

5.1.1 Generation of the MyoC expression constructs

To study if MyoC is capable of complementing MyoA functions, I randomly integrated a second copy of MyoC under two different promoters in the *myoA* null line. For this, the *myoA* KO adapted strain (12 months) was used for stable transfection, since these parasites propagate and recover faster than the freshly induced line.

As shown in Figure 5-1A/B TyMyoC cDNA was preceded by either a strong (p5RT70) or endogenous promoter (pMyoC) (Soldati and Boothroyd, 1995). Additionally, since previous studies failed to incorporate a tag at the C-terminus of MyoC (Andenmatten, unpublished data), I generated an endogenous tagging plasmid to introduce a Ty tag at the N-terminus (Figure 5-1C). This vector contains 1300 bps of the MyoC 5' UTR region (-1000 to -2300 bp upstream ATG), followed by a bleomycin cassette and 1000 bps of the MyoC promoter (0 to – 1000 bp upstream ATG). Then, 500 bps of MyoC genomic DNA was cloned preceded by a Ty tag sequence. Correct integration of the vector was verified by using three sets of primers designed to bind inside and outside the recombination area: (1-1') 5'UTR-Bleomycin, (2-2') Bleomycin-MyoC gene, and (3-3') Ty Tag- MyoC gene (Figure 5-1D).

Overexpression constructs (p5RT70TyMyoC and pMyoCTyMyoC) were randomly integrated in RHΔ*hxgprt* and *myoA* KO genomes. To enhance double homologous recombination of the endogenous tagged MyoC, a CRISPR/CAS9 vector (Curt-Varesano et al., 2016) containing a MyoC specific gRNA was transiently transfected together with TyMyoC plasmid as a donor vector in both the RHΔ*ku80* (Huynh and Carruthers, 2009a) and *myoA* KO (Andenmatten et al., 2013).

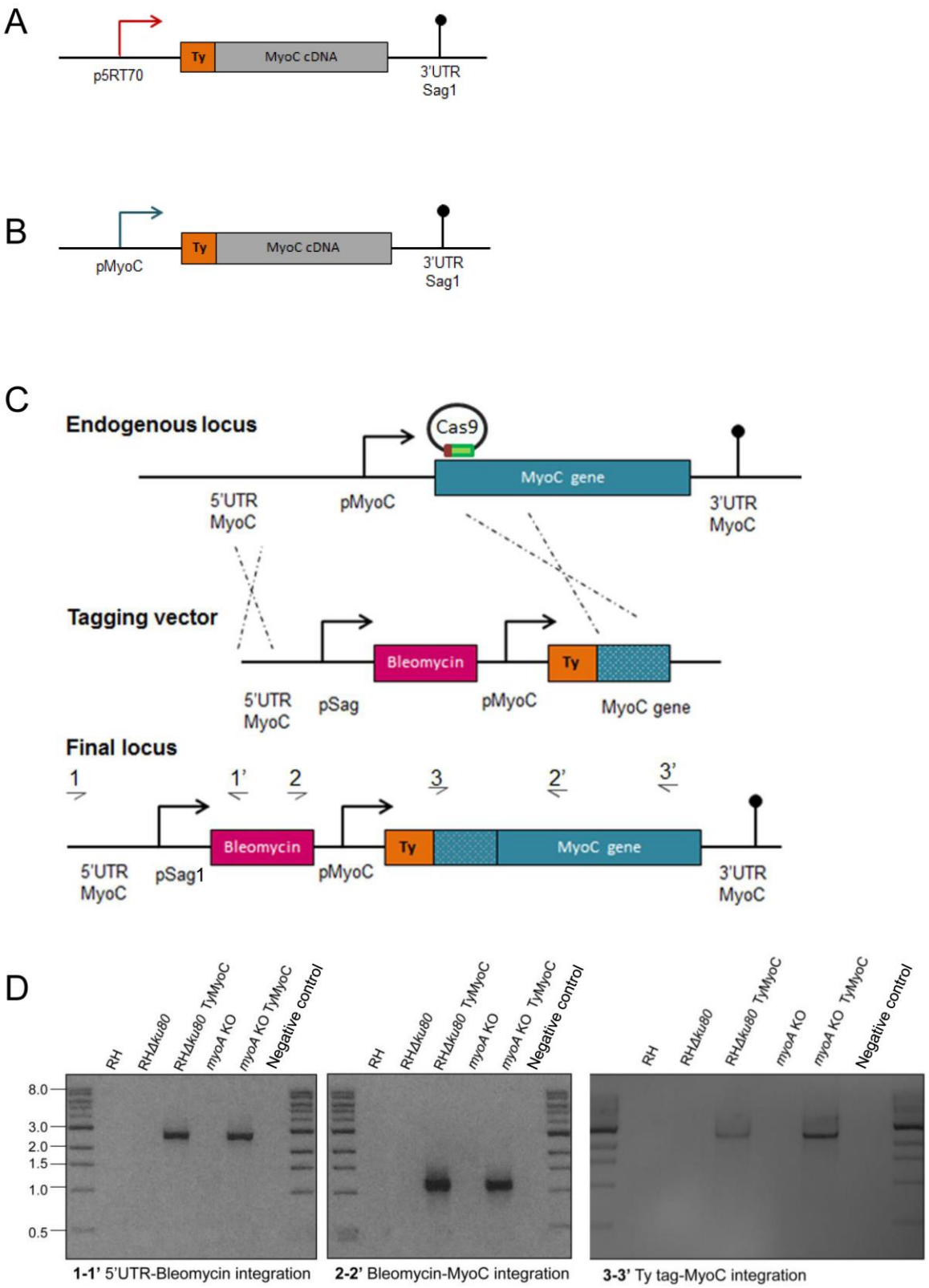

Figure 5-1. Establishment of expression of TyMyoC under different promoters
Scheme of **A.** p5RT70TyMyoC **B.** and pMyoCTyMyoC constructs that were randomly integrated into the RHΔ*hxgprt* and *myoA* KO genome. MyoC cDNA was fused to a ty-tag under p5RT70 and pMyoC promoters **C.** Schematic representation of the endogenous tagging strategy. A Ty tag was added before the MyoC start codon. Double homologous recombination was needed to integrate the construct in the RHΔ*ku80* and *myoA* KO lines. To enhance double homologous recombination insertion, a MyoC-specific CRISPR-Cas9 vector was transiently expressed **D.** Analytical PCR was used to confirm correct integration of the endogenous tagging cassette. To verify correct integration of the bleomycin cassette, primers were used to bind the 5'UTR (1-1') and MyoC (2-2') outside the

recombination area. (3'3') was designed to bind the Ty tag and MyoC outside the recombination area. A no template negative control (NC) was included as a general control for contamination. 1KB ladder was included; numbers show kilobases (kb)

5.1.2 Analysis of different expression levels of MyoC in the *myoA* KO

To analyse if MyoC localisation varies according to different expressions of the protein in the *myoA* KO, the three TyMyoC constructs were stably transfected in both RHΔ*hxgprt* and *myoA* KO strains (section 5.1.1). The expression of the protein was analysed by IFA targeting Ty tag with αTy antibodies in vacuoles and individual parasites (Figure 5-2A/B/C). Structured illumination microscopy (SIM) images were taken using ELYRA PS.1 microscope (Zeiss).

We found that localisation of MyoC varies when expressed under control of different promoters in the *myoA* KO (Figure 5-2A/B/C). While in RHΔ*hxgprt*, MyoC presents a ring-shaped location at the posterior pole of the parasites irrespective of the employed promoter to drive MyoC expression; in the *myoA* KO, however, localisation appears to depend on the expression level. Stable overexpression of MyoC under the p5RT70 promoter results in the relocation of this protein to the periphery of the parasite in both intracellular and extracellular parasites (Figure 5-2A). Similarly, expression of a second copy of MyoC under its endogenous promoter showed a slight relocation of the protein to the pellicle, even though the signal significantly decreased (Figure 5-2B). Finally, expression of endogenously tagged MyoC showed a posterior pole location with minimal relocation to the IMC surrounding the posterior ring (Figure 5-2C). In the case of extracellular parasites, MyoC is brighter in the anterior and posterior rings. Different expression levels of MyoC were verified by western blot using αTy antibodies (Figure 5-2D).

To further analyse the variation of protein levels under different promoters, MyoC expression was quantitively measured by immunofluorescence. An IFA against the Ty Tag was used to measure the cell fluorescence of the three lines expressing TyMyoC. For this, images of vacuoles were obtained using ELYRA PS.1 microscope (Zeiss), these images were taken using the same parameters for exposure and resolution. Analysis of parasites was done using Fiji (ImageJ) drawing tool to trace the area to be measured. For each image, the background was determined by selecting a portion of the image with no signal. Corrected cell fluorescence (CTCF) was calculated using the formula [CTFC = Integrated density – (Area of selected cell x Mean fluorescence of background readings)] (Potapova et al., 2011). As depicted in Figure 5-2E analysis of extracellular and intracellular parasites showed

significant differences in fluorescence among endogenous tagged MyoC and overexpressed MyoC lines in *myoA* KO. A slightly higher signal was found in the endogenous-MyoC tagged line when compared to control parasites, but no statistical differences between them were found.

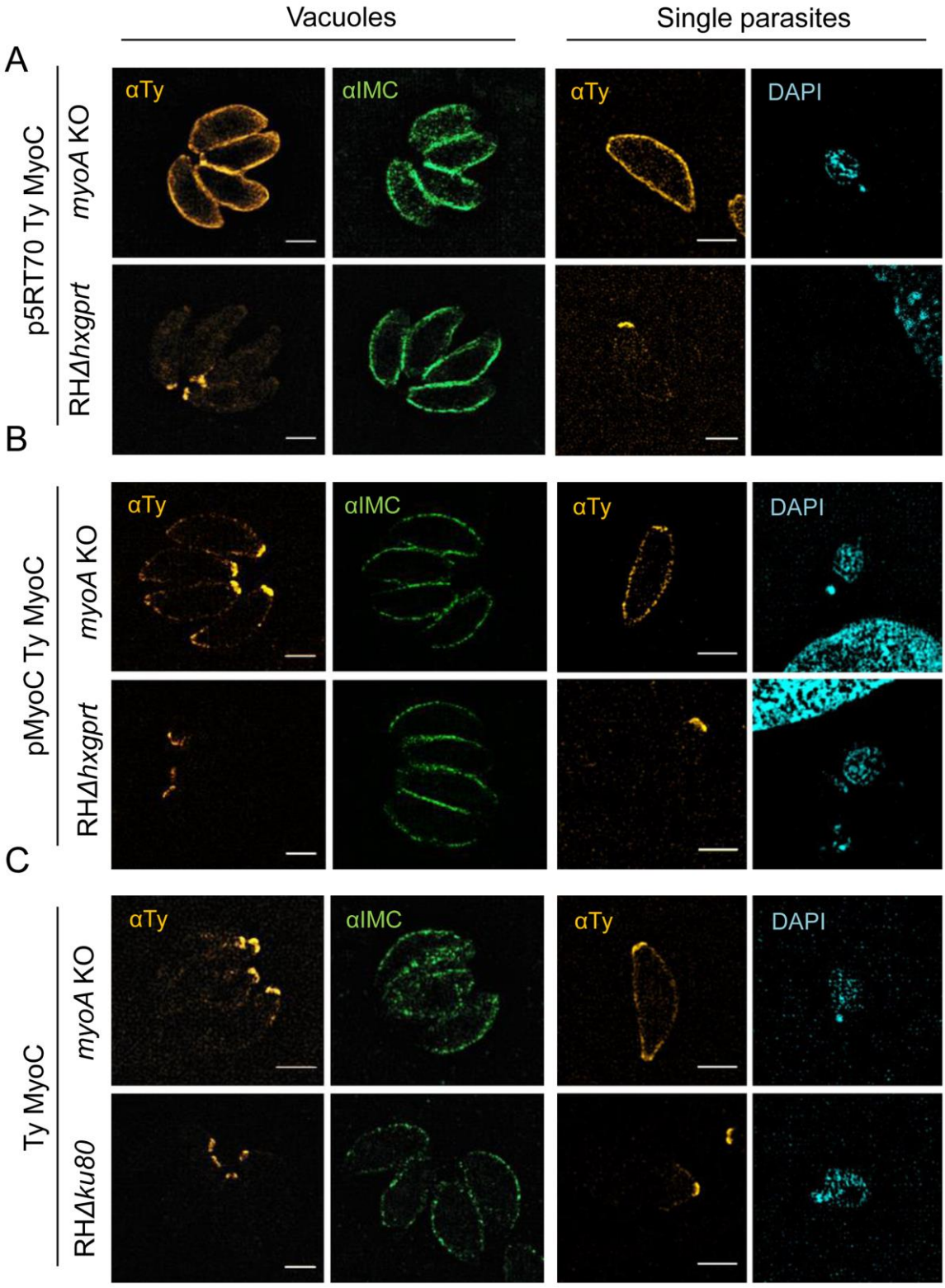

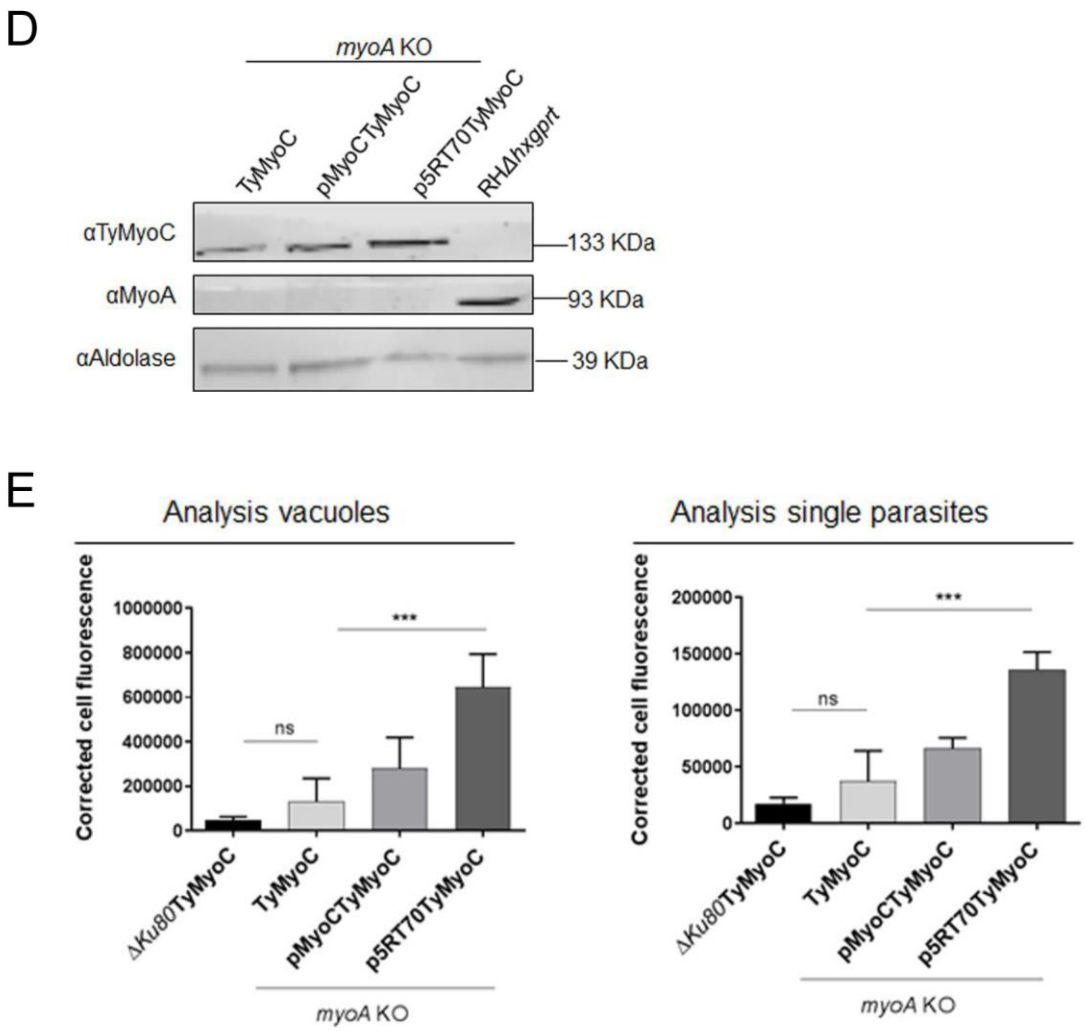

Figure 5-2. Different expression levels of MyoC determine MyoC peripheral localisation
Super-resolution images of vacuoles and single extracellular parasites with MyoC expressed under different promoters **A.** p5RT70TyMyoC **B.** pMyoCTyMyoC **C.** TyMyoC. MyoC was targeted using αTy. Scale bar represents 2μm **D.** Immunoblot analysis of TyMyoC in the *myoA* KO lines using αTy **E.** Corrected cell fluorescence intensities were measured in vacuoles and single parasites expressing different levels of MyoC. MyoC fluorescence was measured using the αTy signal of SIM images. One-way ANOVA followed by Tukey's post hoc test was used to compare means between groups. ***P<0.0001, not significant (ns) P>0.05. Figure modified from (Whitelaw et al., 2017) under Creative Commons Attribution 4.0 International License.

Taken together, these results suggest that MyoC can be relocated to the pellicle in the absence of MyoA upon overexpression. In the case of strong overexpression (p5RT70TyMyoC), a significant relocation of the protein is observed accompanied with a great amount of signal that delineates entirely the parasite periphery. The p5RT70 is a constitutive promoter (Soldati and Boothroyd, 1995) that increases the transcript levels of MyoC ten times when compared to endogenous levels (Andenmatten, unpublished data). This excessive production of the protein was confirmed by our results at both fluorescence and protein level. Even though location in the periphery is evident in the mild overexpression strain (pMyoC-TyMyoC), the signal of MyoC in the endogenously tagged line (TyMyoC) is

still the lowest when compared to strong overexpression levels. Here, most of fluorescence is around the polar ring and a location of the protein to the IMC is observed. Of note, pMyoCTyMyoC was expressed as a second copy of MyoC that had been introduced into the genome. Previous reports studied the possibility of MyoC complementation in the *myoA* KO by i) overexpressing TyMyoC (Andenmatten, unpublished data), and ii) tagging the protein by replacing the endogenous MyoC promoter for a minimal pT7S4 promoter (Frenal et al., 2014). In both situations, peripheral location of the protein was seen, but neither endogenous levels nor quantification were shown (Frenal et al., 2014). For this reason, we considered that the introduction of a Ty Tag at the N-terminal end of the protein gives a better estimate of physiological conditions. Endogenously tagged MyoC does not change significantly its location or protein level upon *myoA* removal. In the case of individual parasites, this signal seems to slightly delineate the periphery of the parasite with a stronger signal in the apical and posterior end. Nonetheless, no significant differences were found when cell fluorescence was compared between Δ*ku80*TyMyoC and *myoA* KO TyMyoC.

5.1.3 Characterisation of TyMyoC expressing lines

Considering the capacity of MyoC to relocate to the pellicle in absence of MyoA, I was curious to study if functional complementation would occur. In this section, I further characterised the three level of expression of TyMyoC in different assays, and analyse their impact in *myoA* KO parasites.

5.1.3.1 Overexpression of MyoC enhances growth in *myoA* KO parasites

The ability of MyoC to complement for MyoA loss in terms of growth was assayed by a five-day plaque assay. As shown in Figure 5-3A, parasites expressing MyoC under p5RT70 and pMyoC grew at faster rates when compared to *myoA* KO parasites. On the other hand, the endogenously tagged MyoC strain showed growth inhibition, comparable to the *myoA* KO itself. This observation was corroborated by quantification of plaque areas shown in Figure 5-3B. While overexpression of MyoC, under either p5RT70 or pMyoC, showed enhanced growth rate, the plaques were still smaller than in RHΔ*hxgprt* parasites, and these differences were statistically significant. This observation showed that overexpressed MyoC has the potential to partially complement for MyoA functions after depleted. As *myoA* KO parasites present defects (Egarter et al., 2014) in terms of attachment, gliding, and egress, I further studied if MyoC can complement these phenotypes, which are directly associated with motor function.

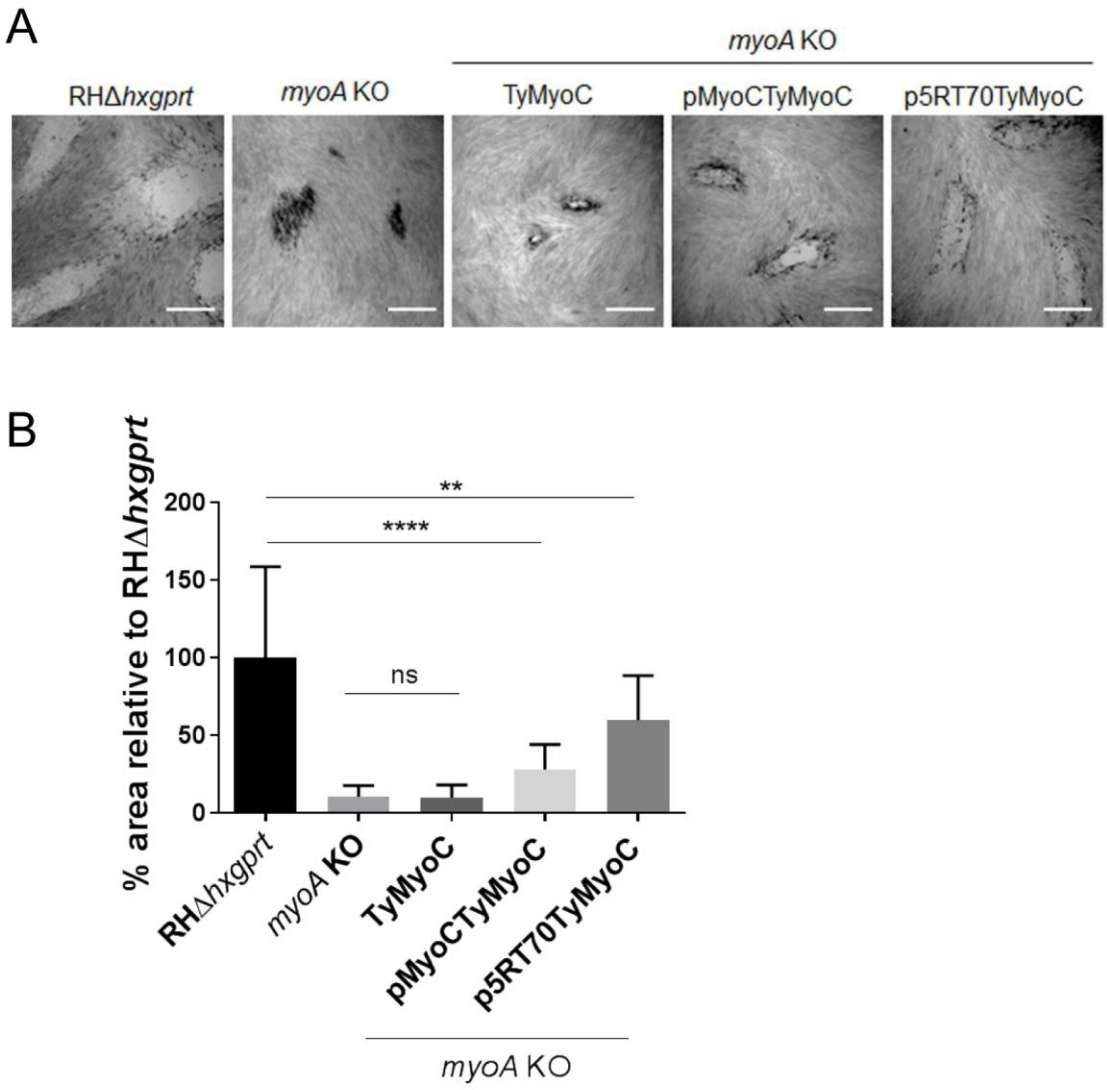

Figure 5-3. Strong overexpression of MyoC can recover growth capacity in *myoA* KO parasites
A. Five-day plaque assay was used to analyse growth ability of p5RT70TyMyoC, pMyoCTyMyoC, and TyMyoC in the *myoA* KO. Giemsa staining was used to visualise the monolayer, scale bar represents 0.5mm **B.** Plaque areas were measured using ImageJ drawing tool. Graphic shows average ± SD. 15 plaques were analysed per each condition. One-way ANOVA followed by Tukey's post hoc test was used to compare means between groups. ***P≤0.0001, **P≤0.01, not significant (ns) P>0.05. Figure modified from (Whitelaw et al., 2017) under Creative Commons Attribution 4.0 International License.

5.1.3.2 Overexpression of MyoC increases gliding rate, but not speed, of *myoA* KO parasites

MyoA depleted parasites present three important features while gliding in 2D environments: i) reduced gliding rates, ii) preference to glide in short circular trails, and iii) arrested "stop and go" gliding motion (Table 4-1) (Egarter et al., 2014). Hence, the ability of MyoC to complement for these processes was examined. First, a trail deposition assay was carried out. As previously described (section 4.1.3), this experiment measures the overall ability of parasites to glide on coated glass slides, but doesn't allow an estimate

regarding gliding speed. The number of parasites moving (gliding rate) and the trail pattern can be assessed by targeting antibodies against the major membrane protein, SAG1, which is left behind following parasite motion (Dobrowolski and Sibley, 1996). As depicted in Figure 5-4A MyoC partially recovers for MyoA gliding rates. This is evident at two levels: the increased number of parasites moving, and the recovery of helical movement. Moreover, longer trails were observed in both helical and circular movements. In addition, 2D gliding kinetics showed that p5RT70TyMyoC *myoA* KO and *myoA* KO strains displayed comparable displacement (11±6 µm and 21±10 µm), and average (0.18±0.1 µm/s and 0.22±0.1 µm/s) speed when moving in circular manner (Figure 5-4B/C). Similarly, even though p5RT70TyMyoC *myoA* KO display helical movement, the travelled trails are slower (0.3±0.1 µm/s) and shorter (24±11 µm) when compared to RHΔ*hxgprt* (1±0.5 µm/s and 55±23 µm, respectively). These results indicate that MyoC is unable to compensate for gliding kinetics phenotype when overexpressed in the *myoA* KO although gliding rates and helical motility are indeed recovered.

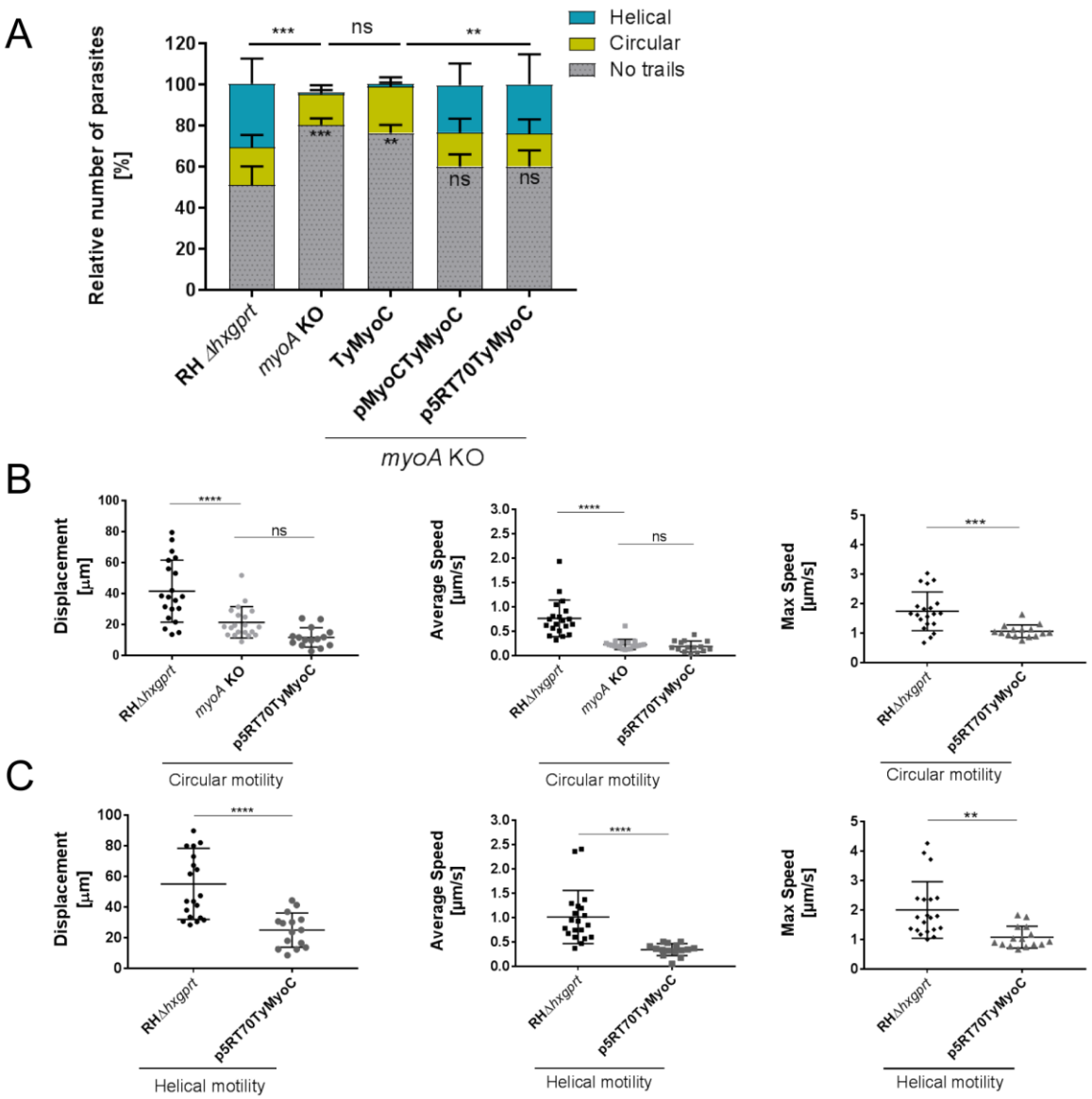

Figure 5-4. MyoC cannot recover for slow gliding speed and distance in the *myoA* KO
A. Quantification of trail deposition assay in p5RT70TyMyoC, pMyoCTyMyoC, and TyMyoC. IFA using αSAG1 antibodies was used to detect trails. Graphic displays mean values of three independent assays in triplicate. Gliding rate and number of helical trails are greatly improved in strains overexpressing MyoC. Two-way ANOVA and Tukey's multiple comparisons test were used to determine differences among means. *** P≤0.001, ** P≤0.01, not significant (ns) P>0.05. 2D gliding motility assays showed p5RT70TyMyoC *myoA* parasites glide in **B.** circular and **C.** helical manner. Nevertheless, displacement (left panel), average speed (mid panel), and maximum speed (right panel) present highly significant differences when compared to RHΔ*hxgprt.* For circular motility statistical analysis, one-way ANOVA together with a Tukey's test were used to compare differences among groups. **** P≤ 0.0001, not significant (ns) P>0.05. For helical motility, statistical analysis was performed using an unpaired t-test **** P≤ 0.0001, ** P≤ 0.01.

To further analyse the MyoC overexpressing line (p5RT70-TyMyoC), we assessed 3D motility data in collaboration with Prof Gary Ward and Dr Jaqueline Leung. As described in section 3.1.6, these experiments were fully standardised and executed at the University of Vermont. Here, a comparative study among loxp*myoA*, *myoA* KO, and p5RT70TyMyoC *myoA* KO parasites to glide in 3D-Matrigel environments was performed. While in 2D environments three different types of motility have been described (Håkansson et al., 1999),

in Matrigel-based 3D motility assays, only an irregular corkscrew-like movement has been described in *Plasmodium* ookinetes and *T. gondii* tachyzoites (Kan et al., 2014, Leung et al., 2014). As shown in Figure 5-5A, the percentage of parasites moving was greatly improved in the MyoC overexpressing *myoA* KO line (40%) when compared to the parental *myoA* KO (11%). However, displacement (7±1 µm and 3±0.3), average speed (0.3±0.03 µm/s and 0.3±0.1 µm/s), and max (1±0.04 µm/s and 0.83±0.35 µm/s) speed were not greatly recovered when MyoC was constitutively overexpressed (Figure 5-5B/C/D). In contrast 40% of control parasites, loxp*myoA,* moved as far as 13±2 µm at an average and max speed of 0.83±0.08 µm/s and 2±0.06 µm/s, respectively.

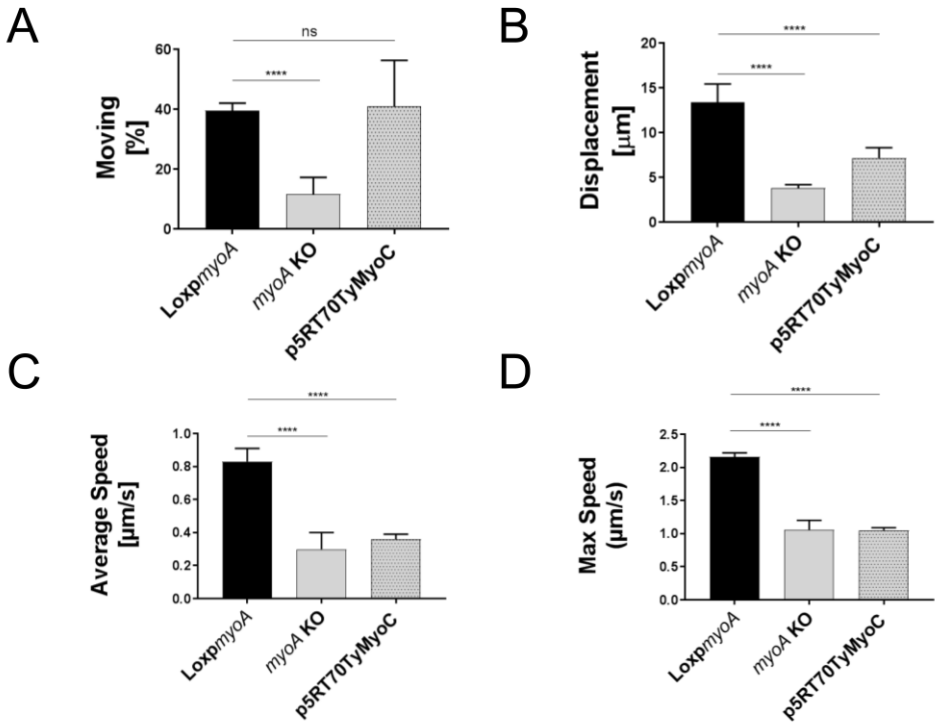

Figure 5-5. 3D gliding kinetics showed overexpressed MyoC cannot compensate for MyoA
3D gliding data were obtained and analysed for loxp*myoA*, *myoA* KO, and p5RT70TyMyoC *myoA* KO lines. Experiments were performed by Dr Jacquelin Leung and Prof Gary Ward. loxp*myoA*, *myoA* KO, and p5RT70TyMyoC *myoA* KO tachyzoites gliding in the 3D matrix were recorded. Percentage of total parasites moving was analysed; only tracks greater than 2µm were considered as moving parasites **A.** Number of p5RT70TyMyoC *myoA* KO parasites moving increases significantly when compared to the *myoA* KO line. However, **B.** gliding distance **C.** average speed, and **D.** maximum speed of tracked parasites present no statistical differences when compared to control parasites. Graphs show mean ± SD of six replicates per sample. Two-way ANOVA followed by Sidak's test were used to compare means between groups. **** P≤0.0001, *** P≤0.001, ** P≤0.01, not significant (ns) P>0.05. Figure modified from (Whitelaw et al., 2017) under Creative Commons Attribution 4.0 International License.

Together with 2D motility, 3D motility assays confirmed that MyoC is indeed able to recover overall motility rates. Nonetheless, total displacement, and average and max speeds are not recovered in the MyoC overexpression line in neither 2D nor 3D

environments. In 2D assays, the max speed of RHΔ*hxgprt70* p5RT70TyMyoC parasites seems to be faster when compared to 3D assay data. This variation may reflect the different resistance the parasites have to overcome when moving in a 3D environment as described in Leung *et al* (2014) and Whitelaw *et al* (2017). In addition, the corkscrew pattern seemed abnormal when compared to control parasites (Prof Gary Ward, personal communication). These results highlight the capacity of peripheral-located MyoC to recover for MyoA upon its removal, but, in terms of motor function, this complementation seems still to have functional consequences. Considering that myosins are molecular motors, the step distance and strength of the stroke on actin are parameters that will vary according to their structural characteristics and interactions with light chains. In the case of MyoA, Williams and colleagues showed that the stabilisation of its lever arm has a direct implication on gliding motility quality in terms of speed and distance (Williams et al., 2015). Under this premise, even though structurally similar to MyoA, MyoC could present different biomechanical characteristics, which somehow affect to fully recover for MyoA loss in terms of gliding quality. Finally, while MyoA lever arm stabilisation and step has been studied (Herm-Gotz et al., 2002, Bookwalter et al., 2014, Tang et al., 2014, Williams et al., 2015), this information is limited for MyoC. Thus, further studies of the composition and stabilisation of the MyoC lever arm are needed to draw greater conclusions.

5.1.3.3 The strong attachment phenotype of *myoA* KO is reduced by overexpression of MyoC

Characterisation of *myoA* KO parasites found that these presented a strong attachment defect in early invasion steps while no replicative phenotype was observed (Egarter et al., 2014). MyoA depleted mutants could penetrate the host cell via canonical TJ formation, but presented an attachment defect prior to, and during, invasion. For this reason, the efficiency of *myoA* KO parasites expressing MyoC to penetrate host cells was evaluated by using a synchronised invasion assay (also known as red/green invasion assay) (Huynh and Carruthers, 2006). Briefly, parasites were left to invade confluent HFF cultures for 15 minutes prior to fixation. An IFA was carried out using αSAG1 antibodies under non-permeabilising conditions. Then, a second staining step was done using αIMC1 antibodies in permeabilising conditions. This differential permeabilization conditions allows recognition of attached (extracellular) versus internalised (intracellular) parasites. As shown in Figure 5-6A, overexpression of MyoC in the *myoA* KO significantly enhanced invasion, almost reaching normal rates. On the other hand, the endogenously tagged MyoC strain presented an equally attachment phenotype when compared to *myoA* KO parasites. This

phenotype again highlights MyoC capacity to recover for MyoA functions, though overexpression of MyoC appears to be required.

Since conditional overexpression of MyoA C-terminal tail (Agop-Nersesian et al., 2009) and MyoB overexpression (Delbac et al., 2001) were found to produce a replication phenotype, I was curious to study if overexpression of MyoC in the *myoA* KO could cause a defect in division. To assess these data, a comparative study of the replication rates of the three TyMyoC expressing lines was performed. For this, parasites were let to infect confluent HFF cultures for 1 hour, followed by 3 washes, which aims to remove extracellular parasites and thus synchronise replication within an hour. Infected cultures were left for 24 hours in normal culturing conditions and fixed after this time. As shown in Figure 5-6B, *myoA* KO lines and the lines expressing tagged MyoC (TyMyoC, pMyoCTyMyoC and p5RT70TyMyoC) showed a replication delay in the first stages of development (vacuoles 2,4, and 8), but no significant differences were found in bigger vacuoles (16 and >32). This delay can be potentially caused by the attachment phenotype and/or aberrant gliding motility observed as described by Andenmatten *et al*. (2013). MyoC overexpression lines show a stronger delay than *myoA* KO parasites; this can be due to the overproduction of the protein causing a slight toxic effect. Although these observations show a delay in replication, no complete abrogation of division is observed as described by Delbac *et al*. (2001).

Together, these results confirm that MyoC can complement some MyoA functions in terms of attachment. One of the most remarkable phenotypes of *myoA* KO line is the strong attachment phenotype while penetrating host cells (Egarter et al., 2014). Thus, its absence was associated with a defect in a step upstream of TJ formation. Neither conoid associated Myosin H (MyoH) (Graindorge et al., 2016), nor any other *T.gondii* myosin, has been linked to host cell attachment to date. Therefore, early invasion events are important functions of MyoA and can be recovered by MyoC in its absence. Additionally, although early studies of MyoC associated this protein with parasite division (Delbac et al., 2001), later studies discarded such function (Egarter et al., 2014). These results support previous studies which showed that absence of MyoA and/or MyoB/C/MLC1 caused a slight delay in replication in *T. gondii* tachyzoites rather than a detrimental defect (section 4.1.4) (Egarter et al., 2014, Frenal et al., 2014). When compared to RhΔ*hxgprt,* lines overexpressing TyMyoC show a delay in replication in early stages vacuoles (2,4 and 8 parasites), although this effect is not observed in later vacuoles (16 and >32). This suggests that two effects can be converging causing division delay: poor gliding kinetics and a potential toxic effect of

TyMyoC; nonetheless, no replication abrogation is seen as suggested in early studies (Delbac et al., 2001).

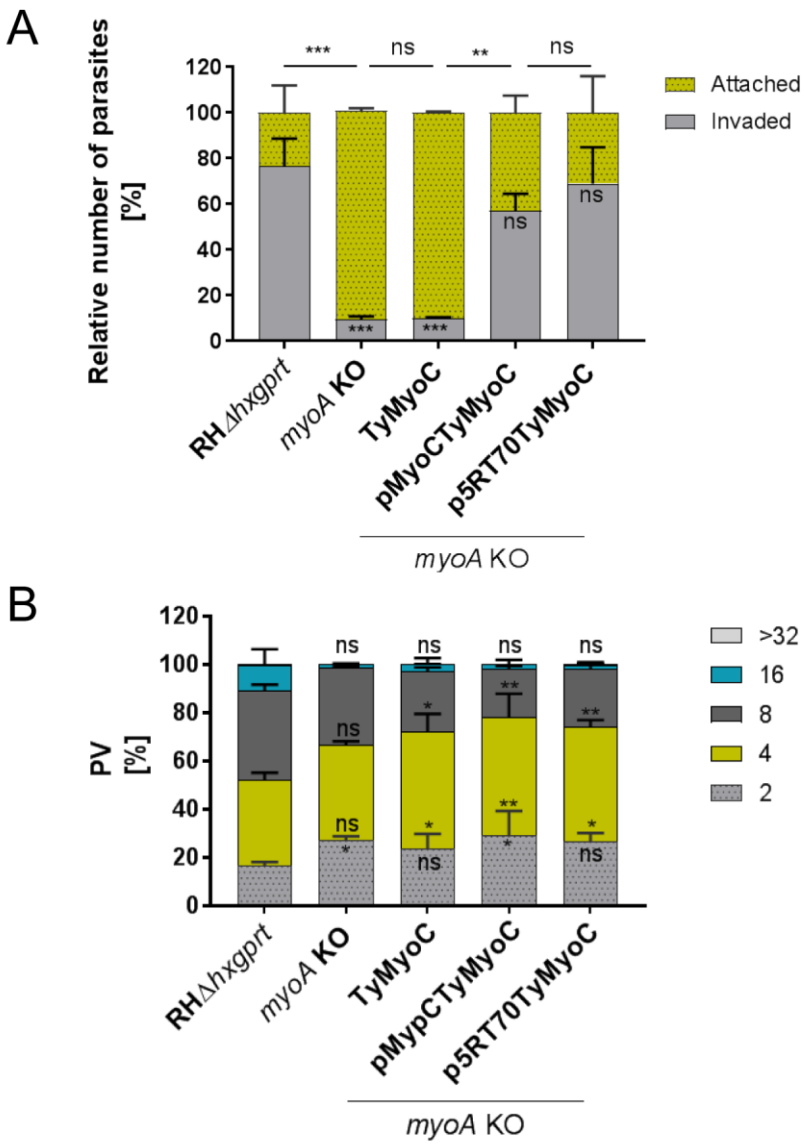

Figure 5-6. MyoC can recover for *myoA* KO host cell attachment phenotype
A. A synchronised invasion assay was performed in p5RT70TyMyoC, pMyoCTyMyoC, and TyMyoC *myoA* KO strains. Parasites were left to invade host cell monolayers for 15 minutes before fixation. Parasites in 10 fields of view were analysed. Parasites overexpressing MyoC can recover for the *myoA* KO host cell attachment phenotype. Graphic depicts mean ± SD. Two-way ANOVA and Tukey's multiple comparisons test were used to determine differences among means. *** P≤0.001, ** P≤0.01, not significant (ns) P>0.05. **B.** Replication assay of p5RT70TyMyoC, pMyoCTyMyoC, and TyMyoC in the *myoA* KO show a replication delay in *myoA* KO lines. The number of parasites per vacuole was counted 24 hours post infection. Graphic depicts mean ± SD. Two-way ANOVA accompanied by Dunnett test for multiple comparisons were used to analyse the data. *** P≤0.001, ** P≤0.01, not significant (ns) P>0.05.

5.1.3.4 MyoC can enhance *myoA* KO egress rates

Upon Ca^{++} stimulation, *myoA* KO parasites showed a clear delay in parasite egress and dissemination *in vitro* (Meissner et al., 2002b, Egarter et al., 2014). The capacity of

MyoC to recover for this egress and dissemination delay in MyoA-depleted parasites was analysed. An egress assay was performed in host cell cultures infected with the three TyMyoC expressing strains that measured the ability of parasites to egress host cells upon ten minutes of Ca^{++} ionophore (A23187) stimulation. The protocol was followed as described in section 3.1.7 and 3.2.5. As shown in Figure 5-7, *myoA* KO and endogenous TyMyoC *myoA* KO parasites show a delay in egress and dissemination that is recovered upon MyoC overexpression. Here, strongly overexpressed MyoC (p5RT70TyMyoC) reached egress rates comparable to RHΔ*hxgprt*, while mildly overexpressed MyoC (pMyoCTyMyoC) showed a slightly reduced capacity.

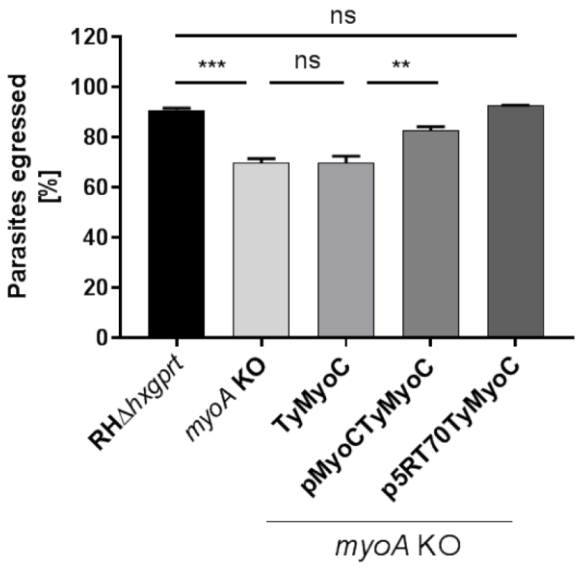

Figure 5-7. Egress is enhanced in the *myoA* KO when overexpressing MyoC
Egress assays of p5RT70TyMyoC, pMyoCTyMyoC, and TyMyoC after 2µM Ca^{++} Ionophore induction (10 minutes). The *myoA* KO presents a slight delay in egress, which improves when MyoC is overexpressed. Graphic displays mean values ± SD of two replicates. One-way ANOVA followed by Tukey's test were used to compare means between groups. *** P≤0.001, ** P≤0.01, not significant (ns) P>0.05

In conclusion, here we have compared the characterised phenotypes of a *myoA* KO strain with *myoA* KO mutants expressing different levels of MyoC. The experiments described above showed that MyoC could take over localisation and function upon MyoA removal. However, this overlap depends on the amount of MyoC expressed in the mutants, with strongly overexpressed MyoC (p5RT70TyMyoC) able to localise in the whole periphery of the parasite whereas mildly overexpressed (pMyoCTyMyoC) and endogenously tagged (TyMyoC) MyoC located mainly in the posterior pole and showed a slight relocation to the periphery. Since the location of MLC1 is not perturbed after MyoA depletion (Andenmatten et al., 2013), it is plausible that it recruits MyoC to this area even at endogenous levels. Additionally, Frenal et al (2014) reported an increase in the amount of

MyoC in MyoA depleted parasites. Here, we observed a slight increase of MyoC fluorescence levels in the *myoA* KO, but this variation is not significant when compared with RHΔ*hxgprt* parasites. Additionally, we observed an immediate partial rescue of the *myo*A KO line when TyMyoC was overexpressed. Growth, gliding rates, invasion, and egress are partially recovered by overexpressed MyoC, but 3D gliding kinetics including distance and average and max speed, are not. Likewise, the *myoB/C/mlc1* KO showed an improvement in gliding kinetics when compared to *myoA* KO (section 4.1.3), meaning that, as a gliding motor, MyoC seems not to be able to complement MyoA loss. Finally, the introduction of extra copies of MyoC did complement MyoA null parasites in several steps of the lytic cycle, but endogenously tagged MyoC showed no significant phenotype recovery.

A closer look at endogenous levels of MyoC indicates this protein is not upregulated in either the *myoA* KO (freshly induced) or the *myoA* KO adapted line (12 months in culture). Here, after one year of continuous culturing of the *myoA* KO, the mutants showed the ability to propagate faster compared to freshly generated *myoA* KO lines. Gliding, invasion, and egress rates increased, indicating that a long-term adaptation process is taking place (Appendix 3). Consequently, since this adaptation happened in a gradual manner, regulation of compensatory myosins may occur and could be detectable at transcription levels. Comparative transcriptomics showed that MyoC, or any other class XIVa or b myosin, is not upregulated in the adapted line; this observation was confirmed by qPCR (Figure 5-8A/B) (Andenmatten unpublished data). The underlying mechanisms driving *myoA* KO adaptation over time remain to be studied; however, it is plausible to think that these parasites regulate important proteins involved in gliding and invasion such as MICs, ROPs, RONs and PM proteins.

Taken together, these data demonstrate that MyoB/C, D, and E transcript levels are not upregulated in the absence of MyoA, indicating that they may not be participating in the adaptation process. Additionally, as MyoC is weakly expressed in *T. gondii* tachyzoites, previous localisation studies in the *myoA* null line have tagged MyoC by either overexpressing the protein (Andenmatten, unpublished data) or by promotor exchange (Frenal et al., 2014). It is important to understand that overexpression of the protein could produce artefactual localisation and characterisation analysis. For instance, as shown above, the importance of the level of MyoC expression to recover for MyoA is critical to consider when studying compensatory mechanisms.

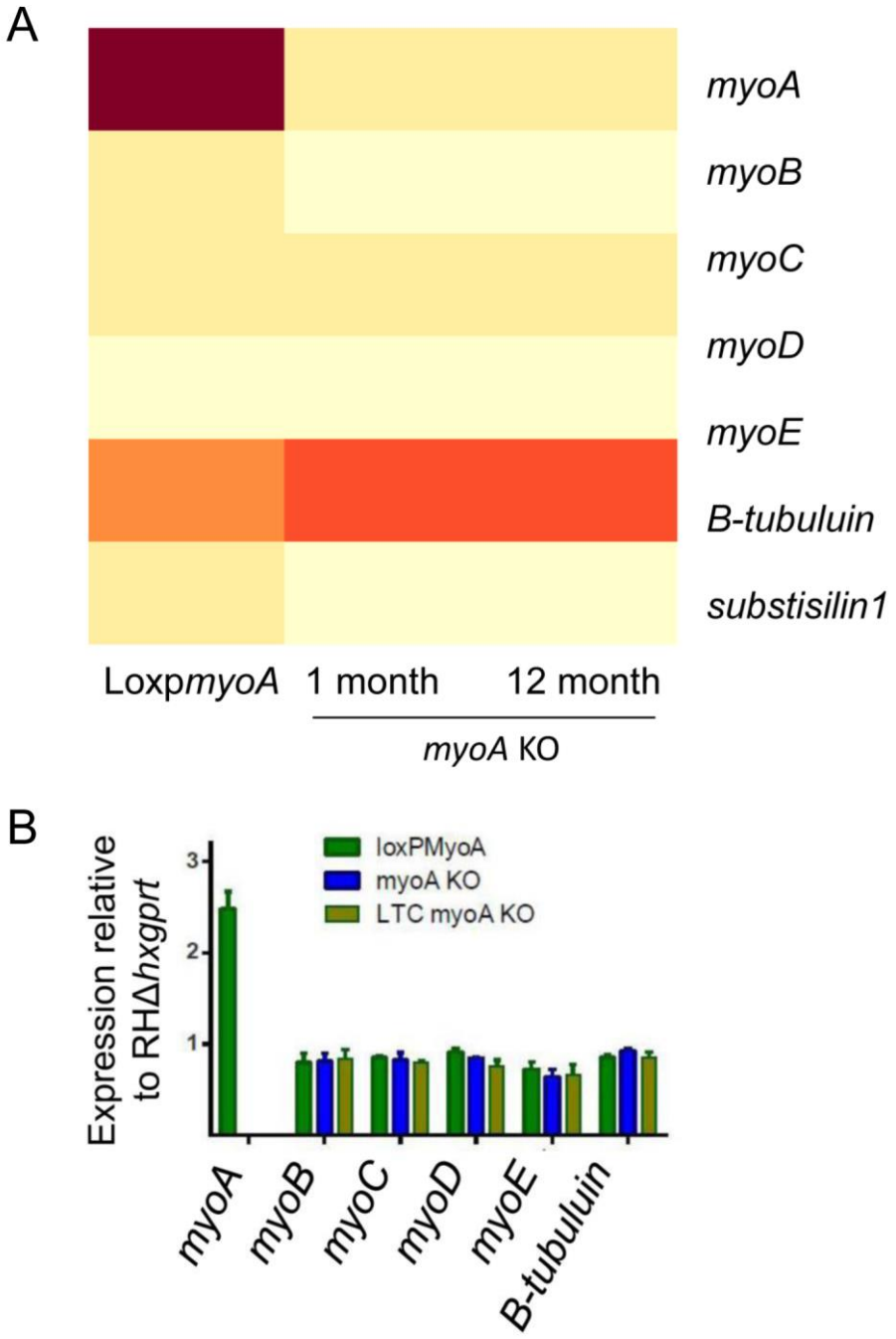

Figure 5-8. Comparative analysis of myosins class XIVa and b in the *myoA* KO line
A. RNA-seq heat map indicating transcript abundance of *myoA*, *B*, *C*, *D*, and *E* in RH*Δhxgprt*, *myoA* KO (1 month in culture), and *myoA* KO (12 months in culture). β-tubulin and SUB1 were used as controls. Relative expression from three independent replicates is shown. Colour key bars represent hundred-fold changes. Analysis performed by Dr. Nick Dickens **B.** Graph showing mRNA levels of *myoA*, *B*, *C*, *D*, and *E* in RH*Δhxgprt*, *myoA* KO (1 month in culture), and *myoA* KO (12 months in culture). α-tubulin was used as control. Bars show mean ± SD of duplicates with three biological replicates. Experiment performed by Dr Nicole Andenmatten.

5.1.4 MyoC localisation is not affected upon MLC1 removal

MyoA interaction with IMC structural proteins (GAPs) is mediated by its light chain MLC1, an orthologue of *Plasmodium* MTIP (Herm-Gotz et al., 2002, Bergman et al., 2003). Although other light chains have been recognised to interact with MyoA in both *Plasmodium* and *T. gondii* (Williams et al., 2015, Bookwalter et al., 2017), it has been shown that only MTIP/MLC1 is responsible for maintaining MyoA subcellular location (section 3.1.3) (Bergman et al., 2003, Egarter et al., 2014). *mtip* KD in *Plasmodium* ookinetes showed that MyoA was degraded upon removal of its molecular partner (Sebastian et al., 2012). In the case of the MyoC-motor complex, immunoprecipitation assays suggested MLC1 interacts with MyoC in the posterior pole (Frenal et al., 2014). However, unlike MyoA, its location does not depend on MLC1, but rather on IMC associated protein 1 (IAP1) (Frenal et al., 2014). In this section, we were interested in further studying MyoC after MLC1 excision.

Previous studies showed that MLC1 is critical for MyoA stabilisation and location in the pellicle of parasites (Bookwalter et al., 2014, Egarter et al., 2014), and that this light chain interacts with both MyoA and MyoC (Frenal et al., 2014). Furthermore, characterisation of both *mlc1* and *myoB/C/mlc1* KOs showed these mutants can be maintained in culture if egress is artificially assisted, and both presented enhanced gliding kinetics when compared to MyoA null mutants. To test if MyoC could relocalise to the pellicle of the parasite upon MLC1-MyoA loss, we expressed TyMyoC in the inducible *mlc1* KO. For this experiment, I transiently transfected TyMyoC overexpression constructs previously described in section 5.1.1, and endogenously tagged MyoC in the loxp*mlc1* strain. As observed in Figure 5-9A/B, in control parasites overexpressed MyoC forms a ring in the posterior pole of the parasite, which does not overlap with MLC1 signal. Similarly, upon MLC1 removal, MyoC is found in its normal location at the posterior pole. These results suggest not only that the presence of MLC1 is critical for MyoA peripheral location, but also for relocation of overexpressed MyoC upon MyoA depletion. Furthermore, endogenously tagged MyoC in the *mlc1* KO does not change its position when compared to control parasites (Figure 5-9C).

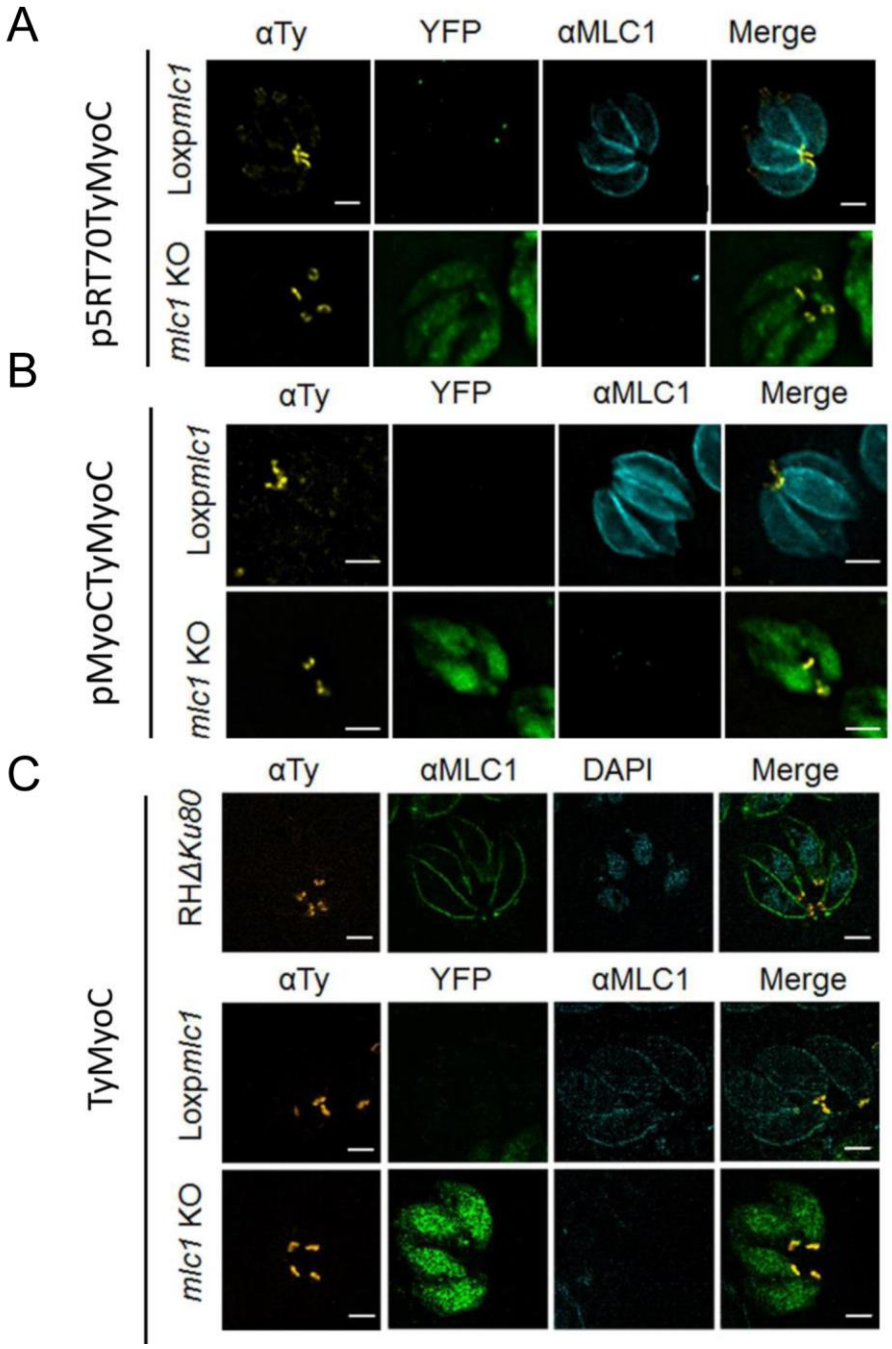

Figure 5-9. MyoC is located in the posterior pole of *mlc1* KO parasites
Immunofluorescence analysis of Ty-tagged MyoC in loxp*mlc1* and *mlc1* KO strains expressing **A.** p5RT70TyMyoC and **B.** pMyoCTyMyoC. Constructs were transiently transfected in the conditional *mlc1* KO strain. MyoC was visualised using αTy. Scale bar represents 2 μm. **C.** SIM images of TyMyoC in RHΔ*hxgprt*, loxp*mlc1,* and *mlc1* KO parasites. Endogenous MyoC was visualised using αTy. Scale bar represents 2 μm. Representative images show that TyMyoC does not change its location in *mlc1* KO parasites under any expression level.

Altogether, these data suggest that neither MyoA nor MyoC are located in the pellicle after MLC1 depletion. While the remarkable capacity of *myoA* KO parasites to glide and invade was explained to be possible by a MyoC-MLC1 interaction, the results obtained in *mlc1* KO parasites showed that such interaction is not essential for recovery of gliding or invasion rates. Interestingly, in terms of gliding and invasion rates, the *mlc1* KO resembles

the *myoA* KO, but the kinetics of the movement is enhanced in the MLC1 null strain. This ability cannot be explained by an immediate MyoC complementation, but we cannot completely discard the possibility that small amounts of MLC1 and MyoA are still able to produce force.

5.2 Study of filamentous actin in mutants of the motor complex

Early studies of apicomplexan gliding motility suggested a conventional architecture for the acto-MyoA motor complex (King, 1988). Thus, MyoA was thought to directly link to transmembrane proteins, and be responsible for moving them across the PM by walking along actin filaments scaffolds which were in contact with the IMC (King, 1988). While this system is still accepted for other myosins, like myosinX (Leijnse et al., 2015), the unusual structure of MyoA and nature of ACT1 did not support this hypothesis in *T. gondii*. For instance, MyoA has a conserved head domain, short neck domain, and an absent tail domain; this structure makes it dependant on MLC1 for function and fixed positioning (Heintzelman and Schwartzman, 1997, Hettmann et al., 2000, Herm-Gotz et al., 2002). Similarly, studies of ACT1 showed that the nature of this protein was not similar to canonical actin-based systems (Dobrowolski et al., 1997b). While long actin filaments were not detected, 97% of this protein was reported to be in its globular form (Dobrowolski et al., 1997b, Pinder et al., 1998). IFA analysis of this protein showed that ACT1 location was diffusive in the cytoplasm with more intense signal in the apical and posterior pole in extracellular parasites (Dobrowolski et al., 1997b, Mehta and Sibley, 2011). Therefore, the actin filaments were suggested to be extremely short and unstable, making its visualisation limited (Dobrowolski et al., 1997b, Schüler and Matuschewski, 2006a). Although evasive, ACT1 filaments have been observed in several instances in *T. gondii*. For instance, use of Jasplakinolide (JAS), an actin polymerization inducing drug, made it possible to observe a posterior spiral structure that was imaged using αACT1 antibodies (Wetzel et al., 2003), corresponding to results obtained by electron microscopy imaging (Shaw and Tilney, 1999). Similar results were obtained when actin depolymerising factor (ADF) was knocked out in *T. gondii* tachyzoites (Mehta and Sibley, 2011). Additionally, an ACT1 network was evident in SEM images when the PM of the parasite was removed (Schatten et al., 2003). Recently, by using actin-Chromobody (Cb) probes, actin filaments have been detected in tachyzoites (Periz et al., 2017). Remarkably, filamentous actin was found to form a highly dynamic network inside parasites, and a stable scaffold in the RB of vacuoles. This RB F-actin formation connects parasites inside the PV, and varies through the development of daughter cells (Periz et al.,

2017). Cb-actin filaments were responsive to actin modulating drugs, such as Cytochalasin (depolymerization) and Jasplakinolide (polymerization), and are completely absent in the *act1* KO (Periz et al., 2017). In good agreement with these findings, a recent study identified a cell-to-cell communication system in *T. gondii* among daughter cells in the PV which is acto-myosin dependant (Frenal et al., 2017b). Here, MyoI and MyoJ have been suggested to maintain the connection among daughter cells while developing inside the host cell (Frenal et al., 2017b). Taken together, these published data elegantly show that *T. gondii* can form long tubular actin networks to communicate between daughter cells in an acto-myosin dependant manner while developing inside the PV (Frenal et al., 2017b, Periz et al., 2017). Additionally, this scaffold is responsible for maintaining organisation of the vacuole, as in the absence of the actin network, the vacuole seemed disorganised and the RB area collapses (Periz et al., 2017). Moreover, this filamentous network would support directed trafficking of proteins as shown for dense granule delivery (Heaslip et al., 2016, Periz et al., 2017).

Considering that the current motor model suggests a critical role of the interaction between MyoA-ACT1, this section focused on visualising the filamentous actin network in the absence of MyoA and MLC1. To observe the F-Actin network described by (Periz et al., 2017), *myoA* KO, inducible *mlc1* KO, and RHΔ*hxgprt* strains were transiently transfected with the construct p5RT70.Cb.haloTag (CbHalo) (Periz et al., 2017) and p5RT70.Cb.SnapTag (CbSnap) (Figure 5-10A). Cb constructs were designed and cloned in our lab by Dr Javier Periz (WTCMP/University of Glasgow).

5.2.1 Cb-actin signal in *myoA* KO and *mlc1* KO

I was interested in observing CbHalo-actin in extracellular parasites using high-resolution microscopy. For this, infected cultures were scratched and syringed. Extracellular parasites were incubated on coverslips previously coated with 0.1% poly-L-lysine for 30 minutes. After this time, parasites were fixed, and an IFA was carried out using αHalo primary antibodies. As depicted in Figure 5-10B (top panel) in RHΔ*hxgprt* parasites, CbHalo signal was mostly found in the cytoplasm of the parasite as previously described (Dobrowolski et al., 1997b, Mehta and Sibley, 2011). This cytoplasmic signal is not equally distributed, as it excludes the parasite nucleus and apicoplast areas (Figure 5-10B, top panel/ expansion). Correspondingly, CbHalo seemed to surround these organelles, and presented a compartmentalised distribution. Additionally, fluorescence images showed CbHalo localisation in the periphery of the parasite, with a slight stronger concentration at the posterior pole. Then, colocalization between the CbHalo peripheral and MLC1 signals was

assessed using Colocalization plugin designed for ImageJ-Fiji on single stack and maximum projection SIM images. The analysis showed that both signals (CbHalo and MLC1) colocalise in the periphery of the parasite above MLC1 in single and maximally projected images (Figure 5-10B, top panel).

The *myoA* and *mlc1* KOs showed a similar cytoplasmic signal of CbHalo (Figure 5-10B, mid and bottom panel). Correspondingly, this signal appears to surround the nucleus and apicoplast (Figure 5-10B, mid and bottom panel/ expansion). Analysis of colocalization in the *myoA* KO parasites showed CbHalo and MLC1 slightly overlapping each other on one side of the periphery (Figure 5-10B, mid panel). As expected, this colocalization is diffuse and lost in the *mlc1* KO (Figure 5-10B, bottom panel).

Following these observations, the signal of CbHalo was studied in intracellular parasites. Figure 5-10C shows that RHΔ*hxgprt*, *myoA* KO, and *mlc1* KO parasites could form a network of CbHalo at the RB. In good agreement with published data (Periz et al., 2017), this filamentous scaffold seems to interconnect all daughter cells, maintaining the organisation of the vacuole. Additionally, individual parasites present cytosolic signal among it, where filaments can be observed (Figure 5-10C). When compared to RHΔ*hxgprt*, the cytosolic signal in the *myoA* KO and *mlc1* KO is more diffuse, but filamentous structures can still be seen (Figure 5-10C, mid and bottom panel).

By using time-lapse imaging, it was demonstrated that parasites expressing CbEmerald have a highly dynamic actin network, which is located in the cytosol of individual parasites (Periz et al., 2017). While this showed a novel feature of *T. gondii* actin, the flow kinetics remained to be studied. In this section, I was curious to see if the network is affected in the absence of MyoA and MLC1-MyoA. In order to enhance visualisation of the filaments, p5RT70.Cb.SnapTag (CbSnap) (Keppler et al., 2003) (Figure 5-10D) was transiently transfected into the parasite lines. Snap tag is a versatile tool that rapidly reacts with labelled substrates; the latter are commercially available in a wide spectrum of fluorophores. This tool, together with the constitutive promoter p5RT70, guarantees the constitutive expression of the protein, aimed to facilitate the signal in live-imaging experiments. Therefore, the use of this construct was meant to enhance the signal-to-noise ratio since CbHalo substrate background was too high to perform live-imaging.

For these experiments, confluent monolayers growing in live-cell imaging dishes were infected with the mutant lines expressing CbSnap. Cultures were incubated with snap ligand (1:10000) for 30 min and washed three times with pre-warmed PBS. Parasites were incubated for 15 min in complete DMEM under normal conditions. Videos were recorded at 1 frame per 100 milliseconds for 30 seconds.

Next, I assessed the dynamics of CbSnap-actin in mutant parasites. Background noise was excessive, which represented a limitation to the study of extracellular parasites - for this reason these data are non-shown.

As depicted in Figure 5-10E, in RHΔ*hxgprt* (Movie 15-16) and loxp*mlc1* (Movie 17-18) vacuoles, I observed actin in three different areas: the periphery, cytosol, and RB. In the periphery, the signal of CbSnap can be seen delineating each individual parasite from the apical to the posterior pole. The cytoplasmic signal is ubiquitous, irregular, and more diffuse than the peripheral signal. In addition, at the 1/3 of the parasite a sharp cytoplasmic signal can be observed closer to the apicoplast. Finally, the third, and strongest, signal comes from the RB, which seems to connect the daughter cells (Periz et al., 2017). In control parasites, the dynamics of these three areas seem to establish a flow connecting them. The nature of this flow seems fast but details about speed and directionality need deeper revision. In both *myoA* KO and *mlc1* KO, the organization of the rosette is disorganised, but they can clearly form RB filaments, which, like RHΔ*hxgprt* parasites, emit the strongest signal of CbSnap (Figure 5-10E). In contrast to the peripheral signal of CbSnap in RHΔ*hxgprt* parasites, in *myoA* KO (Movie 19-20) and *mlc1* KO (Movie 21-22) peripheral filaments are not equally well defined and the signal presented a diffuse pattern (Figure 5-10E). In the cytoplasm, a strong and more diffuse signal was seen in MyoA and MLC1 depleted parasites.

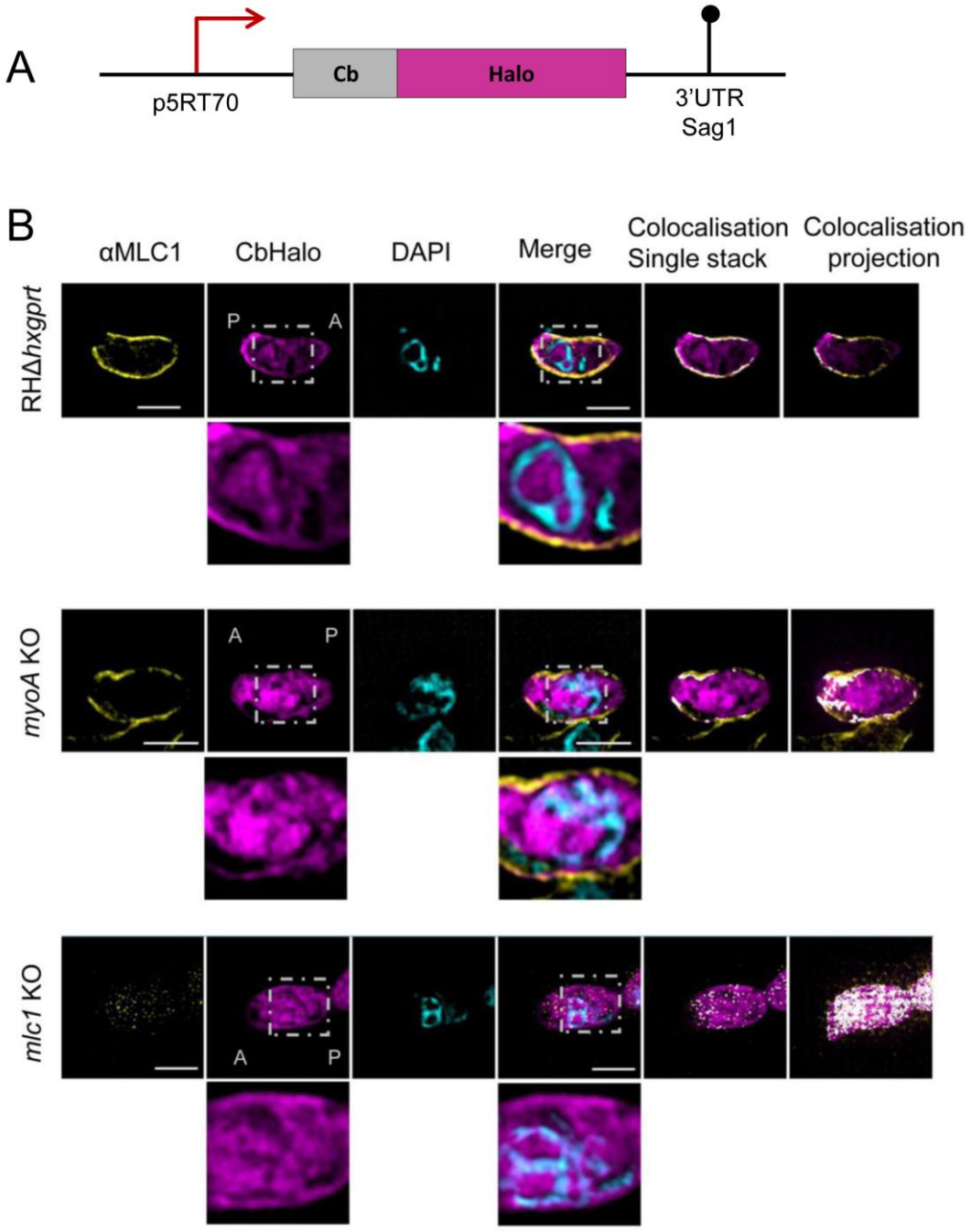
A
Cb
Halo
p5RT70
3'UTR
Sag1
B
αMLC1
CbHalo
DAPI
Merge
Colocalisation
Single stack
Colocalisation
projection
RHΔhxgprt
myoA KO
mlc1 KO
P
A
A
P
A
P

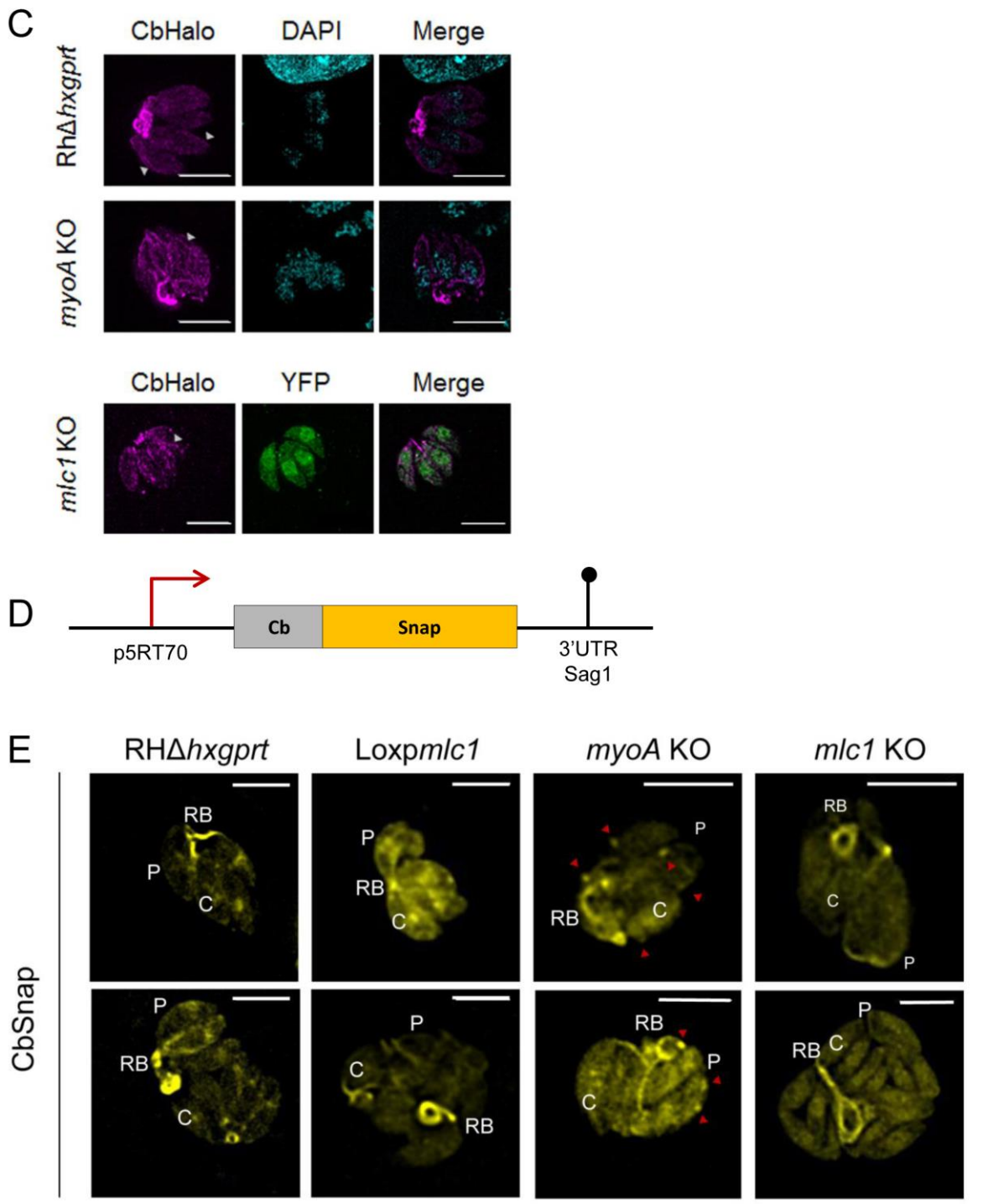

Figure 5-10. Visualisation of actin in *myoA* KO and *mlc1* KO lines
A. Schematic representation of the p5RT70.Cb.Halo construct that was transiently transfected in RHΔ*hxgprt*, loxp*mlc1,* and *myoA* KO strains **B.**SIM images of RHΔ*hxgprt*, loxp*mlc1,* and *myoA* KO extracellular parasites expressing CbHalo. The signal shows an irregular cytosolic distribution of actin. Expansion shows CbHalo signal excluding the nucleus and apicoplast. Posterior pole (P) and apical pole (A) have been localised according to apicoplast position in the image stacks. Colocalisation analysis of MLC1 and CbHalo was performed in single stacks and total projections using Fiji (ImageJ). Colocalised areas are highlighted in white. Scale bar represents 2 µm **C.** SIM images of RHΔ*hxgprt*, loxp*mlc1,* and *myoA* KO vacuoles expressing CbHalo. This signal can be observed in a filamentous network in the posterior end connecting individual parasites in the three lines. Filamentous structures were observed in individual parasites (arrows). Formation of the network is MyoA independent. Scale bar represents 2 µm **D.** Schematic representation of p5RT70.Cb.SnapTag construct that was transiently transfected in RHΔ*hxgprt*, loxp*mlc1,* and *myoA* KO **E.** Time-lapse analysis of RHΔ*hxgprt*, *mlc1* KO, and *myoA* KO vacuoles expressing CbSnap.

Images represent the first frame of each video. Rapid flow of Cb-snap-actin was observed in i) residual body (RB), ii) Periphery (P), and iii) Cytosol (C). RB network can be detected in RHΔ*hxgprt*, *mlc1* KO, and *myoA* KO vacuoles. Peripheral CbSnap signal in RHΔ*hxgprt* delineates the parasite. Cytosolic signal shows a brighter distribution around the apicoplast area in RHΔ*hxgprt.* However, cytosolic and peripheral signal are more diffuse in the knockout lines. Scale bar represents 2 µm

In this section, recently described chromobody-actin tagging (Periz et al., 2017) was used to visualise actin filaments in the *myoA* KO and *mlc1* KO lines. For this, CbHalo and CbSnap constructs were used to assess high-resolution images and the dynamics of the network, respectively. As shown above, in RHΔ*hxgprt,* MyoA, and MLC1 null extracellular parasites, the signal of actin is distributed throughout the cytoplasm, forming compartments that exclude the apicoplast and nucleus. Additionally, a sharp distribution in the periphery can be observed, which, in RHΔ*hxgprt* parasites, seem slightly stronger in the posterior pole.

By high-resolution imaging, we have demonstrated that RHΔ*hxgprt, myoA* KO, and *mlc1* KO parasites can form an interconnecting network among daughter cells in vacuoles. In good agreement with previously published results (Periz et al., 2017), individual parasites form a long actin network among them during their development in the PV, and the absence of MyoA or MLC1-MyoA does not affect the formation of this scaffold. Additionally, RHΔ*hxgprt, myoA* KO, and *mlc1* KO strains present a delineating signal of actin in the periphery of individual parasites and a diffuse signal in the cytoplasm.

This observation was supported by live-imaging in the knockout lines. Here, we observed that F-actin behaviour is highly dynamic (Periz et al., 2017) and the signal of the network comes from three different areas: periphery, cytoplasm, and RB. These actin populations vary in terms of thickness and shape, but video analysis suggests they are interconnected and probably generate a fast flow. Indeed, the RB network was observed in the MyoA and MLC1 null parasites, indicating that the presence of these proteins is not essential for the formation or integrity of the posterior scaffold.

5.3 Summary and conclusions

In this chapter, I have studied the interaction of the important proteins associated with MyoA and MyoA-MLC1 in the respective mutant parasites.

First, the ability of MyoC to take over MyoA functions after its depletion was analysed. Supporting previous data (Egarter et al., 2014, Frenal et al., 2014), our results suggest that MyoC has the capacity to recover MyoA function, but this complementation depends on MyoC localisation in the pellicle. We found that differential expression of MyoC

has biological meaning in terms of recovery of growth, gliding, invasion, and egress rates in the *myoA* KO. This adaptation responded to overexpressed MyoC in the parasite. For instance, when p5RT70TyMyoC was compared to endogenously tagged MyoC in the *myoA* KO, a notable difference in terms of compensation was found. In fact, the average and maximum speed were the only characteristics overexpressed MyoC could not complement in the *myoA* KO. This result showed that MyoC and MyoA may have different mechanistic qualities. While it is known that MyoA interacts with two light chains that stabilise and amplify its step size, insufficient data are available about MyoC lever arm organisation and function.

Second, since both MyoA and MyoC interact with MLC1 (Frenal et al., 2014), we considered that the presence of this protein is critical for leading *myoA* KO remaining invasion rates and MyoC compensatory mechanisms. Here, I tagged MyoC under different expression levels in the conditional *mlc1* KO mutant line. MyoC showed a posterior pole location after MLC1 excision under all three conditions, meaning that MyoC is not interacting with another light chain after MLC1 depletion to relocalize in the pellicle and take over MyoA function and position.

Third, the recently established expression of chromobodies against actin (Periz et al., 2017) was used in the *myoA* KO and *mlc1* KO lines to visualise if filamentous actin structures are evident in these mutants. Previous studies suggested actin is mainly distributed in the periphery and the cytoplasm with a perinuclear concentration in extracellular tachyzoites (Dobrowolski et al., 1997b). In good agreement with these observations, RHΔ*hxgprt*, *myoA* KO, and *mlc1* KO extracellular parasites showed some CbHalo signal at the periphery and most in the cytoplasm where it distributes diffusely, excluding the nucleus and apicoplast. Moreover, these data show that *myoA* KO and *mlc1* KO parasites can form an intravacuolar network made of actin filaments as seen in control parasites, indicating that the formation of these filaments does not depend on the presence of the motor. The signal of peripheral actin and MLC1 in extracellular parasites colocalise underneath MLC1, facing the inner side of the pellicle, and not right beneath the PM as expected (Carruthers and Boothroyd, 2007). Further studies are needed to define if this signal correspond to the cytoplasmic actin meeting the edge of the IMC or if it corresponds to the acto-MyoA motor complex since the exact position of the complex has not been determined and is still a matter of debate (Tardieux and Baum, 2016). Moreover, some studies hypothesised that interaction of actin monomers with MyoA itself will trigger formation and stabilisation of short actin filaments, thus acting as a limiting factor for the assembly of the gliding machinery (Schüler and Matuschewski, 2006b,

Stadler et al., 2017). Here, we have shown that actin filament formation is independent of MyoA function. However, deeper characterisation of the F-actin network is needed to discern if the absence of MyoA-MLC1 influences the dynamics of the flow established either inside (single parasite) or outside of the parasite (PV).

6 Exploring the canonical and novel functions of the acto-MyoA motor complex

Single cells employ different systems of motility based on their shape, force generation mechanism, cytoskeletal arrangement, and adhesion to substrates (Welch, 2015). For instance, tumour cells propagate using two different mechanisms referred to as mesenchymal and amoeboid motility (Paňková et al., 2010). Mesenchymal migration depends on integrins to create focal adhesions that mediate substrate attachment. Cells moving in mesenchymal fashion are usually highly polarised and move at low speeds (Palecek et al., 1997, Paňková et al., 2010). Conversely, amoeboid migration is governed not by adhesin-mediated attachment, but by continuous cycles of cell expansion and contraction. Amoeboid (-like) moving cells are often round shaped, and reach high speeds while moving, corresponding to the low adhesion (traction) to the substrate (Lämmermann and Sixt, 2009, Barry and Bretscher, 2010, Paňková et al., 2010).

Gliding motility in apicomplexan zoites, such as *Plasmodium* and *Toxoplasma,* is mediated by adhesins, which allow parasites to attach to the surface (Heintzelman, 2015). According to the prevailing model for apicomplexan motility, the migration of adhesins is an active process driven by the acto-myosin motor complex. This model was based on the detrimental effects produced by actin modulating and myosin inhibiting drugs on overall motility (Dobrowolski and Sibley, 1996, Dobrowolski et al., 1997a). Therefore, the linear motor proposes that MyoA is a force producer while MIC proteins are force transducers, with both of them associated via ACT1 (Keeley and Soldati, 2004). The observation that both components of the gliding machinery and associated proteins are important for efficient motility, but not essential, has challenged the basis of the current gliding model (Andenmatten et al., 2013, Egarter et al., 2014, Gras et al., 2017, Whitelaw et al., 2017). Further gliding kinetic studies showed that *myoA* KO parasites present a more severe gliding phenotype when compared to *mlc1* and *act1* KOs (Table 4-1) (section 3.1.6) (Egarter et al., 2014, Whitelaw et al., 2017). MyoA null mutants present a slow "stop and go" like movement restricted to circular tracks (Egarter et al., 2014). In contrast, *mlc1* and *act1* KOs present smooth motility in both circular and helical tracks (section 3.1.6, Table 4-1) (Whitelaw et al., 2017). The observations that these three mutants (*myoA*, *mlc1*, and *act1* KOs) can move was corroborated in 3D environments (section 3.1.6 / 5.1.3.2, Table 4-1) (Whitelaw et al., 2017). Additionally, while redundancy between MyoA and MyoC has been suggested to take over MyoA functions in the *myoA* KO strain, overexpression of MyoC can only partially

restore invasion, egress, and gliding rates, but is incapable of recovering motility speed (section 5.1.3/ 5.1.3.2)

In this chapter, the functions of the acto-MyoA motor complex are analysed from both a canonical and newly proposed point of view. Here, it is suggested that the acto-MyoA motor complex is necessary for the correct regulation of attachment to the substrate, but not for global force production. To test this idea, the ability of mutant parasites to remain attached to a substrate under different flow conditions was analysed. Additionally, considering the principle of the linear motor model (Keeley and Soldati, 2004, Soldati and Meissner, 2004), retrograde flow of proteins present in the PM was also studied in parasites with impaired acto-MyoA motor complex function. This was achieved by applying a modified version of the microbead translocation assay (King, 1988). Furthermore, since new evidence has highlighted the importance of retrograde flow in force generation in tachyzoites and *Plasmodium* sporozoites (Quadt et al., 2016, Moreau et al., 2017, Stadler et al., 2017), and considering other models for motility in different organisms (Lämmermann and Sixt, 2009, Barry and Bretscher, 2010, Paňková et al., 2010), new pathways have been tested.

6.1 The acto-MyoA motor complex modulates cell adhesion

Protein-mediated adhesion to the substrate is essential for productive gliding motility in apicomplexan parasites. Previous studies have indicated the importance of multiple proteins involved in this process. For instance, in *T. gondii* the surface antigen (SAG) proteins are localised to the plasma membrane of the parasite and serve as adhesins; however, there is no evidence that these directly interact with the acto-MyoA motor complex (Mineo and Kasper, 1994, Dzierszinski et al., 2000, Lekutis et al., 2001). Furthermore, the micronemes contain a diverse repertoire of micronemal proteins (MICs), among them the thrombospondin-related adhesive (TRAP) family, which has been implicated in substrate attachment (Heintzelman, 2015). The transmembrane adhesive micronemal protein 2 (MIC2) is suggested to be the main substrate adhesion factor (Huynh and Carruthers, 2006, Gras et al., 2017), as it is capable of connecting the acto-MyoA motor complex to the substrate via the glideosome-associated connector (GAC) (Jacot et al., 2016a). The secretion of MICs (*e.g.* MIC2) from the apical pole, and their translocation to the posterior pole generates forward movement, mediated by transient attachment points (Boucher and Bosch, 2015).

To test the ability of acto-MyoA motor complex mutants to attach to a substrate, Dr Gurman Pall employed a microfluidic system with variable flow stress (Whitelaw et al., 2017). This protocol was based on a system established by Harker and colleagues, who elegantly adjusted differential shear levels to physiological conditions in order to demonstrate its impact on adhesion and motility in human vascular endothelium (Harker et al., 2014). For the acto-MyoA motor complex mutant experiments, infected HFF monolayers were scratched and syringed to mechanically induce egress. Extracellular parasites were added to Collagen VI coated chamber slides (Ibidi© IB-80192) and left to attach. The chamber slide was then linked to an open-circuit flow system, in which one side contains a syringe pump that controls the flow rate Figure 6-1A. The first fluidic flow was low at 0.1 ml/min [0.3 dynes/cm^2], used as an initial "wash step" to remove unattached parasites. Subsequently, fluidic flow stress was increased until reaching the range of arterial shear stress, approximately 15 dynes/cm^2 (Papaioannou and Stefanadis, 2005), which in the conditions of this experiment represented around 5 ml/min. To note, as not all parasites in the chamber were within the field of view, many of them could unattach and attach somewhere else in the chamber, and, potentially, stay attached until the highest flow rate outside the field of view. Considering this premise, five images were taken within the same chamber at each fluidic flow rate to reduce the errors associated with quantifying attachment in a limited field of view. As depicted in Figure 6-1B, RHΔ*hxgprt* parasites remain attached to the coated surface with only a slight reduction from initial flow rate to the highest flow rate [15 dynes/cm^2], like *myoA* KO mutants. Unlike *myoA* null parasites, depletion of MIC2 lowered attachment strength; in this case, around 64% of the parasites were lost when increasing flow rate from 1 ml/min to 2 ml/min [3 and 6 dynes/cm^2]. *mlc1* and *act1* KOs showed the weakest attachment strength and were unattached close to the initial flow rate. Thus, after increasing the flow from 0.1 ml/min to 1 ml/min [0.3 dynes/cm^2 and 3 dynes/cm^2], only 26% (*mlc1* KO) and 2% (*act1* KO) remain attached, in contrast to 96% (RHΔ*hxgprt*) and 92% (*myoA* KO). No parasite remained attached when the strongest flow rate of 5ml/min [15 dynes/cm^2] was reached, whereas in the case of RHΔ*hxgprt* (80%) and *myoA* KO (69%) a high number of parasites were observed.

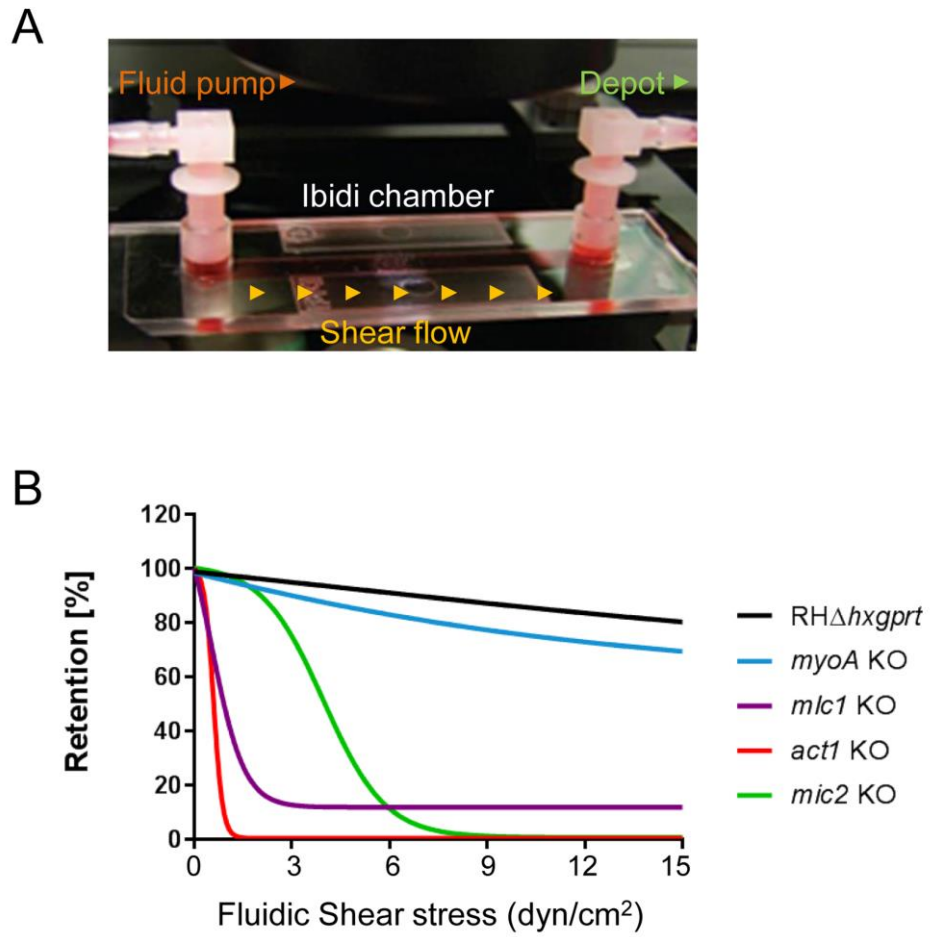

Figure 6-1. Attachment of acto-MyoA motor complex knockouts was measured using fluidic shear flow
Results obtained by Dr Gurman Pall
A. Schematic of the fluidic system. Extracellular parasites were loaded on a slide pre-coated with Collagen in the flow chamber (Ibidi chamber) and left to attach. The fluid was injected into the chamber at different flow rates using a syringe pump controlled by a programmed system. Analysis was initiated after the flow first started. The fluidics system used is an open circuit; after each flow pass through the chamber, fluids and parasites were collected in a reservoir **B.** Graphic displays retention capacity of acto-MyoA motor complex mutants under different flow rates. RHΔ*hxgprt* and *myoA* KO remain retained to the substrate under the highest flow rates. *mic2* KO, *mlc1* KO and *act1* KO were not able to withstand even low flow rates. Figure modified from (Whitelaw et al., 2017) under Creative Commons Attribution 4.0 International License.

These data provide evidence of the potential participation of the acto-MyoA motor complex in substrate attachment. In fact, *myoA* KO parasites present a unique circular "stop and go" like motility that produced slow gliding speed in both 2D and 3D environments (Table 4-1) (Egarter et al., 2014, Whitelaw et al., 2017). This "stop and go" phenotype and slow gliding speed could be caused by strong attachment or "grip" to the substrate, which is supported by the ability of this knockout parasite to be retained under high shear stress. On the contrary, *mic2*, *mlc1*, and *act1* KOs display smooth motility, and their circular gliding kinetics were similar when compared to RHΔ*hxgprt*. In fact, these three knockout lines were

unable to attach under minimal shear stress [0.3 dynes/cm2], indicating they have reduced attachment ability. Thus, there is an inverse correlation between attachment or "grip" and gliding speed (Table 6-1) (Münter et al., 2009, Whitelaw et al., 2017). Considering this, we speculate that the low gliding rates observed in these mutant lines correspond to their deficient attachment capacity, which affects initiation of gliding motility (Table 4-1). Taken together, these data suggest that the acto-MyoA motor complex is involved in the regulation of parasite-substrate interactions, coordinating the engagement and release of transmembrane proteins like MIC2 in the parasite PM without generating the global force for driving gliding.

Table 6-1. Overview of motility speed and retention under flow shear

		Control	*myoA* KO	*mic2* KO	*mlc1* KO	*act1* KO
Gliding speed [µm/s]	2D (circular)	0..7±0.08	0.2±0.08	1±0.3	0.4±0.2	1±0.3
	3D	0.7±0.07	0.3±0.07	0.7±0.1	0.7±0.1	0.7±0.1
Fluid shear stress [dyn/cm2]	0 [% Retention]	100	100	100	100	100
	1 [% Retention]	94	89	75	18	0
	3 [% Retention]	88	78	2.8	11	0
	5 [% Retention]	80	69	0	9	0
Reference		[1] [2]	[1][2]	[3]	[2]	[2]

[1] (Egarter et al., 2014) [2] (Whitelaw et al., 2017) [3] (Gras et al., 2017). In 3 D motility control is considered loxp line while the rest of assays refers to RHΔhxgprt.

6.2 Retrograde flow in *T. gondii* tachyzoites

T. gondii tachyzoites maintain a defined cell polarity, with an organised cytoskeleton and highly specialised apical and posterior complexes (Nichols and Chiappino, 1987, Hu et al., 2006). The linear motor model proposes that, from a fixed position, MyoA generates force to drive the unidirectional transport of ACT1 filaments towards the rear of the parasite, thus translocating or "capping" transmembrane proteins, such as MIC2, from the apical to the posterior pole (Opitz and Soldati, 2002, Soldati and Meissner, 2004). This model was supported by the observation that *Eimeria* and *Plasmodium* sporozoites were able to translocate latex microbeads along the plasma membrane from apical to posterior pole at speeds of 1-10 um/s (King, 1988). More recent studies exploited the principle of membrane protein capping to study the association of the parasite with the substrate employing microbeads. For instance, in order to study the dynamics of attachment, microbeads and traction force microscopy (TFM) was used to assess the tension generated in adhesion sites

along the parasite surface in motile *Plasmodium* sporozoites (Münter et al., 2009). The results of this study suggested that rapid turnover of attachment sites is essential for productive motility (Münter et al., 2009). The antero-posterior transport of lipids and proteins present in the membrane (retrograde flow) was further assessed in *Plasmodium* parasites in order to analyse its importance in cell locomotion (Quadt et al., 2016). Here, the association between retrograde flow and force production was studied in sporozoites by measuring the force necessary to pull out microbeads trapped by optical tweezers, and comparing to the speed that they flow across the parasite surface. Analyses carried out in wild-type parasites, parasites perturbed with actin-modulating drugs, adhesin knockout parasites, and actin-binding protein knockout parasites concluded that efficient motility requires several components, not only involved with force production but also with retrograde flow in the PM together with yet unknown factors. For instance, addition of CytoD did not block retrograde flow, but the force generated on the bead was reduced. Jasplakinolide (JAS) treated parasites showed an increased retrograde flow speed, but less force applied on the bead (Quadt et al., 2016, Moreau et al., 2017). Similar experiments were conducted in *T. gondii* tachyzoites. Here, microbeads trapped by laser tweezers were used to measure the molecular forces involved in the capping of proteins (Stadler et al., 2017). These experiments suggested that in tachyzoites, a period of random movement (apolar phase) precedes directed migration of the microbeads to the rear pole of the parasite (polar phase). Contrary to *Plasmodium* experiments, while addition of CytoD clearly impacted the polarised migration of the bead and reduced the force exerted on it, JAS treatment did not affect the force applied to the bead, but the migration of the bead showed long and random paths (Stadler et al., 2017).

6.2.1 Protein capping is an acto-MyoA independent mechanism

The linear motor proposes that the unidirectional polarised migration of transmembrane proteins depends on the force produced by the acto-MyoA motor complex (Soldati and Meissner, 2004). Therefore, this section was focused on testing the ability of *T. gondii* tachyzoites to translocate microbeads upon depletion of key acto-MyoA motor complex components. This experiment was originally designed by Prof Gary Ward (University of Vermont), and performed by Dr Simon Gras, Dr Jamie Whitelaw, and myself. To give a broad vision of the results, I show data obtained by these members who must be properly acknowledged for sharing their data for this study. Here, extracellular parasites were prepared, and left to attach to live-cell dishes previously coated with poly-L-lysine for 20 minutes on ice. Fluorescent latex 40 nm beads (microbeads) were added and incubated

with the parasites for 10 minutes maintaining cold temperatures, followed by a 15-minute incubation at 37°C in standard culturing conditions to promote microbead translocation. Parasites were fixed with 4%PFA and incubated for 10-15 minutes. After this time, PFA was removed and Hoechst 0.01% was added to stain parasite nuclei. Three outcomes were considered to assess the interaction of the parasites with the microbeads: "Unbound" - no microbead signal is observed at the PM, "Bound" – the microbead signal is observed at the periphery of the parasite, and "Capped" – the microbead signal is polarised (Figure 6-2A) (Whitelaw et al., 2017). Microbead translocation capacity was tested in *myoA* and *mic2* KO clonal lines, and conditional *mlc1* and *act1* KOs 96 hours after rapamycin treatment. As depicted in Figure 6-2B/C, translocation of the microbeads was not blocked in the absence of functional components of the acto-MyoA motor complex. The percentage of capping events with the knockout parasites does not show statistical differences when compared to the RHΔ*hxgprt* strain. However, the percentage of "unbound" microbeads is slightly higher in *myoA* and *mlc1* KOs, and highly significant in *act1* KO mutants (Figure 6-2C). We found no differences in *mic2* KO ability to bind and cap beads when compared to RHΔ*hxgprt*. This result was surprising; however, the interpretation here is that the beads don't bind to MIC2 exclusively, but they can bind to other adhesins present in the membrane as well as to membrane proteins such as SAG1, which covers the parasite surface.

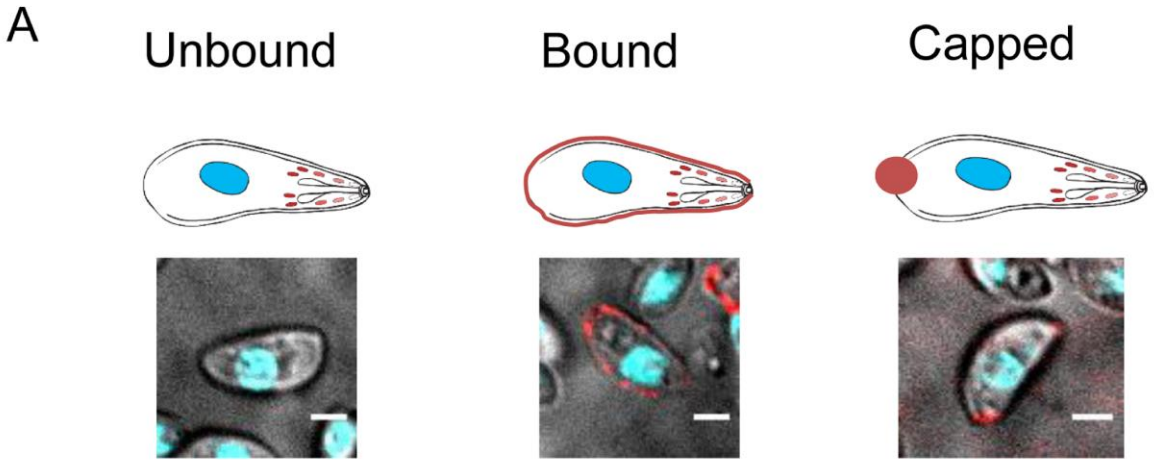
A
Unbound
Bound
Capped

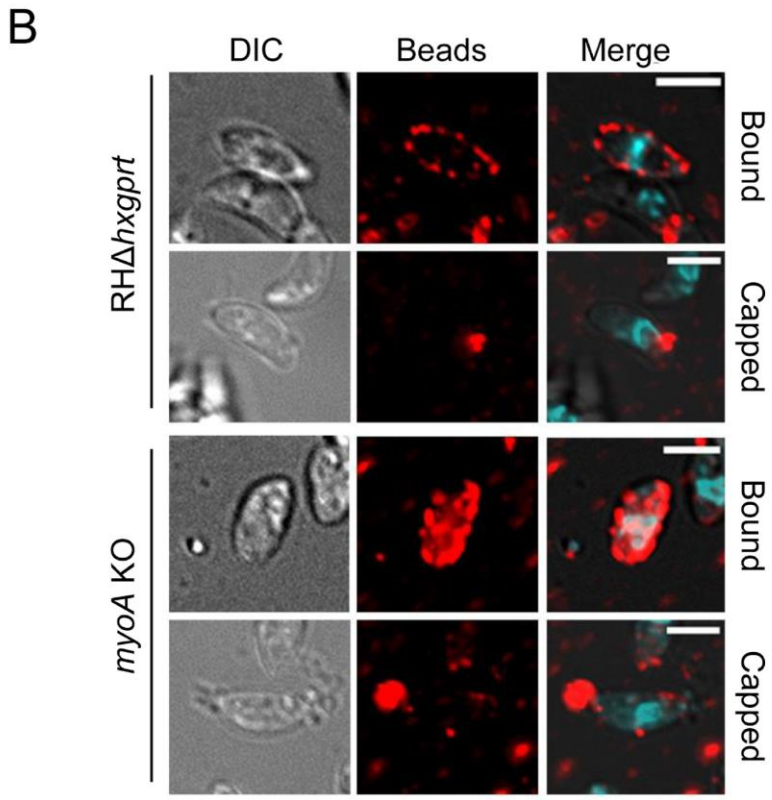
B
DIC
Beads
Merge
RHΔhxgprt
myoA KO
Bound
Capped
Bound
Capped

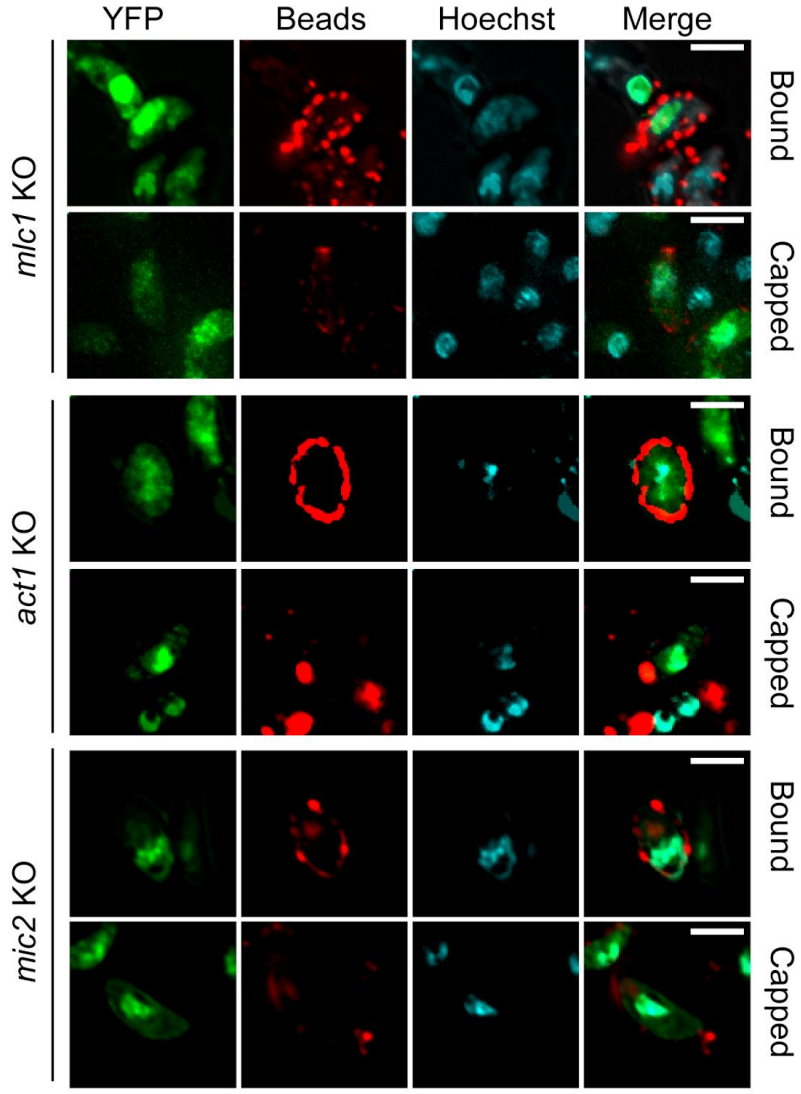

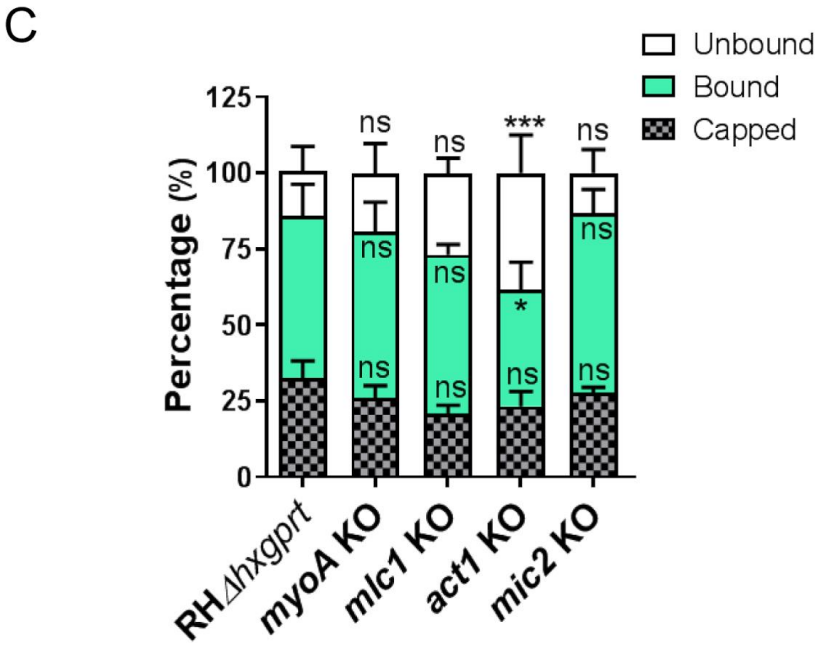

Figure 6-2. Retrograde flow was analysed in the acto-MyoA motor complex knockouts using a bead translocation assay

A. Interaction of parasites with microbeads was analysed after 10 minutes of incubation. Fixed samples were used to analyse microbead translocation. Here, three conditions were considered: Unbound - no beads observed at the parasite surface (left panel), Bound - beads surround parasite surface (middle panel), Capped - beads signal is polarised to the end of the parasite (right panel). **B.** acto-MyoA motor complex KOs can translocate microbeads to the rear. Representative images show RHΔ*hxgprt* and knockout parasites binding and capping microbeads. **C.** Graphic depicts the binding and capping capacity of the acto-MyoA motor complex KOs. The percentage of microbeads capping in the knockout lines presented no significant differences when compared to RHΔ*hxgprt*. Two-way ANOVA followed by Dunnett's multiple test was used to compare knockout lines to RHΔ*hxgprt*. *** P≤0.001, * P≤ 0.05, not significant (ns) P>0.05. Figure modified from (Whitelaw et al., 2017) under Creative Commons Attribution 4.0 International License.

As described above, amoeboid motility requires low levels of cell-substrate attachment indicating that integrin-independent mechanisms drive motility (Friedl and Wolf, 2003). This type of migration is characterised by cycles of extension and retraction of the cell. This cycle is suggested to be driven by actin polymerisation at the leading edge or by a balanced endocytic/exocytic membrane flow (Friedl et al., 2001, Lämmermann and Sixt, 2009, Barry and Bretscher, 2010, Bretscher, 2014). The first option proposes that actin polymerisation in the leading edge pushes the cell forward, and force is transmitted to the trailing edge by the tension generated in the membrane resulting from the changes in cell length (Copos et al., 2017). The exo/endocytic membrane flow hypothesis proposes that cell migration can occur by constant circulation of membrane lipids and proteins. The internalised membrane returns to the leading edge adding "new" surface, so it does not depend on strong cell-substrate adhesion (Bretscher, 1996, Bretscher, 2014).

In *T. gondii,* early studies suggested the general importance of micronemal protein exocytosis and its impact on gliding motility. Here, extracellular parasites incubated with high potassium buffer (endo buffer) or the Ca^{++} chelator (BAPTA-AM), both of which abolish microneme secretion, were blocked in invasion and motility (Endo and Yagita, 1990, Lovett and Sibley, 2003). These results were consistent with the phenotype observed after treatment of tachyzoites with the actin depolymerisation drug cytochalasin D (CytoD) (Carruthers and Sibley, 1999). Conversely, Ca^{++} mediated MIC protein secretion increased the ability of parasites to attach and move on the substrate (Carruthers et al., 1999, Carruthers and Sibley, 1999, Wetzel et al., 2004). Similarly, biogenesis of micronemes depends on functional dynamin-related protein B (DrpB), and hence it directly impacts the ability of the parasite to secrete MIC proteins from the apical pole. Thus, in shield treated DrpB mutant ($DrpB_{DN}$) parasites, MIC proteins are re-routed to the parasite surface through the constitutive secretory pathway; these parasites show clear gliding, invasion, and host cell egress defects (Breinich et al., 2009). Endocytosis refers to the uptake of proteins and lipids by the cell, which can happen via clathrin-dependant and -independent pathways (Le Roy and Wrana, 2005). However, in apicomplexan parasites the existence of endocytic pathways

is largely unknown. In *T. gondii* evidence of clathrin-mediated endocytosis has not been found (Pieperhoff et al., 2013), and is a matter of further study.

Since we have shown that retrograde flow in the PM of *T. gondii* is not blocked in mutants of the acto-myosin system, we analysed the importance of exocytosis-endocytosis in membrane flow and gliding motility by using the described microbead translocation assay. To test this hypothesis a series of controls involved in these pathways were included (Figure 6-3A). Therefore, we used endo buffer and DrpBDN as controls for exocytosis (MIC secretion) and Pitstop®2 (Abcam) as a control for endocytosis. As MIC secretion and their translocation to the posterior pole are essential for normal substrate attachment and parasite motility, a *bona fide* indication of protein capping, microneme secretion was blocked in RHΔ*hxgprt* using Endo buffer (ENDO et al., 1987, Endo and Yagita, 1990). Additionally, endocytosis was tested by using the commercial compound [30µM] Pitstop®2 (Abcam), which has been shown to inhibit clathrin-dependent and -independent endocytic pathways (Dutta et al., 2012, Willox et al., 2014). Next, considering that the $DrpB_{DN}$ line inhibits polarised MICs secretion, this mutant was used to study the effect of capping impairment in protein translocation. Of note, since this was a collaborative project, this section contains data obtained by Dr Simon Gras aimed to give a broader vision of the system.

Unlike results obtained with the *mic2* KO, inhibition of all MICs secretion with endo buffer significantly impacted the ability of parasites to bind and cap microbeads (Figure 6-3A/B). These contrasting results can be explained by the potential capacity of microbeads to bind other microneme proteins aside from MIC2. In the complete absence of MIC proteins in the PM, resulting from endo buffer treatment, abrogation of binding and further translocation of these proteins was observed (Figure 6-3 A/B). [30µM] Pitstop®2 treated parasites showed a significantly defect in capping, while the binding percentage is significantly higher compared to the RHΔ*hxgprt* strain (Figure 6-3). Considering the results obtained with [30µM] Pitstop®2, a trail deposition assay was performed using this compound to assess the percentage of moving parasites (gliding rate) (section 4.1.3). As depicted in Figure 6-3C, these parasites showed a significantly decreased gliding rate (2%) similar that observed in parasites treated with endo buffer (5%). Correspondingly, $DrpB_{DN}$ showed an impressive binding capacity, which significantly exceeded that of RHΔ*hxgprt* (Figure 6-3A/B). These results demonstrate that microbeads indeed bind MIC proteins in the PM, and inhibition of polarised protein translocation blocks microbead capping (Figure 6-3A/B).

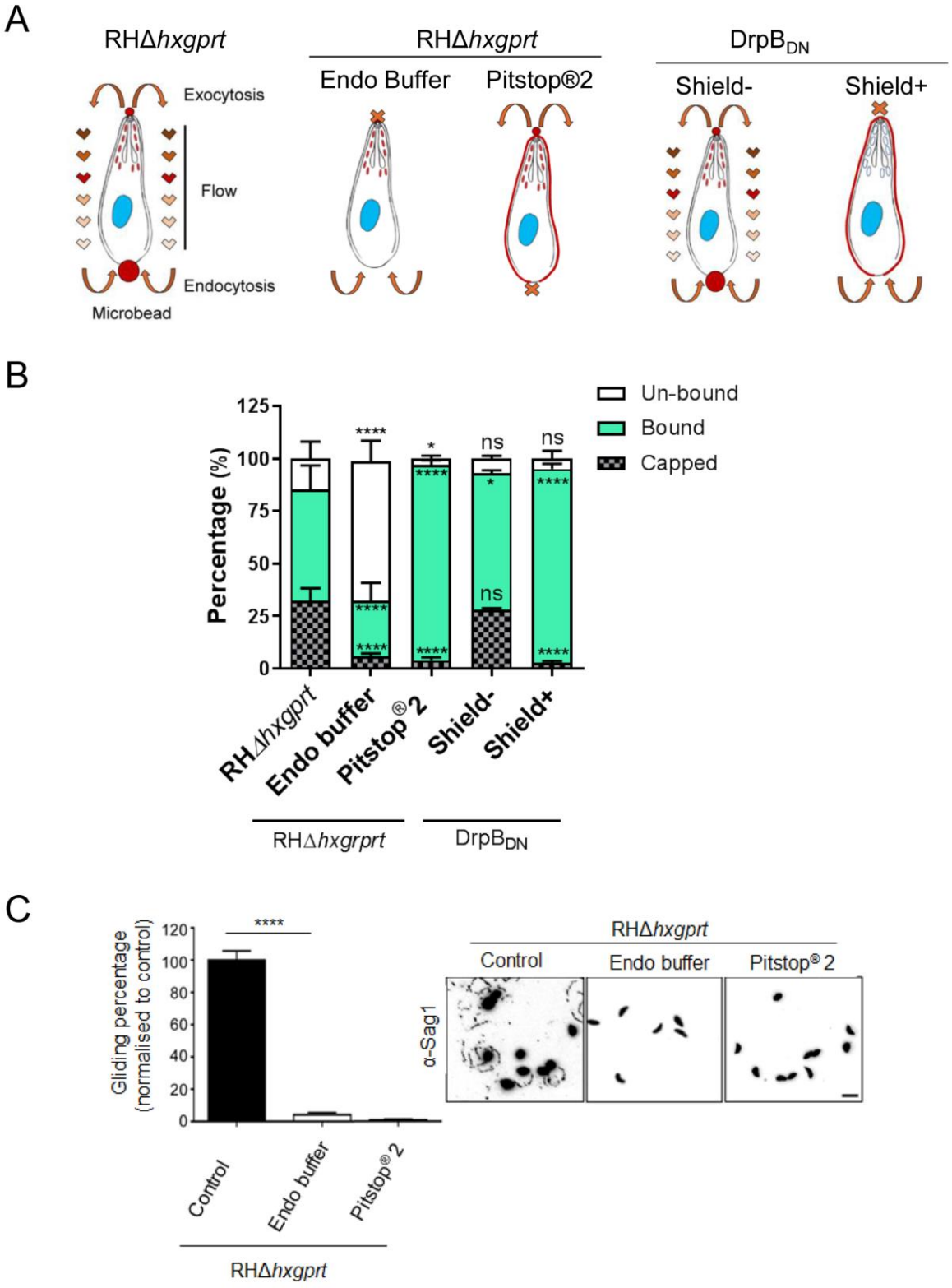

Figure 6-3. Exocytic and endocytic pathways are implicated in retrograde flow maintenance Results obtained by Dr Simon Gras **A.** Schematic of the expected effects of each treatment on the parasite. Figures modified from Dr Simon Gras **B.** Graphic shows binding and translocation capacity of analysed parasites. Parasites treated with endo buffer present a significantly reduced capacity to bind and translocate microbeads. Blocking exocytosis and endocytosis using DrpBDN (+ shield) and Pitstop®2 significantly reduces microbeads translocation, while binding capacity significantly increases. All conditions with treated parasites were statistically compared to RHΔ*hxgprt* using two-way ANOVA followed by Dunnett's multiple test. **** P≤0.0001, * P≤ 0.05, not significant (ns) P>0.05

C. Inhibition of exocytosis and endocytosis blocks motility. Gliding rates (left panel) and trail deposition assay (right panel) of RHΔ*hxgprt*, endo buffer and Pitstop®2 treated parasites show a significantly defect in motility. Graphic displays mean ± SD obtained from three independent replicates. Means were compared using two-tailed Student's t-test. **** P≤0.0001. Scale bar represents 10 µm.

Taken together these results show that retrograde flow can be established in the absence of ACT1, MyoA, MLC1, MIC1, as no statistical differences were found in capping capacity. Consistent with data obtained in *Plasmodium* parasites treated with CytoD (Quadt et al., 2016), the *act1* KO did not show a significant reduction in microbead capping. Instead, these parasites show decreased microbead-binding ability, possibly due to the strong attachment phenotype these parasites exhibit, which we predict is due to the reduced formation of attachment points (Quadt et al., 2016, Whitelaw et al., 2017). In the case of the *mic2* KO, no difference was found in capping or microbead-binding capacity. This result suggests microbeads may be interacting with other proteins, including other MIC proteins, at the tachyzoite plasma membrane; this idea is plausible as a plethora of microneme and surface antigen proteins are present in the PM of extracellular parasites. Similar results were obtained in previous studies testing the capacity of TRAP-like protein (TLP) to translocate microbeads: wild-type and TLP lacking parasites could achieve comparable bead-binding and translocation rates (Quadt et al., 2016).

Additionally, we have employed microbeads capping to study the effect of different exocytosis and endocytosis inhibitors in retrograde flow in *T. gondii* tachyzoites. Here, we have shown that microbeads can bind MIC proteins at the surface of the parasites; thus, inhibition of apical secretion of MIC proteins results in a significantly capping defect as shown in the case of endo buffer and shield-induced $DrpB_{DN}$. Similarly, we have observed that [30µM] Pitstop®2 increased the ability of parasites to bind microbeads, but dramatically inhibited their translocation to the rear, and reduced the ability of the treated parasite to glide.

These examples together show a potential role of exocytosis and endocytosis in generation and maintenance of membrane flow and gliding motility. Here, we suggest that polarised protein secretion and further protein-lipid uptake inhibition produced the arrest of proteins and lipids in the PM. This is evident from the high percentage of bound microbeads but low translocation capacity. Resulting from this "protein arrest" and PM protein and lipid circulation blockage, parasites strongly attach to the substrate and have diminished ability to glide. While these results show the first evidence of a potential function for exo/endocytosis in retrograde flow maintenance and motility, this study need further revision. For example, Pitstop®2 was shown to block not only clathrin-dependent (Dutta et al., 2012), but also

clathrin-independent processes (Willox et al., 2014). As it lacks specificity, validation of these results using other uptake inhibitors or markers is suggested. In addition, since this is the first study using Pitstop® in *T. gondii* as an inhibitor drug, other endocytosis controls are suggested to confirm these results, because potential side effects could be affecting the phenotype reported here. In a similar scenario, endo buffer not only blocks MIC secretion, but can also interfere in other secretion processes, membrane potential, ion channel transport, etc. (ENDO et al., 1987, Endo and Yagita, 1990). Taken together, these preliminary results highlight the potential role of exocytosis and endocytosis in the maintenance of retrograde flow and possibly production of force for gliding in *T. gondii* tachyzoites.

6.3 Summary and conclusions

This chapter was focused analysing the roles of the acto-MyoA motor complex. Considering the relationship between the acto-MyoA motor complex and polarised distribution of MIC proteins, we studied the ability of these parasites to remain attached to a substrate under different flow conditions. While all acto-MyoA mutant parasites remained motile (Andenmatten et al., 2013, Egarter et al., 2014, Whitelaw et al., 2017), their capacity to attach under flow differed. Here, *act1* and *mlc1* KO parasites showed a weak retention capacity, indicating these mutants were unable to attach to the surface even under low flow rate. Both mutants showed motility kinetics comparable to RHΔ*hxgprt* in 2D and 3D assays. In a similar trend, MIC2 depleted parasites showed a weak retention capacity under flow conditions, but no difference in circular motility kinetics when compared to control parasites (Gras et al., 2017). Finally, *myoA* KO mutants showed a remarkable capacity to attach to the substrate, even at high flow rates, like RHΔ*hxgprt*. However, this capacity seems far from "normal" because MyoA null parasites showed a characteristic "stop and go" like circular motility, which was reflected by slow gliding speed in 2D and 3D assays (section 5.1.3.2) (Egarter et al., 2014, Whitelaw et al., 2017). The linear correlation between adhesion site dynamics and speed observed in *P. berghei* sporozoites confirmed there was an association between adhesion and speed, suggesting MyoA, together with other signalling proteins, could participate in adhesion of the parasite to the substrate (Münter et al., 2009). Under this premise, the strong attachment defect observed in gliding *myoA* KO parasites could correspond to a defect in the regulation of attachment sites that cannot be recovered by MyoC (section 5.1.3.2, Table 4-1) (Egarter et al., 2014, Whitelaw et al., 2017). On the other hand, the weak attachment observed in *mlc1* and *act1* KOs could produce gliding speeds comparable to RHΔ*hxgprt* (section 3.1.6/4.1.3, Table 4-1; Table 6-1) (Whitelaw et al., 2017). Therefore, the small percentage of parasites moving and the short trails produced could

correspond to the inability of parasites to engage the substrate. These results show a clear correlation between migration and adhesiveness, a principle of motility that has been shown in other systems (Palecek et al., 1997, Hood and Cheresh, 2002, Kim and Wirtz, 2013). Altogether these data suggest that the acto-MyoA motor complex is participating in host cell attachment.

Additionally, we investigated the principle of the linear motor model that suggests gliding motility is powered by the acto-MyoA motor complex by driving polarised migration of secreted proteins from the apical to the posterior end of the parasite. Under this premise, a bead translocation assay (King, 1988) was employed to analyse the mutants of the acto-MyoA motor complex. All mutants of the acto-MyoA motor complex could translocate the microbeads through the PM to the rear of the parasite. Hence, we demonstrated that mutants of the acto-MyoA motor complex can produce force to move, invade, and establish retrograde flow (Andenmatten et al., 2013, Egarter et al., 2014, Whitelaw et al., 2017), but these conclusions have not led to a complete understanding of how *T. gondii* tachyzoite motility is generated and maintained. Previous studies have shown that a proteic surrounding substrate is not a prerequisite for other organisms to move forward (Barry and Bretscher, 2010), and hypothesised that motility can be powered by polarised secretion and later uptake of proteins and lipids in the PM, resulting in a constant flow on the cell surface (Bretscher, 1996, Bretscher, 2014). Also, the remarkable ability of microbeads to move in a helical path over *T. gondii* tachyzoites (Stadler et al., 2017) can be indicative of the dynamism and fluidity of the PM in "low-adhesion" points. Additionally, the fact that retrograde flow has been suggested to participate in force production in *P. berghei* sporozoites (Quadt et al., 2016) makes plausible the idea that exo/endocytic pathways can generate and maintain retrograde flow, consequently driving motility in *T. gondii* tachyzoites. For this reason, to gain further understanding of the motility system in *T. gondii* tachyzoites, we analysed this hypothesis by determining whether retrograde flow was affected if exo or endocytosis was blocked. Here, when polarised microneme secretion using endo buffer or $DrpB_{DN}$ was blocked (Endo and Yagita, 1990, Breinich et al., 2009), translocation of the microbeads significantly decreased. Similar results were obtained when using the endocytosis inhibitor Pitstop®2 (Dutta et al., 2012) which, also blocked motility. Recent studies analysed the force generated at the parasite's PM using microbeads in a laser trap (Stadler et al., 2017). MIC secretion, induced with Ca^{++} Ionophore (Carruthers and Sibley, 1999), was shown to increase the capping ability and force applied to pull the bead, which was almost double the strength (3.7±0.3pN) compared to untreated parasites (1.9±0.2 pN) (Stadler et al., 2017). These results may be due to the rapid establishment of retrograde flow in response to fast

apical secretion and a great amount of adhesins translocating to the posterior end, contrary to the capping capacity observed when endocytosis is blocked with endo buffer or $DrpB_{DN}$ mutants. Additionally, the apolar phase, an initial period characterised by randomly directed motion, that was reported to precede microbeads translocation in untreated parasites was not observed in Ca^{++} Ionophore treated parasites (Stadler et al., 2017). These results were suggested to correspond to the time until the molecular motor and tracks are assembled (Stadler et al., 2017). However, this could partly correspond to the conditions of the experiment. For instance, these experiments were performed at 24°C temperature, 13°C lower than standard *T. gondii* tachyzoite culture conditions (37°C). Since secretion of MICs is an active process, this detail could slow down the MICs polar secretion and therefore the flow at the PM. The absence of this "apolar" phase in Ca^{++} Ionophore treated parasites may correspond to rapid MIC discharge, which established retrograde flow.

Taken together, our data provide the first suggestion that the acto-myoA motor complex primarily participates in substrate attachment. Moreover, our results suggest that polarised secretion of proteins and further endocytic pathways are necessary to establish retrograde flow in the PM of the parasite, and potentially generate the force necessary to move. Here, while retrograde flow generates the force, the acto-MyoA motor complex would establish the traction or "grip" to move on the substrate (revisited in section 7.3).

7 General discussion and outlook

7.1 Proposed mechanisms recovering functions upon acto-MyoA motor complex components depletion

7.1.1 Functional redundancies among components of the machinery

As disruption of the gliding machinery did not block motility and invasion, legitimate questions were raised about alternative mechanisms to drive these essential steps in the lytic cycle. For instance, it was suggested that redundant proteins may compensate for these processes upon removal of the surface adhesins AMA1 and MIC2, since a plethora of MICs are present in the parasite (Andenmatten et al., 2013, Bargieri et al., 2013, Meissner et al., 2013, Frenal and Soldati-Favre, 2015). Indeed, two orthologues of AMA1 (AMA2 and 3) were suggested to compensate for the loss of AMA1 in the *ama1* KO. In fact, AMA2 was shown to interact to RON2 in the TJ, and to increase its expression in transcript level upon AMA1 removal (Lamarque et al., 2014, Parker et al., 2016). Remarkably, removal of ROM1,4 and 5 -responsible of processing adhesins at TJ- produced an accumulation of MIC2 and AMA1 in the PM; nevertheless, these parasites were still able to invade (Shen et al., 2014b).

A similar scenario was proposed for MyoA given the similarities it shares with MyoC, another class XIVa myosin expressed in *T. gondii* tachyzoites, which, together with MLC1, is part of a posterior motor complex (Egarter et al., 2014, Frenal et al., 2014). Thus, it was suggested that the residual motility and invasiveness exhibited in the *myoA* KO were due to functional compensation by MyoC interacting with the available MLC1 in the periphery (Egarter et al., 2014, Frenal et al., 2014). Indeed, overexpression of MyoC, under either p5RT70 or pMyoC, in the *myoA* KO targets MyoC to the periphery in dividing vacuoles and extracellular parasites. However, with endogenously tagged MyoC, the location of this protein is limited to the posterior pole, while in extracellular parasites a stronger signal is observed in the periphery mostly focused in the apical and posterior poles of the parasite. Moreover, *myoA* KO mutants overexpressing MyoC (under p5RT70 and pMyoC) grew faster in plaque assays, although never reaching RHΔ*hxgprt* growth rate; conversely, endogenous tagged MyoC mutants showed growth inhibition, comparable to the *myoA* KO itself. Together, these results suggest that MyoC can take over MyoA functions in its absence, but this depends on the level of expression of MyoC. MyoC redundancy with

MyoA was further demonstrated by parasites simultaneously lacking MyoA, B, and C (triple KO); these parasites showed an inability to complete the lytic cycle due to an egress defect but remained motile and invasive (Egarter et al., 2014, Frenal et al., 2014). Similarly, conditional disruption of MLC1 in a *myoB/C* KO (*myoB/C/mlc1* KO) demonstrated that these parasites are unable to form plaques in growth assays, like the triple KO and *mlc1* KO (Egarter et al., 2014, Frenal et al., 2014). A closer look at the gliding motility of the *myoB/C/mlc1* KO showed these parasites can move in helical and circular fashion at comparable rates as the *mlc1* KO. Again, in terms of speed and distance, *myoB/C/mlc1* KO glided faster and for longer periods than parasites only depleted for MyoA. Although the gliding rate increases when MyoC is overexpressed in the *myoA* KO, average speed and distance remain unchanged, and these parasites present aberrant corkscrew-like trails in 3D motility assays.

Altogether, these results showed that peripherally located MyoC can recover for MyoA functions in the *myoA* KO parasites in terms of gliding rates, but not kinetics. Curiously, depletion of MyoC seemed to enhance motility rather than produce a detrimental gliding phenotype. Due to its particular degenerated neck domain and short tail domain (Heintzelman and Schwartzman, 1997), MyoA needs to be accompanied by two light chains, MLC1 and -either- ELC1 or 2, to properly function (Bookwalter et al., 2014, Williams et al., 2015, Bookwalter et al., 2017). Together these proteins constitute a conventional lever arm, which amplifies the MyoA step, thus moving actin at fast speeds (Bookwalter et al., 2014, Bookwalter et al., 2017). The association of the light chains to the myosin heavy chain can change motility *in vitro*, but not the dynamics of acto-myosin interaction since this feature is mediated by the MyoA head domain (Bookwalter et al., 2014). Consequently, while MyoA and MyoC contain conserved head domains (Foth et al., 2006), the interactions with actin could differ by phosphorylation dynamics. Similarly, the association of these myosins with the light chains may produce different step sizes; thus, producing changes in overall motility. Under this premise, co-immunoprecipitation studies suggested that MyoC interacts with MLC1 and ELC1 in the posterior pole (Frenal et al., 2014); however, these proteins were precipitated under overexpression conditions, which might cause artificial interactions. In fact, later studies showed ELC1/2 are specific for MyoA, since MyoA depletion both ELCs were relocalised from the periphery to the cytosol (Williams et al., 2015). Similarly, MyoC and MLC1 showed to interact when overexpressed; nevertheless, these results might be taken cautiously since endogenous tagged MyoC in RHΔ*hxgprt* parasites did not show overlapping signal with MLC1 in the posterior pole.

Theoretically, If the characteristics of the MyoC head domain are identical to those in MyoA, the MLC1-MyoC complex could support motility in the *myoA* KO, but the speed actin is moved may be reduced in absence of the ELCs in the periphery, thus causing aberrant motility. To clarify why i) MyoC overexpression produces abnormal motility, and ii) MyoC depletion shows improved gliding kinetics in the *myoA* KO, more information about acto-MyoC interactions, and MyoC lever arm stabilisation and function are needed.

Although the *myoB/C/mlc1* KO exhibited improved gliding kinetics compared to the *myoA* KO, the associated egress defect revealed that MyoC shares function for certain cellular processes with MyoA. In support of this observation, overexpressed MyoC -under p5RT70 or pMyoC- showed a significant increase in the ability to disrupt the cell when compared to *myoA* KO or *myoA* KO with endogenously tagged MyoC. Similarly, depletion of MyoA resulted in an attachment/reorientation and a penetration delay; parasites remained attached to the host-cell PM and penetrated in a "stop and go" motion (Egarter et al., 2014). Overexpression of MyoC recovered for the attachment/reorientation phenotype, suggesting again a redundant function between these myosins. However, to this end, it cannot be discarded that the host cell membrane has a potential role in facilitating the invasion process of these mutants as reported in the *myoA* KO (Bichet et al., 2016).

These data support the idea that MyoA and MyoC could exhibit overlapping functions, which are only evident after MyoA depletion. Furthermore, growth, invasion, motility, and egress rates were all improved under expression of a second copy of -p5RT70 or pMyoC- MyoC, but not in the endogenously tagged MyoC *myoA* KO. This indicates that recovery depends on i) increased expression of MyoC and ii) availability of MLC1 to target MyoC to the pellicle. Nonetheless, *myoA* KO mutants do not show increased levels of MyoC in either the freshly isolated mutant or long term cultured line, contrary to what is currently suggested (Frenal et al., 2017a). Similarly, neither the *mlc1* nor the *myoB/C/mlc1* KO exhibited MyoC or MyoA located in the periphery.

Finally, the presence of a large repertoire of myosin heavy chains and MLCs in *T. gondii* makes it plausible that other complexes (e.g. MLC2-MyoD) recover for the loss of both MyoA-MLC1 and MyoC-MLC1. However, this model doesn't explain how the *gap45* and *act1* KOs move, as their absence has a direct impact on motor complex location and myosin function, respectively.

7.1.2 Host cell contribution during penetration

To enter the host cell, acto-MyoA motor complex mutants employ a canonical TJ (Andenmatten et al., 2013, Egarter et al., 2014). Depletion of GAP45 had a major effect on invasion rates, which may correspond to the round morphology observed in these mutants (Egarter et al., 2014). Like gliding, *myoA* KO parasites presented a slow "stop and go" motion while penetrating the host cell, again indicating an attachment defect (Egarter et al., 2014). ACT1 and MLC1 depleted parasites enter the host cell at variable speeds, but again presented enhanced invasion kinetics when compared to the *myoA* KO mutant (Whitelaw et al., 2017). As apicomplexan zoites contain their own machinery to glide and invade, the contribution of the host cell during penetration remains to be studied in detail (Tardieux and Baum, 2016). Some evidence exists to suggest that the host cell is far from passive during *Plasmodium* (Dasgupta et al., 2014, Koch and Baum, 2016) and *T. gondii* zoite penetration (Meissner et al., 2013, Bichet et al., 2014, Bichet et al., 2016). Host cell projections extend over wild-type tachyzoites during invasion, although this is not observed in all penetration events, which may be due to the fast speed of this process (Meissner et al., 2013, Bichet et al., 2014). Bichet and colleagues showed that host-cell PM protrusions are central for penetration of *myoA* KO parasites (Bichet et al., 2016). These host-cell PM protrusions "wrap" the *myoA* KO mutant, and apply forces that enhance penetration via the TJ, allowing the *myoA* KO to enter the host cell cytosol (Bichet et al., 2014). These results indicate that the host cell partially contributes to the force required to drive invasion in the *myoA* KO mutant; thus, it cannot be discarded that the same process may enhance host cell penetration in the *act1* and *mlc1* KOs as well. Another recent study has demonstrated that the RON complex, injected into the host cell, indirectly associates to the host cell cytoskeleton by recruiting adaptor proteins in the TJ. This recruitment would provide the parasite with a substantial anchor during penetration (Guérin et al., 2017), and might reduce the energy that parasites employ for this process. In fact, these host-cell mediated processes are interesting observations that should be addressed in deeper detail to study if the overall process differs, not only among acto-MyoA motor mutants, but among secretory organelle mutants as well.

Taken together, these results explain how gliding and invasion could be uncoupled; however, the understanding of this mechanism is in the early stages and further studies will extend our knowledge about host cell contribution.

7.2 Updated functions of the acto-MyoA motor complex

The characterisation of the conditional knockouts of the acto-MyoA motor complex components gave insights into new elements and put under consideration the functions attributed by the linear motor model (Andenmatten et al., 2013, Bargieri et al., 2013, Mueller et al., 2013, Egarter et al., 2014, Shen and Sibley, 2014, Bichet et al., 2016, Harding et al., 2016, Jacot et al., 2016b, Gras et al., 2017). For instance, depletion of GAP40 and GAP50 resulted in a dramatic collapse of the IMC, and caused a detrimental defect during IMC biogenesis in dividing parasites, which impeded the analysis of extracellular tachyzoites (Harding et al., 2016). On the other hand, the rest of the acto-MyoA motor complex mutants could glide and invade; however, *act1*, *mlc1*, and *gap45* KOs were not viable in culture due to an egress phenotype (Andenmatten et al., 2013, Egarter et al., 2014).

7.2.1 Acto-myosin dependent organelle transport

Considering the vital importance of the processes driven by the acto-MyoA motor complex, it was proposed that remaining protein present in the conditional mutants after depletion could drive the remaining invasion and gliding rates (Drewry and Sibley, 2015). In fact, excision of a specific gene does not guarantee protein function loss since small amounts of the protein can maintain remnants of the function, especially in a non-clonal line (Meissner et al., 2013, Frenal and Soldati-Favre, 2015). In this scenario, it was suggested that the ACT1 polymerisation mechanism does not depend on a critical concentration of G-actin, as canonical actins do, but it rather polymerises in a isodesmic manner (Skillman et al., 2013). Isodesmic polymerisation proposes that there is no minimal G-actin concentration; thus, actin dimers, trimers or polymers can be formed at any given concentration of actin (Skillman et al., 2013). Consequently, it was suggested that small amounts of ACT1 present in the *act1* KO were enough to form filaments, and drive remaining invasion and motility (Drewry and Sibley, 2015). These observations were recently challenged by a study demonstrating that ACT1 polymerisation depends on a critical concentration of G-actin, and has elongation and treadmilling rates similar to canonical actins (Kumpula et al., 2017). Thus, the isodesmic polymerisation hypothesis should no longer be considered in future models of actin dynamics in Apicomplexa.

This study was supported by the fact that depletion of the acto-MyoA motor complex affected other parasite functions. For instance, depletion of ACT1 produced a dramatic defect in dense granule directed motion and apicoplast inheritance leading to a delayed death

phenotype; thus, confirming that this process is acto-MyoF dependent (Fichera and Roos, 1997, Andenmatten et al., 2013, Jacot et al., 2013, Heaslip et al., 2016). On the contrary, even though MLC1 was shown to interact with different myosins -MyoA, MyoC, and MyoH- (Herm-Gotz et al., 2002, Egarter et al., 2014, Frenal et al., 2014, Graindorge et al., 2016), no phenotype in terms of replication and apicoplast segregation was observed in *mlc1* KO parasites. This indicates that if MyoF and MLC1 interact, this contact is not essential for apicoplast inheritance.

7.2.2 Assembly and association of the acto-MyoA motor complex

The association among the components of the motor complex is affected upon removal of anchorage elements such as MLC1 and GAP45 (Egarter et al., 2014). MLC1 and MyoA are lost in the conditional *mlc1* KO line 48 hours post induction; thus, absence of MLC1 drives MyoA relocation and, probably, degradation as observed in *Plasmodium* MTIP-MyoA (Sebastian et al., 2012, Egarter et al., 2014). Similarly, depletion of GAP45 results in the mislocation of MLC1 and MyoA to the cytosol of parasites (Egarter et al., 2014). Therefore, MyoA associated ELCs (ELC1/2) are also mislocalised since their peripheral distribution depends solely on MyoA presence (Nebl et al., 2011, Williams et al., 2015). These results confirm previous studies which suggested that i) MLC1 is indispensable for MyoA anchorage to the GAP proteins and ii) GAP45 is central for assembly of the motor complex because it spans the space between the PM and the IMC, and targets MyoA to the periphery via MLC1 (Hettmann et al., 2000, Herm-Gotz et al., 2002, Gaskins et al., 2004, Frenal et al., 2010).

7.2.3 Cell-cell communication among daughter cells

Periz and colleagues recently established Cb-based technology for actin visualisation, and showed that individual daughter cells remain connected during division by a filamentous structure that resides in the RB (Periz et al., 2017). This network is suggested to support acto-MyoI and J functions associated to maintain synchronicity, connection and PV organisation during division (Frenal et al., 2017b, Periz et al., 2017). Expectedly, the filamentous Cb-actin signal is affected when using actin drug inhibitors and in *act1* KO mutants as soon as 24 hours post induction (Periz et al., 2017).

Given the unusual dynamics of apicomplexan ACT1, it was suggested that MyoA might induce ACT1 filament formation, acting like a limiting factor to drive motility just

upon acto-MyoA contact (Schüler and Matuschewski, 2006b, Stadler et al., 2017). Here, depletion of MyoA and MLC1 presented similar ACT1 structures in the residual body, periphery, and cytosol of the parasite as in RHΔ*hxgprt.* While these results are preliminary, it sets a precedent for further work to explore this in deeper detail. Although the Cb-actin signal in the mutant parasites does not show strong differences when compare to control parasites, actin dynamics could be affected by the lack of MyoA-MLC1 in the periphery.

7.2.4 The acto-MyoA motor complex is necessary for substrate attachment

The linear motor model proposes that the acto-MyoA motor complex drives gliding motility by actively translocating adhesins (e.g. MIC2) from apical to posterior pole; thus, this rearward migration would produce forward motion at the same speed as MIC translocation (King, 1988, Keeley and Soldati, 2004, Heintzelman, 2015, Frenal et al., 2017a). Nevertheless, parasites lacking its key components are all able to move, albeit at variable speeds and in reduced numbers (Andenmatten et al., 2013, Egarter et al., 2014).

Trail deposition assays showed that *myoA* and *mlc1* KOs move exclusively in a circular manner (Andenmatten et al., 2013, Egarter et al., 2014). A closer look at 2D gliding kinetics showed that *mlc1* KO mutants can move not only in a circular, but also in a helical, manner and did not present "stop and go"-like movement as reported for the *myoA* KO. The helical paths travelled yield shorter trails and slower speeds when compared to RHΔ*hxgprt*, while circular trails are as long as control parasites and with an enhanced speed when compared to *myoA* KO parasites. Similarly, *gap45* and *act1* KOs showed longer and faster gliding kinetics when compared to the *myoA* KO (Egarter et al., 2014, Whitelaw et al., 2017).

In 3D Matrigel motility assays, all mutants travelled in a typical corkscrew-like pattern reported for both *T. gondii* tachyzoites (Leung et al., 2014) and *Plasmodium* ookinete (Kan et al., 2014). In the case of *myoA* KO parasites, the 2D and 3D kinetics of the trails travelled showed shorter distance and significantly decreased average speed, which could not be recovered by overexpression of MyoC. On the Other hand, *act1* and *mlc1* KOs showed short corkscrew-like trails, but the average speed remained comparable to loxp*act1* and loxp*mlc1*, respectively, albeit at considerably reduced gliding rates (Whitelaw et al., 2017).

In cell motility, the relationship between motion and traction is inversely proportional; therefore, optimal motility is a balance between these two parameters, which

would be regulated according to cell signalling and environment. Indeed, abrogation of motility can happen either by poor adhesion (low traction) or strong attachment (high traction) (DiMilla et al., 1991, Welch, 2015). Cell traction is governed by the variation of adhesin-receptor bond strength and distribution of the focal adhesion points, thus, affecting overall cell motility (DiMilla et al., 1991). Considering the role of the MyoA-motor complex in connecting adhesins (MICs) to the cytoskeleton, it was conceivable to propose its function for attachment. In fact, the different speeds and overall motility fashion observed in these mutants indicated an attachment phenotype. Indeed, under shear conditions, the acto-MyoA motor complex mutants showed different characteristics. For instance, the *myoA* KO retained to the substrate under high flow at comparable levels as RHΔ*hxgprt,* indicating a strong attachment. This could be reflected in the "stop and go" motility observed in 2D environments and reduced speed in both 2D and 3D gliding assays. On the other hand, the relatively enhanced 2D and 3D motility kinetics observed in *mic2*, *mlc1,* and *act1* KOs could be the result of an attachment deficit, since these mutants detached from the substrate under relatively weak flow conditions (Harker et al., 2014, Gras et al., 2017, Whitelaw et al., 2017).

Additionally, depletion of the gliding machinery failed to block translocation of beads along the PM. This was apparent from the fact that *act1*, *myoA*, *mlc1,* and *mic2* KOs could cap beads previously attached to the PM; in fact, the degree of capping of all these mutants are comparable to RHΔ*hxgprt*. Similarly, analysis of motility using high speed microscopy and laser trapped beads in *Plasmodium* sporozoites showed that retrograde flow and regulation of attachment sites are directly implicated in efficient motility (Quadt et al., 2016). Even though addition of CytoD decreased force and motility rate, retrograde flow was not blocked (Quadt et al., 2016). A similar study was developed in *T. gondii* and showed that polar translocation of proteins in tachyzoites is preceded by an apolar phase of random movement. Addition of CytoD (200nM) affected the force applied to the bead and the speed of capping (Stadler et al., 2017). Still, CytoD decreases the ability of parasites to bind the bead, but translocation was still evident upon addition of 500 nM CytoD (Whitelaw et al., 2017). These results can be explained by i) the production of less overall force or ii) the beads not binding efficiently to the parasite's PM, thus decreasing force transmission. In addition, it was observed that the migration of the microbead in the polar phase was not always constant and directional, but showed pauses and reversals and capped at an average speed of 0.03 µm/s (Stadler et al., 2017). *Plasmodium* sporozoites did not show an apolar and polar phase as suggested for tachyzoites, but pulled the bead out of the trap shortly after first contact. In these parasites, translocation of the bead was directional and presented some speed variations while migrating but reached average speeds of 6 µm/s (Quadt et al., 2016).

To conclude, microbeads translocation in *T. gondii* tachyzoites was done at room temperature [24ºC] (Stadler et al., 2017); however, since flow is an active process, a change of temperature could have affected the translocation kinetics. For this reason, it would be recommended to work at 37ºC (standard culture temperature) to study this mechanism. Finally, considering that the acto-MyoA mutants can all cap beads, but present great differences in attachment, it would be interesting to characterise the process of translocation in these parasites.

7.2.5 Egress depends on a functional acto-MyoA motor complex

Acto-MyoA motor complex mutants remained invasive and motile in around 20% of the population, yet in *act1*, *mlc1*, and *gap45* KOs egress was severely affected since <4% can egress (Andenmatten et al., 2013, Egarter et al., 2014). The fact that the *mlc1* KO could be kept in culture for up to 6 weeks by enriching the mutant population and bypassing egress indicates that the main limitation of this mutant line is based on its ability to egress. Compared to the *mlc1* KO, *act1*, *gap40*, *gap45,* and *gap 50* KOs present detrimental phenotypes associated with apicoplast and dense granule maintenance, morphological defects, and IMC biogenesis and stabilisation, respectively, which limited their *in vitro* survival (Andenmatten et al., 2013, Egarter et al., 2014, Harding et al., 2016, Whitelaw et al., 2017). A study of *mlc1* KO egress showed that the majority of these parasites remained internalised even upon Ca^{++} induction, supporting previous observations (Egarter et al., 2014).

Following 10 minutes of Ca^{++} mediated egress, virtually all RHΔ*hxgprt* parasites disrupted the host cells; in contrast, 4% of *mlc1* KO parasites egressed, whereas 70% *mlc1* KO could permeabilise the PV but remained intracellular. A closer examination of this process indicated that these mutants respond to Ca^{++} ionophore (A23187) treatment by changing morphology, and disrupting organization of the vacuole, but further apparent motility, PV and host cell disruption is not evident. Besides, non-egressed *mlc1* KO vacuoles became immobile inside the PV might be due the physical confinement; however, sporadic discrete egress of individual parasites could be observed. Together, these results demonstrated that MLC1 mutants fail to exit perforated PVs, likely due to lack of mechanical force to rupture the membranes surrounding them.

Discussions focused on egress phenotypes observed in acto-MyoA motor complex mutants suggested that the correct assembly of these proteins may act as a checkpoint, such

that only parasites able to invade could egress (Boucher and Bosch, 2015). As with host cell invasion, host cell egress is a multistep process in which PV and host cell perforation is initiated by internal Ca^{++} signalling, followed by MIC secretion and motility to provide mechanical rupture of the PV and host cell (Kafsack et al., 2009, Blackman and Carruthers, 2013, Frenal et al., 2017a). Ca^{++} signalling plays an important role during egress; consequently, the presence of CDPKs may regulate egress by modulating MIC secretion, phosphorylating the motor complex proteins, and even supressing Ca^{++}dependent egress (Arrizabalaga and Boothroyd, 2004, Lourido et al., 2012, McCoy et al., 2017). For instance, CDPK3 was suggested to regulate MyoA function, which would make it able to control egress (Gaji et al., 2015). Under this premise, the egress defect observed in MLC1 depleted parasites might be due to the absence of MyoA in the periphery. Additionally, *in vitro* studies suggested MTIP contains two phosphorylatable sites that might modulate MyoA function (Douse et al., 2012). However, these results were not observed in MLC1; thus, from the eight described phosphorylation sites, four were reported to have no critical function in invasion or egress (Jacot et al., 2014). Nonetheless, as not all phosphorylation sites were studied, it cannot be excluded that the remaining ones participate in MyoA function during egress (Jacot et al., 2014), causing a detrimental defect in the *mlc1* KO. In addition, a recent visual report suggests *T. gondii* egress can occur in both a lytic and non-lytic manner (Caldas et al., 2010, Caldas et al., 2017). In fact, individual parasites can egress from the host cell with the host PM resealing behind them while others -single or collective- rupture the PV structure (Caldas et al., 2017). A similar phenomenon was observed in *Plasmodium* sporozoites which are able to egress the cell inside a vesicle collectively or egress the host cell individually in a point of exit (Klug and Frischknecht, 2017). While the specific process driving these different mechanisms of egress are unknown, it would be interesting to study if *mlc1* KO parasites have preference for non-lytic egress; thus, releasing less parasites to the extracellular milieu. To this end, it is clear that the absence of a myosin in the periphery severely affects egress in tachyzoites; interestingly, this phenotype is not observed in *Plasmodium* merozoites lacking ACT1, meaning this process is acto-myosin independent (Das et al., 2017). These results suggest that some processes, previously considered conserved among Apicomplexan parasites, can hold important differences, which should be taken in consideration for future research.

These results together show that the acto-MyoA motor complex depletion impacts different cellular functions that are evident 24-48 hours after induction, meaning no sufficient protein is present in the mutants to fulfil these important roles. However, gliding was still observed in *act1*, *myoA*, *mlc1* and *gap45* KOs after these time points, and in some

cases the kinetics were comparable to control parasites (Andenmatten et al., 2013, Egarter et al., 2014).

7.3 Can acto-myosin independent forces drive motility?

Amoeboid motility broadly studied in *Dictyostelium discodeum* is characterised by fast alternation between expansion and contraction of the cell. This motility has a low affinity for the substrate caused by weak and fast integrin attachment of the cell to the extracellular matrix (Copos et al., 2017). Similar to *D. discodeum*, a plethora of leukocytes and tumour cells display amoeboid motility. For instance, fast gliding in lymphocytes and neutrophils is reported to happen by weak engagement of the cell with the substrate (Friedl and Wolf, 2003). Moreover, a study in *D. discodeum* and neutrophils demonstrated that these cells are able to swim in Ficoll, which creates a viscous and isodense environment, using similar amoeboid motility (Barry and Bretscher, 2010). Although the speed was reduced to one-third of that in normal medium, these experiments highlighted that motility can occur in a substrate-independent manner (Barry and Bretscher, 2010). How these cells can move in an integrin-independent manner can be explained by low adhesion mechanisms such as amoeboid propulsion, cell shape change, cytoplasmic streaming, or endocytic/exocytic membrane flow (Friedl and Wolf, 2003, Barry and Bretscher, 2010, Bretscher, 2014). The latter suggests that motility can be powered by membrane flow at the cell's surface generated by a cycle of exocytosis at the apical end and endocytosis at random spots of the PM towards the posterior end. The spatial separation between exocytic and endocytic sites maintain the antero-posterior flow of lipids and proteins in the membrane (Bretscher, 1996, Bretscher, 2014).

To this end, both membrane flow and gliding can happen in the absence of acto-MyoA motor complex components (section 7.2.4). For this reason, the potential role of microneme secretion and endocytosis for gliding and retrograde flow establishment was studied. Blocking microneme secretion by inducing the expression of mutant DrpB (Breinich et al., 2009) or using endo buffer (Endo and Yagita, 1990) blocked both motility (Breinich et al., 2009, Kafsack et al., 2009) and retrograde flow. While moving, tachyzoites leave behind a trail derived from membrane proteins (Håkansson et al., 1999), but even now it is not known if membranous material is somehow recycled at the posterior pole (Pieperhoff et al., 2013). For this reason, the endocytosis inhibitor, Pitstop®2 (Dutta et al., 2012, Willox et al., 2014), was used to study retrograde flow and gliding rates. Interestingly, both processes were blocked when using the drug. These preliminary results suggest that the establishment

of membrane flow, and therefore, gliding motility might rely on a constant cycle of exocytosis in the apical pole and endocytosis/shedding in the posterior pole; in this view, the acto-MyoA motor complex would participate in attachment site regulation.

7.3.1 Hypothetical model for gliding motility in *T. gondii* tachyzoites

Previous data support the idea that neither gliding motility nor retrograde flow fully depends on the acto-MyoA motor complex. On the contrary, new emerging evidence has shown that other mechanisms can be implicated in the regulation of these processes, replacing the model based solely on a unidirectional acto-MyoA motor complex system (Münter et al., 2009, Bargieri et al., 2014, Egarter et al., 2014, Quadt et al., 2016, Tardieux and Baum, 2016, Gras et al., 2017, Moreau et al., 2017, Whitelaw et al., 2017). Here, a hypothetical model for *T. gondii* tachyzoites gliding motility is presented based on the compilation of data presented in this thesis and other studies.

Retrograde flow in the PM of the parasite is generated by a combination of i) protein secretion at the apical pole and ii) shedding and uptake of proteins in the basal pore. The maintenance of the flow in the PM will depend on the constant circulation of proteins and lipids in a polarised manner. Therefore, this movement would be able to produce the force necessary for motility and invasion (Figure 7-1A); however, retrograde flow, on its own, does not produce the necessary traction. The latter requires the participation of the acto-Myo machinery residing underneath the PM which connects cytoskeletal components to the surface via transmembrane proteins (MICs). Consequently, in this hypothetical model, the acto-MyoA motor complex is proposed to be involved in the regulation of attachment sites, providing the parasite traction or "grip" for gliding. The acto-MyoA motor complex will serve as a "molecular clutch" (Lin et al., 1994) instead of a force generator (Whitelaw et al., 2017). Here, the secreted MIC proteins would play the role of adhesins by indirectly connecting the cytoskeleton of the parasite to the substrate. Under this premise, when ACT1 filaments and MyoA, the "clutch", are engaged, the attachment with the substrate is strengthened in the specific point of contact. On the other hand, when the "clutch" is disengaged, by i) ACT1 filament-MyoA disengagement or ii) ACT1 depolymerisation, the attachment to the substrate is weakened because the attachment sites are released, which would let the adhesive protein flow towards the posterior pole until another "clutch" is reached (Figure 7-1B).

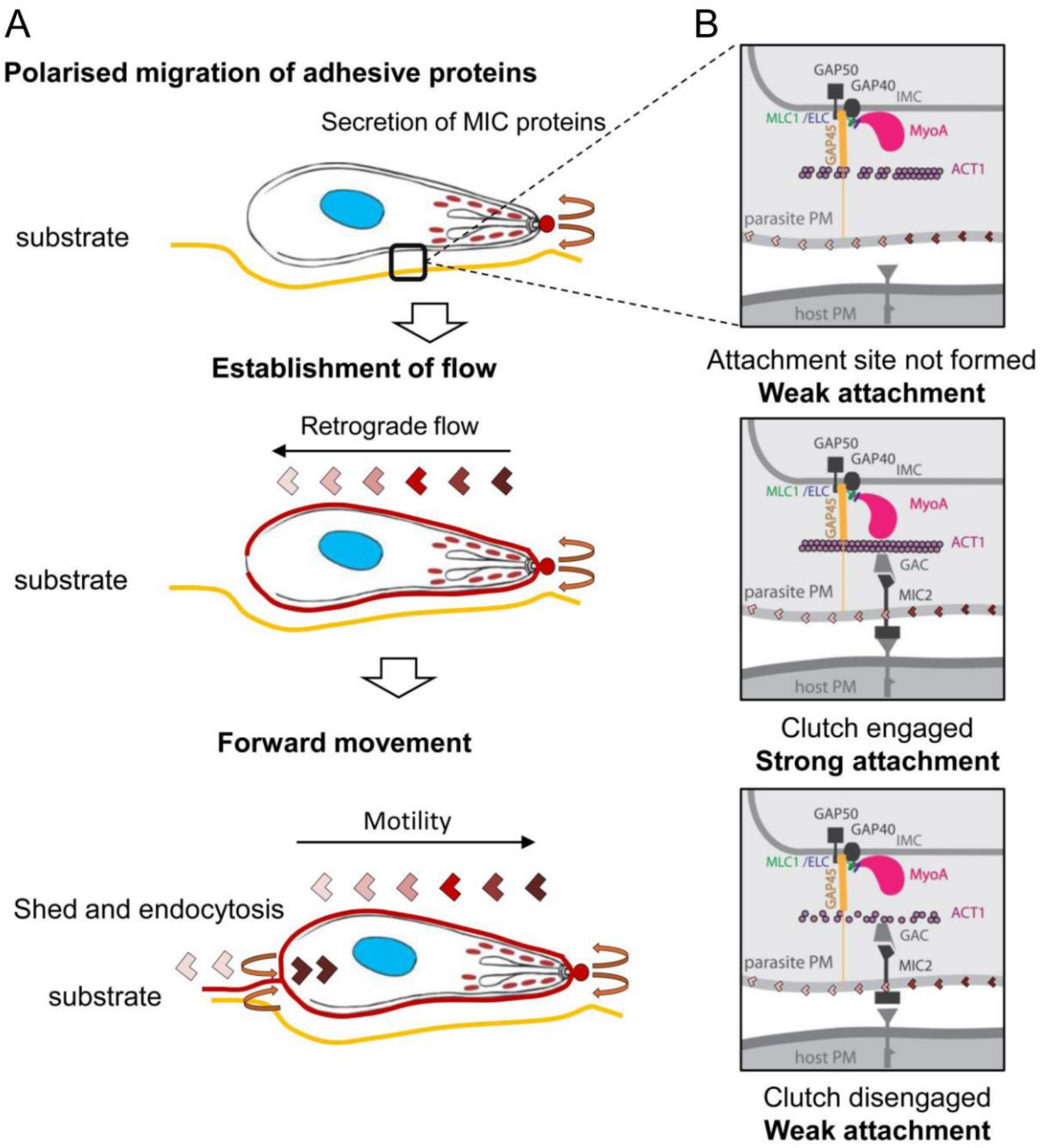

Figure 7-1.Hypothetical model for gliding motility comprising force generation and regulation of attachment sites
A. Schematic representation of retrograde flow in the PM of tachyzoites. Flow is initiated by secretion of MIC proteins into the PM (upper panel). Distribution and polarised translocation of MIC proteins from the apical to the posterior pole establishes flow in the surface (mid panel). Flow in the PM is maintained by constant endocytosis and shedding of lipids and proteins. The force for motility is generated by a continuous cycle of polarised secretion and translocation of proteins, and further uptake and shedding of membrane components **B.** Diagram of the acto-MyoA motor complex actively regulating attachment sites. The proposed model suggests that the acto-MyoA motor complex acts as a molecular clutch. When the clutch is disengaged by lack of interaction between MyoA and ACT1 filaments, it produces a weak attachment to the substrate (upper and bottom panel). When the clutch is engaged by the active interaction between MyoA and ACT1 filaments, the attachment sites are strengthened (mid panel). These two mechanisms together will produce efficient gliding motility by generating force for moving and regulating the strength of attachment to the substrate. Scheme was modified from an original template provided by Dr Simon Gras.

In conclusion, a combination of these data and new evidence emerging in recent years, suggest that apicomplexan gliding motility is more complex than expected, and

comprises several mechanisms that have not been studied in depth before. Here, we propose that, together with the force generated by retrograde flow in the PM, the acto-MyoA motor complex provides traction producing efficient and directed gliding motility. Even though this hypothetical model corresponds to previous suggestions for amoeboid motility (Bretscher, 1996, Bretscher, 2014), many points still need to be studied. For instance, the continuous circulation of proteins and lipids, produced by exo/endocytic pathways, are proposed to partially balance the loss of shed membrane components left behind while gliding. However, little evidence of endocytic pathways in extracellular tachyzoites exists (Pieperhoff et al., 2013). Additionally, as the capping of proteins in the acto-myoA motor complex mutants seems to be comparable to RHΔ*hxgprt* parasites, this translocation, in terms of force employed and speed of transmission, remains to be studied. Moreover, the use of different exocytosis and endocytosis inhibitors and stimulators is expected to give more support to this model. For instance, microneme secretion is largely studied for the release of adhesins to the PM (Boucher and Bosch, 2015), but further studies of the function of exocytosis as a mechanism to maintain retrograde flow are recommended. Since endo buffer does not specifically affects MIC secretion, a good place to start would be using mutant parasites with reduced or blocked MIC discharge. For instance, RNG2 that is an apical complex protein directly implicated in MIC discharge regulation, which depletion showed a marked reduction of microneme and rhoptry proteins discharge; thus, gliding motility abrogation (Katris et al., 2014). Another interesting candidate is AKMT, a methyltransferase, which depletion does not affect secretory organelle discharge or acto-MyoA motor complex overall integrity, but affects motility activation (Heaslip et al., 2011).

Moreover, results presented here suggest that the acto-MyoA motor complex may function as a regulator of attachment sites. Therefore, more research is needed to understand how the attachment sites are regulated and distributed along a motile tachyzoite, as was successfully shown in *Plasmodium* (Münter et al., 2009, Hegge et al., 2012). Finally, in order to prove or discard the suggested motility models (*i.e.* linear or retrograde flow-clutch), future approaches involving biophysics and mathematical models are necessary. Here, it is recommended to further drive a detailed characterisation of the motility phenotypes observed in the acto-MyoA motor complex mutants.

7.4 Final highlights

Given the remarkable ability of the acto-MyoA motor complex mutants to glide and invade (Andenmatten et al., 2013, Egarter et al., 2014), four different explanations were

suggested to explain such phenotypes; these are further discussed below. Firstly, redundancies among myosins were suggested to compensate upon MyoA depletion (Frenal and Soldati-Favre, 2015). In this thesis, it was shown that MyoC can partially recover for MyoA loss, but this depends on the overexpression of the protein; however, no recovery was observed in the *myoA* KO with endogenously tagged MyoC or in the *mlc1* KO. To support this observation, the *myoB/C/mlc1*, *act1*, *mlc1*, and *gap45* KOs showed enhanced gliding kinetics compared to the *myoA* KO, indicating that gliding motility can occur in the absence of a peripherally located myosin (Egarter et al., 2014, Whitelaw et al., 2017). Second, as suggested for the *act1* KO (Drewry and Sibley, 2015), considering the window between induction and characterisation in the mutants that cannot be maintained in culture, the remaining protein could power gliding motility. For this reason, in this thesis, a careful quantification of MLC1 levels showed this protein is indistinguishable from background signal as soon as 48 hours after induction. This result is supported by the relocation of MyoA from the periphery at the same time point, and that egress is affected after the first round of the lytic cycle (36 hours), thus suggesting there is not sufficient protein to support these essential functions; however, gliding motility remains observed in around 28% of the mutants. Even though these results suggest absence of a functional amount of MLC1, the complete depletion of a protein, using any system, is a quasi-impossible approach since remnants of the protein of interest could be passed over generations (Meissner et al., 2013, Frenal and Soldati-Favre, 2015). Similarly, depletion of ACT1 showed a defect in apicoplast segregation and organelle transport as soon as 24 hours post induction, but parasites remained motile even after 96 hours post induction (Whitelaw et al., 2017). Actin pyrene labelling and dynamic light scattering measurements elegantly showed that, like canonical actins, ACT1 polymerisation depends on a critical concentration (Kumpula et al., 2017). This suggests that minimal levels of actin in the *act1* KO cannot form functional filaments to support gliding, as previously suggested (Drewry and Sibley, 2015). Third, acto-MyoA independent invasion and gliding mechanisms were proposed to exist and contribute to these vital processes (Meissner et al., 2013, Egarter et al., 2014). Indeed, recent studies have highlighted the ability of parasites to subvert host cell components in order to enter (Bichet et al., 2016, Guérin et al., 2017). The most striking example was observed in the *myoA* KO mutants, which rely on host cell PM protrusions to access the cytosol and establish the nascent PV (Bichet et al., 2016). Consequently, it cannot be discarded that other mutants of the motor complex components exploit this pathway to enter the host cell.

Additionally, the gelation/solation model for motility predicted that microneme secretion at the apical end of the parasite can generate new attachment sites, which,

combined with pressure generated inside the cytosol, pushes the parasite forward (Egarter et al., 2014). Here, based on the evidence suggested in previously published data and this thesis (Egarter et al., 2014, Kan et al., 2014, Leung et al., 2014, Quadt et al., 2016, Tardieux and Baum, 2016, Moreau et al., 2017, Whitelaw et al., 2017), we propose a new hypothetical model for gliding motility. This new model suggests that motility in apicomplexans may involve different interactors able to combine and produce the necessary forces for motility and invasion (Figure 7-2). Efficient motility goes further than the linear motor model, but is the product of three independent factors: cell shape, force generation, and force transmission. 3D corkscrew trails and 2D helical motion were associated to the left-handed torsion of the microtubules (Håkansson et al., 1999, Kan et al., 2014, Leung et al., 2014). It was suggested that the participation of other cytoskeletal factors would "relax" the necessity of a pre-assembled motor complex in the periphery, but proposed a "free" motor model (Tardieux and Baum, 2016). This suggests that actin filaments are directly associated to the inner side of the PM and MyoA would not move adhesins *per se* but "patches" of PM associated adhesins. The directional movement is proposed to rely on actin filament orientation but not on the fixed position of MyoA maintained by GAP proteins (Tardieux and Baum, 2016). This model does not anticipate the requirement of a linker between actin and MICs in the PM. In fact, despite that GAC is proposed to fulfil this position, the interaction between this linker and ACT1, again, was based on immunoprecipitation studies of overexpressed proteins (Jacot et al., 2016b). In addition, actin binding proteins would be of great importance for maintaining the dynamics of actin filament formation, elongation, and depolymerisation in the periphery; thus, having a direct role on motility kinetics and directionality (Quadt et al., 2016, Moreau et al., 2017, Stadler et al., 2017). Finally, retrograde flow establishment would support translocation of the MICs, which are regulated by actin dynamics and the MyoA motor complex step; therefore, these factors together would be able to produce forward motility. Even though this model tries to consolidate current data, further studies are needed to confirm several aspects, such as how retrograde flow is produced and maintained and how actin binding proteins can modulate motility.

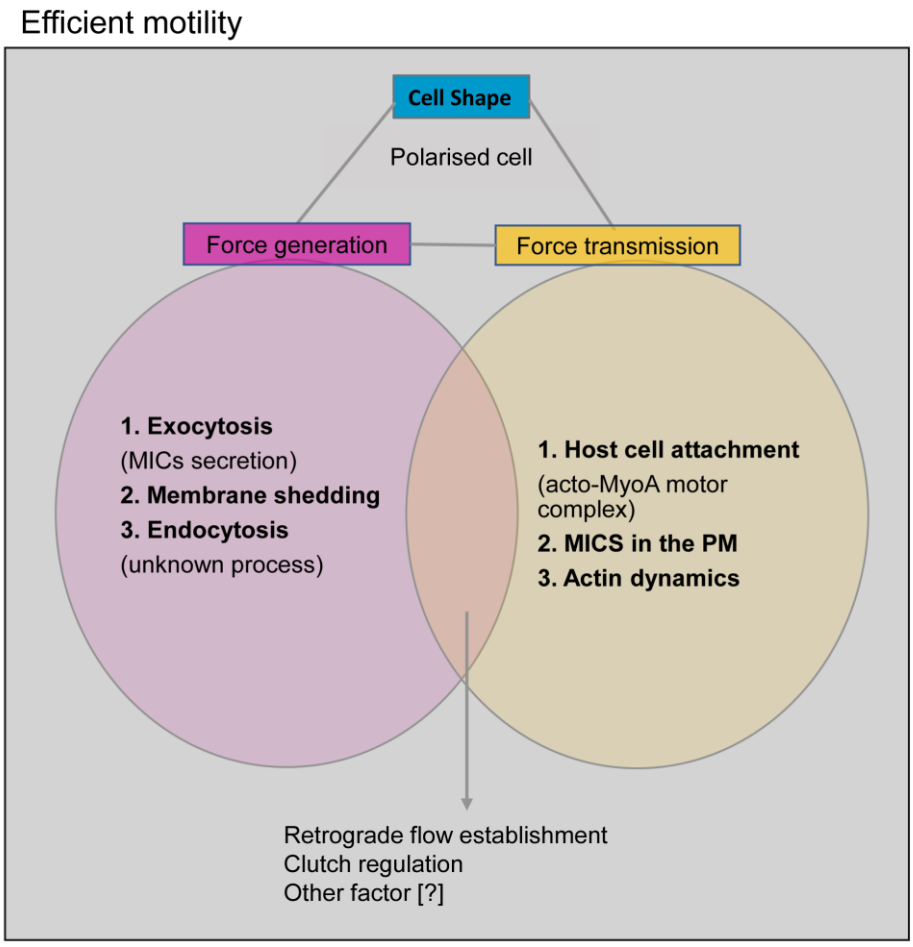

Figure 7-2. Efficient gliding motility relies on different mechanisms
The relationship among cell shape (Kan et al., 2014, Leung et al., 2014), force generation (Quadt et al., 2016, Moreau et al., 2017), and force transmission (Münter et al., 2009, Harker et al., 2014, Quadt et al., 2016, Gras et al., 2017, Whitelaw et al., 2017) is necessary for efficient gliding motility. Here, it is hypothesised that retrograde flow is established upon a constant cycle of exocytosis in the apical end and endocytosis/shedding towards the rear. Therefore, translocation of integrins depends on flow in the PM and not the acto-MyoA motor complex. Accordingly, substrate attachment will be produced by the "molecular clutch" comprising the acto-MyoA motor complex and the MICs in the PM. Thus, the engagement and disengagement of the MICs -adhesins- will depend on actin dynamics and the myoA motor complex. Finally, both the establishment of retrograde flow and the distribution and regulation of attachment sites are responsible for gliding kinetics. The possibility of other potential contributors is left open in this scheme since further studies are needed to elucidate this process.

7.5 Outlook for future remarks

The debate centred around the remaining motility and invasiveness of acto-MyoA motor complex mutants proposed several models to explain these phenomena. In this study, it is shown that neither residual protein in the conditional KOs nor redundancy among myosins in *T. gondii* explains the observed phenotypes in the mutant parasites. Additionally, moving from qualitative analysis of motility and invasion, a deep characterisation of these processes provided evidence that the acto-MyoA motor complex has further functions in regulation of attachment sites rather than force production. Conceptually, the acto-MyoA

motor complex will act in line with the molecular clutch model (Lin et al., 1994). Moreover, pulling together data obtained in this study with previous results, a new model for tachyzoite motility is proposed. However, further studies are required to solidify and expand knowledge of apicomplexan motility. For addressing future studies, it is important to consider that conditional mutants of the acto-MyoA motor complex in *Plasmodium* present slightly different phenotypes than their orthologues in *T. gondii* (Siden-Kiamos et al., 2011, Sebastian et al., 2012, Das et al., 2017). While some functions, such as apicoplast segregation, seem to be maintained between *T. gondii* and *Plasmodium*, depletion of ACT1 caused a detrimental invasion defect in the latter but no egress, indicating that this protein may have conserved and specific functions in each organism (Das et al., 2017).

While 2D and 3D motility assays give a broad vision of how single cells move, the conditions of each environment may require different interactors (Lämmermann and Sixt, 2009, Paluch et al., 2016). For example, intestinal leukocytes employ integrin-mediated attachment for migrating in 2D environments. However, depletion of 24 integrins showed that they were dispensable for motility in 3D milieu, indicating that protrusive actin polymerisation alone was sufficient to drive migration (Lämmermann et al., 2008). The confinement of the 3D environment immobilises the cell and, thus, adhesins are not required to attach to the substrate, while in 2D environments adhesins are required for immobilising the parasite on the substrate prior to migration (Lämmermann and Sixt, 2009, Paluch et al., 2016). Under this premise, it would be interesting to further study if there is a difference in MIC release in 2D and 3D environments. Considering that these parasites have different attachment characteristics, acto-MyoA motor complex mutants represent a good model to start characterising this process. In addition, to gain more knowledge about the interaction between the parasite and the substrate, surface sensitive imaging techniques can be employed. For instance, total internal reflection fluorescence microscopy (TIRFM) could be a useful tool to visualise adhesin structure and regulation, since this technique permits selective illumination of proteins in the immediate juncture between the substrate and the adhesin (Bretschneider et al., 2004, De Niz et al., 2017). Another powerful microscopy technique is traction force microscopy (TFM), which was employed to study how attachment sites are distributed and regulated in gliding *Plasmodium* sporozoites (Münter et al., 2009). This study indicated that while moving in 2D surfaces, sporozoite attachment sites are not evenly distributed along the surface, but change rapidly and present a stick-slip fashion (Münter et al., 2009) Furthermore, as the loss of acto-MyoA motor complex components affected adhesion; and therefore, most probably membrane tension, it would be interesting to scan the membrane of these parasites using atomic force microscopy (AFM). This

technique is widely used to study cell topography, cell-substrate/cell-cell interaction and high speed live cell imaging (De Niz et al., 2017). The latter application could be a good place to start the analysis of actin dynamics with the recently established Cb-actin technology (Periz et al., 2017). Here, preliminary data suggested actin filament formation does not depend on the presence of the MyoA-MLC1 complex, but more studies to expand our knowledge on the real impact of MyoA depletion on actin dynamics are needed. Thus, it is suggested to establish stable expression of the Cb-actin constructs under less strong promoters in the MyoA-motor complex KOs. Also, the addition of ligands to the sample to detect Cb-halo and Cb-snap increased background noise, limiting the quality and analysis of the resulting images. For this reason, the use of ligand-free fluorochromes (e.g. emerald green fluorescent protein) will give a better estimate of the real distribution of actin in the mutants. With this in mind, transient transfection and overexpression of the vectors can potentially interfere with actin functions (Periz et al., 2017), and also potentially with dynamics. Finally, considering the highly dynamic nature of the actin network, live-cell imaging based studies can be used to characterise mutants expressing Cb-actin in intracellular and extracellular stages. This would provide necessary data to expand our knowledge of the impact that the absence of peripheral MyoA has on actin dynamics.

8 Appendices

Appendix 1. License number obtained to use Figure 1-2 here entitled *Toxoplasma gondii* life cycle. To note, additional reprinted figures do not need license number, but appropriate citation

License Number	4212531498449
License date	Oct 19, 2017
Licensed Content Publisher	Nature Publishing Group
Licensed Content Publication	Nature Reviews Microbiology
Licensed Content Title	Modulation of innate immunity by Toxoplasma gondii virulence effectors
Licensed Content Author	Christopher A. Hunter, L. David Sibley
Licensed Content Date	Oct 16, 2012
Licensed Content Volume	10
Licensed Content Issue	11
Type of Use	reuse in a dissertation / thesis
Requestor type	academic/educational
Format	print and electronic
Portion	figures/tables/illustrations
Number of figures/tables/illustrations	1
High-res required	no
Figures	Figure 1-1. Toxoplasma gondii life cycle
Author of this NPG article	no
Your reference number	
Title of your thesis / dissertation	From force generation to host cell attachment: novel functions of the acto-MyoA motor complex
Expected completion date	Nov 2017
Estimated size (number of pages)	250
Requestor Location	University of Glasgow 120 university place Glasgow, Lanarkshire G12 8TA United Kingdom Attn: University of Glasgow
Billing Type	Invoice
Billing address	University of Glasgow 120 university place Glasgow, United Kingdom G12 8TA Attn: University of Glasgow
Total	0.00 GBP

Appendix 2. Immunoblot of loxp*mlc1* induced line A. $1x10^6$ sorted YFP+ events and B. $1x10^6$ induced parasites were analysed using western blot. Antibodies used were αMyoA and αMLC1. αCatalase was used as an internal control. As observed, no signal of Catalase can be clearly seen in sorted parasites in 24 and 72 hours post induction. Unsorted parasites show a slight decrease of MLC1 signal in later time points. However, this signal never disappears because of the presence of induced parasites in the sample.

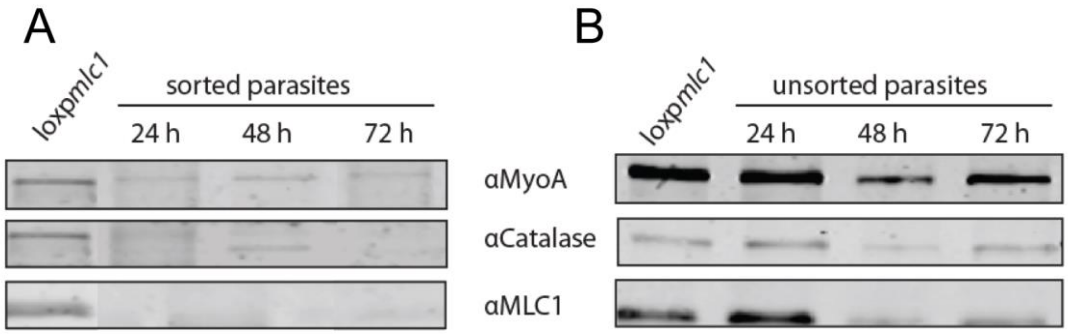

Appendix 3. *myoA* KO adaptation over time. A. 7-day plaque assay showing the adaptation of *myoA* KO parasites over time. Increase in the plaque area is observed in the parasites kept in culture for longer periods B. The number of trails deposited by 12-month cultured *myoA* KO increases when compared to 1-month cultured mutants C. Gliding kinetics show *myoA* KO (12 month) did not adapt in terms of speed and distance of the trails. Mean values of three independent experiment in triplicate are shown, ±SD, ***P≤0.001 D. 20-minute egress assay shows the ability of *myoA* KO adapted line to egress the host cell. In contrast, *myoA* KO parasites (1 month) show an obvious egress delay. Data and Graphics obtained by Dr. Nicole Andenmatten

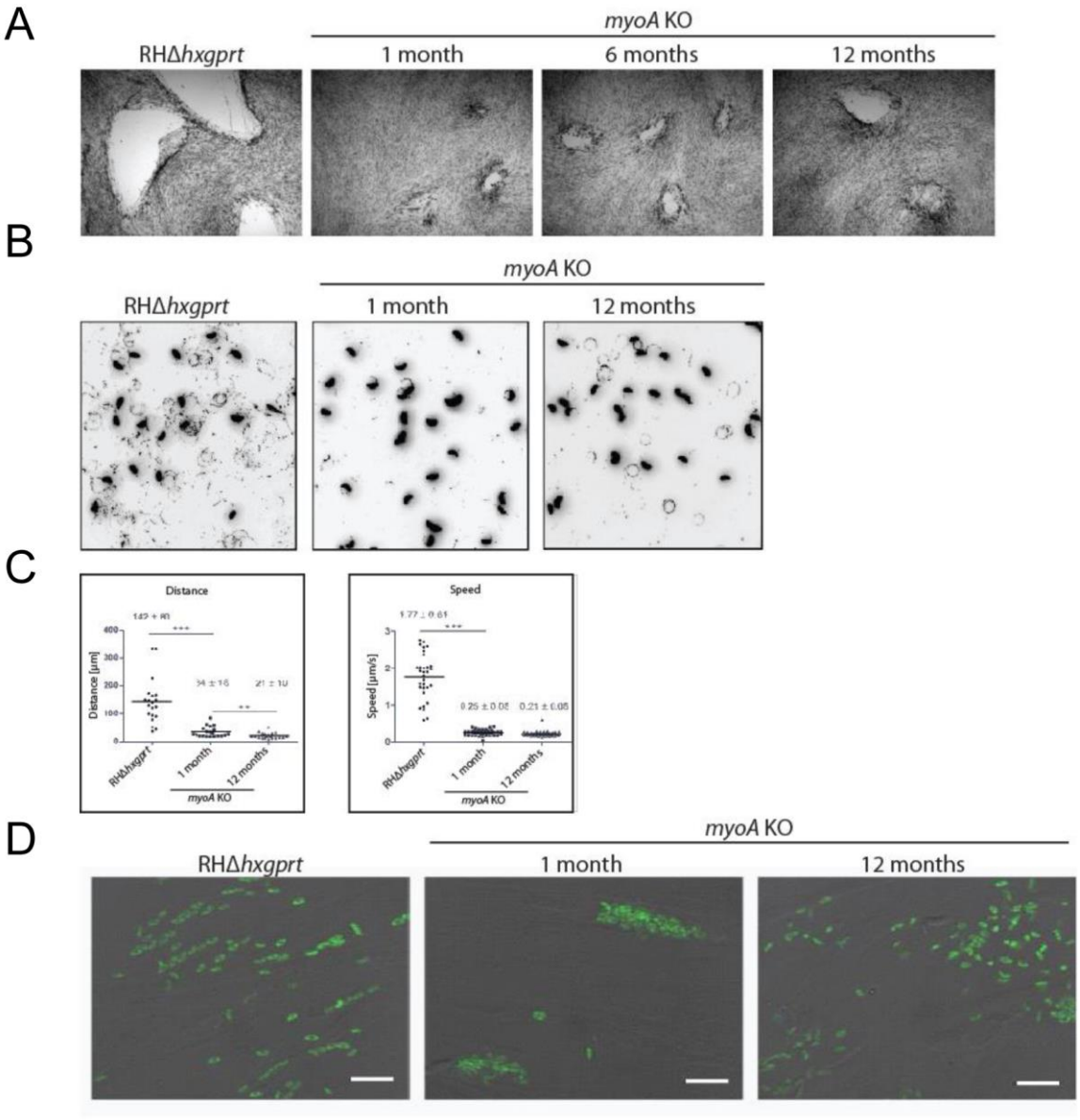

9 References

ADL, S. M., LEANDER, B. S., SIMPSON, A. G., ARCHIBALD, J. M., ANDERSON, O. R., BASS, D., BOWSER, S. S., BRUGEROLLE, G., FARMER, M. A., KARPOV, S., KOLISKO, M., LANE, C. E., LODGE, D. J., MANN, D. G., MEISTERFELD, R., MENDOZA, L., MOESTRUP, O., MOZLEY-STANDRIDGE, S. E., SMIRNOV, A. V. & SPIEGEL, F. 2007. Diversity, nomenclature, and taxonomy of protists. *Syst Biol,* 56**,** 684-9.

AGOP-NERSESIAN, C., NAISSANT, B., BEN RACHED, F., RAUCH, M., KRETZSCHMAR, A., THIBERGE, S., MENARD, R., FERGUSON, D. J. P., MEISSNER, M. & LANGSLEY, G. 2009. Rab11A-Controlled Assembly of the Inner Membrane Complex Is Required for Completion of Apicomplexan Cytokinesis. *PLOS Pathogens,* 5**,** e1000270.

ALEXANDER, D. L., MITAL, J., WARD, G. E., BRADLEY, P. & BOOTHROYD, J. C. 2005. Identification of the moving junction complex of *Toxoplasma gondii*: a collaboration between distinct secretory organelles. *PLoS Pathog,* 1**,** e17.

ALTSCHUL, S. F., GISH, W., MILLER, W., MYERS, E. W. & LIPMAN, D. J. 1990. Basic local alignment search tool. *Journal of molecular biology,* 215**,** 403-410.

AMBROISE-THOMAS, P. & PELLOUX, H. 1993. Toxoplasmosis - congenital and in immunocompromised patients: a parallel. *Parasitol Today,* 9**,** 61-3.

ANDENMATTEN, N., EGARTER, S., JACKSON, A. J., JULLIEN, N., HERMAN, J. P. & MEISSNER, M. 2013. Conditional genome engineering in *Toxoplasma gondii* uncovers alternative invasion mechanisms. *Nat Methods,* 10**,** 125-7.

ARANDA, P. S., LAJOIE, D. M. & JORCYK, C. L. 2012. Bleach gel: a simple agarose gel for analyzing RNA quality. *Electrophoresis,* 33**,** 366-9.

ARMSTRONG, C. M. & GOLDBERG, D. E. 2007. An FKBP destabilization domain modulates protein levels in Plasmodium falciparum. *Nat Methods,* 4**,** 1007-9.

ARRIZABALAGA, G. & BOOTHROYD, J. C. 2004. Role of calcium during *Toxoplasma gondii* invasion and egress. *International Journal for Parasitology,* 34**,** 361-368.

BANASZYNSKI, L. A., CHEN, L. C., MAYNARD-SMITH, L. A., OOI, A. G. & WANDLESS, T. J. 2006. A rapid, reversible, and tunable method to regulate protein function in living cells using synthetic small molecules. *Cell,* 126**,** 995-1004.

BANE, K. S., LEPPER, S., KEHRER, J., SATTLER, J. M., SINGER, M., REINIG, M., KLUG, D., HEISS, K., BAUM, J., MUELLER, A.-K. & FRISCHKNECHT, F. 2016. The Actin Filament-Binding Protein Coronin Regulates Motility in Plasmodium Sporozoites. *PLOS Pathogens,* 12**,** e1005710.

BARGIERI, D., LAGAL, V., ANDENMATTEN, N., TARDIEUX, I., MEISSNER, M. & MENARD, R. 2014. Host cell invasion by apicomplexan parasites: the junction conundrum. *PLoS Pathog,* 10**,** e1004273.

BARGIERI, D. Y., ANDENMATTEN, N., LAGAL, V., THIBERGE, S., WHITELAW, J. A., TARDIEUX, I., MEISSNER, M. & MÉNARD, R. 2013. Apical membrane antigen 1 mediates apicomplexan parasite attachment but is dispensable for host cell invasion. *Nature communications,* 4**,** 2552.

BARRAGAN, A. & SIBLEY, L. D. 2002. Transepithelial migration of *Toxoplasma gondii* is linked to parasite motility and virulence. *Journal of Experimental Medicine,* 195**,** 1625-1633.

BARRY, N. P. & BRETSCHER, M. S. 2010. Dictyostelium amoebae and neutrophils can swim. *Proceedings of the National Academy of Sciences,* 107**,** 11376-11380.

BAUM, J., PAPENFUSS, A. T., BAUM, B., SPEED, T. P. & COWMAN, A. F. 2006. Regulation of apicomplexan actin-based motility. *Nat Rev Micro,* 4**,** 621-628.

BERGMAN, L. W., KAISER, K., FUJIOKA, H., COPPENS, I., DALY, T. M., FOX, S., MATUSCHEWSKI, K., NUSSENZWEIG, V. & KAPPE, S. H. I. 2003. Myosin A tail domain interacting protein (MTIP) localizes to the inner membrane complex of Plasmodium sporozoites. *Journal of Cell Science,* 116**,** 39-49.

BESTEIRO, S., DUBREMETZ, J. F. & LEBRUN, M. 2011. The moving junction of apicomplexan parasites: a key structure for invasion. *Cell Microbiol,* 13**,** 797-805.

BICHET, M., JOLY, C., HENNI, A. H., GUILBERT, T., XEMARD, M., TAFANI, V., LAGAL, V., CHARRAS, G. & TARDIEUX, I. 2014. The toxoplasma-host cell junction is anchored to the cell cortex to sustain parasite invasive force. *BMC Biol,* 12**,** 773.

BICHET, M., TOUQUET, B., GONZALEZ, V., FLORENT, I., MEISSNER, M. & TARDIEUX, I. 2016. Genetic impairment of parasite myosin motors uncovers the contribution of host cell membrane dynamics to Toxoplasma invasion forces. *BMC biology,* 14**,** 97.

BILLKER, O., LOURIDO, S. & SIBLEY, L. D. 2009. Calcium-dependent signaling and kinases in apicomplexan parasites. *Cell host & microbe,* 5**,** 612-622.

BLACK, M., SEEBER, F., SOLDATI, D., KIM, K. & BOOTHROYD, J. C. 1995. Restriction enzyme-mediated integration elevates transformation frequency and enables co-transfection of *Toxoplasma gondii*. *Molecular and biochemical parasitology,* 74**,** 55-63.

BLACK, M. W., ARRIZABALAGA, G. & BOOTHROYD, J. C. 2000. Ionophore-resistant mutants of *Toxoplasma gondii* reveal host cell permeabilization as an early event in egress. *Mol Cell Biol,* 20**,** 9399-408.

BLACK, M. W. & BOOTHROYD, J. C. 2000. Lytic cycle of *Toxoplasma gondii*. *Microbiology and Molecular Biology Reviews,* 64**,** 607-623.

BLACKMAN, M. J. & CARRUTHERS, V. B. 2013. Recent insights into apicomplexan parasite egress provide new views to a kill. *Current Opinion in Microbiology,* 16**,** 459-464.

BLACKMAN, M. J., FUJIOKA, H., STAFFORD, W. H., SAJID, M., CLOUGH, B., FLECK, S. L., AIKAWA, M., GRAINGER, M. & HACKETT, F. 1998. A subtilisin-like protein in secretory organelles of Plasmodium falciparum merozoites. *J Biol Chem,* 273**,** 23398-409.

BLAKE, D. P. & TOMLEY, F. M. 2014. Securing poultry production from the ever-present Eimeria challenge. *Trends in Parasitology,* 30**,** 12-19.

BLANCHOIN, L., BOUJEMAA-PATERSKI, R., SYKES, C. & PLASTINO, J. 2014. Actin dynamics, architecture, and mechanics in cell motility. *Physiological reviews,* 94**,** 235-263.

BOOKWALTER, C. S., KELSEN, A., LEUNG, J. M., WARD, G. E. & TRYBUS, K. M. 2014. A *Toxoplasma gondii* class XIV myosin, expressed in Sf9 cells with a parasite co-chaperone, requires two light chains for fast motility. *Journal of Biological Chemistry,* 289**,** 30832-30841.

BOOKWALTER, C. S., TAY, C. L., MCCRORIE, R., PREVIS, M. J., KREMENTSOVA, E. B., FAGNANT, P. M., BAUM, J. & TRYBUS, K. M. 2017. Binding Of A Newly Identified Essential Light Chain To Expressed Plasmodium falciparum Class XIV Myosin Enhances Actin Motility. *bioRxiv***,** 127118.

BOOTHROYD, J. C. 2013. Have It Your Way: How Polymorphic, Injected Kinases and Pseudokinases Enable Toxoplasma to Subvert Host Defenses. *PLOS Pathogens,* 9**,** e1003296.

BOOTHROYD, J. C. & DUBREMETZ, J. F. 2008. Kiss and spit: the dual roles of Toxoplasma rhoptries. *Nat Rev Microbiol,* 6**,** 79-88.

BOUCHER, L. E. & BOSCH, J. 2015. The apicomplexan glideosome and adhesins - Structures and function. *J Struct Biol,* 190**,** 93-114.

BOUGDOUR, A., DURANDAU, E., BRENIER-PINCHART, M.-P., ORTET, P., BARAKAT, M., KIEFFER, S., CURT-VARESANO, A., CURT-BERTINI, R.-L., BASTIEN, O., COUTE, Y., PELLOUX, H. & HAKIMI, M.-A. 2013. Host Cell Subversion by Toxoplasma GRA16, an Exported Dense Granule Protein that Targets the Host Cell Nucleus and Alters Gene Expression. *Cell Host & Microbe,* 13**,** 489-500.

BOUGDOUR, A., TARDIEUX, I. & HAKIMI, M. A. 2014. Toxoplasma exports dense granule proteins beyond the vacuole to the host cell nucleus and rewires the host genome expression. *Cellular microbiology,* 16**,** 334-343.

BRAUN, L., BRENIER-PINCHART, M. P., YOGAVEL, M., CURT-VARESANO, A., CURT-BERTINI, R. L., HUSSAIN, T., KIEFFER-JAQUINOD, S., COUTE, Y., PELLOUX, H., TARDIEUX, I., SHARMA, A., BELRHALI, H., BOUGDOUR, A. & HAKIMI, M. A. 2013. A Toxoplasma dense granule protein, GRA24, modulates the early immune response to infection by promoting a direct and sustained host p38 MAPK activation. *J Exp Med,* 210**,** 2071-86.

BREINICH, M. S., FERGUSON, D. J. P., FOTH, B. J., VAN DOOREN, G. G., LEBRUN, M., QUON, D. V., STRIEPEN, B., BRADLEY, P. J., FRISCHKNECHT, F., CARRUTHERS, V. B. & MEISSNER, M. 2009. A Dynamin Is Required for the Biogenesis of Secretory Organelles in *Toxoplasma gondii*. *Current Biology,* 19**,** 277-286.

BRETSCHER, M. S. 1996. Getting membrane flow and the cytoskeleton to cooperate in moving cells. *Cell,* 87**,** 601-6.

BRETSCHER, M. S. 2014. Asymmetry of single cells and where that leads. *Annual review of biochemistry,* 83**,** 275-289.

BRETSCHNEIDER, T., DIEZ, S., ANDERSON, K., HEUSER, J., CLARKE, M., MÜLLER-TAUBENBERGER, A., KÖHLER, J. & GERISCH, G. 2004. Dynamic Actin Patterns and Arp2/3 Assembly at the Substrate-Attached Surface of Motile Cells. *Current Biology,* 14**,** 1-10.

BUGULISKIS, J. S., BROSSIER, F., SHUMAN, J. & SIBLEY, L. D. 2010. Rhomboid 4 (ROM4) affects the processing of surface adhesins and facilitates host cell invasion by *Toxoplasma gondii*. *PLoS pathogens,* 6**,** e1000858.

CALDAS, L. A., ATTIAS, M. & DE SOUZA, W. 2017. A structural analysis of the natural egress of *Toxoplasma gondii*. *Microbes and Infection*.

CALDAS, L. A., DE SOUZA, W. & ATTIAS, M. 2010. Microscopic analysis of calcium ionophore activated egress of *Toxoplasma gondii* from the host cell. *Veterinary Parasitology,* 167**,** 8-18.

CAMEJO, A., GOLD, D. A., LU, D., MCFETRIDGE, K., JULIEN, L., YANG, N., JENSEN, K. D. C. & SAEIJ, J. P. J. 2014. Identification of three novel *Toxoplasma gondii* rhoptry proteins. *International Journal for Parasitology,* 44**,** 147-160.

CARPENTER, A. E., JONES, T. R., LAMPRECHT, M. R., CLARKE, C., KANG, I. H., FRIMAN, O., GUERTIN, D. A., CHANG, J. H., LINDQUIST, R. A., MOFFAT, J., GOLLAND, P. & SABATINI, D. M. 2006. CellProfiler: image analysis software for identifying and quantifying cell phenotypes. *Genome Biology,* 7**,** R100.

CARRUTHERS, V. & BOOTHROYD, J. C. 2007. Pulling together: an integrated model of Toxoplasma cell invasion. *Curr Opin Microbiol,* 10**,** 83-9.

CARRUTHERS, V. B. 2002. Host cell invasion by the opportunistic pathogen *Toxoplasma gondii*. *Acta tropica,* 81**,** 111-122.

CARRUTHERS, V. B. & BLACKMAN, M. J. 2005. A new release on life: emerging concepts in proteolysis and parasite invasion. *Mol Microbiol,* 55**,** 1617-30.

CARRUTHERS, V. B., HÅKANSSON, S., GIDDINGS, O. K. & SIBLEY, L. D. 2000. *Toxoplasma gondii* uses sulfated proteoglycans for substrate and host cell attachment. *Infection and immunity,* 68**,** 4005-4011.

CARRUTHERS, V. B., MORENO, S. N. & SIBLEY, L. D. 1999. Ethanol and acetaldehyde elevate intracellular [Ca2+] and stimulate microneme discharge in *Toxoplasma gondii*. *Biochem J,* 342 (Pt 2)**,** 379-86.

CARRUTHERS, V. B. & SIBLEY, L. D. 1997. Sequential protein secretion from three distinct organelles of *Toxoplasma gondii* accompanies invasion of human fibroblasts. *Eur J Cell Biol,* 73**,** 114-23.

CARRUTHERS, V. B. & SIBLEY, L. D. 1999. Mobilization of intracellular calcium stimulates microneme discharge in *Toxoplasma gondii*. *Molecular microbiology,* 31**,** 421-428.

CARRUTHERS, V. B. & TOMLEY, F. M. 2008. Microneme proteins in apicomplexans. *Subcell Biochem,* 47**,** 33-45.

CINTRA, W. M. & DE SOUZA, W. 1985. Distribution of intramembranous particles and filipin-sterol complexes in the cell membranes of *Toxoplasma gondii*. *European journal of cell biology,* 37**,** 63-69.

CLOUGH, B. & FRICKEL, E. M. 2017. The Toxoplasma Parasitophorous Vacuole: An Evolving Host-Parasite Frontier. *Trends Parasitol,* 33**,** 473-488.

COLEMAN, B. I. & GUBBELS, M. J. 2012. A genetic screen to isolate *Toxoplasma gondii* host-cell egress mutants. *J Vis Exp*.

COLLINS, C. R., DAS, S., WONG, E. H., ANDENMATTEN, N., STALLMACH, R., HACKETT, F., HERMAN, J. P., MÜLLER, S., MEISSNER, M. & BLACKMAN, M. J. 2013. Robust inducible Cre recombinase activity in the human malaria parasite Plasmodium falciparum enables efficient gene deletion within a single asexual erythrocytic growth cycle. *Molecular microbiology,* 88**,** 687-701.

COPOS, C. A., WALCOTT, S., DEL ÁLAMO, J. C., BASTOUNIS, E., MOGILNER, A. & GUY, R. D. 2017. Mechanosensitive Adhesion Explains Stepping Motility in Amoeboid Cells. *Biophysical Journal,* 112**,** 2672-2682.

CURT-VARESANO, A., BRAUN, L., RANQUET, C., HAKIMI, M. A. & BOUGDOUR, A. 2016. The aspartyl protease TgASP5 mediates the export of the Toxoplasma GRA16 and GRA24 effectors into host cells. *Cell Microbiol,* 18**,** 151-67.

DAHER, W., KLAGES, N., CARLIER, M.-F. & SOLDATI-FAVRE, D. 2012. Molecular characterization of *Toxoplasma gondii* formin 3, an actin nucleator dispensable for tachyzoite growth and motility. *Eukaryotic cell,* 11**,** 343-352.

DAHER, W., PLATTNER, F., CARLIER, M. & SOLDATI-FAVRE, D. 2010. Concerted Action of Two Formins in Gliding Motility and Host Cell Invasion by Toxoplasma.

DARD, XE, L., M., BOUTEILLE, B. & PESTRE-ALEXANDRE, M. 1992. Isoenzyme Analysis of 35 *Toxoplasma gondii* Isolates and the Biological and Epidemiological Implications. *The Journal of Parasitology,* 78**,** 786-794.

DAS, S., HERTRICH, N., PERRIN, ABIGAIL J., WITHERS-MARTINEZ, C., COLLINS, CHRISTINE R., JONES, MATTHEW L., WATERMEYER, JEAN M., FOBES, ELMAR T., MARTIN, STEPHEN R., SAIBIL, HELEN R., WRIGHT, GAVIN J., TREECK, M., EPP, C. & BLACKMAN, MICHAEL J. 2015. Processing of Plasmodium falciparum Merozoite Surface Protein MSP1 Activates a Spectrin-Binding Function Enabling Parasite Egress from RBCs. *Cell Host & Microbe,* 18**,** 433-444.

DAS, S., LEMGRUBER, L., TAY, C. L., BAUM, J. & MEISSNER, M. 2017. Multiple essential functions of Plasmodium falciparum actin-1 during malaria blood-stage development. *BMC Biol,* 15**,** 70.

DASGUPTA, S., AUTH, T., GOV, N. S., SATCHWELL, T. J., HANSSEN, E., ZUCCALA, E. S., RIGLAR, D. T., TOYE, A. M., BETZ, T. & BAUM, J. 2014. Membrane-wrapping contributions to malaria parasite invasion of the human erythrocyte. *Biophysical journal,* 107**,** 43-54.

DE-LA-TORRE, A., SAUER, A., PFAFF, A. W., BOURCIER, T., BRUNET, J., SPEEG-SCHATZ, C., BALLONZOLI, L., VILLARD, O., AJZENBERG, D. & SUNDAR, N. 2013. Severe South American ocular toxoplasmosis is associated with decreased Ifn-γ/Il-17a and increased Il-6/Il-13 intraocular levels. *PLoS neglected tropical diseases,* 7**,** e2541.

DE AZEVEDO, M. F., GILSON, P. R., GABRIEL, H. B., SIMOES, R. F., ANGRISANO, F., BAUM, J., CRABB, B. S. & WUNDERLICH, G. 2012. Systematic analysis of FKBP inducible degradation domain tagging strategies for the human malaria parasite Plasmodium falciparum. *PLoS One,* 7**,** e40981.

DE NIZ, M., BURDA, P.-C., KAISER, G., DEL PORTILLO, H. A., SPIELMANN, T., FRISCHKNECHT, F. & HEUSSLER, V. T. 2017. Progress in imaging methods: insights gained into Plasmodium biology. *Nat Rev Micro,* 15**,** 37-54.

DELBAC, F., SANGER, A., NEUHAUS, E. M., STRATMANN, R., AJIOKA, J. W., TOURSEL, C., HERM-GOTZ, A., TOMAVO, S., SOLDATI, T. & SOLDATI, D. 2001. *Toxoplasma gondii* myosins B/C: one gene, two tails, two localizations, and a role in parasite division. *J Cell Biol,* 155**,** 613-23.

DESMONTS, G. & COUVREUR, J. 1974. Congenital toxoplasmosis: a prospective study of 378 pregnancies. *New England Journal of Medicine,* 290**,** 1110-1116.

DIMILLA, P. A., BARBEE, K. & LAUFFENBURGER, D. A. 1991. Mathematical model for the effects of adhesion and mechanics on cell migration speed. *Biophysical Journal,* 60**,** 15-37.

DOBROWOLSKI, J. & SIBLEY, L. D. 1997. The role of the cytoskeleton in host cell invasion by *Toxoplasma gondii*. *Behring Inst Mitt***,** 90-6.

DOBROWOLSKI, J. M., CARRUTHERS, V. B. & SIBLEY, L. D. 1997a. Participation of myosin in gliding motility and host cell invasion by *Toxoplasma gondii*. *Mol Microbiol,* 26**,** 163-73.

DOBROWOLSKI, J. M., NIESMAN, I. R. & SIBLEY, L. D. 1997b. Actin in the parasite *Toxoplasma gondii* is encoded by a single copy gene, ACT1 and exists primarily in a globular form. *Cell Motil Cytoskeleton,* 37**,** 253-62.

DOBROWOLSKI, J. M. & SIBLEY, L. D. 1996. Toxoplasma invasion of mammalian cells is powered by the actin cytoskeleton of the parasite. *Cell,* 84**,** 933-9.

DONALD, R. G., CARTER, D., ULLMAN, B. & ROOS, D. S. 1996. Insertional tagging, cloning, and expression of the *Toxoplasma gondii* hypoxanthine-xanthine-guanine phosphoribosyltransferase gene Use as a selectable marker for stable transformation. *Journal of Biological Chemistry,* 271**,** 14010-14019.

DONALD, R. G. & ROOS, D. S. 1993. Stable molecular transformation of *Toxoplasma gondii*: a selectable dihydrofolate reductase-thymidylate synthase marker based on drug-resistance mutations in malaria. *Proc Natl Acad Sci U S A,* 90**,** 11703-7.

DOUSE, C. H., GREEN, J. L., SALGADO, P. S., SIMPSON, P. J., THOMAS, J. C., LANGSLEY, G., HOLDER, A. A., TATE, E. W. & COTA, E. 2012. Regulation of the Plasmodium motor

complex: phosphorylation of myosin A tail-interacting protein (MTIP) loosens its grip on MyoA. *J Biol Chem,* 287**,** 36968-77.

DREWRY, L. L. & SIBLEY, L. D. 2015. Toxoplasma Actin Is Required for Efficient Host Cell Invasion. *MBio,* 6**,** e00557.

DUBEY, J., MILLER, N. L. & FRENKEL, J. 1970. The *Toxoplasma gondii* oocyst from cat feces. *Journal of Experimental Medicine,* 132**,** 636-662.

DUBEY, J. P. 2009. History of the discovery of the life cycle of *Toxoplasma gondii*. *International Journal for Parasitology,* 39**,** 877-882.

DUBEY, J. P. & FRENKEL, J. K. 1972. Cyst-induced toxoplasmosis in cats. *J Protozool,* 19**,** 155-77.

DUBEY, J. P., LINDSAY, D. S. & SPEER, C. A. 1998. Structures of *Toxoplasma gondii* tachyzoites, bradyzoites, and sporozoites and biology and development of tissue cysts. *Clin Microbiol Rev,* 11**,** 267-99.

DUNN, D., WALLON, M., PEYRON, F., PETERSEN, E., PECKHAM, C. & GILBERT, R. 1999. Mother-to-child transmission of toxoplasmosis: risk estimates for clinical counselling. *The Lancet,* 353**,** 1829-1833.

DUTTA, D., WILLIAMSON, C. D., COLE, N. B. & DONALDSON, J. G. 2012. Pitstop 2 Is a Potent Inhibitor of Clathrin-Independent Endocytosis. *PLOS ONE,* 7**,** e45799.

DVORIN, J. D., MARTYN, D. C., PATEL, S. D., GRIMLEY, J. S., COLLINS, C. R., HOPP, C. S., BRIGHT, A. T., WESTENBERGER, S., WINZELER, E., BLACKMAN, M. J., BAKER, D. A., WANDLESS, T. J. & DURAISINGH, M. T. 2010. A Plant-Like Kinase in Plasmodium falciparum Regulates Parasite Egress from Erythrocytes. *Science,* 328**,** 910-912.

DZIERSZINSKI, F., MORTUAIRE, M., CESBRON-DELAUW, M. F. & TOMAVO, S. 2000. Targeted disruption of the glycosylphosphatidylinositol-anchored surface antigen SAG3 gene in *Toxoplasma gondii* decreases host cell adhesion and drastically reduces virulence in mice. *Molecular Microbiology,* 37**,** 574-582.

EGARTER, S., ANDENMATTEN, N., JACKSON, A. J., WHITELAW, J. A., PALL, G., BLACK, J. A., FERGUSON, D. J., TARDIEUX, I., MOGILNER, A. & MEISSNER, M. 2014. The Toxoplasma Acto-MyoA Motor Complex Is Important but Not Essential for Gliding Motility and Host Cell Invasion. *PLoS One,* 9**,** e91819.

EIDELL, K. P., BURKE, T. & GUBBELS, M.-J. 2010. Development of a screen to dissect *Toxoplasma gondii* egress. *Molecular and Biochemical Parasitology,* 171**,** 97-103.

ELSHEIKHA, H. M., BÜSSELBERG, D. & ZHU, X.-Q. 2016. The known and missing links between *Toxoplasma gondii*. *Metabolic brain disease,* 31**,** 749-759.

ENDO, T., SETHI, K. K. & PIEKARSKI, G. 1982. *Toxoplasma gondii*: Calcium lonophore A23187-mediated exit of trophozoites from infected murine macrophages. *Experimental Parasitology,* 53**,** 179-188.

ENDO, T., TOKUDA, H., YAGITA, K. & KOYAMA, T. 1987. Effects of extracellular potassium on acid release and motility initiation in *Toxoplasma gondii*. *Journal of Eukaryotic Microbiology,* 34**,** 291-295.

ENDO, T. & YAGITA, K. 1990. Effect of Extracellular Ions on Motility and Cell Entry in *Toxoplasma gondii*. *The Journal of Protozoology,* 37**,** 133-138.

ETHERIDGE, RONALD D., ALAGANAN, A., TANG, K., LOU, HUA J., TURK, BENJAMIN E. & SIBLEY, L. D. 2014. The Toxoplasma Pseudokinase ROP5 Forms Complexes with ROP18 and ROP17 Kinases that Synergize to Control Acute Virulence in Mice. *Cell Host & Microbe,* 15**,** 537-550.

FAGARASANU, A., MAST, F. D., KNOBLACH, B. & RACHUBINSKI, R. A. 2010. Molecular mechanisms of organelle inheritance: lessons from peroxisomes in yeast. *Nat Rev Mol Cell Biol,* 11**,** 644-54.

FENTRESS, S. J., BEHNKE, M. S., DUNAY, I. R., MASHAYEKHI, M., ROMMEREIM, L. M., FOX, B. A., BZIK, D. J., TAYLOR, G. A., TURK, B. E., LICHTI, C. F., TOWNSEND, R. R., QIU, W., HUI, R., BEATTY, W. L. & SIBLEY, L. D. 2010. Phosphorylation of Immunity-Related GTPases by a *Toxoplasma gondii*-Secreted Kinase Promotes Macrophage Survival and Virulence. *Cell Host & Microbe,* 8**,** 484-495.

FICHERA, M. E., BHOPALE, M. K. & ROOS, D. S. 1995. In vitro assays elucidate peculiar kinetics of clindamycin action against *Toxoplasma gondii*. *Antimicrobial agents and chemotherapy,* 39**,** 1530-1537.

FICHERA, M. E. & ROOS, D. S. 1997. A plastid organelle as a drug target in apicomplexan parasites. *Nature,* 390**,** 407-9.

FORTIER, B., COIGNARD-CHATAIN, C., SOETE, M. & DUBREMETZ, J. F. 1996. [Structure and biology of *Toxoplasma gondii* bradyzoites]. *C R Seances Soc Biol Fil,* 190**,** 385-94.

FOTH, B. J., GOEDECKE, M. C. & SOLDATI, D. 2006. New insights into myosin evolution and classification. *Proc Natl Acad Sci U S A,* 103**,** 3681-6.

FOX, B. A., RISTUCCIA, J. G., GIGLEY, J. P. & BZIK, D. J. 2009. Efficient gene replacements in *Toxoplasma gondii* strains deficient for nonhomologous end joining. *Eukaryotic cell,* 8**,** 520-529.

FOX, B. A., ROMMEREIM, L. M., GUEVARA, R. B., FALLA, A., HORTUA TRIANA, M. A., SUN, Y. & BZIK, D. J. 2016. The *Toxoplasma gondii* Rhoptry Kinome Is Essential for Chronic Infection. *MBio,* 7.

FRANCIA, M. E. & STRIEPEN, B. 2014. Cell division in apicomplexan parasites. *Nat Rev Micro,* 12**,** 125-136.

FRENAL, K., DUBREMETZ, J.-F., LEBRUN, M. & SOLDATI-FAVRE, D. 2017a. Gliding motility powers invasion and egress in Apicomplexa. *Nature Reviews Microbiology*.

FRENAL, K., JACOT, D., HAMMOUDI, P. M., GRAINDORGE, A., MACO, B. & SOLDATI-FAVRE, D. 2017b. Myosin-dependent cell-cell communication controls synchronicity of division in acute and chronic stages of *Toxoplasma gondii*. *Nat Commun,* 8**,** 15710.

FRENAL, K., MARQ, J. B., JACOT, D., POLONAIS, V. & SOLDATI-FAVRE, D. 2014. Plasticity between MyoC- and MyoA-glideosomes: an example of functional compensation in *Toxoplasma gondii* invasion. *PLoS Pathog,* 10**,** e1004504.

FRENAL, K., POLONAIS, V., MARQ, J. B., STRATMANN, R., LIMENITAKIS, J. & SOLDATI-FAVRE, D. 2010. Functional dissection of the apicomplexan glideosome molecular architecture. *Cell Host Microbe,* 8**,** 343-57.

FRENAL, K. & SOLDATI-FAVRE, D. 2015. Plasticity and Redundancy in Proteins Important for Toxoplasma Invasion. *PLoS Pathog,* 11**,** e1005069.

FRENKEL, J. 1973. Toxoplasma in and around us. *Bioscience,* 23**,** 343-352.

FREVERT, U., ENGELMANN, S., ZOUGBÉDÉ, S., STANGE, J., NG, B., MATUSCHEWSKI, K., LIEBES, L. & YEE, H. 2005. Intravital Observation of Plasmodium berghei Sporozoite Infection of the Liver. *PLoS Biology,* 3**,** e192.

FRIEDL, P., BORGMANN, S. & BROCKER, E. B. 2001. Amoeboid leukocyte crawling through extracellular matrix: lessons from the Dictyostelium paradigm of cell movement. *J Leukoc Biol,* 70**,** 491-509.

FRIEDL, P. & WOLF, K. 2003. Tumour-cell invasion and migration: diversity and escape mechanisms. *Nature reviews. Cancer,* 3**,** 362.

FRIXIONE, E., MONDRAGON, R. & MEZA, I. 1996. Kinematic analysis of *Toxoplasma gondii* motility. *Cell Motil Cytoskeleton,* 34**,** 152-63.

GAJI, R. Y., JOHNSON, D. E., TREECK, M., WANG, M., HUDMON, A. & ARRIZABALAGA, G. 2015. Phosphorylation of a Myosin Motor by TgCDPK3 Facilitates Rapid Initiation of Motility during *Toxoplasma gondii* egress. *PLOS Pathogens,* 11**,** e1005268.

GAJRIA, B., BAHL, A., BRESTELLI, J., DOMMER, J., FISCHER, S., GAO, X., HEIGES, M., IODICE, J., KISSINGER, J. C. & MACKEY, A. J. 2007. ToxoDB: an integrated *Toxoplasma gondii* database resource. *Nucleic acids research,* 36**,** D553-D556.

GANDHI, M. & GOODE, B. L. 2008. Coronin: the double-edged sword of actin dynamics. *The Coronin Family of Proteins***,** 72-87.

GARG, S., AGARWAL, S., KUMAR, S., YAZDANI, S. S., CHITNIS, C. E. & SINGH, S. 2013. Calcium-dependent permeabilization of erythrocytes by a perforin-like protein during egress of malaria parasites. *Nat Commun,* 4**,** 1736.

GARRISON, E., TREECK, M., EHRET, E., BUTZ, H., GARBUZ, T., OSWALD, B. P., SETTLES, M., BOOTHROYD, J. & ARRIZABALAGA, G. 2012. A forward genetic screen reveals that calcium-dependent protein kinase 3 regulates egress in Toxoplasma. *PLoS Pathog,* 8**,** e1003049.

GASKINS, E., GILK, S., DEVORE, N., MANN, T., WARD, G. & BECKERS, C. 2004. Identification of the membrane receptor of a class XIV myosin in *Toxoplasma gondii*. *J Cell Biol,* 165**,** 383-93.

GATIGNOL, A., BARON, M. & TIRABY, G. 1987. Phleomycin resistance encoded by the ble gene from transposon Tn 5 as a dominant selectable marker in Saccharomyces cerevisiae. *Molecular and General Genetics MGG,* 207**,** 342-348.

GAVRILESCU, L. C. & DENKERS, E. Y. 2001. IFN-γ overproduction and high level apoptosis are associated with high but not low virulence *Toxoplasma gondii* infection. *The Journal of Immunology,* 167**,** 902-909.

GIFFORD, J. L., WALSH, M. P. & VOGEL, H. J. 2007. Structures and metal-ion-binding properties of the Ca2+-binding helix–loop–helix EF-hand motifs. *Biochemical Journal,* 405**,** 199-221.

GOLD, DANIEL A., KAPLAN, AARON D., LIS, A., BETT, GLENNA C. L., ROSOWSKI, EMILY E., CIRELLI, KIMBERLY M., BOUGDOUR, A., SIDIK, SAIMA M., BECK, JOSH R., LOURIDO, S., EGEA, PASCAL F., BRADLEY, PETER J., HAKIMI, M.-A., RASMUSSON, RANDALL L. & SAEIJ, JEROEN P. J. 2015. The Toxoplasma Dense Granule Proteins GRA17 and GRA23 Mediate the Movement of Small Molecules between the Host and the Parasitophorous Vacuole. *Cell Host & Microbe,* 17**,** 642-652.

GOULD, S. B., MAIER, U.-G. & MARTIN, W. F. 2015. Protein import and the origin of red complex plastids. *Current Biology,* 25**,** R515-R521.

GOULD, S. B., THAM, W.-H., COWMAN, A. F., MCFADDEN, G. I. & WALLER, R. F. 2006. Alveolins, a new family of cortical proteins that define the protist infrakingdom Alveolata. *Molecular biology and evolution,* 25**,** 1219-1230.

GRAINDORGE, A., FRENAL, K., JACOT, D., SALAMUN, J., MARQ, J. B. & SOLDATI-FAVRE, D. 2016. The Conoid Associated Motor MyoH Is Indispensable for *Toxoplasma gondii* Entry and Exit from Host Cells. *PLoS Pathog,* 12**,** e1005388.

GRAS, S., JACKSON, A., WOODS, S., PALL, G., WHITELAW, J., LEUNG, J. M., WARD, G. E., ROBERTS, C. W. & MEISSNER, M. 2017. Parasites lacking the micronemal protein MIC2 are deficient in surface attachment and host cell egress, but remain virulent in vivo. *Wellcome open research,* 2.

GREEN, J. L., WALL, R. J., VAHOKOSKI, J., YUSUF, N. A., RIDZUAN, M. A. M., STANWAY, R. R., STOCK, J., KNUEPFER, E., BRADY, D., MARTIN, S. R., HOWELL, S. A., PIRES, I. P., MOON, R. W., MOLLOY, J. E., KURSULA, I., TEWARI, R. & HOLDER, A. A. 2017. Compositional and expression analyses of the glideosome during the Plasmodium life cycle reveal an additional myosin light chain required for maximum motility. *J Biol Chem.*

GUBBELS, M.-J., WHITE, M. & SZATANEK, T. 2008. The cell cycle and *Toxoplasma gondii* cell division: tightly knit or loosely stitched? *International journal for parasitology,* 38**,** 1343-1358.

GUBBELS, M. J., VAISHNAVA, S., BOOT, N., DUBREMETZ, J. F. & STRIEPEN, B. 2006. A MORN-repeat protein is a dynamic component of the *Toxoplasma gondii* cell division apparatus. *J Cell Sci,* 119**,** 2236-45.

GUÉRIN, A., CORRALES, R. M., PARKER, M. L., LAMARQUE, M. H., JACOT, D., EL HAJJ, H., SOLDATI-FAVRE, D., BOULANGER, M. J. & LEBRUN, M. 2017. Efficient invasion by Toxoplasma depends on the subversion of host protein networks. *Nature Microbiology,* 2**,** 1358.

GUPTA, C. M., THIYAGARAJAN, S. & SAHASRABUDDHE, A. A. 2015. Unconventional actins and actin-binding proteins in human protozoan parasites. *Int J Parasitol,* 45**,** 435-47.

HÅKANSSON, S., MORISAKI, H., HEUSER, J. & SIBLEY, L. D. 1999. Time-Lapse Video Microscopy of Gliding Motility in*Toxoplasma gondii* Reveals a Novel, Biphasic Mechanism of Cell Locomotion. *Molecular biology of the cell,* 10**,** 3539-3547.

HAKIMI, M.-A., OLIAS, P. & SIBLEY, L. D. 2017. Toxoplasma effectors targeting host signaling and transcription. *Clinical microbiology reviews,* 30**,** 615-645.

HAMMER, J. A., 3RD & SELLERS, J. R. 2011. Walking to work: roles for class V myosins as cargo transporters. *Nat Rev Mol Cell Biol,* 13**,** 13-26.

HARDING, C. R., EGARTER, S., GOW, M., JIMÉNEZ-RUIZ, E., FERGUSON, D. J. P. & MEISSNER, M. 2016. Gliding Associated Proteins Play Essential Roles during the Formation of the Inner Membrane Complex of *Toxoplasma gondii*. *PLOS Pathogens,* 12**,** e1005403.

HARDING, C. R. & MEISSNER, M. 2014. The inner membrane complex through development of *Toxoplasma gondii* and Plasmodium. *Cellular Microbiology,* 16**,** 632-641.

HARKER, K. S., JIVAN, E., MCWHORTER, F. Y., LIU, W. F. & LODOEN, M. B. 2014. Shear forces enhance *Toxoplasma gondii* tachyzoite motility on vascular endothelium. *MBio,* 5**,** e01111-13.

HARTMAN, M. A., FINAN, D., SIVARAMAKRISHNAN, S. & SPUDICH, J. A. 2011. Principles of unconventional myosin function and targeting. *Annu Rev Cell Dev Biol,* 27**,** 133-55.

HARVEY, K. L., YAP, A., GILSON, P. R., COWMAN, A. F. & CRABB, B. S. 2014. Insights and controversies into the role of the key apicomplexan invasion ligand, Apical Membrane Antigen 1. *Int J Parasitol,* 44**,** 853-7.

HEASLIP, A. T., LEUNG, J. M., CAREY, K. L., CATTI, F., WARSHAW, D. M., WESTWOOD, N. J., BALLIF, B. A. & WARD, G. E. 2010. A Small-Molecule Inhibitor of *T. gondii* Motility Induces the Posttranslational Modification of Myosin Light Chain-1 and Inhibits Myosin Motor Activity. *PLOS Pathogens,* 6**,** e1000720.

HEASLIP, A. T., NELSON, S. R. & WARSHAW, D. M. 2016. Dense granule trafficking in *Toxoplasma gondii* requires a unique class 27 myosin and actin filaments. *Mol Biol Cell,* 27**,** 2080-9.

HEASLIP, A. T., NISHI, M., STEIN, B. & HU, K. 2011. The motility of a human parasite, *Toxoplasma gondii*, is regulated by a novel lysine methyltransferase. *PLoS pathogens,* 7**,** e1002201.

HEGGE, S., UHRIG, K., STREICHFUSS, M., KYNAST-WOLF, G., MATUSCHEWSKI, K., SPATZ, J. P. & FRISCHKNECHT, F. 2012. Direct manipulation of malaria parasites with optical tweezers reveals distinct functions of Plasmodium surface proteins. *ACS nano,* 6**,** 4648-4662.

HEINTZELMAN, M. B. 2015. Gliding motility in apicomplexan parasites. *Semin Cell Dev Biol,* 46**,** 135-42.

HEINTZELMAN, M. B. & SCHWARTZMAN, J. D. 1997. A novel class of unconventional myosins from *Toxoplasma gondii*. Elsevier.

HEISSLER, S. M. & SELLERS, J. R. 2014. Myosin light chains: Teaching old dogs new tricks. *Bioarchitecture,* 4**,** 169-188.

HELLERSCHMIED, D. & CLAUSEN, T. 2014. Myosin chaperones. *Current Opinion in Structural Biology,* 25**,** 9-15.

HERM-GÖTZ, A., AGOP-NERSESIAN, C., MÜNTER, S., GRIMLEY, J. S., WANDLESS, T. J., FRISCHKNECHT, F. & MEISSNER, M. 2007. Rapid control of protein level in the apicomplexan *Toxoplasma gondii*. *Nature methods,* 4**,** 1003.

HERM-GOTZ, A., DELBAC, F., WEISS, S., NYITRAI, M., STRATMANN, R., TOMAVO, S., SIBLEY, L. D., GEEVES, M. A. & SOLDATI, D. 2006. Functional and biophysical analyses of the class XIV *Toxoplasma gondii* myosin D. *J Muscle Res Cell Motil,* 27**,** 139-51.

HERM-GOTZ, A., WEISS, S., STRATMANN, R., FUJITA-BECKER, S., RUFF, C., MEYHOFER, E., SOLDATI, T., MANSTEIN, D. J., GEEVES, M. A. & SOLDATI, D. 2002. *Toxoplasma gondii* myosin A and its light chain: a fast, single-headed, plus-end-directed motor. *EMBO J,* 21**,** 2149-58.

HETTMANN, C., HERM, A., GEITER, A., FRANK, B., SCHWARZ, E., SOLDATI, T. & SOLDATI, D. 2000. A dibasic motif in the tail of a class XIV apicomplexan myosin is an essential determinant of plasma membrane localization. *Molecular biology of the cell,* 11**,** 1385-1400.

HILL, D. & DUBEY, J. 2002. *Toxoplasma gondii*: transmission, diagnosis and prevention. *Clinical microbiology and infection,* 8**,** 634-640.

HOFF, E. F. & CARRUTHERS, V. B. 2002. Is Toxoplasma egress the first step in invasion? *Trends in Parasitology,* 18**,** 251-255.

HOHLFELD, P., DAFFOS, F., THULLIEZ, P., AUFRANT, C., COUVREUR, J., MACALEESE, J., DESCOMBEY, D. & FORESTIER, F. 1989. Fetal toxoplasmosis: outcome of pregnancy and infant follow-up after in utero treatment. *J Pediatr,* 115**,** 765-9.

HOOD, J. D. & CHERESH, D. A. 2002. Role of integrins in cell invasion and migration. *Nat Rev Cancer,* 2**,** 91-100.

HOUDUSSE, A. & SWEENEY, H. L. 2016. How Myosin Generates Force on Actin Filaments. *Trends in Biochemical Sciences,* 41**,** 989-997.

HOWE, D. K. & SIBLEY, L. D. 1995. *Toxoplasma gondii* Comprises Three Clonal Lineages: Correlation of Parasite Genotype with Human Disease. *The Journal of Infectious Diseases,* 172**,** 1561-1566.

HU, K., JOHNSON, J., FLORENS, L., FRAUNHOLZ, M., SURAVAJJALA, S., DILULLO, C., YATES, J., ROOS, D. S. & MURRAY, J. M. 2006. Cytoskeletal components of an invasion machine--the apical complex of *Toxoplasma gondii*. *PLoS Pathog,* 2**,** e13.

HU, K., MANN, T., STRIEPEN, B., BECKERS, C. J., ROOS, D. S. & MURRAY, J. M. 2002a. Daughter cell assembly in the protozoan parasite*Toxoplasma gondii*. *Molecular biology of the cell,* 13**,** 593-606.

HU, K., ROOS, D. S. & MURRAY, J. M. 2002b. A novel polymer of tubulin forms the conoid of *Toxoplasma gondii*. *J Cell Biol,* 156**,** 1039-50.

HUNTER, C. A. & SIBLEY, L. D. 2012. Modulation of innate immunity by *Toxoplasma gondii* virulence effectors. *Nat Rev Microbiol,* 10**,** 766-78.

HUYNH, M.-H. & CARRUTHERS, V. B. 2006. Toxoplasma MIC2 Is a Major Determinant of Invasion and Virulence. *PLOS Pathogens,* 2**,** e84.

HUYNH, M.-H. & CARRUTHERS, V. B. 2009a. Tagging of endogenous genes in a *Toxoplasma gondii* strain lacking Ku80. *Eukaryotic cell,* 8**,** 530-539.

HUYNH, M. H. & CARRUTHERS, V. B. 2009b. Tagging of endogenous genes in a *Toxoplasma gondii* strain lacking Ku80. *Eukaryot Cell,* 8**,** 530-9.

INGRAM, W. M., GOODRICH, L. M., ROBEY, E. A. & EISEN, M. B. 2013. Mice infected with low-virulence strains of *Toxoplasma gondii* lose their innate aversion to cat urine, even after extensive parasite clearance. *PloS one,* 8**,** e75246.

ISHINO, T., CHINZEI, Y. & YUDA, M. 2005. A Plasmodium sporozoite protein with a membrane attack complex domain is required for breaching the liver sinusoidal cell layer prior to hepatocyte infection. *Cell Microbiol,* 7**,** 199-208.

JACOT, D., DAHER, W. & SOLDATI-FAVRE, D. 2013. *Toxoplasma gondii* myosin F, an essential motor for centrosomes positioning and apicoplast inheritance. *EMBO J,* 32**,** 1702-16.

JACOT, D., FRENAL, K., MARQ, J. B., SHARMA, P. & SOLDATI-FAVRE, D. 2014. Assessment of phosphorylation in Toxoplasma glideosome assembly and function. *Cell Microbiol,* 16**,** 1518-32.

JACOT, D., TOSETTI, N., PIRES, I., STOCK, J., GRAINDORGE, A., HUNG, Y.-F., HAN, H., TEWARI, R., KURSULA, I. & SOLDATI-FAVRE, D. 2016a. An Apicomplexan Actin-Binding Protein Serves as a Connector and Lipid Sensor to Coordinate Motility and Invasion. *Cell Host & Microbe,* 20**,** 731-743.

JACOT, D., TOSETTI, N., PIRES, I., STOCK, J., GRAINDORGE, A., HUNG, Y. F., HAN, H., TEWARI, R., KURSULA, I. & SOLDATI-FAVRE, D. 2016b. An Apicomplexan Actin-Binding Protein Serves as a Connector and Lipid Sensor to Coordinate Motility and Invasion. *Cell Host Microbe,* 20**,** 731-743.

JENSEN, K. D., WANG, Y., WOJNO, E. D. T., SHASTRI, A. J., HU, K., CORNEL, L., BOEDEC, E., ONG, Y.-C., CHIEN, Y.-H. & HUNTER, C. A. 2011. Toxoplasma polymorphic effectors determine macrophage polarization and intestinal inflammation. *Cell host & microbe,* 9**,** 472-483.

JEWETT, T. J. & SIBLEY, L. D. 2003. Aldolase Forms a Bridge between Cell Surface Adhesins and the Actin Cytoskeleton in Apicomplexan Parasites. *Molecular Cell,* 11**,** 885-894.

JIMENEZ-RUIZ, E., WONG, E. H., PALL, G. S. & MEISSNER, M. 2014. Advantages and disadvantages of conditional systems for characterization of essential genes in *Toxoplasma gondii*. *Parasitology,* 141**,** 1390-8.

JULLIEN, N., SAMPIERI, F., ENJALBERT, A. & HERMAN, J. P. 2003. Regulation of Cre recombinase by ligand-induced complementation of inactive fragments. *Nucleic Acids Res,* 31**,** e131.

KAFSACK, B. F. C., PENA, J. D. O., COPPENS, I., RAVINDRAN, S., BOOTHROYD, J. C. & CARRUTHERS, V. B. 2009. Rapid Membrane Disruption by a Perforin-Like Protein Facilitates Parasite Exit from Host Cells. *Science,* 323**,** 530-533.

KAN, A., TAN, Y. H., ANGRISANO, F., HANSSEN, E., ROGERS, K. L., WHITEHEAD, L., MOLLARD, V. P., COZIJNSEN, A., DELVES, M. J. & CRAWFORD, S. 2014. Quantitative analysis of Plasmodium ookinete motion in three dimensions suggests a critical role for cell shape in the biomechanics of malaria parasite gliding motility. *Cellular microbiology,* 16**,** 734-750.

KANNAN, G., MOLDOVAN, K., XIAO, J.-C., YOLKEN, R. H., JONES-BRANDO, L. & PLETNIKOV, M. V. 2010. *Toxoplasma gondii* strain-dependent effects on mouse behaviour. *Folia parasitologica,* 57**,** 151.

KATRIS, N. J., VAN DOOREN, G. G., MCMILLAN, P. J., HANSSEN, E., TILLEY, L. & WALLER, R. F. 2014. The apical complex provides a regulated gateway for secretion of invasion factors in Toxoplasma. *PLoS pathogens,* 10**,** e1004074.

KEELEY, A. & SOLDATI, D. 2004. The glideosome: a molecular machine powering motility and host-cell invasion by Apicomplexa. *Trends in Cell Biology,* 14**,** 528-532.

KEPPLER, A., GENDREIZIG, S., GRONEMEYER, T., PICK, H., VOGEL, H. & JOHNSSON, K. 2003. A general method for the covalent labeling of fusion proteins with small molecules in vivo. *Nature biotechnology,* 21**,** 86.

KHAN, A., DUBEY, J., SU, C., AJIOKA, J. W., ROSENTHAL, B. M. & SIBLEY, L. D. 2011. Genetic analyses of atypical *Toxoplasma gondii* strains reveal a fourth clonal lineage in North America. *International journal for parasitology,* 41**,** 645-655.

KHAN, A., FUX, B., SU, C., DUBEY, J., DARDÉ, M.-L., AJIOKA, J., ROSENTHAL, B. & SIBLEY, L. 2007. Recent transcontinental sweep of *Toxoplasma gondii* driven by a single monomorphic chromosome. *Proceedings of the National Academy of Sciences,* 104**,** 14872-14877.

KHAN, A., TAYLOR, S., SU, C., MACKEY, A. J., BOYLE, J., COLE, R., GLOVER, D., TANG, K., PAULSEN, I. T. & BERRIMAN, M. 2005. Composite genome map and recombination parameters derived from three archetypal lineages of *Toxoplasma gondii*. *Nucleic acids research,* 33**,** 2980-2992.

KIARA, H., STEINAA, L., NENE, V. & SVITEK, N. 2018. Theileria in Ruminants. *In:* FLORIN-CHRISTENSEN, M. & SCHNITTGER, L. (eds.) *Parasitic Protozoa of Farm Animals and Pets.* Cham: Springer International Publishing.

KIBBE, W. A. 2007. OligoCalc: an online oligonucleotide properties calculator. *Nucleic Acids Res,* 35**,** W43-6.

KIJLSTRA, A. & PETERSEN, E. 2014. Epidemiology, Pathophysiology, and the Future of Ocular Toxoplasmosis. *Ocular Immunology and Inflammation,* 22**,** 138-147.

KIM, D., LANGMEAD, B. & SALZBERG, S. L. 2015. HISAT: a fast spliced aligner with low memory requirements. *Nature methods,* 12**,** 357.

KIM, D. H. & WIRTZ, D. 2013. Focal adhesion size uniquely predicts cell migration. *Faseb j,* 27**,** 1351-61.

KIM, K., SOLDATI, D. & BOOTHROYD, J. C. 1993. Gene replacement in *Toxoplasma gondii* with chloramphenicol acetyltransferase as selectable marker. *SCIENCE-NEW YORK THEN WASHINGTON-,* 262**,** 911-911.

KIM, K. & WEISS, L. M. 2008. Toxoplasma: the next 100years. *Microbes and Infection,* 10**,** 978-984.

KING, C. A. 1988. Cell motility of sporozoan protozoa. *Parasitology Today,* 4**,** 315-319.

KLINGER, C. M., KARNKOWSKA, A., HERMAN, E. K., HAMPL, V. & DACKS, J. B. 2016. Phylogeny and Evolution. *Molecular Parasitology.* Springer.

KLUG, D. & FRISCHKNECHT, F. 2017. Motility precedes egress of malaria parasites from oocysts. *eLife,* 6**,** e19157.

KNOBLACH, B. & RACHUBINSKI, R. A. 2016. How peroxisomes partition between cells. A story of yeast, mammals and filamentous fungi. *Current Opinion in Cell Biology,* 41**,** 73-80.

KOCH, M. & BAUM, J. 2016. The mechanics of malaria parasite invasion of the human erythrocyte–towards a reassessment of the host cell contribution. *Cellular microbiology,* 18**,** 319-329.

KOHLER, S. 2005. Multi-membrane-bound structures of Apicomplexa: I. the architecture of the *Toxoplasma gondii* apicoplast. *Parasitol Res,* 96**,** 258-72.

KOHLER, S., DELWICHE, C. F., DENNY, P. W., TILNEY, L. G., WEBSTER, P., WILSON, R. J., PALMER, J. D. & ROOS, D. S. 1997. A plastid of probable green algal origin in Apicomplexan parasites. *Science,* 275**,** 1485-9.

KORPELAINEN, E., TUIMALA, J., SOMERVUO, P., HUSS, M. & WONG, G. 2014. *RNA-seq data analysis: a practical approach,* Chapman and Hall/CRC.

KREIDENWEISS, A., HOPKINS, A. V. & MORDMÜLLER, B. 2013. 2A and the auxin-based degron system facilitate control of protein levels in Plasmodium falciparum. *PloS one,* 8**,** e78661.

KREMER, K., KAMIN, D., RITTWEGER, E., WILKES, J., FLAMMER, H., MAHLER, S., HENG, J., TONKIN, C. J., LANGSLEY, G., HELL, S. W., CARRUTHERS, V. B., FERGUSON, D. J. & MEISSNER, M. 2013. An overexpression screen of *Toxoplasma gondii* Rab-GTPases reveals distinct transport routes to the micronemes. *PLoS Pathog,* 9**,** e1003213.

KRENDEL, M. & MOOSEKER, M. S. 2005. Myosins: tails (and heads) of functional diversity. *Physiology (Bethesda),* 20**,** 239-51.

KUDRYASHEV, M., LEPPER, S., BAUMEISTER, W., CYRKLAFF, M. & FRISCHKNECHT, F. 2010. Geometric constrains for detecting short actin filaments by cryogenic electron tomography. *PMC biophysics,* 3**,** 6.

KUMPULA, E.-P., PIRES, I., LASIWA, D., PIIRAINEN, H., BERGMANN, U., VAHOKOSKI, J. & KURSULA, I. 2017. Apicomplexan actin polymerization depends on nucleation. *Scientific Reports,* 7**,** 12137.

KUMPULA, E. P. & KURSULA, I. 2015. Towards a molecular understanding of the apicomplexan actin motor: on a road to novel targets for malaria remedies? *Acta Crystallogr F Struct Biol Commun,* 71**,** 500-13.

KURSULA, I., KURSULA, P., GANTER, M., PANJIKAR, S., MATUSCHEWSKI, K. & SCHULER, H. 2008. Structural basis for parasite-specific functions of the divergent profilin of Plasmodium falciparum. *Structure,* 16**,** 1638-48.

LAEMMLI, U. K. 1970. Cleavage of structural proteins during the assembly of the head of bacteriophage T4. *nature,* 227**,** 680-685.

LAGAL, V., BINDER, E. M., HUYNH, M. H., KAFSACK, B. F., HARRIS, P. K., DIEZ, R., CHEN, D., COLE, R. N., CARRUTHERS, V. B. & KIM, K. 2010. *Toxoplasma gondii* protease TgSUB1 is required for cell surface processing of micronemal adhesive complexes and efficient adhesion of tachyzoites. *Cellular microbiology,* 12**,** 1792-1808.

LAMARQUE, M., BESTEIRO, S., PAPOIN, J., ROQUES, M., VULLIEZ-LE NORMAND, B., MORLON-GUYOT, J., DUBREMETZ, J. F., FAUQUENOY, S., TOMAVO, S., FABER, B. W., KOCKEN, C. H., THOMAS, A. W., BOULANGER, M. J., BENTLEY, G. A. & LEBRUN, M. 2011. The RON2-AMA1 interaction is a critical step in moving junction-dependent invasion by apicomplexan parasites. *PLoS Pathog,* 7**,** e1001276.

LAMARQUE, M. H., ROQUES, M., KONG-HAP, M., TONKIN, M. L., RUGARABAMU, G., MARQ, J.-B., PENARETE-VARGAS, D. M., BOULANGER, M. J., SOLDATI-FAVRE, D. & LEBRUN, M. 2014. Plasticity and redundancy among AMA–RON pairs ensure host cell entry of Toxoplasma parasites. *Nature communications,* 5.

LÄMMERMANN, T., BADER, B. L., MONKLEY, S. J., WORBS, T., WEDLICH-SÖLDNER, R., HIRSCH, K., KELLER, M., FÖRSTER, R., CRITCHLEY, D. R. & FÄSSLER, R. 2008. Rapid leukocyte migration by integrin-independent flowing and squeezing. *Nature,* 453**,** 51-55.

LÄMMERMANN, T. & SIXT, M. 2009. Mechanical modes of 'amoeboid' cell migration. *Current Opinion in Cell Biology,* 21**,** 636-644.

LANGOUSIS, G. & HILL, K. L. 2014. Motility and more: the flagellum of Trypanosoma brucei. *Nature reviews. Microbiology,* 12**,** 505.

LAVINE, M. D. & ARRIZABALAGA, G. 2008. Exit from Host Cells by the Pathogenic Parasite *Toxoplasma gondii* Does Not Require Motility. *Eukaryotic Cell,* 7**,** 131-140.

LE ROY, C. & WRANA, J. L. 2005. Clathrin-and non-clathrin-mediated endocytic regulation of cell signalling. *Nature reviews Molecular cell biology,* 6**,** 112-126.

LEANDER, B. S. & KEELING, P. J. 2003. Morphostasis in alveolate evolution. *Trends in Ecology & Evolution,* 18**,** 395-402.

LEE, M. C. & FIDOCK, D. A. 2014. CRISPR-mediated genome editing of Plasmodium falciparum malaria parasites. *Genome medicine,* 6**,** 63.

LEE, P. Y., COSTUMBRADO, J., HSU, C.-Y. & KIM, Y. H. 2012. Agarose gel electrophoresis for the separation of DNA fragments. *Journal of visualized experiments: JoVE*.

LEIJNSE, N., ODDERSHEDE, L. B. & BENDIX, P. M. 2015. An updated look at actin dynamics in filopodia. *Cytoskeleton,* 72**,** 71-79.

LEKUTIS, C., FERGUSON, D. J. P., GRIGG, M. E., CAMPS, M. & BOOTHROYD, J. C. 2001. Surface antigens of *Toxoplasma gondii*: variations on a theme. *International Journal for Parasitology,* 31**,** 1285-1292.

LEUNG, J. M., ROULD, M. A., KONRADT, C., HUNTER, C. A. & WARD, G. E. 2014. Disruption of TgPHIL1 Alters Specific Parameters of *Toxoplasma gondii* Motility Measured in a Quantitative, Three-Dimensional Live Motility Assay. *PLOS ONE,* 9**,** e85763.

LEVINE, N. D. 1988. Progress in taxonomy of the Apicomplexan protozoa. *J Protozool,* 35**,** 518-20.

LEW, A. E., DLUZEWSKI, A. R., JOHNSON, A. M. & PINDER, J. C. 2002. Myosins of Babesia bovis: molecular characterisation, erythrocyte invasion, and phylogeny. *Cell Motil Cytoskeleton,* 52**,** 202-20.

LI, H., HANDSAKER, B., WYSOKER, A., FENNELL, T., RUAN, J., HOMER, N., MARTH, G., ABECASIS, G. & DURBIN, R. 2009. The sequence alignment/map format and SAMtools. *Bioinformatics,* 25**,** 2078-2079.

LIN, C.-H., THOMPSON, C. A. & FORSCHER, P. 1994. Cytoskeletal reorganization underlying growth cone motility. *Current Opinion in Neurobiology,* 4**,** 640-647.

LIN, J. W., MEIRELES, P., PRUDÊNCIO, M., ENGELMANN, S., ANNOURA, T., SAJID, M., CHEVALLEY-MAUREL, S., RAMESAR, J., NAHAR, C., AVRAMUT, C. M. C., KOSTER, A. J., MATUSCHEWSKI, K., WATERS, A. P., JANSE, C. J., MAIR, G. R. & KHAN, S. M. 2013. Loss-of-function analyses defines vital and redundant functions of the Plasmodium rhomboid protease family. *Molecular Microbiology,* 88**,** 318-338.

LONG, S. 2017. Functional characterization of apically localized calmodulins that regulate motility and cell invasion in *Toxoplasma gondii*. *The FASEB Journal,* 31**,** 620.2-620.2.

LONG, S., BROWN, K. M., DREWRY, L. L., ANTHONY, B., PHAN, I. Q. H. & SIBLEY, L. D. 2017. Calmodulin-like proteins localized to the conoid regulate motility and cell invasion by *Toxoplasma gondii*. *PLOS Pathogens,* 13**,** e1006379.

LOURIDO, S. & MORENO, S. N. 2015. The calcium signaling toolkit of the Apicomplexan parasites *Toxoplasma gondii* and Plasmodium spp. *Cell Calcium,* 57**,** 186-93.

LOURIDO, S., SHUMAN, J., ZHANG, C., SHOKAT, K. M., HUI, R. & SIBLEY, L. D. 2010. Calcium-dependent protein kinase 1 is an essential regulator of exocytosis in Toxoplasma. *Nature,* 465**,** 359-62.

LOURIDO, S., TANG, K. & SIBLEY, L. D. 2012. Distinct signalling pathways control Toxoplasma egress and host-cell invasion. *The EMBO Journal,* 31**,** 4524-4534.

LOVETT, J. L. & SIBLEY, L. D. 2003. Intracellular calcium stores in *Toxoplasma gondii* govern invasion of host cells. *Journal of Cell Science,* 116**,** 3009-3016.

LYONS, R. E., MCLEOD, R. & ROBERTS, C. W. 2002. *Toxoplasma gondii* tachyzoite–bradyzoite interconversion. *Trends in parasitology,* 18**,** 198-201.

MA, J. S., SASAI, M., OHSHIMA, J., LEE, Y., BANDO, H., TAKEDA, K. & YAMAMOTO, M. 2014. Selective and strain-specific NFAT4 activation by the *Toxoplasma gondii* polymorphic dense granule protein GRA6. *Journal of Experimental Medicine,* 211**,** 2013-2032.

MANN, T. & BECKERS, C. 2001. Characterization of the subpellicular network, a filamentous membrane skeletal component in the parasite *Toxoplasma gondii*. *Mol Biochem Parasitol,* 115**,** 257-68.

MATRAJT, M., PLATT, C. D., SAGAR, A. D., LINDSAY, A., MOULTON, C. & ROOS, D. S. 2004. Transcript initiation, polyadenylation, and functional promoter mapping for the dihydrofolate reductase-thymidylate synthase gene of *Toxoplasma gondii*. *Molecular and Biochemical Parasitology,* 137**,** 229-238.

MCCOY, J. M., STEWART, R. J., UBOLDI, A. D., LI, D., SCHRODER, J., SCOTT, N. E., PAPENFUSS, A. T., LEHANE, A. M., FOSTER, L. J. & TONKIN, C. J. 2017. A forward genetic screen identifies a negative regulator of rapid Ca2+-dependent cell egress (MS1) in the intracellular parasite *Toxoplasma gondii*. *J Biol Chem,* 292**,** 7662-7674.

MCCOY, J. M., WHITEHEAD, L., VAN DOOREN, G. G. & TONKIN, C. J. 2012. TgCDPK3 regulates calcium-dependent egress of *Toxoplasma gondii* from host cells. *PLoS Pathog,* 8**,** e1003066.

MCFADDEN, G. I. 2011. The apicoplast. *Protoplasma,* 248**,** 641-650.

MCFADDEN, G. I., REITH, M. E., MUNHOLLAND, J. & LANG-UNNASCH, N. 1996. Plastid in human parasites. *Nature,* 381**,** 482.

MCFADDEN, G. I. & YEH, E. 2017. The apicoplast: now you see it, now you don't. *International Journal for Parasitology,* 47**,** 137-144.

MEHTA, S. & SIBLEY, L. D. 2010. *Toxoplasma gondii* actin depolymerizing factor acts primarily to sequester G-actin. *J Biol Chem,* 285**,** 6835-47.

MEHTA, S. & SIBLEY, L. D. 2011. Actin depolymerizing factor controls actin turnover and gliding motility in *Toxoplasma gondii*. *Mol Biol Cell,* 22**,** 1290-9.

MEISSNER, M., BRECHT, S., BUJARD, H. & SOLDATI, D. 2001. Modulation of myosin A expression by a newly established tetracycline repressor-based inducible system in *Toxoplasma gondii*. *Nucleic acids research,* 29**,** e115-e115.

MEISSNER, M., FERGUSON, D. J. & FRISCHKNECHT, F. 2013. Invasion factors of apicomplexan parasites: essential or redundant? *Curr Opin Microbiol,* 16**,** 438-44.

MEISSNER, M., KREJANY, E., GILSON, P. R., DE KONING-WARD, T. F., SOLDATI, D. & CRABB, B. S. 2005. Tetracycline analogue-regulated transgene expression in Plasmodium falciparum blood stages using *Toxoplasma gondii* transactivators. *Proc Natl Acad Sci U S A,* 102**,** 2980-5.

MEISSNER, M., REISS, M., VIEBIG, N., CARRUTHERS, V. B., TOURSEL, C., TOMAVO, S., AJIOKA, J. W. & SOLDATI, D. 2002a. A family of transmembrane microneme proteins of *Toxoplasma gondii* contain EGF-like domains and function as escorters. *J Cell Sci,* 115**,** 563-74.

MEISSNER, M., SCHLUTER, D. & SOLDATI, D. 2002b. Role of *Toxoplasma gondii* myosin A in powering parasite gliding and host cell invasion. *Science,* 298**,** 837-40.

MENARD, R. 2001. Gliding motility and cell invasion by Apicomplexa: insights from the Plasmodium sporozoite. *Cellular microbiology,* 3**,** 63-73.

MERCIER, C., DUBREMETZ, J. F., RAUSCHER, B., LECORDIER, L., SIBLEY, L. D. & CESBRON-DELAUW, M. F. 2002. Biogenesis of nanotubular network in Toxoplasma parasitophorous vacuole induced by parasite proteins. *Mol Biol Cell,* 13**,** 2397-409.

MESSINA, M., NIESMAN, I., MERCIER, C. & SIBLEY, L. D. 1995. Stable DNA transformation of *Toxoplasma gondii* using phleomycin selection. *Gene,* 165**,** 213-217.

MINEO, J. R. & KASPER, L. H. 1994. Attachment of *Toxoplasma gondii* to host cells involves major surface protein, SAG-1 (P30). *Exp Parasitol,* 79**,** 11-20.

MITAL, J., MEISSNER, M., SOLDATI, D. & WARD, G. E. 2005. Conditional expression of *Toxoplasma gondii* apical membrane antigen-1 (TgAMA1) demonstrates that TgAMA1 plays a critical role in host cell invasion. *Mol Biol Cell,* 16**,** 4341-9.

MONDRAGON, R. & FRIXIONE, E. 1996. Ca2+-Dependence of Conoid Extrusion in *Toxoplasma gondii* Tachyzoites. *Journal of Eukaryotic Microbiology,* 43**,** 120-127.

MONTOYA, J. G. & LIESENFELD, O. 2004. Toxoplasmosis. *The Lancet,* 363**,** 1965-1976.

MORDUE, D. G., HÅKANSSON, S., NIESMAN, I. & SIBLEY, L. D. 1999. *Toxoplasma gondii* resides in a vacuole that avoids fusion with host cell endocytic and exocytic vesicular trafficking pathways. *Experimental parasitology,* 92**,** 87-99.

MOREAU, C. A., BHARGAV, S. P., KUMAR, H., QUADT, K. A., PIIRAINEN, H., STRAUSS, L., KEHRER, J., STREICHFUSS, M., SPATZ, J. P., WADE, R. C., KURSULA, I. & FRISCHKNECHT, F. 2017. A unique profilin-actin interface is important for malaria parasite motility. *PLOS Pathogens,* 13**,** e1006412.

MORISAKI, J. H., HEUSER, J. E. & SIBLEY, L. D. 1995. Invasion of *Toxoplasma gondii* occurs by active penetration of the host cell. *Journal of Cell Science,* 108**,** 2457-2464.

MORRISON, D. A. 2009. Evolution of the Apicomplexa: where are we now? *Trends Parasitol,* 25**,** 375-82.

MORRISON, W. I. 2015. The aetiology, pathogenesis and control of theileriosis in domestic animals. *Rev Sci Tech,* 34**,** 599-611.

MORRISSETTE, N. S., MURRAY, J. M. & ROOS, D. S. 1997. Subpellicular microtubules associate with an intramembranous particle lattice in the protozoan parasite *Toxoplasma gondii*. *J Cell Sci,* 110 (Pt 1)**,** 35-42.

MORRISSETTE, N. S. & SIBLEY, L. D. 2002. Cytoskeleton of apicomplexan parasites. *Microbiol Mol Biol Rev,* 66**,** 21-38; table of contents.

MOUDY, R., MANNING, T. J. & BECKERS, C. J. 2001. The loss of cytoplasmic potassium upon host cell breakdown triggers egress of *Toxoplasma gondii*. *J Biol Chem,* 276**,** 41492-501.

MUELLER, C., GRAINDORGE, A. & SOLDATI-FAVRE, D. 2017. Functions of myosin motors tailored for parasitism. *Current Opinion in Microbiology,* 40**,** 113-122.

MUELLER, C., KLAGES, N., JACOT, D., SANTOS, J. M., CABRERA, A., GILBERGER, T. W., DUBREMETZ, J. F. & SOLDATI-FAVRE, D. 2013. The Toxoplasma protein ARO

mediates the apical positioning of rhoptry organelles, a prerequisite for host cell invasion. *Cell Host Microbe,* 13**,** 289-301.

MÜNTER, S., SABASS, B., SELHUBER-UNKEL, C., KUDRYASHEV, M., HEGGE, S., ENGEL, U., SPATZ, J. P., MATUSCHEWSKI, K., SCHWARZ, U. S. & FRISCHKNECHT, F. 2009. Plasmodium Sporozoite Motility Is Modulated by the Turnover of Discrete Adhesion Sites. *Cell Host & Microbe,* 6**,** 551-562.

NAGY, A. 2000. Cre recombinase: the universal reagent for genome tailoring. *genesis,* 26**,** 99-109.

NAIR, S. C., BROOKS, C. F., GOODMAN, C. D., STRURM, A., MCFADDEN, G. I., SUNDRIYAL, S., ANGLIN, J. L., SONG, Y., MORENO, S. N. J. & STRIEPEN, B. 2011. Apicoplast isoprenoid precursor synthesis and the molecular basis of fosmidomycin resistance in *Toxoplasma gondii*. *The Journal of Experimental Medicine,* 208**,** 1547-1559.

NEBL, T., PRIETO, J. H., KAPP, E., SMITH, B. J., WILLIAMS, M. J., YATES, J. R., 3RD, COWMAN, A. F. & TONKIN, C. J. 2011. Quantitative in vivo analyses reveal calcium-dependent phosphorylation sites and identifies a novel component of the Toxoplasma invasion motor complex. *PLoS Pathog,* 7**,** e1002222.

NGUYEN, T., BIGAIGNON, G., MARKINE-GORIAYNOFF, D., HEREMANS, H., NGUYEN, T., WARNIER, G., DELMEE, M., WARNY, M., WOLF, S. & UYTTENHOVE, C. 2003. Virulent *Toxoplasma gondii* strain RH promotes T-cell-independent overproduction of proinflammatory cytokines IL12 and γ-interferon. *Journal of medical microbiology,* 52**,** 869-876.

NICHOLS, B. A. & CHIAPPINO, M. L. 1987. Cytoskeleton of *Toxoplasma gondii*. *Journal of Eukaryotic Microbiology,* 34**,** 217-226.

NICOLLE, C. 1908. Sur une infection a corps de Leishman (on organismes voisons) du gondi. *CR Acad Sci,* 147**,** 736.

NICOLLE, M. 1909. Sur un protozoaire nouveau du gondi.(Toxopasma N. GEN.). *Arch Inst Pasteur Tunis,* 2**,** 97-103.

NISHI, M., HU, K., MURRAY, J. M. & ROOS, D. S. 2008. Organellar dynamics during the cell cycle of *Toxoplasma gondii*. *J Cell Sci,* 121**,** 1559-68.

NISHIMURA, K., FUKAGAWA, T., TAKISAWA, H., KAKIMOTO, T. & KANEMAKI, M. 2009. An auxin-based degron system for the rapid depletion of proteins in nonplant cells. *Nat Meth,* 6**,** 917-922.

NUSSBAUM-KRAMMER, C. I., NETO, M. F., BRIELMANN, R. M., PEDERSEN, J. S. & MORIMOTO, R. I. 2015. Investigating the spreading and toxicity of prion-like proteins using the metazoan model organism C. elegans. *Journal of visualized experiments: JoVE***,** 52321.

OGINO, N. & YONEDA, C. 1966. The fine structure and mode of division of *Toxoplasma gondii*. *Arch Ophthalmol,* 75**,** 218-27.

OKUMURA, T., SASAMURA, T., INATOMI, M., HOZUMI, S., NAKAMURA, M., HATORI, R., TANIGUCHI, K., NAKAZAWA, N., SUZUKI, E., MAEDA, R., YAMAKAWA, T. & MATSUNO, K. 2015. Class I Myosins Have Overlapping and Specialized Functions in Left-Right Asymmetric Development in Drosophila. *Genetics,* 199**,** 1183-1199.

OLIVIERI, A., COLLINS, C. R., HACKETT, F., WITHERS-MARTINEZ, C., MARSHALL, J., FLYNN, H. R., SKEHEL, J. M. & BLACKMAN, M. J. 2011. Juxtamembrane Shedding of Plasmodium falciparum AMA1 Is Sequence Independent and Essential, and Helps Evade Invasion-Inhibitory Antibodies. *PLOS Pathogens,* 7**,** e1002448.

OLSHINA, M. A., ANGRISANO, F., MARAPANA, D. S., RIGLAR, D. T., BANE, K., WONG, W., CATIMEL, B., YIN, M.-X., HOLMES, A. B. & FRISCHKNECHT, F. 2015. Plasmodium falciparum coronin organizes arrays of parallel actin filaments potentially guiding directional motility in invasive malaria parasites. *Malaria journal,* 14**,** 280.

OPITZ, C. & SOLDATI, D. 2002. 'The glideosome': a dynamic complex powering gliding motion and host cell invasion by *Toxoplasma gondii*. *Mol Microbiol,* 45**,** 597-604.

OUOLOGUEM, D. T. & ROOS, D. S. 2014. Dynamics of the *Toxoplasma gondii* inner membrane complex. *Journal of Cell Science,* 127**,** 3320-3330.

PALECEK, S. P., LOFTUS, J. C., GINSBERG, M. H., LAUFFENBURGER, D. A. & HORWITZ, A. F. 1997. Integrin-ligand binding properties govern cell migration speed through cell-substratum adhesiveness. *Nature,* 385**,** 537-540.

PALUCH, E. K., ASPALTER, I. M. & SIXT, M. 2016. Focal Adhesion–Independent Cell Migration. *Annual review of cell and developmental biology,* 32**,** 469-490.

PAŇKOVÁ, K., RÖSEL, D., NOVOTNÝ, M. & BRÁBEK, J. 2010. The molecular mechanisms of transition between mesenchymal and amoeboid invasiveness in tumor cells. *Cellular and Molecular Life Sciences,* 67**,** 63-71.

PAPAIOANNOU, T. G. & STEFANADIS, C. 2005. Vascular wall shear stress: basic principles and methods. *Hellenic J Cardiol,* 46**,** 9-15.

PAPPAS, G., ROUSSOS, N. & FALAGAS, M. E. 2009. Toxoplasmosis snapshots: global status of *Toxoplasma gondii* seroprevalence and implications for pregnancy and congenital toxoplasmosis. *International journal for parasitology,* 39**,** 1385-1394.

PAQUET, C., YUDIN, M. H., YUDIN, M. H., ALLEN, V. M., BOUCHARD, C., BOUCHER, M., CADDY, S., CASTILLO, E., MONEY, D. M., MURPHY, K. E., OGILVIE, G., PAQUET, C., VAN SCHALKWYK, J. & SENIKAS, V. 2013. Toxoplasmosis in Pregnancy: Prevention, Screening, and Treatment. *Journal of Obstetrics and Gynaecology Canada,* 35**,** 78-79.

PARKER, M. L., PENARETE-VARGAS, D. M., HAMILTON, P. T., GUÉRIN, A., DUBEY, J. P., PERLMAN, S. J., SPANO, F., LEBRUN, M. & BOULANGER, M. J. 2016. Dissecting the interface between apicomplexan parasite and host cell: Insights from a divergent AMA–RON2 pair. *Proceedings of the National Academy of Sciences,* 113**,** 398-403.

PERIZ, J., WHITELAW, J., HARDING, C., GRAS, S., DEL ROSARIO MININA, M. I., LATORRE-BARRAGAN, F., LEMGRUBER, L., REIMER, M. A., INSALL, R., HEASLIP, A. & MEISSNER, M. 2017. *Toxoplasma gondii* F-actin forms an extensive filamentous network required for material exchange and parasite maturation. *Elife,* 6.

PERNAS, L., ADOMAKO-ANKOMAH, Y., SHASTRI, A. J., EWALD, S. E., TREECK, M., BOYLE, J. P. & BOOTHROYD, J. C. 2014. Toxoplasma effector MAF1 mediates recruitment of host mitochondria and impacts the host response. *PLoS biology,* 12**,** e1001845.

PHILIP, N. & WATERS, A. P. 2015. Conditional degradation of Plasmodium calcineurin reveals functions in parasite colonization of both host and vector. *Cell host & microbe,* 18**,** 122-131.

PIEPERHOFF, M. S., PALL, G. S., JIMENEZ-RUIZ, E., DAS, S., MELATTI, C., GOW, M., WONG, E. H., HENG, J., MULLER, S., BLACKMAN, M. J. & MEISSNER, M. 2015. Conditional U1 Gene Silencing in *Toxoplasma gondii*. *PLoS One,* 10**,** e0130356.

PIEPERHOFF, M. S., SCHMITT, M., FERGUSON, D. J. P. & MEISSNER, M. 2013. The Role of Clathrin in Post-Golgi Trafficking in *Toxoplasma gondii*. *PLOS ONE,* 8**,** e77620.

PINDER, J. C., FOWLER, R. E., DLUZEWSKI, A. R., BANNISTER, L. H., LAVIN, F. M., MITCHELL, G. H., WILSON, R. J. & GRATZER, W. B. 1998. Actomyosin motor in the merozoite of the malaria parasite, Plasmodium falciparum: implications for red cell invasion. *Journal of Cell Science,* 111**,** 1831-1839.

PLATTNER, F., YAROVINSKY, F., ROMERO, S., DIDRY, D., CARLIER, M. F., SHER, A. & SOLDATI-FAVRE, D. 2008. Toxoplasma profilin is essential for host cell invasion and TLR11-dependent induction of an interleukin-12 response. *Cell Host Microbe,* 3**,** 77-87.

POLLARD, T. D., BLANCHOIN, L. & MULLINS, R. D. 2000a. Molecular mechanisms controlling actin filament dynamics in nonmuscle cells. *Annu Rev Biophys Biomol Struct,* 29.

POLLARD, T. D., BLANCHOIN, L. & MULLINS, R. D. 2000b. Molecular mechanisms controlling actin filament dynamics in nonmuscle cells. *Annual review of biophysics and biomolecular structure,* 29**,** 545-576.

POLONAIS, V., JAVIER FOTH, B., CHINTHALAPUDI, K., MARQ, J. B., MANSTEIN, D. J., SOLDATI-FAVRE, D. & FRENAL, K. 2011. Unusual anchor of a motor complex (MyoD-MLC2) to the plasma membrane of *Toxoplasma gondii*. *Traffic,* 12**,** 287-300.

PORTER, S. B. & SANDE, M. A. 1992. Toxoplasmosis of the central nervous system in the acquired immunodeficiency syndrome. *New England Journal of Medicine,* 327**,** 1643-1648.

PORTMAN, N. & ŠLAPETA, J. 2013. The flagellar contribution to the apical complex: a new tool for the eukaryotic Swiss Army knife? *Trends in Parasitology,* 30**,** 58-64.

POTAPOVA, T. A., SIVAKUMAR, S., FLYNN, J. N., LI, R. & GORBSKY, G. J. 2011. Mitotic progression becomes irreversible in prometaphase and collapses when Wee1 and Cdc25 are inhibited. *Mol Biol Cell,* 22**,** 1191-206.

QUADT, K. A., STREICHFUSS, M., MOREAU, C. A., SPATZ, J. P. & FRISCHKNECHT, F. 2016. Coupling of Retrograde Flow to Force Production During Malaria Parasite Migration. *ACS Nano,* 10**,** 2091-102.

RIDZUAN, M. A. M., MOON, R. W., KNUEPFER, E., BLACK, S., HOLDER, A. A. & GREEN, J. L. 2012. Subcellular location, phosphorylation and assembly into the motor complex of GAP45 during Plasmodium falciparum schizont development. *PloS one,* 7**,** e33845.

ROBERT-GANGNEUX, F. & DARDE, M. L. 2012. Epidemiology of and diagnostic strategies for toxoplasmosis. *Clin Microbiol Rev,* 25**,** 264-96.

ROGERS, S. L. & GELFAND, V. I. 2000. Membrane trafficking, organelle transport, and the cytoskeleton. *Curr Opin Cell Biol,* 12**,** 57-62.

ROOS, D. S., DONALD, R. G., MORRISSETTE, N. S. & MOULTON, A. L. C. 1995. Molecular tools for genetic dissection of the protozoan parasite *Toxoplasma gondii*. *Methods in cell biology,* 45**,** 27-63.

RUGARABAMU, G., MARQ, J. B., GUERIN, A., LEBRUN, M. & SOLDATI-FAVRE, D. 2015. Distinct contribution of *Toxoplasma gondii* rhomboid proteases 4 and 5 to micronemal protein protease 1 activity during invasion. *Mol Microbiol,* 97**,** 244-62.

RUSSELL, D. & BURNS, R. 1984. The polar ring of coccidian sporozoites: a unique microtubule-organizing centre. *Journal of cell science,* 65**,** 193-207.

RUSSELL, D. G. & SINDEN, R. E. 1981. The role of the cytoskeleton in the motility of coccidian sporozoites. *Journal of Cell Science,* 50**,** 345-359.

SAHOO, N., BEATTY, W., HEUSER, J., SEPT, D. & SIBLEY, L. D. 2006. Unusual kinetic and structural properties control rapid assembly and turnover of actin in the parasite *Toxoplasma gondii*. *Molecular biology of the cell,* 17**,** 895-906.

SALAMUN, J., KALLIO, J. P., DAHER, W., SOLDATI-FAVRE, D. & KURSULA, I. 2014. Structure of *Toxoplasma gondii* coronin, an actin-binding protein that relocalizes to the posterior pole of invasive parasites and contributes to invasion and egress. *Faseb j,* 28**,** 4729-47.

SANTOS, J. M., FERGUSON, D. J., BLACKMAN, M. J. & SOLDATI-FAVRE, D. 2011. Intramembrane cleavage of AMA1 triggers Toxoplasma to switch from an invasive to a replicative mode. *Science,* 331**,** 473-477.

SCHATTEN, H., SIBLEY, L. D. & RIS, H. 2003. Structural evidence for actin-like filaments in *Toxoplasma gondii* using high-resolution low-voltage field emission scanning electron microscopy. *Microsc Microanal,* 9**,** 330-5.

SCHINDELIN, J., ARGANDA-CARRERAS, I., FRISE, E., KAYNIG, V., LONGAIR, M., PIETZSCH, T., PREIBISCH, S., RUEDEN, C., SAALFELD, S. & SCHMID, B. 2012. Fiji: an open-source platform for biological-image analysis. *Nature methods,* 9**,** 676-682.

SCHINDELIN, J., RUEDEN, C. T., HINER, M. C. & ELICEIRI, K. W. 2015. The ImageJ ecosystem: An open platform for biomedical image analysis. *Molecular reproduction and development,* 82**,** 518-529.

SCHLÜTER, D., DÄUBENER, W., SCHARES, G., GROß, U., PLEYER, U. & LÜDER, C. 2014. Animals are key to human toxoplasmosis. *International Journal of Medical Microbiology,* 304**,** 917-929.

SCHMITZ, S., GRAINGER, M., HOWELL, S., CALDER, L. J., GAEB, M., PINDER, J. C., HOLDER, A. A. & VEIGEL, C. 2005. Malaria Parasite Actin Filaments are Very Short. *Journal of Molecular Biology,* 349**,** 113-125.

SCHÜLER, H. & MATUSCHEWSKI, K. 2006a. Plasmodium motility: actin not actin' like actin. *Trends in Parasitology,* 22**,** 146-147.

SCHÜLER, H. & MATUSCHEWSKI, K. 2006b. Regulation of Apicomplexan Microfilament Dynamics by a Minimal Set of Actin-Binding Proteins. *Traffic,* 7**,** 1433-1439.

SEBASTIAN, S., BROCHET, M., COLLINS, MARK O., SCHWACH, F., JONES, MATTHEW L., GOULDING, D., RAYNER, JULIAN C., CHOUDHARY, JYOTI S. & BILLKER, O. 2012. A Plasmodium Calcium-Dependent Protein Kinase Controls Zygote Development and Transmission by Translationally Activating Repressed mRNAs. *Cell Host & Microbe,* 12**,** 9-19.

SEBÉ-PEDRÓS, A., GRAU-BOVÉ, X., RICHARDS, T. A. & RUIZ-TRILLO, I. 2014. Evolution and classification of myosins, a paneukaryotic whole-genome approach. *Genome biology and evolution,* 6**,** 290-305.

SHARMAN, P., SMITH, N., WALLACH, M. & KATRIB, M. 2010. Chasing the golden egg: vaccination against poultry coccidiosis. *Parasite immunology,* 32**,** 590-598.

SHAW, M. K. & TILNEY, L. G. 1999. Induction of an acrosomal process in *Toxoplasma gondii*: visualization of actin filaments in a protozoan parasite. *Proc Natl Acad Sci U S A,* 96**,** 9095-9.

SHEFFIELD, H. G. & MELTON, M. L. 1968. The Fine Structure and Reproduction of *Toxoplasma gondii*. *The Journal of Parasitology,* 54**,** 209-226.

SHEINER, L., VAIDYA, A. B. & MCFADDEN, G. I. 2013. The metabolic roles of the endosymbiotic organelles of Toxoplasma and Plasmodium spp. *Current Opinion in Microbiology,* 16**,** 452-458.

SHEN, B., BROWN, K. M., LEE, T. D. & SIBLEY, L. D. 2014a. Efficient gene disruption in diverse strains of *Toxoplasma gondii* using CRISPR/CAS9. *MBio,* 5**,** e01114-14.

SHEN, B., BUGULISKIS, J. S., LEE, T. D. & SIBLEY, L. D. 2014b. Functional analysis of rhomboid proteases during Toxoplasma invasion. *MBio,* 5**,** e01795-14.

SHEN, B. & SIBLEY, L. D. 2014. Toxoplasma aldolase is required for metabolism but dispensable for host-cell invasion. *Proc Natl Acad Sci U S A,* 111**,** 3567-72.

SIBLEY, L. D. 2010. How apicomplexan parasites move in and out of cells. *Curr Opin Biotechnol,* 21**,** 592-8.

SIBLEY, L. D. & BOOTHROYD, J. C. 1992. Virulent strains of *Toxoplasma gondii* comprise a single clonal lineage. *Nature,* 359**,** 82.

SIBLEY, L. D., KHAN, A., AJIOKA, J. W. & ROSENTHAL, B. M. 2009. Genetic diversity of *Toxoplasma gondii* in animals and humans. *Philos Trans R Soc Lond B Biol Sci,* 364**,** 2749-61.

SIDEN-KIAMOS, I., GANTER, M., KUNZE, A., HLISCS, M., STEINBUCHEL, M., MENDOZA, J., SINDEN, R. E., LOUIS, C. & MATUSCHEWSKI, K. 2011. Stage-specific depletion of myosin A supports an essential role in motility of malarial ookinetes. *Cell Microbiol,* 13**,** 1996-2006.

SIDEN-KIAMOS, I., LOUIS, C. & MATUSCHEWSKI, K. 2012. Evidence for filamentous actin in ookinetes of a malarial parasite. *Mol Biochem Parasitol,* 181**,** 186-9.

SIDIK, S. M., HACKETT, C. G., TRAN, F., WESTWOOD, N. J. & LOURIDO, S. 2014. Efficient genome engineering of *Toxoplasma gondii* using CRISPR/Cas9. *PloS one,* 9**,** e100450.

SIDIK, S. M., HUET, D., GANESAN, S. M., HUYNH, M.-H., WANG, T., NASAMU, A. S., THIRU, P., SAEIJ, J. P., CARRUTHERS, V. B. & NILES, J. C. 2016. A genome-wide CRISPR screen in toxoplasma identifies essential apicomplexan genes. *Cell,* 166**,** 1423-1435. e12.

SINAI, A. P., WEBSTER, P. & JOINER, K. A. 1997. Association of host cell endoplasmic reticulum and mitochondria with the *Toxoplasma gondii* parasitophorous vacuole membrane: a high affinity interaction. *Journal of cell science,* 110**,** 2117-2128.

SKARIAH, S., MCINTYRE, M. K. & MORDUE, D. G. 2010. *Toxoplasma gondii*: determinants of tachyzoite to bradyzoite conversion. *Parasitology research,* 107**,** 253-260.

SKILLMAN, K. M., DAHER, W., MA, C. I., SOLDATI-FAVRE, D. & SIBLEY, L. D. 2012. *Toxoplasma gondii* profilin acts primarily to sequester G-actin while formins efficiently nucleate actin filament formation in vitro. *Biochemistry,* 51**,** 2486-95.

SKILLMAN, K. M., MA, C. I., FREMONT, D. H., DIRAVIYAM, K., COOPER, J. A., SEPT, D. & SIBLEY, L. D. 2013. The unusual dynamics of parasite actin result from isodesmic polymerization. *Nature communications,* 4**,** 2285.

ŠLAPETA, J. & MORIN-ADELINE, V. 2011. Apicomplexa Levine 1970 Sporozoa Leucart 1879. http://tolweb.org/Apicomplexa/2446/2011.05.18 *in The Tree of Life Web Project*.

SOLDATI, D. & BOOTHROYD, J. C. 1993. Transient transfection and expression in the obligate intracellular parasite *Toxoplasma gondii*. *SCIENCE-NEW YORK THEN WASHINGTON-*, 260**,** 349-349.

SOLDATI, D. & BOOTHROYD, J. C. 1995. A selector of transcription initiation in the protozoan parasite *Toxoplasma gondii*. *Mol Cell Biol,* 15**,** 87-93.

SOLDATI, D., DUBREMETZ, J. F. & LEBRUN, M. 2001. Microneme proteins: structural and functional requirements to promote adhesion and invasion by the apicomplexan parasite *Toxoplasma gondii*. *International Journal for Parasitology,* 31**,** 1293-1302.

SOLDATI, D. & MEISSNER, M. 2004. Toxoplasma as a novel system for motility. *Curr Opin Cell Biol,* 16**,** 32-40.

SPEER, C. A., CLARK, S. & DUBEY, J. P. 1998. Ultrastructure of the oocysts, sporocysts, and sporozoites of *Toxoplasma gondii*. *J Parasitol,* 84**,** 505-12.

SPEER, C. A. & DUBEY, J. P. 1998. Ultrastructure of early stages of infections in mice fed *Toxoplasma gondii* oocysts. *Parasitology,* 116 (Pt 1)**,** 35-42.

SPEER, C. A. & DUBEY, J. P. 2005. Ultrastructural differentiation of *Toxoplasma gondii* schizonts (types B to E) and gamonts in the intestines of cats fed bradyzoites. *Int J Parasitol,* 35**,** 193-206.

STADLER, R. V., WHITE, L. A., HU, K., HELMKE, B. P. & GUILFORD, W. H. 2017. Direct measurement of cortical force generation and polarization in a living parasite. *Mol Biol Cell,* 28**,** 1912-1923.

STEWARD, M. J. & VANDERBERG, J. P. 1988. Malaria sporozoites leave behind trails of circumsporozoite protein during gliding motility. *Journal of Eukaryotic Microbiology,* 35**,** 389-393.

STOMMEL, E. W., ELY, K. H., SCHWARTZMAN, J. D. & KASPER, L. H. 1997. *Toxoplasma gondii*:Dithiol-Induced Ca2+Flux Causes Egress of Parasites from the Parasitophorous Vacuole. *Experimental Parasitology,* 87**,** 88-97.

STRIEPEN, B. 2013. Time to tackle cryptosporidiosis. *Nature,* 503**,** 189-191.

STRIEPEN, B., CRAWFORD, M. J., SHAW, M. K., TILNEY, L. G., SEEBER, F. & ROOS, D. S. 2000. The Plastid of *Toxoplasma gondii* Is Divided by Association with the Centrosomes. *The Journal of Cell Biology,* 151**,** 1423-1434.

SU, C., KHAN, A., ZHOU, P., MAJUMDAR, D., AJZENBERG, D., DARDÉ, M.-L., ZHU, X.-Q., AJIOKA, J. W., ROSENTHAL, B. M. & DUBEY, J. P. 2012. Globally diverse *Toxoplasma gondii* isolates comprise six major clades originating from a small number of distinct ancestral lineages. *Proceedings of the National Academy of Sciences,* 109**,** 5844-5849.

SUAREZ, C., BISHOP, R., ALZAN, H., POOLE, W. & COOKE, B. 2017. Advances in the application of genetic manipulation methods to Apicomplexan parasites. *International journal for parasitology*.

SUGDEN, K., MOFFITT, T. E., PINTO, L., POULTON, R., WILLIAMS, B. S. & CASPI, A. 2016. Is Toxoplasma Gondii Infection Related to Brain and Behavior Impairments in Humans? Evidence from a Population-Representative Birth Cohort. *PLOS ONE,* 11**,** e0148435.

SUSS-TOBY, E., ZIMMERBERG, J. & WARD, G. 1996. Toxoplasma invasion: the parasitophorous vacuole is formed from host cell plasma membrane and pinches off via a fission pore. *Proceedings of the National Academy of Sciences,* 93**,** 8413-8418.

SWAPNA, L. S. & PARKINSON, J. 2017. Genomics of apicomplexan parasites. *Critical Reviews in Biochemistry and Molecular Biology,* 52**,** 254-273.

TANG, Q., ANDENMATTEN, N., HORTUA TRIANA, M. A., DENG, B., MEISSNER, M., MORENO, S. N., BALLIF, B. A. & WARD, G. E. 2014. Calcium-dependent phosphorylation alters class XIVa myosin function in the protozoan parasite *Toxoplasma gondii*. *Mol Biol Cell,* 25**,** 2579-91.

TARDIEUX, I. & BAUM, J. 2016. Reassessing the mechanics of parasite motility and host-cell invasion. *J Cell Biol,* 214**,** 507-15.

TAYLOR, S., BARRAGAN, A., SU, C., FUX, B., FENTRESS, S., TANG, K., BEATTY, W., EL HAJJ, H., JEROME, M. & BEHNKE, M. 2006. A secreted serine-threonine kinase determines virulence in the eukaryotic pathogen *Toxoplasma gondii*. *Science,* 314**,** 1776-1780.

TENTER, A. M., HECKEROTH, A. R. & WEISS, L. M. 2000. *Toxoplasma gondii*: from animals to humans. *International Journal for Parasitology,* 30**,** 1217-1258.

TORGERSON, P. R. & MASTROIACOVO, P. 2013. The global burden of congenital toxoplasmosis: a systematic review. *Bulletin of the World Health Organization,* 91**,** 501-508.

TRAPNELL, C., ROBERTS, A., GOFF, L., PERTEA, G., KIM, D., KELLEY, D. R., PIMENTEL, H., SALZBERG, S. L., RINN, J. L. & PACHTER, L. 2012. Differential gene and transcript expression analysis of RNA-seq experiments with TopHat and Cufflinks. *Nature protocols,* 7**,** 562.

TREECK, M., SANDERS, J. L., ELIAS, J. E. & BOOTHROYD, J. C. 2011. The phosphoproteomes of Plasmodium falciparum and *Toxoplasma gondii* reveal unusual adaptations within and beyond the parasites' boundaries. *Cell Host Microbe,* 10**,** 410-9.

TREES, A., DAVISON, H., INNES, E. & WASTLING, J. 1999. Towards evaluating the economic impact of bovine neosporosis. *International journal for parasitology,* 29**,** 1195-1200.

TRYBUS, K. M. 1994. Role of myosin light chains. *Journal of muscle research and cell motility,* 15**,** 587-594.

UETI, M. W. & KNOWLES, D. P. 2018. Equine Piroplasmids. *In:* FLORIN-CHRISTENSEN, M. & SCHNITTGER, L. (eds.) *Parasitic Protozoa of Farm Animals and Pets.* Cham: Springer International Publishing.

UILENBERG, G. 2006. Babesia—A historical overview. *Veterinary Parasitology,* 138**,** 3-10.

VAHOKOSKI, J., BHARGAV, S. P., DESFOSSES, A., ANDREADAKI, M., KUMPULA, E.-P., MARTINEZ, S. M., IGNATEV, A., LEPPER, S., FRISCHKNECHT, F. & SIDÉN-KIAMOS, I. 2014. Structural differences explain diverse functions of Plasmodium actins. *PLoS pathogens,* 10**,** e1004091.

VANDERBERG, J. P. 1974. Studies on the motility of Plasmodium sporozoites. *Journal of Eukaryotic Microbiology,* 21**,** 527-537.

VENIT, T., DZIJAK, R., KALENDOVÁ, A., KAHLE, M., ROHOŽKOVÁ, J., SCHMIDT, V., RÜLICKE, T., RATHKOLB, B., HANS, W., BOHLA, A., EICKELBERG, O., STOEGER, T., WOLF, E., YILDIRIM, A. Ö., GAILUS-DURNER, V., FUCHS, H., DE ANGELIS, M. H. & HOZÁK, P. 2013. Mouse Nuclear Myosin I Knock-Out Shows Interchangeability and Redundancy of Myosin Isoforms in the Cell Nucleus. *PLOS ONE,* 8**,** e61406.

VINAYAK, S., PAWLOWIC, M. C., SATERIALE, A., BROOKS, C. F., STUDSTILL, C. J., BAR-PELED, Y., CIPRIANO, M. J. & STRIEPEN, B. 2015. Genetic modification of the diarrheal pathogen Cryptosporidium parvum. *Nature,* 523**,** 477-480.

VIVIER, E. & PETITPREZ, A. 1969. The outer membrane complex and its development at the time of the formation of daughter cells in *Toxoplasma gondii*. *The Journal of cell biology,* 43**,** 329-342.

WAGNER, J. C., PLATT, R. J., GOLDFLESS, S. J., ZHANG, F. & NILES, J. C. 2014. Efficient CRISPR-Cas9-mediated genome editing in Plasmodium falciparum. *Nature methods,* 11**,** 915-918.

WALLER, R. F. & MCFADDEN, G. I. 2005. The apicoplast: a review of the derived plastid of apicomplexan parasites. *Curr Issues Mol Biol,* 7**,** 57-79.

WEBER, E., GRUETZNER, R., WERNER, S., ENGLER, C. & MARILLONNET, S. 2011. Assembly of designer TAL effectors by Golden Gate cloning. *PLoS One,* 6**,** e19722.

WEISS, L. M. & DUBEY, J. P. 2009. Toxoplasmosis: A history of clinical observations. *Int J Parasitol,* 39**,** 895-901.

WEISS, L. M. & KIM, K. 2000. The development and biology of bradyzoites of *Toxoplasma gondii*. *Frontiers in bioscience: a journal and virtual library,* 5**,** D391.

WELCH, MATTHEW D. 2015. Cell Migration, Freshly Squeezed. *Cell,* 160**,** 581-582.

WELLS, A. L., LIN, A. W., LI-QIONG, C. & SAFER, D. 1999. Myosin VI is an actin-based motor that moves backwards. *Nature,* 401**,** 505.

WETZEL, D. M., CHEN, L. A., RUIZ, F. A., MORENO, S. N. J. & SIBLEY, L. D. 2004. Calcium-mediated protein secretion potentiates motility in *Toxoplasma gondii*. *Journal of Cell Science,* 117**,** 5739-5748.

WETZEL, D. M., HAKANSSON, S., HU, K., ROOS, D. & SIBLEY, L. D. 2003. Actin filament polymerization regulates gliding motility by apicomplexan parasites. *Mol Biol Cell,* 14**,** 396-406.

WETZEL, D. M., SCHMIDT, J., KUHLENSCHMIDT, M. S., DUBEY, J. & SIBLEY, L. D. 2005. Gliding motility leads to active cellular invasion by Cryptosporidium parvum sporozoites. *Infection and immunity,* 73**,** 5379-5387.

WHITELAW, J. A., LATORRE-BARRAGAN, F., GRAS, S., PALL, G. S., LEUNG, J. M., HEASLIP, A., EGARTER, S., ANDENMATTEN, N., NELSON, S. R., WARSHAW, D. M., WARD, G. E. & MEISSNER, M. 2017. Surface attachment, promoted by the actomyosin system of *Toxoplasma gondii* is important for efficient gliding motility and invasion. *BMC Biol,* 15**,** 1.

WHO 2016. World Malaria Report 2016. *Geneva: World Health Organization; 2016,* License CC BY-NC-SA 3.0 IGO.

WILLIAMS, M. J., ALONSO, H., ENCISO, M., EGARTER, S., SHEINER, L., MEISSNER, M., STRIEPEN, B., SMITH, B. J. & TONKIN, C. J. 2015. Two Essential Light Chains Regulate the MyoA Lever Arm To Promote Toxoplasma Gliding Motility. *MBio,* 6**,** e00845-15.

WILLOX, A. K., SAHRAOUI, Y. M. E. & ROYLE, S. J. 2014. Non-specificity of Pitstop 2 in clathrin-mediated endocytosis. *Biology Open,* 3**,** 326-331.

WOHLFERT, E. A., BLADER, I. J. & WILSON, E. H. 2017. Brains and Brawn: Toxoplasma Infections of the Central Nervous System and Skeletal Muscle. *Trends in Parasitology,* 33**,** 519-531.

WOLF, A., COWEN, D. & PAIGE, B. 1939a. HUMAN TOXOPLASMOSIS: OCCURRENCE IN INFANTS AS AN ENCEPHALOMYELITIS VERIFICATION BY TRANSMISSION TO ANIMALS. *Science,* 89**,** 226-7.

WOLF, A., COWEN, D. & PAIGE, B. 1939b. Human toxoplasmosis: occurrence in infants as an encephalomyelitis verification by transmission to animals. *Science (Washington),* 89.

WOO, Y. H., ANSARI, H., OTTO, T. D., KLINGER, C. M., KOLISKO, M., MICHALEK, J., SAXENA, A., SHANMUGAM, D., TAYYROV, A., VELUCHAMY, A., ALI, S., BERNAL, A., DEL CAMPO, J., CIHLAR, J., FLEGONTOV, P., GORNIK, S. G., HAJDUSKOVA, E., HORAK, A., JANOUSKOVEC, J., KATRIS, N. J., MAST, F. D., MIRANDA-SAAVEDRA, D., MOURIER, T., NAEEM, R., NAIR, M., PANIGRAHI, A. K., RAWLINGS, N. D., PADRON-REGALADO, E., RAMAPRASAD, A., SAMAD, N., TOMCALA, A., WILKES, J., NEAFSEY, D. E., DOERIG, C., BOWLER, C., KEELING, P. J., ROOS, D. S., DACKS, J. B., TEMPLETON, T. J., WALLER, R. F., LUKES, J., OBORNIK, M. & PAIN, A. 2015. Chromerid genomes reveal the evolutionary path from photosynthetic algae to obligate intracellular parasites. *Elife,* 4**,** e06974.

WOOLNER, S. & BEMENT, W. M. 2009. Unconventional myosins acting unconventionally. *Trends Cell Biol,* 19**,** 245-52.

XIAO, J., VISCIDI, R. P., KANNAN, G., PLETNIKOV, M. V., LI, Y., SEVERANCE, E. G., YOLKEN, R. H. & DELHAES, L. 2013. The Toxoplasma MAG1 peptides induce sex-based humoral immune response in mice and distinguish active from chronic human infection. *Microbes and infection,* 15**,** 74-83.

XIAO, J. & YOLKEN, R. H. 2015. Strain hypothesis of *Toxoplasma gondii* infection on the outcome of human diseases. *Acta Physiologica,* 213**,** 828-845.

XU, P., WIDMER, G., WANG, Y., OZAKI, L. S., ALVES, J. M., SERRANO, M. G., PUIU, D., MANQUE, P., AKIYOSHI, D., MACKEY, A. J., PEARSON, W. R., DEAR, P. H., BANKIER, A. T., PETERSON, D. L., ABRAHAMSEN, M. S., KAPUR, V., TZIPORI, S. & BUCK, G. A. 2004. The genome of Cryptosporidium hominis. *Nature,* 431**,** 1107-12.

YANG, A. S. P., O'NEILL, M. T., JENNISON, C., LOPATICKI, S., ALLISON, C. C., ARMISTEAD, J. S., ERICKSON, S. M., ROGERS, K. L., ELLISDON, A. M., WHISSTOCK, J. C., TWEEDELL, R. E., DINGLASAN, R. R., DOUGLAS, D. N., KNETEMAN, N. M. & BODDEY, J. A. 2017. Cell Traversal Activity Is Important for Plasmodium falciparum Liver Infection in Humanized Mice. *Cell Reports,* 18**,** 3105-3116.

YAP, A., AZEVEDO, M. F., GILSON, P. R., WEISS, G. E., O'NEILL, M. T., WILSON, D. W., CRABB, B. S. & COWMAN, A. F. 2014. Conditional expression of apical membrane antigen 1 in Plasmodium falciparum shows it is required for erythrocyte invasion by merozoites. *Cellular microbiology,* 16**,** 642-656.

YEH, E. & DERISI, J. L. 2011. Chemical Rescue of Malaria Parasites Lacking an Apicoplast Defines Organelle Function in Blood-Stage Plasmodium falciparum. *PLOS Biology,* 9**,** e1001138.

YEOH, S., O'DONNELL, R. A., KOUSSIS, K., DLUZEWSKI, A. R., ANSELL, K. H., OSBORNE, S. A., HACKETT, F., WITHERS-MARTINEZ, C., MITCHELL, G. H. & BANNISTER, L. H. 2007. Subcellular discharge of a serine protease mediates release of invasive malaria parasites from host erythrocytes. *Cell,* 131**,** 1072-1083.

YUSUF, N. A., GREEN, J. L., WALL, R. J., KNUEPFER, E., MOON, R. W., SCHULTE-HUXEL, C., STANWAY, R. R., MARTIN, S. R., HOWELL, S. A. & DOUSE, C. H. 2015. The Plasmodium class XIV myosin, MyoB, has a distinct subcellular location in invasive and motile stages of the malaria parasite and an unusual light chain. *Journal of biological chemistry,* 290**,** 12147-12164.

ZHANG, C., XIAO, B., JIANG, Y., ZHAO, Y., LI, Z., GAO, H., LING, Y., WEI, J., LI, S. & LU, M. 2014. Efficient editing of malaria parasite genome using the CRISPR/Cas9 system. *MBio,* 5**,** e01414-14.

ZHENG, B., SAGE, M., SHEPPEARD, E. A., JURECIC, V. & BRADLEY, A. 2000. Engineering mouse chromosomes with Cre-loxP: range, efficiency, and somatic applications. *Molecular and cellular biology,* 20**,** 648-655.

ZHU, G., MARCHEWKA, M. J. & KEITHLY, J. S. 2000. Cryptosporidium parvum appears to lack a plastid genome. *Microbiology,* 146 (Pt 2)**,** 315-21.

ZINCHUK, V., ZINCHUK, O. & OKADA, T. 2007. Quantitative colocalization analysis of multicolor confocal immunofluorescence microscopy images: pushing pixels to explore biological phenomena. *Acta Histochem Cytochem,* 40**,** 101-11.